CZECH TECHNICAL UNIVERSITY IN PRAGUE
FACULTY OF NUCLEAR SCIENCES AND PHYSICAL ENGINEERING

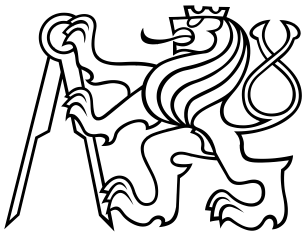

DOCTORAL THESIS

ADVANCED MOMENT INVARIANTS FOR PATTERN MATCHING

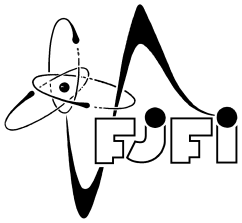

PRAGUE 2020

JITKA KOSTKOVÁ

DECLARATION

I declare that I carried out this Thesis independently and only with the cited sources, literature and other professional sources.

Prague, June 2020

Jitka Kostková

BIBLIOGRAFICKÝ ZÁZNAM

Autor	Ing. Jitka Kostková České vysoké učení technické v Praze Fakulta jaderná a fyzikálně inženýrská Katedra matematiky
Název práce	Pokročilé momentové invarianty pro rozpoznávání vzorů
Studijní obor	Matematické inženýrství
Školitel	Prof. Ing. Jan Flusser, DrSc. Ústav teorie informace a automatizace, v.v.i. Akademie věd České republiky
Akademický rok	2020
Počet stran	114
Klíčová slova	digitální zpracování obrazu, momenty, invarianty, vektorová pole, ortogonální polynomy, gaussovské rozmazání, afinní transformace

BIBLIOGRAPHIC ENTRY

Author	Ing. Jitka Kostková Czech Technical University in Prague Faculty of Nuclear Sciences and Physical Engineering Department of Mathematics
Title of Dissertation	Advanced moment invariants for pattern matching
Field of Study	Mathematical Engineering
Supervisor	Prof. Ing. Jan Flusser, DrSc. Institute of Information Theory and Automation Czech Academy of Sciences
Academic Year	2020
Number of Pages	114
Keywords	Image Processing, Moments, Invariants, Vector fields, Orthogonal polynomials, Gaussian blur, Affine transformation

This thesis is dedicated to my loved ones.

ABSTRAKT

Tato práce se zabývá dvěma aktuálními trendy momentových metod v rozpoznávání obrazu – momentovými invarianty vektorových polí a momentovými invarianty ke konvoluci s Gaussovou funkcí.

Vektorová pole jsou speciálním typem dat objevujícím se v mnoha aplikacích, přitahujícím v posledních letech stále větší pozornost. Vektorová pole jsou v jistém smyslu podobná barevným obrázkům, ale některé jejich vlastnosti se výrazně liší. Vektor je veličina, kterou můžeme popsat velikostí a směrem. V této práci navrhujeme metodu popisu a vyhledávání ve vektorových polích při neznámé rotaci, respektive afinní transformaci pole. Transformace vektorových polí na rozdíl od obrázků nepůsobí pouze na prostorové souřadnice, ale ovlivňuje také hodnoty vektorového pole. Prezentujeme invarianty vektorových polí vůči totální rotaci z ortogonálních momentů a invarianty vůči totální afinní transformaci a jejich souvislost s vícevrstvými grafy.

Druhá část práce se věnuje nové teorii invariantů vůči gaussovskému rozmazání, jehož jádro může být libovolně otočené, protažené a škálované. Předpoklad anizotropní gaussovské funkce nám umožňuje snadno konstruovat kombinované invarianty vůči gaussovskému rozmazání a afinní transformaci. Navrhujeme nelineární projekční operátor, který extrahuje část obrázku necitlivou vůči šumu. Momenty této části pak reprezentují invarianty původního obrázku. Metoda nepotřebuje žádnou apriorní znalost parametrů Gaussovy funkce a nepoužívá dekonvoluci. Tato teorie může být upravena pro popis vícerozměrných histogramů obrázků necitlivý k aditivnímu gaussovskému šumu.

ABSTRACT

The thesis covers two areas of moment-based methods in image processing – moment invariants for vector field images and moment invariants to convolution with Gaussian function.

Vector fields are a special type of multidimensional data that comes from numerous scientific and engineering areas. They have been drawing increasing attention in the last few years. Although vector fields are similar in a certain sense to color images, they differ significantly in several ways. A vector is a quantity with a magnitude and a direction that can be visualized as an arrow. In this thesis, we propose a method for the description and matching of vector field patterns under an unknown rotation and affine transformation of the field. In contrast to digital images, transformations of vector fields may act not only on the spatial coordinates but also on the field values. Invariants of vector fields w.r.t. total rotation are constructed from orthogonal moments. Invariants to total affine transformation of vector fields in explicit form are derived and their connection to multi-layer graphs is shown.

The second part of the thesis presents a new theory of invariants to Gaussian blur. The blur kernel may be arbitrarily oriented, scaled, and elongated. The assumption of an anisotropic Gaussian kernel allows the construction of combined invariants to Gaussian blur and spatial affine transformation. We propose a non-linear projection operator which extracts blur-insensitive component of the image. The invariants are formally defined as moments of this component. The method does not require any prior knowledge of the blur kernel parameters and it avoids the usage of deconvolution. The theory can be modified for the description of multidimensional image histograms insensitive to additive Gaussian noise in the image.

PUBLICATIONS

INTERNATIONAL JOURNALS WITH IMPACT FACTOR

- J. Kostková, J. Flusser, M. Lébl, and M. Pedone, "Handling Gaussian blur without deconvolution," *Pattern Recognition*, vol. 103, 2020, art. no. 107264
- J. Kostková and J. Flusser, "Robust multivariate density estimation under Gaussian noise," *Multidimensional Systems and Signal Processing*, vol. 31, pp. 1113–1143, 2020
- J. Kostková, T. Suk, and J. Flusser, "Affine invariants of vector fields," *IEEE Transactions on Pattern Analysis and Machine Intelligence*, 2019. DOI: 10.1109/TPAMI.2019.2951664
- B. Yang, J. Kostková, J. Flusser, T. Suk, and R. Bujack, "Rotation invariants of vector fields from orthogonal moments," *Pattern Recognition*, vol. 74, pp. 110–121, 2018
- B. Yang, J. Kostková, J. Flusser, and T. Suk, "Scale invariants from Gaussian–Hermite moments," *Signal Processing*, vol. 132, pp. 77–84, 2017

INTERNATIONAL CONFERENCE PROCEEDINGS INDEXED BY SCOPUS AND WEB OF SCIENCE

- J. Kostková and J. Flusser, "On the null-space of the shape-color moment invariants," in *International Conference on Computer Analysis of Images and Patterns CAIP'19*, Springer, vol. LNCS 11678, 2019, pp. 402–408
- J. Kostková and J. Flusser, "Robust histogram estimation under Gaussian noise," in *International Conference on Computer Analysis of Images and Patterns CAIP'19*, Springer, vol. LNCS 11678, 2019, pp. 421–432
- J. Kostková, J. Flusser, M. Lébl, and M. Pedone, "Image invariants to anisotropic Gaussian blur," in *Scandinavian Conference on Image Analysis SCIA'19*, Springer, vol. LNCS 11482, 2019, pp. 140–151
- J. Kostková, T. Suk, and J. Flusser, "Affine moment invariants of vector fields," in *2018 25th IEEE International Conference on Image Processing (ICIP)*, IEEE, 2018, pp. 1338–1342

- B. Yang, J. Kostková, T. Suk, J. Flusser, and R. Bujack, "Recognition of patterns in vector fields by Gaussian–Hermite invariants," in *International Conference on Image Processing ICIP'17*, J. Luo, W. Zeng, and Y.-J. Zhang, Eds., Beijing, China: IEEE, 2017, pp. 2350–2363

ACKNOWLEDGMENTS

My work in the field of science would have not been possible without my mom ***Jitka***, who have been there for me my whole life. The completion of my dissertation would not have been possible without the support and loving care of ***Tom***. You make me a better person.

All results described in this Thesis were accomplished with the help and support of my associates from the Institute of Information Theory and Automation which falls under the Czech Academy of Sciences.

I am deeply indebted to my supervisor ***Jan Flusser***. Thank you for your time, patience, ideas, and comments during this long period of my life.

I must also thank to my special friend ***Barney*** for proofreading of the English manuscript.

I am also grateful to the entire Department of Image Processing for the great working environment where I always feel comfortable and supported. Special thanks goes to ***Matěj***, who is always willing to stay up late and help me.

Last but not least, I would like to thank the Group of Applied Mathematics and Stochastics – it was great to be a part of your team. I cannot leave the Czech Technical University without mentioning ***Milan Krbálek***, who sparked my interest in mathematics.

My PhD studies were supported by these grants:

- GAČR - GA18-07247S - *Methods and Algorithms for Vector and Tensor Field Image Analysis*
- GAČR - GA15-16928S - *Invariants and Adaptive Representations of Digital Images*
- Akademická prémie AV ČR 2017 - *Praemium Academiae*
- Studentská grantová soutěž (SGS) - SGS18/188/OHK4/3T/14 - *Fyzikální a socio-fyzikální aplikace stochastického modelování*
- Studentská grantová soutěž (SGS) - SGS15/214/OHK4/3T/14 - *Aplikace stochastických modelů na vybrané socio-fyzikální monitorovací systémy*

Institute of Information Theory and Automation

Department of Image Processing

Czech Technical University

Grant Agency of the Czech Republic

Group of Applied Mathematics and Stochastics

CONTENTS

Part I

INTRODUCTION

1 INTRODUCTION

> "... and your tongue will be parched with thirst and your body overcome by sleep and hunger before you can describe with words what a painter is able to show you in an instant."
>
> –Leonardo da Vinci
> Excerpt from A Comparison Between Poetry and Painting
> From his undated manuscripts

1.1 MOTIVATION

The modern equivalent of the da Vinci's quotation is the English language adage: "A picture is worth a thousand words". While in the past pictures were represented by paintings, currently, the most common source of visual information is a photograph. The number of photographs taken every year is growing rapidly (see Fig. 1) owing to the boom of smartphones and social networks. Estimates suggest that more than 1 *trillion* (10^{12}) photos were taken in 2018.[1] These images are not only personal memories but many of them were acquired for professional purposes in medicine, biology, astronomy, industry and other areas. All the data has to be stored, processed, and analyzed. Each photo contains several megabytes of information. There is not enough human power to do that manually. This is why there is such a dramatic need for automatic image analysis methods.

Image analysis is the process of extraction, understanding, and interpretation of useful information from an image. Typical examples are detection and counting of cells in microscopic images in biology or detection of tumors in MRI images of the brain in medicine. Nowadays, image analysis is an omnipresent component of modern AI systems and allows for substantial advances in automation. Image analysis pipeline consists basically of 5 steps – image acquisition, preprocessing, object detection, computing of features, and classification. Figure 2 shows an illustrative example of image analysis.

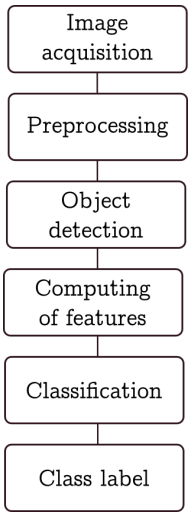

Image analysis pipeline.

1 www.theconversation.com/of-the-trillion-photos-taken-in-2018-which-were-the-most-memorable-108815

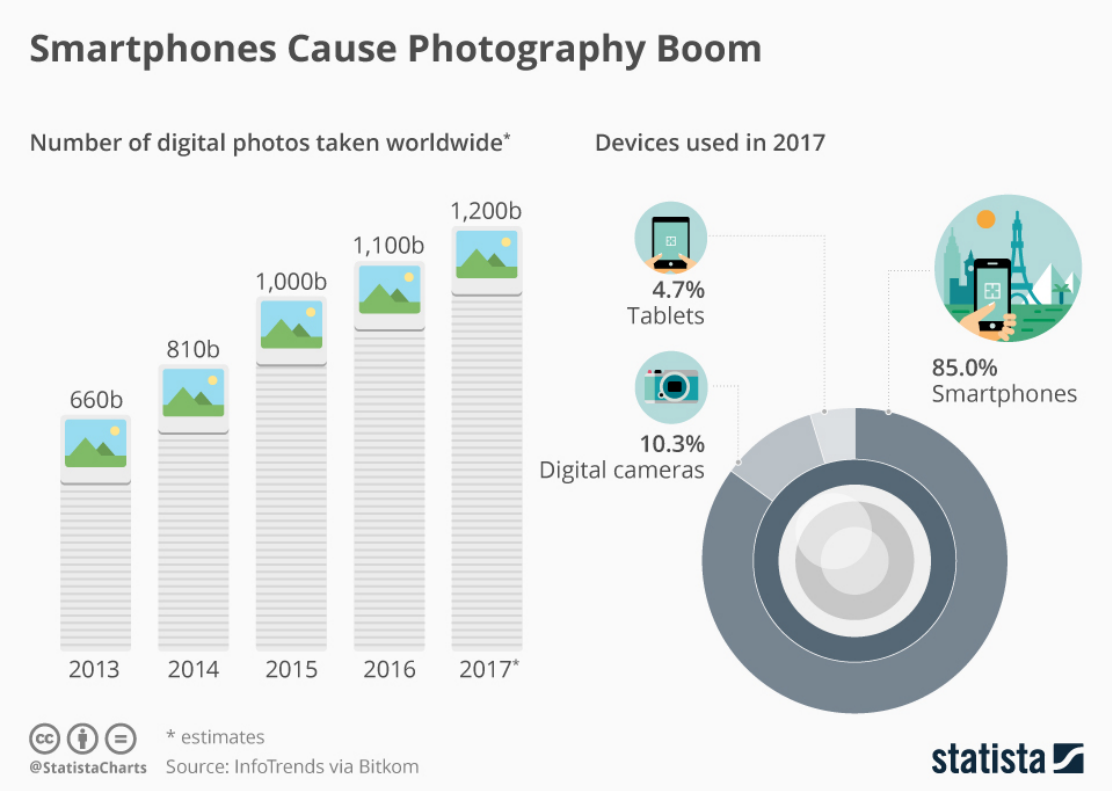

Figure 1: *Felix Richter: "Smartphones Cause Photography Boom"*, Statista, *13 February 2020*, https://www.statista.com/chart/10913/number-of-photos-taken-worldwide/.

Image acquisition

Real imaging systems and imaging conditions are imperfect, as a result, the observed image is only a degraded version of the original scene. Various kinds of degradations may be introduced during the acquisition process due to sampling, motion of the imaging device, lens imperfections, defocus, noise, etc. In the general case, the relationship between the original image f and its degraded version g can be described as $g = \mathcal{D}(f)$, where $\mathcal{D}$ is the degradation operator. In a 2D linear shift-invariant system, $\mathcal{D}$ is in the form

$$g(\tau(x,y)) = (f * h)(x,y) + n(x,y)\,, \tag{1}$$

where n is an additive random noise, h is the point-spread function (PSF) of the system and τ is a transform of spatial coordinates, $*$ denotes a 2D convolution. However, for non-image functions and in a higher dimension the degradation model may be highly complicated. The goal of recognition algorithms is to analyze the unknown image function f provided we know only the function g.

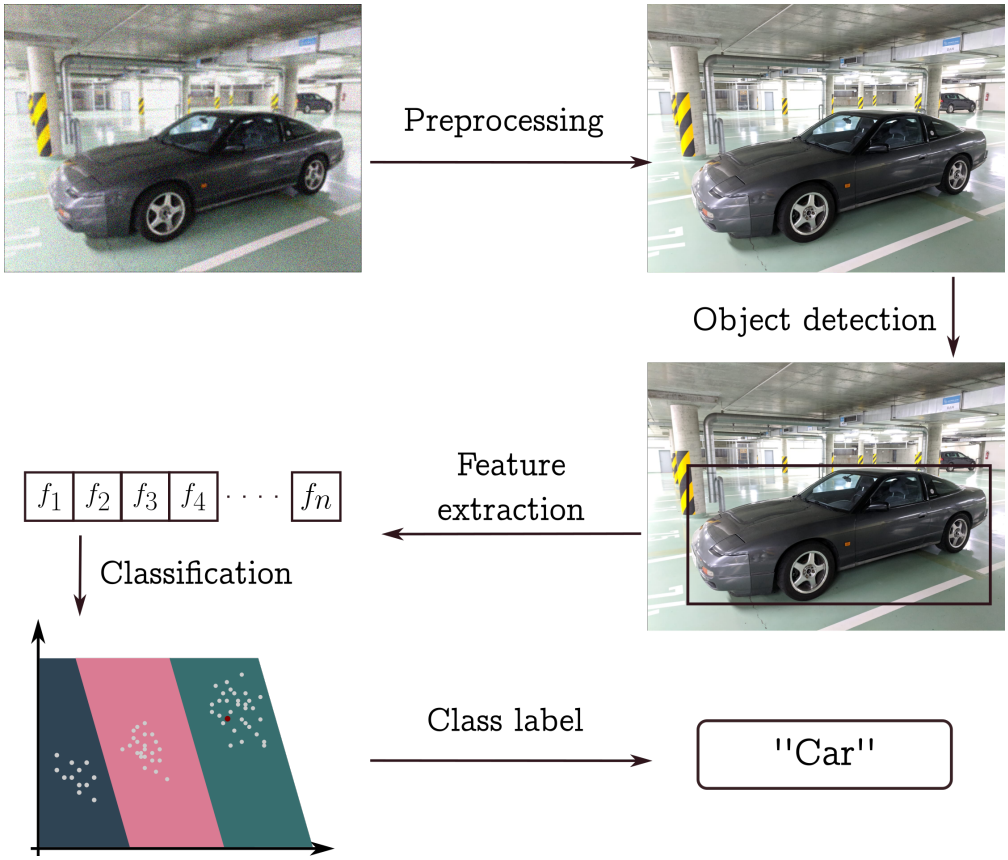

Figure 2: *Example of analysis of a photograph.*

Preprocessing

Suppression or removal of these artifacts to enhance the visual quality of the image is the main goal of the second step – image preprocessing. The resulting image is easier to analyze and process computationally. This step belongs to so-called *low-level processing*, i.e. the input and output are images. Some examples of image enhancement methods are histogram equalization, contrast adjustment, deblurring/sharpening, noise removal, morphological operations, and many others.

Object detection

Object detection is the process of finding instances of objects in the image – their precise localization and correct identification of all their pixels (segmentation). Feature-based object detection (e.g. RANSAC [11]) or state-of-the-art detection using deep learning methods [12] can be used to produce high-quality results depending on the specific application. A basic survey of the algorithms for object detection and image

segmentation can be found in the book [13] or the tutorial article on image segmentation [14].

Feature description

A *feature* is a measurable quantitative characteristic of the object. It can be viewed as a point in a metric space – *feature space* – which describes the object/image. Their design belongs to the challenging tasks in image processing. The features should describe the objects accurately and unambiguously. The following properties of the features are desirable for image analysis applications.

- Quantity – a single value is in most cases insufficient for the description and it is necessary to construct an $r - D$ *feature vector* to improve the recognition power. However, the dimension of the feature space should be reasonably low to maintain a low computational complexity.
- Discriminability – the features of objects of one class should differ significantly from the features of other classes.
- Invariance – the feature vector should remain unchanged regardless of the intra-class variation.
- Independence – none of the components of the feature vector is a function of the others. Dependent features are redundant, do not contribute to the discrimination power, and only increase the dimensionality of the feature space.
- Completeness – a loss-less reconstruction of the object from the features is possible, i.e. no other independent features exist. In practical applications, e.g. classification, completeness is often superfluous.

There are plenty of existing features, they always have to be chosen according to the application area and its objective. There is no single optimal solution that can be used in all cases.

Classification and class labeling

The last two steps are performed in the feature space. Every object/image is now represented by a feature vector. Constructing a classifier is equivalent to a partition of the feature space. The classification result depends solely on the position of the respective point in the feature space. The classification can be either *supervised* or *unsupervised* – *clustering*. In the case of supervised classification, the classes are specified beforehand through a training set – a set of objects with known class membership. In unsupervised classification, the training set is not available and the data with similar features are grouped to form "clusters". Because the classification takes place in the feature

space, it is not restricted to image analysis applications only and can be used in numerous applications – artificial intelligence, decision making, statistical data analysis, social sciences, and many others. Classification methods are thoroughly discussed in classical books [15] or [16].

1.2 INVARIANTS

In the previous section, invariance was mentioned as one of the desired properties of the features. As it is the central term of the thesis, we devote this section to the explanation of this notion.

Invariance is a property of an object which remains unchanged under certain transformations. More precisely, the *invariant feature* or *(absolute) invariant* is a functional I which maps the image space into the feature space such that $I(f)$ does not depend on particular appearance of f but only on the class f belongs to.

In other words, the functional I fulfils the condition $I(f) = I(\mathcal{D}(f))$ for any f and any admissible degradation $\mathcal{D}$. $\mathcal{D}$ is sometimes called the operator of the intra-class variation.

The functional I defines the relation of equivalence on the image space. We say that functions f and g are equivalent $f \sim g$ if and only if $I(f) = I(g)$. The invariants stay constant within each equivalence class, while should distinguish any two images belonging to different classes.

Not all invariants are useful for classification purposes either. For instance, if I is the same constant for all objects, then it is invariant but useless. Hence, it is important for I to differ significantly on objects from different classes. The ideal situation is depicted in Figure 3. The blue points and red points form two compact clusters (invariance) and at the same time, the clusters are well separated (discriminability).

In practical applications, we have to take into account which degradations can occur. Invariance and discriminability are opposite properties, i.e. an increase in invariance leads to a decrease in discriminability. Choosing a suitable compromise between invariance and discrimination power is the key task in feature-based object recognition.

Categories of invariants

Invariant features can be divided into various categories depending on the point of view. The most often used criteria are

- the dimension of objects and the type of data,
- the type of invariance (intra-class variation),
- the part of an object which is necessary for the invariant computation,
- the mathematical tools used for the construction of invariants.

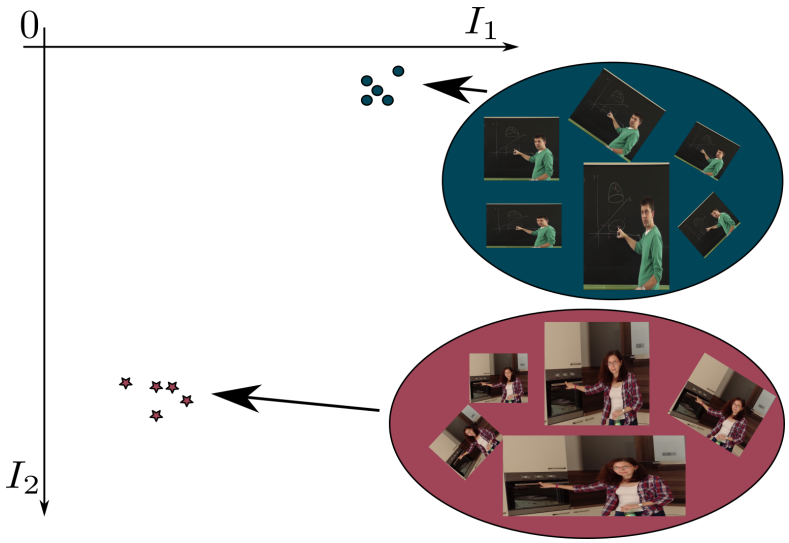

Figure 3: *Invariance and discriminability. The affinely transformed images of a man and a woman form two compact clusters (invariance) in the feature space which are far enough from each other (discriminability).*

In the following section, we focus on invariants constructed from so-called *image moments*.

1.3 IMAGE MOMENTS AND MOMENT INVARIANTS

In mathematics, the moment of a function is a specific quantitative measure of the shape of the function. Moments are often used in statistics as a tool for the description of a probability density function. They are popular as they have one remarkable property. For a function defined on a bounded interval, they are complete features, i.e. the collection of all the moments of all orders uniquely determines the distribution [17] – *Hausdorff moment problem*.

Image moments

Before we proceed to the definition of the central term of the thesis it is necessary to recall some basic definitions and notations important for the understanding of the text.

Definition 1. *By an* image function *(or* image*) we understand any piecewise continuous real function* $f : \mathbb{R}^d \to \mathbb{R}$ *defined on a compact support* $\Omega \subset \mathbb{R}^d$.

The image function does not have to be non-negative in general. This simple assumption ensures that mathematical operations on the image are well defined. Sometimes additional constraints, such as non-zero integral or square integrability, are re-

quired to meet the assumptions of a given mathematical theory. The continuous representation of the image function is convenient for the mathematical description because of its formal simplicity.

Moments can be viewed as "projections" of the image function onto a polynomial basis. According to the polynomial basis, we can divide moments into several categories (see Fig. 4 for the overview). Although all of them are theoretically equivalent, i.e. every element of one basis can be expressed as a linear combination of elements from any other basis, some of them possess better numerical properties or enable simple derivation of invariants.

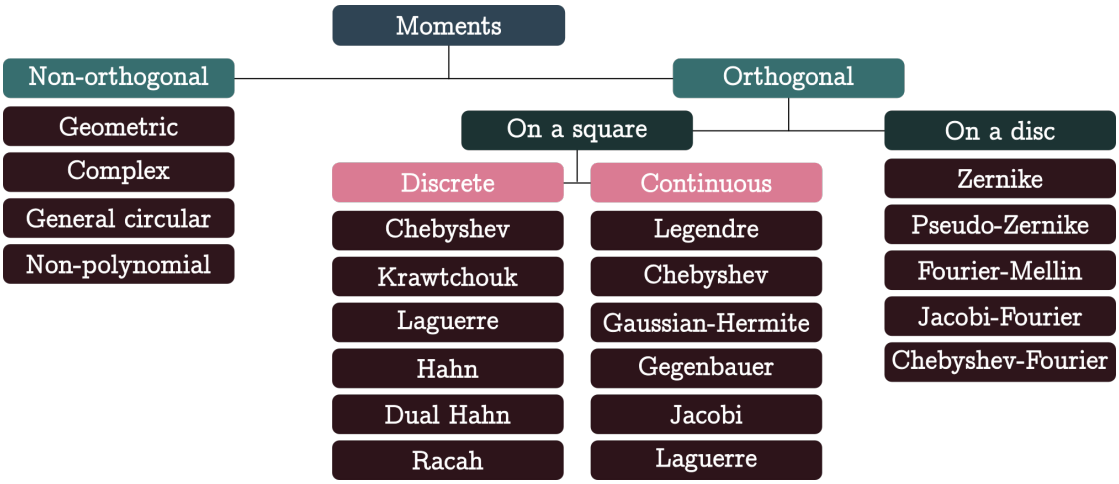

Figure 4: *Moment functions taxonomy.*

Definition 2. *Let* $\{\pi_{\mathbf{p}}(\mathbf{x})\}$ *be a* d*-variable polynomial basis of the space of image functions defined on* Ω *and let* $\mathbf{p} = (p_1, \ldots, p_d)$ *be a multi-index of non-negative integers which show the highest power of the respective variables in* $\pi_{\mathbf{p}}(\mathbf{x})$*. Then the* general moment $M_{\mathbf{p}}^{(f)}$ *of image* f *is defined as*

$$M_{\mathbf{p}}^{(f)} = \int_{\Omega} \pi_{\mathbf{p}}(\mathbf{x}) f(\mathbf{x}) \, \mathrm{d}\mathbf{x} \,. \tag{2}$$

The number $|\mathbf{p}| = \sum_{i=1}^{d} p_i$ *is called the* order *of the moment.*

It is advantageous sometimes to allow weight functions in the integrand. The most common choice of the basis is $\pi_{\mathbf{p}}(\mathbf{x}) = \mathbf{x}^{\mathbf{p}}$ which leads to geometric moments

$$m_{\mathbf{p}} = \int_{\mathbb{R}^d} \mathbf{x}^{\mathbf{p}} f(\mathbf{x}) \, \mathrm{d}\mathbf{x} \,. \tag{3}$$

Geometric moments (GM) are popular thanks to their formal simplicity. However, they suffer from several drawbacks – they transform in a complicated way during rotation,

the values are growing rapidly with the order, etc. The basis of GM is non-orthogonal and this property is inherited by the moments. Consequently, the monomials provide a highly correlated description which can result in the important descriptive information being contained within small differences between moments and the need for high computational precision. To overcome the shortcomings associated with GM, one should use moments constructed from orthogonal bases – *orthogonal (OG) moments* – whenever possible. Although they are theoretically equivalent, OG moments can be computed via recursions and they need lower computational precision to achieve the same accuracy as geometric and other non-orthogonal moments.

Moment invariants are functions of moments, they have the same properties as moments but unlike them allow us to distinguish among images from different classes without recovering f.

2 MODERN TRENDS IN INVARIANT THEORY

Image analysis is a fast-developing area of computer science and the same applies to the theory and applications of invariants. There are several directions of state-of-the-art research – some of them take advantage of the existing theory and try to improve, generalize or make it more convenient for practical applications, while the other explore new possibilities and push the current limits.

Invariants have a much longer history than image processing or even computers. The (algebraic) invariants can be traced back more than 100 years to David Hilbert who gave an introductory course in invariant theory at the University of Göttingen in 1897. Since then, the theory of algebraic invariants has been studied exhaustively, some of the references may be found in [18].

Moment invariants were first introduced in 1962 by Hu [19], who used the theory of algebraic invariants to derive his 7 famous moment invariants w.r.t. translation, scaling, and rotation of 2D objects. Thousands of articles and books have been published on moment invariants ever since. While in 2014 Papakostas reported in [20] that about 18 000 research papers relevant to moments and/or moment invariants in image analysis have appeared in SCOPUS, more than 12 000 new articles were published between years 2014 and 2019 (see Figure 5 for a detailed analysis). This demonstrates that even in the age of deep learning moment invariants are still attracting attention.

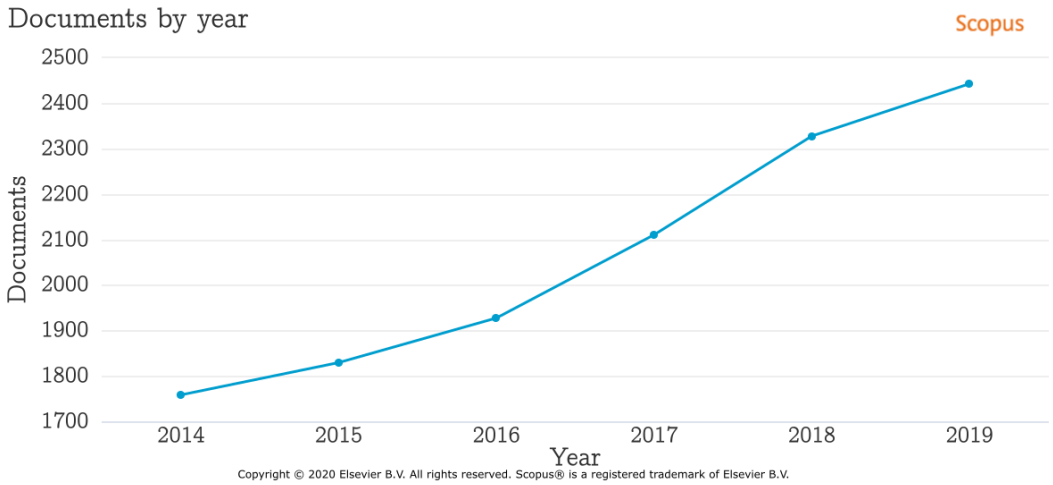

Figure 5: *The number of papers about moments and moment invariants published between the years 2014 and 2019 according to the SCOPUS database.*

The evolution of moment invariants in image analysis was summarized in five monographs. In 1998 Mukundan et al. [21] wrote a short introduction into this area. The book by Pawlak [17] deals with the numerical aspects of image moments. An overview of important theoretical results and their practical application in image analysis was given in 2009 by Flusser et al. [22]. On the occasion of the 50th anniversary of moment invariants, Papakostas published in 2014 the book [20] summarizing the latest development in this area. Each chapter was written by invited researchers specialized in the field of moments. The latest monograph published two years later by Flusser et al. [23] reviews the development after 2009, explores thoroughly both the theory and the practical usage of moment invariants. Currently, Papakostas is preparing a new monograph [24] summarizing the latest progress in the field of moments. We can also find specialized monographs, e.g. Rahman et al. [25] devoted to orthogonal moment-based features in a fingerprint, iris, face and expression recognition.

Moment invariants have become an important tool for shape description, because of their versatility. Moments can be applied to binary, grayscale, color, or multispectral images, defined in 2D, 3D, and higher-dimensional space. Currently, even moment invariants for vector and tensor fields are developed. They can deal with various degradations such as similarity and affine transformation of objects or image blurring (see Figure 6 for detailed classification). In what follows, we will briefly summarize the progress in the design of moment invariants.

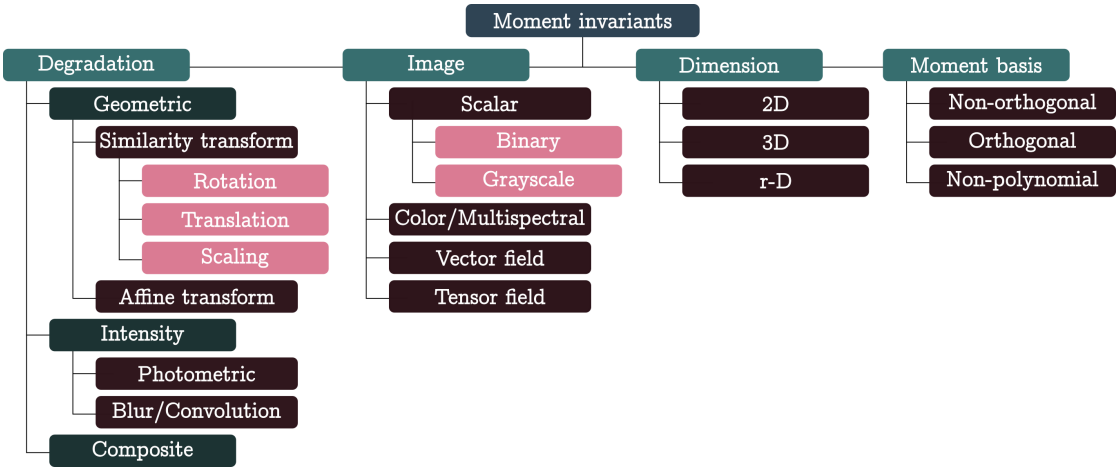

Figure 6: *Taxonomy of moment invariants.*

2.1 TOPICS OF CURRENT RESEARCH ON MOMENT INVARIANTS

Traditional topics that had been intensively studied from the 1970s to 2000s, namely the design of rotation and affine 2D moment invariants, were resolved successfully in the turn of the millennium. We can divide the current research in the area of moment

invariants into five principal categories – invariants for new types of data, invariants to specific degradations, local invariants, efficient computation of moments, and design of non-polynomial moments and invariants.

2.1.1 *Invariants for new types of data*

Since moments of grayscale images have been thoroughly studied for decades, it is only natural that other types of data are drawing attention.

The rapid development of 3D imaging technologies and scanning devices, such as Computer Tomography (CT), Magnetic Resonance Imaging (MRI), and Light Detection And Ranging (LiDAR) caused the need for methods for 3D data. Some of the algorithms are only modifications of the 2D versions but some of them need a completely different approach. The majority of the articles for 3D moment invariants deal with TRS transformation. We can find invariants constructed from geometric moments [26–29], 3D analogue of complex moments (using *spherical harmonics* in the basis functions) [30–34], or from various orthogonal moments [35–41]. The 3D affine transformation [27] is much less common degradation in practice and thus no extensive research was done in this area.

The 3D moment invariants found practical applications in numerous areas, e.g. testing handedness and gender from brain MRI snaps [42], 3D image registration [43, 44], prediction of rupture of intracranial saccular aneurysms [45], ATS drug identification [46, 47], semantic segmentation of outdoor areas recorded by LiDAR [48], liver segmentation of magnetic resonance images [49].

In the last decade, increasing attention has been paid to *vector field* (VF) images and the tools for their analysis. The images of vector fields arise in mechanical engineering, fluid dynamics, computer vision, meteorology, etc. They may be obtained as a result of computer processing of standard digital images or video, numerical solution of Navier–Stokes equation, or from real physical measurements.

The 2D vector field invariants were introduced by Schlemmer et al. [50] and later further investigated by Yang et al. [4] and Kostková et al. [3, 9]. The invariants of 3D vector fields were studied by Langbein and Hagen [51] and Bujack et al. [52, 53].

Color images can be viewed as a special case of vector fields or three gray-level images. The RGB channels should not be handled separately, because the geometric transform acting on the image is the same for all channels. This leads to the idea of joint invariants [54–56]. Many authors have used the quaternion formalism for the description of color images [57–64].

2.1.2 *Invariants to specific degradations*

When dealing with invariants one should always keep in mind, what degradations may occur. Considering broader invariance than necessary decreases the recognition

power of the features. In the last twenty years, a large amount of effort has been spent to study invariants to image blurring [65–68]. When analyzing blurred images the crucial problem is to identify the particular blurring kernel, to which should the invariance be achieved. The first papers on this subject focused on various symmetric kernels [69–71]. In this context, Gaussian blur invariants [1, 72, 73] play an important role among other blur invariants since they are the only ones that have actually used the parametric form of the point–spread function.

In practice, the degradations are often coupled, which leads to a need for construction of combined invariants. Unfortunately, the derivation of such features might be very complicated. In the literature, we can find combined invariants to, e.g. Gaussian blur and rotation [74], Gaussian blur and affine transformation [1], shape and color affine transformation [56], or circularly symmetric blur and similarity transformation [75].

2.1.3 *Local invariants*

Moment invariants are naturally global features, i.e. they are calculated from the whole image. On the one hand, they have many advantages, e.g. robustness to noise. On the other hand, a small change in the scene influences all the invariants. Hence, they are not suitable for applications, where the objects can be partially occluded, some part of the object is not visible, etc. The main purpose of the local invariants is to recognize objects, that are visible only partially.

Unlike the other moment families, Krawtchouk moments [76, 77] and dual Hahn moments [78] can extract local features from any region of interest in an image by varying the parameters of the polynomials. Some authors noticed that the localization property is preserved when constructing hybrid (or separable) moments, particularly as a combination of Chebyshev and Krawtchouk polynomials [79–82]. However, the choice of the parameters is a difficult task since the position of the object in the image is usually unknown.

Semi-local invariants combine the best of both global and local invariants and try to suppress their drawbacks. They divide the object into smaller parts and describe each part by some kind of global invariants [83, 84]. The main disadvantage of the semi-local invariants is the ambiguity in the choice of the part size.

2.1.4 *Efficient computation of moments*

Another remarkable trend in the theory of moments is the development of efficient algorithms providing high computational speed. One possible way to reduce the computational time is by reducing the number of pixels, where the polynomials are evaluated without loss of information. This includes the decomposition methods of binary images [85–95] and methods using boundary-based methods [96–110].

The method of intensity slicing [111] and bit slicing [112] transforms the problem of calculating gray-level moments to the previous task of calculating binary moments. The computational speed can be also improved at the expense of accuracy by using approximation methods, e.g. Chung et al. [113].

Another possibility to speed-up the algorithms is to use the specific properties of the particular polynomials. In the case of orthogonal polynomials, we can use the three-term recurrence relation or the symmetry of the polynomials. Such algorithms were applied to the polynomials orthogonal on a square [114–124] and the polynomials orthogonal on a disk [125–128].

2.1.5 *Non-polynomial moments and invariants*

Some authors allow basis functions which are non-polynomial in the Definition 2 of the moments.

Increasing attention has been paid to so-called fractional-order moments, e.g. fractional Fourier–Mellin [129], Chebyshev [130], Charlier [131], Jacobi–Fourier [132], Legendre–Fourier [133], or discrete Chebyshev moments [134]. Fractional-order moments were reported to be superior to classical moments in terms of accuracy, stability, noise resistance, invariance to similarity transformations, recognition rates, and computational times [133].

In some papers, the polynomial basis was entirely replaced by another, where the basis functions are products of a polynomial and some other function. We can find papers on wavelet moments [135–139], radial harmonic Fourier moments [59, 140–142], log-polar Exponent-Fourier moments [143], Radon odd radial harmonic Fourier moments [144], Bessel–Fourier moments [145, 146], moments based on polar harmonic transformation [147–150] and binary step-wise radial function [151].

Furthermore, Hosny et al. [152] proposed a new class of fractional-order radial harmonic Fourier moments, which combine both fractional-order polynomials with other basis function.

3 GOALS AND CONTRIBUTION

After a thorough exploration of the state-of-the-art invariant image analysis, we identified two areas of interest with a high potential – moment invariants to a total transformation of vector fields and moment invariants of scalar images to intensity degradations.

3.1 GOALS OF THE THESIS

- Invariants for vector fields – designing invariants to total transformation (rotation and affine transformation) and creating stable algorithms for analysis of vector field data.
- Invariants to convolution with Gaussian function – considering unconstrained Gaussian kernel, examining the possibility of construction of combined invariants.

3.2 CONTRIBUTION OF THE THESIS

The thesis consists of four papers attached in Part ii covering two areas.

1. Vector field analysis
   - B. Yang, J. Kostková, J. Flusser, T. Suk, and R. Bujack, "Rotation invariants of vector fields from orthogonal moments," *Pattern Recognition*, vol. 74, pp. 110–121, 2018

     We proposed a stable algorithm for the computation of invariants w.r.t. total rotation of the vector field from orthogonal moments.
   - J. Kostková, T. Suk, and J. Flusser, "Affine invariants of vector fields," *IEEE Transactions on Pattern Analysis and Machine Intelligence*, 2019. DOI: 10.1109/TPAMI.2019.2951664

     We introduced invariants w.r.t. a total affine transformation based on the moments of the vector field.
2. Scalar image analysis
   - J. Kostková, J. Flusser, M. Lébl, and M. Pedone, "Handling Gaussian blur without deconvolution," *Pattern Recognition*, vol. 103, 2020, art. no. 107264

New invariants w.r.t. arbitrary oriented and elongated Gaussian blur were presented together with the substitution theorem for the construction of combined invariants to blur and affine transform.

- J. Kostková and J. Flusser, "Robust multivariate density estimation under Gaussian noise," *Multidimensional Systems and Signal Processing*, vol. 31, pp. 1113–1143, 2020

  We introduced a novel approach to the description of a multidimensional image histogram insensitive with respect to additive Gaussian noise in the image.

4 THE THESIS IN BRIEF

4.1 DESIGNING INVARIANTS FOR VECTOR FIELDS

Vector fields are a special kind of multidimensional data that appears in many engineering areas. The increasing amount of data goes hand in hand with the increasing need for automatic processing of the data. In some aspects, they are similar to color images, but there are some substantial differences. Consequently, the methods for image analysis cannot be used directly but the traditional methods must be either further generalized or entirely new methods must be developed.

A 2D vector field $\mathbf{f}$ can be viewed as a pair of scalar images $\mathbf{f}(\mathbf{x}) = (f_1(\mathbf{x}), f_2(\mathbf{x}))^{\mathrm{T}}$. At each point $\mathbf{x} = (x, y)$, the value of $\mathbf{f}(\mathbf{x})$ shows the magnitude and the orientation of a certain vector.

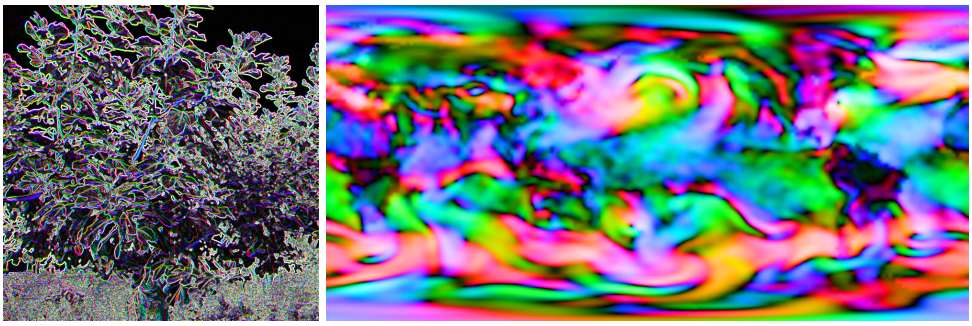

Figure 7: *Color coded vector fields: gradient VF (left) and wind velocity map (right).*

The most significant difference between vector fields and digital images is the behavior under geometric transformation. Unlike images, transformations of vector fields may act not only on the spatial coordinates but also on the field values. We have to distinguish four kinds of transformation.

- *Inner rotation* acts only on spatial coordinates.
- *Outer rotation* acts only on vector values and does not affect spatial coordinates.
- *Total rotation* is a combination of an inner and outer transformation of the same transformation matrices.
- *Independent total rotation* is the most general rotation. It acts on both spatial coordinates and vector values but the transformation matrices may differ.

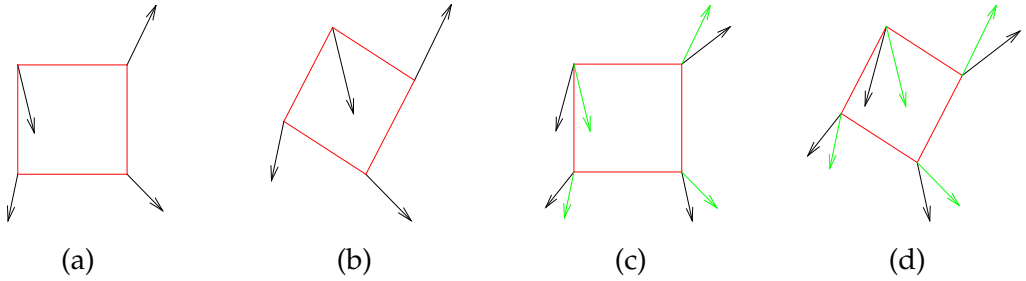

Figure 8: *Vector field transformations: (a) the original vector field, (b) its inner affine transformation, (c) its outer affine transformation, (d) its total affine transformation. The green arrows in (c) and (d) show the vector field without the outer transformation.*

In practice, the most common is the total transformation of the field, i.e. if the field is transformed in the spatial domain, the vector values are transformed by the same transformation.

To detect singularities such as sinks, vortices, saddle points, or arbitrary patterns of interest special methods for vector fields must be developed. The problem of invariants w.r.t. total rotation was first studied by Schlemmer et al. [50] who introduced *flow vector moment invariants*. Schlemmer proposed to treat 2D vector field (VF) as a field of complex numbers $\mathbf{f}(x,y) = f_1(x,y) + if_2(x,y)$ and use the standard definition of complex moments. As complex moments change only their phase under total rotation, the invariance can be reached through phase cancellation by multiplication of proper moments. To overcome the numerical problems of complex moments Yang et al. [4] introduced invariants w.r.t. total rotation constructed from orthogonal moments – Gaussian–Hermite and Zernike moments.

In practice, vector field transformation is often more general than rotation. An acceptable compromise between simplicity and generality is provided by *affine transform*. A generalization of the graph method for scalar images [153, 154] can be used for the derivation of the affine moment invariants of 2D vector fields (VFAMIs). The construction of VFAMIs was first published in the papers by Kostková et al. in [3, 9].

4.2 DESIGNING INVARIANTS TO IMAGE BLURRING

Another relevant problem in image processing are uniform changes in image intensity function. The most important class of intensity degradations is image blurring. Blurring can be caused by numerous factors such as out-of-focus and motion of the imaging device or due to acquiring image through some turbulent medium.

Assuming that the imaging system is linear and space invariant, blurring can be described by a convolution of the original image f with a point-spread function (PSF). The degradation model (1) has the form

$$g(x,y) = (f * h)(x,y)\,, \tag{4}$$

Figure 9: *Examples of space variant out-of-focus blur, motion blur and Gaussian blur.*

where * denotes a 2D convolution, and h is the PSF of the system.

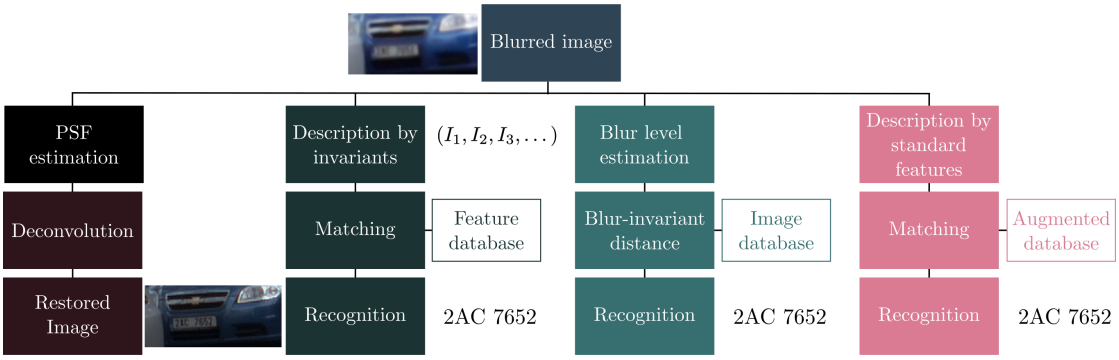

Figure 10: *Four approaches to the analysis of blurred images. Image restoration via deconvolution (first branch), description and recognition by blur invariants (second branch), matching by minimum blur-invariant distance (third branch), and brute-force searching an augmented database (last branch).*

There are several ways of dealing with blurred images (see Figure 10 for an overview). They may or may not be convenient depending on the task we are solving. The invariant description of blurred images is very advantageous and effective if we do not need to reconstruct the original image but for example, only localize some objects in it. We need to find the description of the image g independent of the particular realization of the PSF h which is usually unknown. In other words, we are searching for the functional I fulfilling $I(f) = I(f * h)$ for any admissible PSF h.

The invariants cannot be constructed for arbitrary PSF. The necessary (but not sufficient) condition is the closure to composition – convolution is the operator of the intra-class variation which must be closed. It holds that the more specific the class of the PSFs is, the higher the recognition power of the invariants. For example, all centrosymmetric objects are indistinguishable by invariants to centrosymmetric blur, invariants to circularly symmetric blur are not able to discriminate the circularly symmetric objects, etc.

Blur invariants were first introduced in the '90s in the series of papers by Flusser et al. [65, 155, 156]. They assumed the PSFs with *central symmetry*, $h(x, y) = h(-x, -y)$,

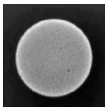

Circular symmetric blur.

Motion blur.

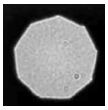

9-FRS blur.

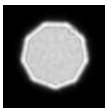

9-fold dihedral blur.

and the majority of the articles published so far adopted this assumption in their studies [66, 67, 70, 71]. Invariants to convolution with PSFs with *circular symmetry*, i.e. $h(x, y) = h(r)$, from complex moments were proposed in [69]. Other authors expressed them later equivalently employing orthogonal moments – Zernike moments [74, 75, 157], pseudo–Zernike moments [158], Chebyshev moments [159], and Fourier–Mellin moments [160]. Invariants to *linear motion blur* or more precisely *symmetric directional blur* were presented in the papers [161, 162]. A substantial generalization of previous work was made by introducing *N-fold rotation symmetric (N-FRS) blur* moment invariants [68] and later further generalized to *N-fold dihedral blur* in [163].

All the above-mentioned invariants can be described by a unified theory regardless of the particular PSF class. The mathematical approach is based on the theory of projection operators. The construction of blur invariants is described by the *Fundamental Theorem of blur invariants* [23] which is a very strong theorem. However, its applicability depends on our ability to construct a subspace of all admissible PSFs and a projector onto this subspace.

The theory can be used with slight modification for the derivation of invariants to *Gaussian blur*. These are the only invariants that use the parametric form of the PSF rather than some of its specific properties. A complete set of moment invariants w.r.t. Gaussian blur was introduced by Flusser et al. in [72, 73] but it was limited to PSFs with diagonal covariance matrices. Most recently, Kostková et al. [1] generalized the theory for Gaussians with general covariance matrices – the blur kernel may be arbitrary oriented, scaled, and elongated (see Figure 11 for examples). The main contribution of this generalization is that it enables to construct the combined invariants to both blur and affine transform.

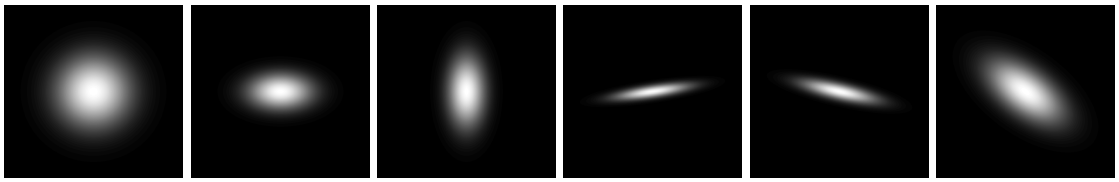

Figure 11: *Gaussian blur with diagonal (1–3) and general (4–6) covariance matrices.*

The theory of moment invariants to Gaussian blur was adjusted by Höschl et al. [164] for a noise-robust PDF estimation, which was motivated by histogram-based image retrieval. Their invariants were based on moments of a histogram of the noisy gray-level image. The extension of the theory for histograms of color images was proposed by Kostková et al. in [2].

BIBLIOGRAPHY

[1] J. Kostková, J. Flusser, M. Lébl, and M. Pedone, "Handling Gaussian blur without deconvolution," *Pattern Recognition*, vol. 103, 2020, art. no. 107264.

[2] J. Kostková and J. Flusser, "Robust multivariate density estimation under Gaussian noise," *Multidimensional Systems and Signal Processing*, vol. 31, pp. 1113–1143, 2020.

[3] J. Kostková, T. Suk, and J. Flusser, "Affine invariants of vector fields," *IEEE Transactions on Pattern Analysis and Machine Intelligence*, 2019. DOI: 10.1109/TPAMI.2019.2951664.

[4] B. Yang, J. Kostková, J. Flusser, T. Suk, and R. Bujack, "Rotation invariants of vector fields from orthogonal moments," *Pattern Recognition*, vol. 74, pp. 110–121, 2018.

[5] B. Yang, J. Kostková, J. Flusser, and T. Suk, "Scale invariants from Gaussian–Hermite moments," *Signal Processing*, vol. 132, pp. 77–84, 2017.

[6] J. Kostková and J. Flusser, "On the null-space of the shape-color moment invariants," in *International Conference on Computer Analysis of Images and Patterns CAIP'19*, Springer, vol. LNCS 11678, 2019, pp. 402–408.

[7] J. Kostková and J. Flusser, "Robust histogram estimation under Gaussian noise," in *International Conference on Computer Analysis of Images and Patterns CAIP'19*, Springer, vol. LNCS 11678, 2019, pp. 421–432.

[8] J. Kostková, J. Flusser, M. Lébl, and M. Pedone, "Image invariants to anisotropic Gaussian blur," in *Scandinavian Conference on Image Analysis SCIA'19*, Springer, vol. LNCS 11482, 2019, pp. 140–151.

[9] J. Kostková, T. Suk, and J. Flusser, "Affine moment invariants of vector fields," in *2018 25th IEEE International Conference on Image Processing (ICIP)*, IEEE, 2018, pp. 1338–1342.

[10] B. Yang, J. Kostková, T. Suk, J. Flusser, and R. Bujack, "Recognition of patterns in vector fields by Gaussian–Hermite invariants," in *International Conference on Image Processing ICIP'17*, J. Luo, W. Zeng, and Y.-J. Zhang, Eds., Beijing, China: IEEE, 2017, pp. 2350–2363.

[11] K. G. Derpanis, "Overview of the RANSAC algorithm," *Image Rochester NY*, vol. 4, no. 1, pp. 2–3, 2010.

[12] P. Druzhkov and V. Kustikova, "A survey of deep learning methods and software tools for image classification and object detection," *Pattern Recognition and Image Analysis*, vol. 26, no. 1, pp. 9–15, 2016.

[13] M. Šonka, V. Hlaváč, and R. Boyle, *Image Processing, Analysis and Machine Vision*, 3rd. Toronto, Canada: Thomson, 2007.

[14] Y.-H. Wang, "Tutorial: image segmentation," *National Taiwan University, Taipei*, pp. 1–36, 2010.

[15] R. O. Duda, P. E. Hart, and D. G. Stork, *Pattern Classification*, 2nd. New York, USA: Wiley Interscience, 2001.

[16] S. Theodoridis and K. Koutroumbas, *Pattern Recognition*, 4th. Academic Press, 2009.

[17] M. Pawlak, *Image Analysis by Moments: Reconstruction and Computational Aspects*. Wrocław, Poland: Oficyna Wydawnicza Politechniki Wrocławskiej, 2006.

[18] D. Hilbert, *Theory of Algebraic Invariants*. Cambridge, U.K.: Cambridge University Press, 1993.

[19] M.-K. Hu, "Visual pattern recognition by moment invariants," *IRE Transactions on Information Theory*, vol. 8, no. 2, pp. 179–187, 1962.

[20] G. A. Papakostas, Ed., *Moments and Moment Invariants: Theory and Applications*, ser. Gate to Computer Science and Research. Xanthi, Greece: Science Gate Publishing, 2014, vol. 1.

[21] R. Mukundan and K. R. Ramakrishnan, *Moment Functions in Image Analysis*. Singapore: World Scientific, 1998.

[22] J. Flusser, T. Suk, and B. Zitová, *Moments and Moment Invariants in Pattern Recognition*. Chichester, U.K.: Wiley, 2009.

[23] J. Flusser, T. Suk, and B. Zitová, *2D and 3D Image Analysis by Moments*. Chichester, U.K.: Wiley, 2016.

[24] G. A. Papakostas, Ed., *Recent Progress in Moments and Moment Invariants*, ser. Gate to Computer Science and Research. Xanthi, Greece: Science Gate Publishing, to appear in November 2020.

[25] S. M. Rahman, T. Howlader, and D. Hatzinakos, *Orthogonal Image Moments for Human-Centric Visual Pattern Recognition*. Springer, 2019.

[26] D. Cyganski and J. A. Orr, "Object recognition and orientation determination by tensor methods," in *Advances in Computer Vision and Image Processing*, T. S. Huang, Ed., Greenwich, Connecticut, USA: JAI Press, 1988, pp. 101–144.

[27] D. Xu and H. Li, "3-D affine moment invariants generated by geometric primitives," in *Proceedings of the 18th International Conference on Pattern Recognition ICPR'06*, Hong Kong: IEEE Computer Society, 2006, pp. 544–547.

[28] D. Xu and H. Li, "Geometric moment invariants," *Pattern Recognition*, vol. 41, no. 1, pp. 240–249, 2008.

[29] T. Suk and J. Flusser, "Tensor method for constructing 3D moment invariants," in *Computer Analysis of Images and Patterns CAIP'11*, P. Real, D. Diaz-Pernil, H. Molina-Abril, A. Berciano, and W. Kropatsch, Eds., ser. Lecture Notes in Computer Science, vol. 6854–6855, Seville, Spain: Springer, Aug. 2011, pp. 212–219.

[30] C.-H. Lo and H.-S. Don, "3-D moment forms: Their construction and application to object identification and positioning," *IEEE Transactions on Pattern Analysis and Machine Intelligence*, vol. 11, no. 10, pp. 1053–1064, 1989.

[31] J. Flusser, J. Boldyš, and B. Zitová, "Moment forms invariant to rotation and blur in arbitrary number of dimensions," *IEEE Transactions on Pattern Analysis and Machine Intelligence*, vol. 25, no. 2, pp. 234–246, 2003.

[32] J. M. Galvez and M. Canton, "Normalization and shape recognition of three-dimensional objects by 3D moments," *Pattern Recognition*, vol. 26, no. 5, pp. 667–681, 1993.

[33] T. Suk, J. Flusser, and J. Boldyš, "3D rotation invariants by complex moments," *Pattern Recognition*, vol. 48, no. 11, pp. 3516–3526, 2015.

[34] T. Suk and J. Flusser, "Recognition of symmetric 3D bodies," *Symmetry*, vol. 6, no. 3, pp. 722–757, 2014.

[35] N. Canterakis, "3D Zernike moments and Zernike affine invariants for 3D image analysis and recognition," in *Proceedings of the 11th Scandinavian Conference on Image Analysis SCIA'99*, B. K. Ersbøll and P. Johansen, Eds., Kangerlussuaq, Greenland: DSAGM, 1999.

[36] B. Yang, J. Flusser, and T. Suk, "3D rotation invariants of Gaussian–Hermite moments," *Pattern Recognition Letters*, vol. 54, no. 1, pp. 18–26, 2015.

[37] M. El Mallahi, A. Zouhri, A. El Affar, A. Tahiri, and H. Qjidaa, "Radial Hahn moment invariants for 2D and 3D image recognition," *International Journal of Automation and Computing*, vol. 15, no. 3, pp. 277–289, 2018.

[38] R. Benouini, I. Batioua, K. Zenkouar, S. Najah, and H. Qjidaa, "Efficient 3D object classification by using direct Krawtchouk moment invariants," *Multimedia Tools and Applications*, vol. 77, no. 20, pp. 27 517–27 542, 2018.

[39] I. Batioua, R. Benouini, K. Zenkouar, A. Zahi, and H. El Fadili, "3D image analysis by separable discrete orthogonal moments based on Krawtchouk and Tchebichef polynomials," *Pattern Recognition*, vol. 71, pp. 264–277, 2017.

[40] M. El Mallahi, A. Zouhri, and H. Qjidaa, "Radial Meixner moment invariants for 2D and 3D image recognition," *Pattern Recognition and Image Analysis*, vol. 28, no. 2, pp. 207–216, 2018.

[41] M. El Mallahi, A. Zouhri, A. Mesbah, A. Berrahou, I. El Affar, and H. Qjidaa, "Radial invariant of 2D and 3D Racah moments," *Multimedia Tools and Applications*, vol. 77, no. 6, pp. 6583–6604, 2018.

[42] J.-F. Mangin, F. Poupon, E. Duchesnay, D. Rivière, A. Cachia, D. L. Collins, A. C. Evans, and J. Régis, "Brain morphometry using 3D moment invariants," *Medical Image Analysis*, vol. 8, no. 3, pp. 187–196, 2004.

[43] M. Kazhdan, "An approximate and efficient method for optimal rotation alignment of 3D models," *IEEE Transactions on Pattern Analysis and Machine Intelligence*, vol. 29, no. 7, pp. 1221–1229, 2007.

[44] M. Trummer, H. Suesse, and J. Denzler, "Coarse registration of 3D surface triangulations based on moment invariants with applications to object alignment and identification," in *Proceedings of the 12th International Conference on Computer Vision, ICCV'09*, Washington, DC, USA: IEEE, 2009, pp. 1273–1279.

[45] R. D. Millán, M. Hernandez, D. Gallardo, J. R. Cebral, C. Putman, L. Dempere-Marco, and A. F. Frangi, "Characterization of cerebral aneurysms using 3D moment invariants," in *Proceedings of the conference SPIE Medical Imaging 2005: Image Processing*, vol. 5747, 2005, pp. 743–754.

[46] S. F. Pratama, A. K. Muda, Y.-H. Choo, and A. Abraham, "Exact computation of 3D geometric moment invariants for ATS drugs identification," in *Innovations in Bio-Inspired Computing and Applications*, Springer, 2016, pp. 347–358.

[47] S. F. Pratama, A. K. Muda, Y.-H. Choo, J. Flusser, and A. Abraham, "ATS drugs molecular structure representation using refined 3D geometric moment invariants," *Journal of Mathematical Chemistry*, vol. 55, no. 10, pp. 1951–1963, 2017.

[48] S. Sickert and J. Denzler, "Semantic segmentation of outdoor areas using 3D moment invariants and contextual cues," in *German Conference on Pattern Recognition*, Springer, 2017, pp. 165–176.

[49] A. Abdalbari, J. Ren, and M. Green, "Seeds classification for image segmentation based on 3-D affine moment invariants," *Biomedical Engineering Letters*, vol. 6, no. 4, pp. 224–233, 2016.

[50] M. Schlemmer, M. Heringer, F. Morr, I. Hotz, M.-H. Bertram, C. Garth, W. Kollmann, B. Hamann, and H. Hagen, "Moment invariants for the analysis of 2D flow fields," *IEEE Transactions on Visualization and Computer Graphics*, vol. 13, no. 6, pp. 1743–1750, 2007.

[51] M. Langbein and H. Hagen, "A generalization of moment invariants on 2D vector fields to tensor fields of arbitrary order and dimension," in *Proceedings of 5th International Symposium Advances in Visual Computing, ISVC'09, Part II*, ser. Lecture Notes in Computer Science, vol. 5876, Las Vegas, Nevada, USA: Springer, 2009, pp. 1151–1160.

[52] R. Bujack, "Orientation invariant pattern detection in vector fields with Clifford algebra and moment invariants," PhD thesis, Fakultät für Mathematik und Informatik, Universität Leipzig, Leipzig, Germany, 2014.

[53] R. Bujack, J. Kasten, I. Hotz, G. Scheuermann, and E. Hitzer, "Moment invariants for 3D flow fields via normalization," in *Pacific Visualization Symposium, PacificVis'15*, Hangzhou, China: IEEE, 2015, pp. 9–16.

[54] B. Yang, T. Suk, J. Flusser, Z. Shi, and X. Chen, "Rotation invariants from Gaussian–Hermite moments of color images," *Signal Processing*, vol. 143, pp. 282–291, 2018.

[55] T. Suk and J. Flusser, "Affine moment invariants of color images," in *Computer Analysis of Images and Patterns CAIP'09*, X. Jiang and N. Petkov, Eds., vol. LNCS 5702, Münster, Germany: Springer, Sep. 2009, pp. 334–341.

[56] M. Gong, Y. Hao, H. Mo, and H. Li, "Naturally combined shape-color moment invariants under affine transformations," *Computer Vision and Image Understanding*, vol. 162, pp. 46–56, 2017.

[57] B. Chen, H. Shu, H. Zhang, G. Chen, C. Toumoulin, J. Dillenseger, and L. Luo, "Quaternion Zernike moments and their invariants for color image analysis and object recognition," *Signal Processing*, vol. 92, no. 2, pp. 308–318, 2012.

[58] L.-Q. Guo and M. Zhu, "Quaternion Fourier–Mellin moments for color images," *Pattern Recognition*, vol. 44, no. 2, pp. 187–195, 2011.

[59] X.-Y. Wang, W.-Y. Li, H.-Y. Yang, P.-P. Niu, and Y.-W. Li, "Invariant quaternion radial harmonic Fourier moments for color image retrieval," *Optics & Laser Technology*, vol. 66, pp. 78–88, 2015.

[60] L. Guo, M. Dai, and M. Zhu, "Quaternion moment and its invariants for color object classification," *Information Sciences*, vol. 273, pp. 132–143, Jul. 2014.

[61] K. M. Hosny and M. M. Darwish, "New set of quaternion moments for color images representation and recognition," *Journal of Mathematical Imaging and Vision*, vol. 60, no. 5, pp. 717–736, 2018.

[62] K. M. Hosny and M. M. Darwish, "Invariant color images representation using accurate quaternion Legendre–Fourier moments," *Pattern Analysis and Applications*, vol. 22, no. 3, pp. 1105–1122, 2019.

[63] C. Singh and J. Singh, "Multi-channel versus quaternion orthogonal rotation invariant moments for color image representation," *Digital Signal Processing*, vol. 78, pp. 376–392, 2018.

[64] I. Elouariachi, R. Benouini, K. Zenkouar, and A. Zarghili, "Robust hand gesture recognition system based on a new set of quaternion Tchebichef moment invariants," *Pattern Analysis and Applications*, 2020. DOI: 10.1007/s10044-020-00866-9.

[65] J. Flusser and T. Suk, "Degraded image analysis: an invariant approach," *IEEE Transactions on Pattern Analysis and Machine Intelligence*, vol. 20, no. 6, pp. 590–603, 1998.

[66] H. Zhang, H. Shu, G.-N. Han, G. Coatrieux, L. Luo, and J. L. Coatrieux, "Blurred image recognition by Legendre moment invariants," *IEEE Transactions on Image Processing*, vol. 19, no. 3, pp. 596–611, 2010.

[67] C.-Y. Wee and R. Paramesran, "Derivation of blur-invariant features using orthogonal Legendre moments," *IET Computer Vision*, vol. 1, no. 2, pp. 66–77, 2007.

[68] J. Flusser, T. Suk, J. Boldyš, and B. Zitová, "Projection operators and moment invariants to image blurring," *IEEE Transactions on Pattern Analysis and Machine Intelligence*, vol. 37, no. 4, pp. 786–802, 2015.

[69] J. Flusser and B. Zitová, "Invariants to convolution with circularly symmetric PSF," in *Proceedings of the 17th International Conference on Pattern Recognition ICPR'04*, Cambridge, U.K.: IEEE Computer Society, 2004, pp. 11–14.

[70] X. Dai, H. Zhang, H. Shu, and L. Luo, "Image recognition by combined invariants of Legendre moment," in *Proceedings of the IEEE International Conference on Information and Automation ICIA'10*, Harbin, China, Jun. 2010, pp. 1793–1798.

[71] J. Kautsky and J. Flusser, "Blur invariants constructed from arbitrary moments," *IEEE Transactions on Image Processing*, vol. 20, no. 12, pp. 3606–3611, 2011.

[72] J. Flusser, T. Suk, S. Farokhi, and C. Höschl IV, "Recognition of images degraded by Gaussian blur," in *Computer Analysis of Images and Patterns CAIP'15*, G. Azzopardi and N. Petkov, Eds., ser. Lecture Notes in Computer Science, vol. 9256–9257, Valletta, Malta: Springer, 2015, 88–99, part I.

[73] J. Flusser, S. Farokhi, C. Höschl IV, T. Suk, B. Zitová, and M. Pedone, "Recognition of images degraded by Gaussian blur," *IEEE Transactions on Image Processing*, vol. 25, no. 2, pp. 790–806, 2016.

[74] H. Zhu, M. Liu, H. Ji, and Y. Li, "Combined invariants to blur and rotation using Zernike moment descriptors," *Pattern Analysis and Applications*, vol. 13, no. 3, pp. 309–319, 2010.

[75] B. Chen, H. Shu, H. Zhang, G. Coatrieux, L. Luo, and J. L. Coatrieux, "Combined invariants to similarity transformation and to blur using orthogonal Zernike moments," *IEEE Transactions on Image Processing*, vol. 20, no. 2, pp. 345–360, 2011.

[76] P.-T. Yap, R. Paramesran, and S.-H. Ong, "Image analysis by Krawtchouk moments," *IEEE Transactions on Image Processing*, vol. 12, no. 11, pp. 1367–1377, 2003.

[77] A. Sit and D. Kihara, "Comparison of image patches using local moment invariants," *IEEE Transactions on Image Processing*, vol. 23, no. 5, pp. 2369–2379, 2014.

[78] E. G. Karakasis, G. Papakostas, D. E. Koulouriotis, and V. Tourassis, "Generalized dual Hahn moment invariants," *Pattern Recognition*, vol. 46, no. 7, pp. 1998–2014, 2013.

[79] W. A. Jassim, P. Raveendran, and R. Mukundan, "New orthogonal polynomials for speech signal and image processing," *IET Signal Processing*, vol. 6, no. 8, pp. 713–723, 2012.

[80] B. M. Mahmmod, A. R. bin Ramli, S. H. Abdulhussain, S. A. R. Al-Haddad, and W. A. Jassim, "Signal compression and enhancement using a new orthogonal-polynomial-based discrete transform," *IET Signal Processing*, vol. 12, no. 1, pp. 129–142, 2017.

[81] S. H. Abdulhussain, A. R. Ramli, B. M. Mahmmod, M. I. Saripan, S. Al-Haddad, and W. A. Jassim, "A new hybrid form of Krawtchouk and Tchebichef polynomials: Design and application," *Journal of Mathematical Imaging and Vision*, vol. 61, no. 4, pp. 555–570, 2019.

[82] Z. N. Idan, S. H. Abdulhussain, and S. A. R. Al-Haddad, "A new separable moments based on Tchebichef–Krawtchouk polynomials," *IEEE Access*, vol. 8, pp. 41 013–41 025, 2020.

[83] E. Sariyanidi, V. Dagli, S. C. Tek, B. Tunc, and M. Gokmen, "Local Zernike moments: A new representation for face recognition," in *19th IEEE International Conference on Image Processing ICIP'12*, Orlando, FL, USA: IEEE, 2012, pp. 585–588.

[84] P. Patil and K Vasanth, "Iris recognition using local and global iris image moment features," in *2019 Innovations in Power and Advanced Computing Technologies (i-PACT)*, IEEE, vol. 1, 2019, pp. 1–5.

[85] M. F. Zakaria, L. J. Vroomen, P. Zsombor-Murray, and J. M. van Kessel, "Fast algorithm for the computation of moment invariants," *Pattern Recognition*, vol. 20, no. 6, pp. 639–643, 1987.

[86] M. Dai, P. Baylou, and M. Najim, "An efficient algorithm for computation of shape moments from run-length codes or chain codes," *Pattern Recognition*, vol. 25, no. 10, pp. 1119–1128, 1992.

[87] B. C. Li, "A new computation of geometric moments," *Pattern Recognition*, vol. 26, no. 1, pp. 109–113, 1993.

[88] I. M. Spiliotis and B. G. Mertzios, "Real-time computation of two-dimensional moments on binary images using image block representation," *IEEE Transactions on Image Processing*, vol. 7, no. 11, pp. 1609–1615, 1998.

[89] J. Flusser, "Refined moment calculation using image block representation," *IEEE Transactions on Image Processing*, vol. 9, no. 11, pp. 1977–1978, 2000.

[90] E. Kawaguchi and T. Endo, "On a method of binary-picture representation and its application to data compression," *IEEE Transactions on Pattern Analysis and Machine Intelligence*, vol. 2, no. 1, pp. 27–35, 1980.

[91] C.-H. Wu, S.-J. Horng, and P.-Z. Lee, "A new computation of shape moments via quadtree decomposition," *Pattern Recognition*, vol. 34, no. 7, pp. 1319–1330, 2001.

[92] J. H. Sossa-Azuela, C. Yáñez-Márquez, and J. L. Díaz de León Santiago, "Computing geometric moments using morphological erosions," *Pattern Recognition*, vol. 34, no. 2, pp. 271–276, 2001.

[93] T. Suk and J. Flusser, "Refined morphological methods of moment computation," in *20th International Conference on Pattern Recognition ICPR'10*, Istanbul, Turkey: IEEE Computer Society, Aug. 2010, pp. 966–970.

[94] T. Suk, C. Höschl IV, and J. Flusser, "Decomposition of binary images – A survey and comparison," *Pattern Recognition*, vol. 45, no. 12, pp. 4279–4291, 2012.

[95] C. Höschl IV and J. Flusser, "Decomposition of 3D binary objects into rectangular blocks," in *2016 International Conference on Digital Image Computing: Techniques and Applications (DICTA)*, IEEE, 2016, pp. 1–8.

[96] B.-C. Li and J. Shen, "Fast computation of moment invariants," *Pattern Recognition*, vol. 24, no. 8, pp. 807–813, 1991.

[97] X. Y. Jiang and H. Bunke, "Simple and fast computation of moments," *Pattern Recognition*, vol. 24, no. 8, pp. 801–806, 1991.

[98] W. Philips, "A new fast algorithm for moment computation," *Pattern Recognition*, vol. 26, no. 11, pp. 1619–1621, 1993.

[99] L. Yang and F. Albregtsen, "Fast and exact computation of Cartesian geometric moments using discrete Green's theorem," *Pattern Recognition*, vol. 29, no. 11, pp. 1061–1073, 1996.

[100] J. H. Sossa-Azuela, I. Mazaira, and J. I. Zannatha, "An extension to Philip's algorithm for moment calculation," *Computación y Sistemas*, vol. 3, no. 1, pp. 5–16, 1999.

[101] J. Flusser, "Fast calculation of geometric moments of binary images," in *Proceedings of the 22nd Workshop on Pattern Recognition and Medical Computer Vision OAGM'98*, Illmitz, Austria: ÖCG, 1998, pp. 265–274.

[102] R. Mukundan and K. R. Ramakrishnan, "Fast computation of Legendre and Zernike moments," *Pattern Recognition*, vol. 28, no. 9, pp. 1433–1442, 1995.

[103] J. G. Leu, "Computing a shape's moments from its boundary," *Pattern Recognition*, vol. 24, no. 10, pp. 949–957, 1991.

[104] M. H. Singer, "A general approach to moment calculation for polygons and line segments," *Pattern Recognition*, vol. 26, no. 7, pp. 1019–1028, 1993.

[105] J. Flusser, "Effective boundary-based calculation of object moments," in *Proceedings of the International Conference on Image and Vision Computing '98 New Zealand IVCNZ '98*, Auckland, New Zealand: The University of Auckland, 1998, pp. 369–374.

[106] L. Yang, F. Albregtsen, and T. Taxt, "Fast computation of three-dimensional geometric moments using a discrete divergence theorem and a generalization to higher dimensions," *Graphical Models and Image Processing*, vol. 59, no. 2, pp. 97–108, 1997.

[107] B. C. Li and S. D. Ma, "Efficient computation of 3D moments," in *Proceedings of the 12th International Conference on Pattern Recognition ICPR'94*, vol. I, Jerusalem, Israel: IEEE Computer Society, 1994, pp. 22–26.

[108] S. A. Sheynin and A. V. Tuzikov, "Explicit formulae for polyhedra moments," *Pattern Recognition Letters*, vol. 22, no. 10, pp. 1103–1109, 2001.

[109] B. C. Li, "The moment calculation of polyhedra," *Pattern Recognition*, vol. 26, no. 8, pp. 1229–1233, 1993.

[110] A. G. Mamistvalov, "*n*-dimensional moment invariants and conceptual mathematical theory of recognition *n*-dimensional solids," *IEEE Transactions on Pattern Analysis and Machine Intelligence*, vol. 20, no. 8, pp. 819–831, 1998.

[111] G. A. Papakostas, E. G. Karakasis, and D. E. Koulouriotis, "Efficient and accurate computation of geometric moments on gray-scale images," *Pattern Recognition*, vol. 41, no. 6, pp. 1895–1904, 2008.

[112] I. M. Spiliotis and Y. S. Boutalis, "Parameterized real-time moment computation on gray images using block techniques," *Journal of Real-Time Image Processing*, vol. 6, no. 2, pp. 81–91, 2011.

[113] K.-L. Chung and P.-C. Chen, "An efficient algorithm for computing moments on a block representation of a grey-scale image," *Pattern Recognition*, vol. 38, no. 12, pp. 2578–2586, 2005.

[114] K.-H. Chang, R. Paramesran, B. Honarvar, and C.-L. Lim, "Efficient hardware accelerators for the computation of Tchebichef moments," *IEEE Transactions on Circuits and Systems for Video Technology*, vol. 22, no. 3, pp. 414–425, 2012.

[115] B. Honarvar, R. Paramesran, and C.-L. Lim, "The fast recursive computation of Tchebichef moment and its inverse transform based on Z-transform," *Digital Signal Processing*, vol. 23, no. 5, pp. 1738–1746, 2013.

[116] P.-T. Yap and R. Paramesran, "An efficient method for the computation of Legendre moments," *IEEE Transactions on Pattern Analysis and Machine Intelligence*, vol. 27, no. 12, pp. 1996–2002, 2005.

[117] K. M. Hosny, "Exact Legendre moment computation for gray level images," *Pattern Recognition*, vol. 40, no. 12, pp. 3597–3605, 2007.

[118] K. M. Hosny, "Fast and low-complexity method for exact computation of 3D Legendre moments," *Pattern Recognition Letters*, vol. 32, no. 9, pp. 1305–1314, 2011.

[119] K. M. Hosny, "Fast computation of accurate Gaussian–Hermite moments for image processing applications," *Digital Signal Processing*, vol. 22, no. 3, pp. 476–485, 2012.

[120] Z. Bahaoui, H. E. Fadili, K. Zenkouar, H. Qjidaa, and A. Zarghili, "Image analysis by efficient Gegenbauer moments computation for 3D objects reconstruction," *International Journal of Information and Communication Technology*, vol. 14, no. 3, pp. 263–276, 2019.

[121] I. M. Spiliotis, N. D. Karampasis, and Y. S. Boutalis, "Fast computation of Hahn moments on gray images using block representation," *Journal of Electronic Imaging*, vol. 29, no. 1, 2020. DOI: 10.1117/1.JEI.29.1.013020.

[122] H. Karmouni, A. Hmimid, T. Jahid, M. Sayyouri, H. Qjidaa, and A. Rezzouk, "Fast and stable computation of the Charlier moments and their inverses using digital filters and image block representation," *Circuits, Systems, and Signal Processing*, vol. 37, no. 9, pp. 4015–4033, 2018.

[123] A. Mesbah, M. El Mallahi, H. El Fadili, K. Zenkouar, A. Berrahou, and H. Qjidaa, "An algorithm for fast computation of 3D Krawtchouk moments for volumetric image reconstruction," in *Proceedings of the Mediterranean Conference on Information & Communication Technologies 2015*, Springer, 2016, pp. 267–276.

[124] R. Benouini, I. Batioua, K. Zenkouar, A. Zahi, H. El Fadili, and H. Qjidaa, "Fast and accurate computation of Racah moment invariants for image classification," *Pattern Recognition*, vol. 91, pp. 100–110, 2019.

[125] Y. Xuan, D. Li, and W. Han, "Efficient optimization approach for fast GPU computation of Zernike moments," *Journal of Parallel and Distributed Computing*, vol. 111, pp. 104–114, 2018.

[126] A.-W. Deng and C.-Y. Gwo, "Fast and stable algorithms for high-order pseudo Zernike moments and image reconstruction," *Applied Mathematics and Computation*, vol. 334, pp. 239–253, 2018.

[127] E. Walia, C. Singh, and A. Goyal, "On the fast computation of orthogonal Fourier–Mellin moments with improved numerical stability," *Journal of Real-Time Image Processing*, vol. 7, no. 4, pp. 247–256, 2012.

[128] R. Upneja and C. Singh, "Fast computation of Jacobi–Fourier moments for invariant image recognition," *Pattern Recognition*, vol. 48, no. 5, pp. 1836–1843, 2015.

[129] H. Zhang, Z. Li, and Y. Liu, "Fractional orthogonal Fourier–Mellin moments for pattern recognition," in *Chinese Conference on Pattern Recognition*, Springer, 2016, pp. 766–778.

[130] R. Benouini, I. Batioua, K. Zenkouar, A. Zahi, S. Najah, and H. Qjidaa, "Fractional-order orthogonal Chebyshev moments and moment invariants for image representation and pattern recognition," *Pattern Recognition*, vol. 86, pp. 332–343, 2019.

[131] M. Yamni, A. Daoui, H. Karmouni, M. Sayyouri, H. Qjidaa, and J. Flusser, "Fractional Charlier moments for image reconstruction and image watermarking," *Signal Processing*, vol. 171, 2020. DOI: 10.1016/j.sigpro.2020.107509.

[132] K. M. Hosny, M. M. Darwish, and T. Aboelenan, "Novel fractional-order generic Jacobi–Fourier moments for image analysis," *Signal Processing*, vol. 172, 2020, art. no. 107545.

[133] K. M. Hosny, M. M. Darwish, and T. Aboelenen, "New fractional-order Legendre–Fourier moments for pattern recognition applications," *Pattern Recognition*, vol. 103, 2020, art. no. 107324.

[134] B. Xiao, J. Luo, X. Bi, W. Li, and B. Chen, "Fractional discrete Tchebyshev moments and their applications in image encryption and watermarking," *Information Sciences*, vol. 516, pp. 545–559, 2020.

[135] H. Pan and L. Xia, "Wavelet moment invariants based on multiresolution image analysis," in *Third International Symposium on Multispectral Image Processing and Pattern Recognition*, International Society for Optics and Photonics, vol. 5286, 2003, pp. 271–276.

[136] J. Hu, J.-X. Sun, and Y. Wei, "Wavelet moment for images," *Journal of Circuits and Systems*, vol. 10, no. 6, pp. 132–136, 2005.

[137] F. Zhang, S.-Q. Liu, D.-B. Wang, and W. Guan, "Aircraft recognition in infrared image using wavelet moment invariants," *Image and Vision Computing*, vol. 27, no. 4, pp. 313–318, 2009.

[138] X.-Y. Wang, Y.-P. Yang, and H.-Y. Yang, "Invariant image watermarking using multi-scale Harris detector and wavelet moments," *Computers & electrical engineering*, vol. 36, no. 1, pp. 31–44, 2010.

[139] C. Singh and A. M. Sahan, "Face recognition using complex wavelet moments," *Optics & Laser Technology*, vol. 47, pp. 256–267, 2013.

[140] H. Ren, Z. Ping, W. Bo, W. Wu, and Y. Sheng, "Multidistortion-invariant image recognition with radial harmonic Fourier moments," *Journal of the Optical Society of America A*, vol. 20, no. 4, pp. 631–637, 2003.

[141] C. Wang, X. Wang, Z. Xia, and C. Zhang, "Ternary radial harmonic Fourier moments based robust stereo image zero-watermarking algorithm," *Information Sciences*, vol. 470, pp. 109–120, 2019.

[142] C.-P. Wang, X.-Y. Wang, and Z.-Q. Xia, "Geometrically invariant image watermarking based on fast radial harmonic Fourier moments," *Signal Processing: Image Communication*, vol. 45, pp. 10–23, 2016.

[143] H.-Y. Yang, S.-R. Qi, W. Chao, S.-B. Yang, and X.-Y. Wang, "Image analysis by log-polar Exponent-Fourier moments," *Pattern Recognition*, vol. 101, 2020, art. no. 107177.

[144] J. Zhong, Y. Gan, and S. Xie, "Radon odd radial harmonic Fourier moments in detecting cloned forgery image," *Chaos, Solitons & Fractals*, vol. 89, pp. 115–129, 2016.

[145] B. Xiao, J.-F. Ma, and X. Wang, "Image analysis by Bessel–Fourier moments," *Pattern Recognition*, vol. 43, no. 8, pp. 2620–2629, 2010.

[146] Z. Shao, H. Shu, J. Wu, B. Chen, and J. L. Coatrieux, "Quaternion Bessel–Fourier moments and their invariant descriptors for object reconstruction and recognition," *Pattern Recognition*, vol. 47, no. 2, pp. 603–611, 2014.

[147] P.-T. Yap, X. Jiang, and A. C. Kot, "Two-dimensional polar harmonic transforms for invariant image representation," *IEEE Transactions on Pattern Analysis and Machine Intelligence*, vol. 32, no. 7, pp. 1259–1270, 2010.

[148] Y. N. Li, "Quaternion polar harmonic transforms for color images," *IEEE Signal Processing Letters*, vol. 20, no. 8, pp. 803–806, 2013.

[149] X.-Y. Wang, W.-Y. Li, H.-Y. Yang, P. Wang, and Y.-W. Li, "Quaternion polar complex exponential transform for invariant color image description," *Applied Mathematics and Computation*, vol. 256, pp. 951–967, 2015.

[150] K. M. Hosny and M. M. Darwish, "Highly accurate and numerically stable higher order QPCET moments for color image representation," *Pattern Recognition Letters*, vol. 97, pp. 29–36, 2017.

[151] S. Dominguez, "Image analysis by moment invariants using a set of step-like basis functions," *Pattern Recognition Letters*, vol. 34, no. 16, pp. 2065–2070, 2013.

[152] K. M. Hosny, M. M. Darwish, and M. M. Eltoukhy, "Novel multi-channel fractional-order radial harmonic Fourier moments for color image analysis," *IEEE Access*, vol. 8, pp. 40 732–40 743, 2020.

[153] T. Suk and J. Flusser, "Graph method for generating affine moment invariants," in *Proceedings of the 17th International Conference on Pattern Recognition ICPR'04*, Cambridge, U.K.: IEEE Computer Society, 2004, pp. 192–195.

[154] T. Suk and J. Flusser, "Affine moment invariants generated by graph method," *Pattern Recognition*, vol. 44, no. 9, pp. 2047–2056, 2011.

[155] J. Flusser, T. Suk, and S. Saic, "Image features invariant with respect to blur," *Pattern Recognition*, vol. 28, no. 11, pp. 1723–1732, 1995.

[156] J. Flusser, T. Suk, and S. Saic, "Recognition of blurred images by the method of moments," *IEEE Transactions on Image Processing*, vol. 5, no. 3, pp. 533–538, 1996.

[157] H. Ji and H. Zhu, "Degraded image analysis using Zernike moment invariants," in *Proceedings of the International Conference on Acoustics, Speech and Signal Processing ICASSP'09*, 2009, pp. 1941–1944.

[158] X. Dai, T. Liu, H. Shu, and L. Luo, "Pseudo-Zernike moment invariants to blur degradation and their use in image recognition," in *Intelligent Science and Intelligent Data Engineering IScIDE'12*, J. Yang, F. Fang, and C. Sun, Eds., ser. Lecture Notes in Computer Science, vol. 7751, Nanjing, China: Springer, 2013, pp. 90–97.

[159] Q. Liu, H. Zhu, and Q. Li, "Image recognition by combined affine and blur Tchebichef moment invariants," in *Proceedings of 4th International Conference on Image and Signal Processing (CISP)*, Shanghai, China, 2011, pp. 1517–1521.

[160] Q. Liu, H. Zhu, and Q. Li, "Object recognition by combined invariants of orthogonal Fourier–Mellin moments," in *Proceedings of 8th International Conference on Information, Communications and Signal Processing ICICS'11*, Singapore: IEEE, Dec. 2011, pp. 1–5.

[161] J. Flusser, T. Suk, and S. Saic, "Recognition of images degraded by linear motion blur without restoration," *Computing Supplement*, Supplement, vol. 11, pp. 37–51, 1996.

[162] A. Stern, I. Kruchakov, E. Yoavi, and S. Kopeika, "Recognition of motion-blured images by use of the method of moments," *Applied Optics*, vol. 41, pp. 2164–2172, 2002.

[163] J. Boldyš and J. Flusser, "Invariants to symmetrical convolution with application to dihedral kernel symmetry," in *Proceedings of the 17th International Conference on Image Analysis and Processing ICIAP'13*, A. Petrosino, Ed., ser. Lecture Notes in Computer Science, vol. 8157, Neapol, Italy: Springer, 2013, 369–378, part II.

[164] C. Höschl IV and J. Flusser, "Robust histogram-based image retrieval," *Pattern Recognition Letters*, vol. 69, pp. 72–81, 2016.

[165] H. Gould and J. Quaintance, "Double fun with double factorials," *Mathematics Magazine*, vol. 85, no. 3, pp. 177–192, 2012.

Part II

PAPERS

Pattern Recognition 74 (2018) 110–121

Contents lists available at ScienceDirect

Pattern Recognition

journal homepage: www.elsevier.com/locate/patcog

Rotation invariants of vector fields from orthogonal moments

Bo Yang[a], Jitka Kostková[b], Jan Flusser[b,*], Tomáš Suk[b], Roxana Bujack[c]

[a] School of Automation, Northwestern Polytechnical University, 127 West Youyi Road, 710 072 Xi'an Shaanxi, P.R. China
[b] Institute of Information Theory and Automation of the CAS, Pod vodárenskou věží 4, 182 08 Praha 8, Czech Republic
[c] Data Science at Scale Team, Los Alamos National Laboratory, P.O. Box 1663, Los Alamos, NM 87545, USA

ARTICLE INFO

Article history:
Received 31 March 2017
Revised 2 September 2017
Accepted 5 September 2017
Available online 11 September 2017

Keywords:
Vector field
Total rotation
Invariants
Gaussian–Hermite moments
Zernike moments
Numerical stability

ABSTRACT

Vector field images are a type of new multidimensional data that appear in many engineering areas. Although the vector fields can be visualized as images, they differ from graylevel and color images in several aspects. To analyze them, special methods and algorithms must be originally developed or substantially adapted from the traditional image processing area. In this paper, we propose a method for the description and matching of vector field patterns under an unknown rotation of the field. Rotation of a vector field is so-called total rotation, where the action is applied not only on the spatial coordinates but also on the field values. Invariants of vector fields with respect to total rotation constructed from orthogonal Gaussian–Hermite moments and Zernike moments are introduced. Their numerical stability is shown to be better than that of the invariants published so far. We demonstrate their usefulness in a real world template matching application of rotated vector fields.

1. Introduction

In the last decade, an increasing attention has been paid to *vector field* images and to the tools for their analysis. Vector fields arise in mechanical engineering, fluid dynamics, computer vision, meteorology, and many other application areas. They describe particle velocity, wind velocity, optical/motion flow, image gradient, and other phenomena, for instance, flowing water in a pipe, an air flow around an aircraft wing or around a coachwork, or a wind velocity map. Vector fields are obtained as a result of computer processing of standard digital images or videos, numerical solutions of the Navier–Stokes equations, or from real physical measurements (see Fig. 1).

A 2D vector field $\mathbf{f}(\mathbf{x})$ can be mathematically described as a pair of scalar fields (images) $\mathbf{f}(\mathbf{x}) = (f_1(\mathbf{x}), f_2(\mathbf{x}))$. At each point $\mathbf{x} = (x, y)$, the value of $\mathbf{f}(\mathbf{x})$ shows the orientation and the magnitude of a certain vector.

A common task in vector field analysis is the detection of various patterns of interest. It comprises not only detection of singularities such as sinks, vortices, saddle points, vortex-saddle combinations, and double vortices, but also detection of patterns which are not specific but are similar to the pattern stored in the database. For engineers and designers, it is very important to identify these patterns of interest in the flow, because they may increase the friction, vary the pressure, or decrease the speed of the medium, which consequently increases the power and cost necessary to transport it through the pipe or the object through the air or water. We also may just look for an appearance of certain pattern because it may indicate the presence of the physical phenomenon in the fluid we are interested in. The detection of these features is typically accomplished by template matching.[1] Sample templates of these patterns, obtained from similar fields or as a result of a simulation, are stored in the template database and searched in the given field. The search algorithm must be primarily *rotation invariant*, because the particular orientation of the template is unknown (see Fig. 2 for illustration). It is further important that the algorithm is robust with respect to noise in the measurements.

Many template-matching techniques have been developed for scalar images. The key point to avoid a brute-force search is to find rotation-invariant template descriptors. The matching is then performed by a search of all possible template locations (which may be sped-up by a pyramidal representation of the image) and

* Corresponding author.
E-mail addresses: bo.yang@hotmail.fr (B. Yang), kostkova@utia.cas.cz (J. Kostková), flusser@utia.cas.cz (J. Flusser), suk@utia.cas.cz (T. Suk), bujack@lanl.gov (R. Bujack).

[1] If the patterns to be detected were only singularities or other mathematically well-described patterns, we could alternatively use other methods. Template matching is a general method suitable for any pattern which is defined by example rather than by mathematical description.

http://dx.doi.org/10.1016/j.patcog.2017.09.004

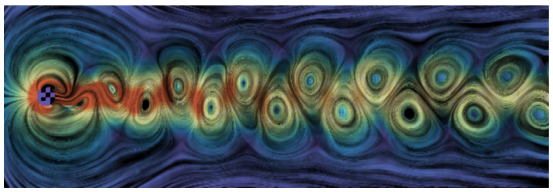

Fig. 1. Fluid flow behind an obstacle. The flow direction is visualized using line integral convolution and the velocity is encoded in the color.

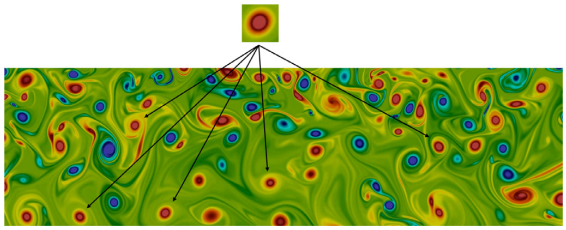

Fig. 2. Vortex detection in a swirling fluid by template matching. The detection method must be invariant to the template orientation.

the matching position is determined as that one which minimizes certain "distance" (usually derived from ℓ_2-norm) in the high-dimensional feature-space of descriptors. The first method of this kind was proposed by Goshtasby [1], who used rotation invariants from geometric moments as the descriptors, but in principle any invariants from any kind of features [2–7] can be used for this purpose.

The methods (or, more precisely, the invariant descriptors) originally designed for scalar images cannot be applied directly to vector fields, because the behavior of a vector field under rotation is substantially different. The rotation of scalar image f by the angle α can be described as

$$f'(\mathbf{x}) = f(\mathbf{R}_{-\alpha} \cdot \mathbf{x}),$$

where

$$\mathbf{R}_\alpha = \begin{pmatrix} \cos\alpha & -\sin\alpha \\ \sin\alpha & \cos\alpha \end{pmatrix}$$

is a rotation matrix. This rotation, called *inner rotation*, affects the spatial coordinates only.

However, when rotating a vector field, the situation is different. The vectors rotate inversely to the in-plane rotation such that their relative orientation to the image content stays constant. The underlying model, which is called *total rotation*, is

$$\mathbf{f}'(\mathbf{x}) = \mathbf{R}_\alpha \mathbf{f}(\mathbf{R}_{-\alpha} \cdot \mathbf{x}).$$

The total rotation of a sample vector field is illustrated in Fig. 3(b) for $\alpha = 22.5^\circ$. Each arrow is rotated around the image center to the new position and its direction is also rotated by the same angle.

In order to implement a rotation-invariant template matching algorithm, we first need to find descriptors that are invariant with respect to the total rotation of a vector field. This problem was raised for the first time by Schlemmer et al. [8], who adapted the scalar moment invariants proposed by Mostafa and Psaltis [9] and Flusser [3,10] and designed invariants composed of geometric complex moments of the field. Schlemmer et al. used these invariants to detect specific patterns in a turbulent swirling jet flow. Rotation invariants from geometric complex moments have found several applications. Liu and Ribeiro [11] used them, along with a local approximation of the vector field by a polynomial, to detect singularities on meteorological satellite images showing wind velocity. Basically the same kind of rotation invariants were used by Liu and Yap [12] for the indexing and recognition of fingerprint images. Bujack et al. [13,14] studied the invariants of complex moments thoroughly, generalized the previous works, and showed that the invariants can be derived also by means of the field normalization approach. These authors demonstrated the use of the invariants in several pattern matching tasks including fluid dynamics simulation of a Kármán vortex street.

In all of the above-mentioned papers, despite of certain differences, the invariants are essentially based on standard geometric moments. It is well known from many studies of scalar images, that the geometric (and consequently the complex) moments have rather poor numerical properties, in particular they cannot be calculated in a stable way up to high orders [2]. This is caused by the fact that their basis functions $x^p y^q$ are not orthogonal. In scalar image analysis, this finding led to the design of invariants from orthogonal moments and from other orthogonal projections of the image (see, for instance, [2] for a survey). However, nothing like that has been published for vector fields so far.

In this paper, we introduce vector field invariants w.r.t. total rotation composed of orthogonal Gaussian–Hermite moments and of Zernike moments. We demonstrate that they have better numerical properties than the invariants of geometric/complex moments and they can be advantageously used in the vector field template matching tasks.

In the next section, we briefly recall Gaussian–Hermite moments. In Section 3, we show how the Gaussian–Hermite moments can be used for designing rotation invariants of vector fields. Section 4 introduces vector field invariants based on Zernike moments. Finally, numerical experiments and comparison are presented in Section 5.

2. Gaussian–Hermite polynomials and moments

Hermite polynomials are popular basis functions introduced by C. Hermite [15]. They have been widely used in signal analysis and in many other applications.

The Hermite polynomial of the n-th degree is defined as

$$H_n(x) = (-1)^n e^{x^2} \frac{\mathrm{d}^n}{\mathrm{d}x^n} e^{-x^2}. \tag{1}$$

Hermite polynomials are orthogonal on $(-\infty, \infty)$ with the weight $w(x) = e^{-x^2}$. For numerical calculations, Hermite polynomials can be evaluated in a fast and stable way by means of the three-term recurrence relation

$$H_n(x) = 2xH_{n-1}(x) - 2(n-1)H_{n-2}(x) \tag{2}$$

with the initialization $H_0(x) = 1$ and $H_1(x) = 2x$. If they are not modulated, they have a high range of values and poor localization, which makes them difficult to use directly for image description. To overcome this, we modulate Hermite polynomials with a Gaussian function and scale them. This normalization yields *Gaussian–Hermite (GH) polynomials*

$$H_n(x, \sigma) = H_n(x/\sigma) e^{-\frac{x^2}{2\sigma^2}}. \tag{3}$$

In most cases, we work with *orthonormal* GH polynomials $\hat{H}_n$, which differ from Eq. (3) just by the scalar factor:

$$\hat{H}_n(x, \sigma) = \frac{1}{\sqrt{n! 2^n \sigma \sqrt{\pi}}} H_n(x, \sigma). \tag{4}$$

As can be seen in Fig. 4, the GH polynomials have a range of values inside $(-1, 1)$. Although they are formally defined on $(-\infty, \infty)$, they are effectively localized into a small neighborhood of the origin controlled by σ.

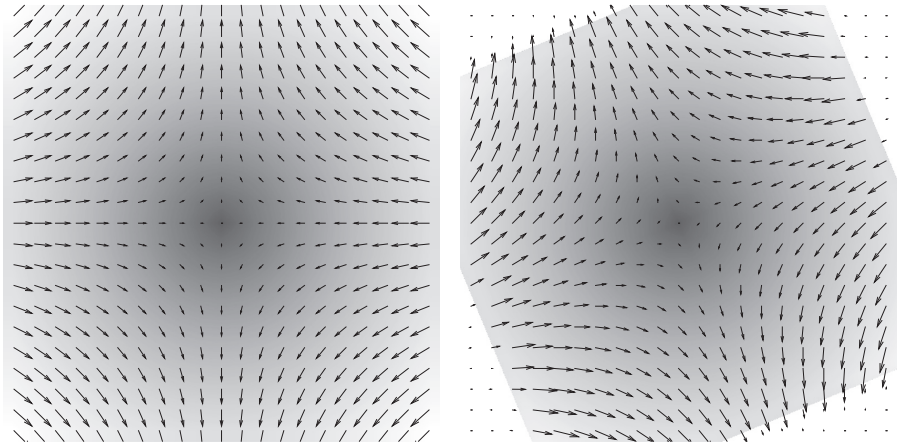

(a) (b)

Fig. 3. Vector field transformation: (a) original vector field, (b) its total rotation.

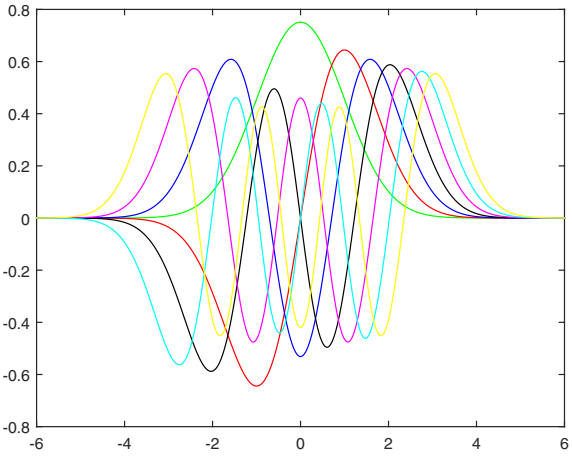

Fig. 4. The graphs of the Gaussian–Hermite polynomials up to degree 6 with $\sigma = 1$.

2D Gaussian–Hermite moments of a function $f(x, y)$ are defined as

$$\hat{\eta}_{pq} = \int_{-\infty}^{\infty}\int_{-\infty}^{\infty} \hat{H}_p(x,\sigma)\hat{H}_q(y,\sigma) f(x,y)\mathrm{d}x\mathrm{d}y. \tag{5}$$

The GH moments were introduced to the image analysis community by Shen [16,17]. They were proved to be robust w.r.t. additive noise [18,19] and were successfully employed in several applications, such as in the detection of moving objects in videos [20], in license plate recognition [21], in image registration as landmark descriptors [4], in fingerprint classification [22], in face recognition [23,24], in 3D object reconstruction [25], and as directional feature extractors [26].

The main advantage of the GH moments for using in image processing is their simple transformation under a rotation of the spatial coordinates, as was discovered by Yang et al. [27,28] and employed to design GH rotation invariants of scalar images [29]. This property of the GH moments has been known as the *Yang's theorem*: If there exists rotation invariant $I(m_{p_1q_1}, m_{p_2q_2}, \ldots, m_{p_dq_d})$ of geometric moments

$$m_{pq} = \int_{-\infty}^{\infty}\int_{-\infty}^{\infty} x^p y^q f(x,y)\mathrm{d}x\mathrm{d}y, \tag{6}$$

then the same function of the corresponding Hermite moments is also a rotation invariant (see [28] for the detailed proof). Furthermore, Gaussian weighting and scaling do not violate this property provided that the scale parameter σ is the same for x and y and that the normalizing coefficient has been set up as

$$\hat{\eta}_{pq} = \frac{1}{\sigma\sqrt{\pi\,(p+q)!2^{p+q}}}\int_{-\infty}^{\infty}\int_{-\infty}^{\infty} H_p(x,\sigma)H_q(y,\sigma) f(x,y)\mathrm{d}x\mathrm{d}y. \tag{7}$$

The Yang's theorem still holds well and the functional $I(\hat{\eta}_{p_1q_1}, \hat{\eta}_{p_2q_2}, \ldots, \hat{\eta}_{p_dq_d})$ is a rotation invariant of the Gaussian–Hermite moments of scalar images [28].

In the next section, we adapt the Yang's theorem for vector fields and show how to construct GH invariants w.r.t. total rotation, which is the main theoretical contribution of the paper.

3. Gaussian–Hermite rotation invariants of vector fields

A vector field can be treated as a complex-valued function (or matrix in a discrete case)

$$\mathbf{f}(x,y) = f_1(x,y) + i f_2(x,y),$$

which allows us to use the standard definition of moments. It holds, for arbitrary moment M_{pq},

$$M_{pq}^{(\mathbf{f})} = M_{pq}^{(f_1)} + iM_{pq}^{(f_2)},$$

where M_{pq} may stand for geometric, GH, or any other moment. Since the outer rotation (i.e. the rotation of the vector values) can be modeled as a multiplication of the vector field by a constant factor $e^{-i\alpha}$, any moment M_{pq} suffices

$$M'_{pq} = e^{-i\alpha}M_{pq}.$$

Hence, the GH moments are transformed exactly in the same way as the geometric moments. This allows us to formulate a generalization of the Yang's theorem to vector fields:

If there exists invariant to total rotation of a vector field $I(m_{p_1q_1}, m_{p_2q_2}, \ldots, m_{p_dq_d})$ of geometric moments, then the same

functional $I(\hat{\eta}_{p_1q_1}, \hat{\eta}_{p_2q_2}, \ldots, \hat{\eta}_{p_dq_d})$ of the Gaussian–Hermite moments is also an invariant.

Practical applicability of the Yang's vector-field theorem depends on our ability to find rotation invariant I composed of geometric moments (in practice, a single invariant is not sufficient and we are looking for a set providing a sufficient discriminability). That is, however, not easy. Already in the theory of moments of scalar images, it was shown [30] that the rotation invariants are hard to construct directly from the geometric moments. The same applies for vector fields, where the problem is even more difficult. In scalar moment invariants, the problem was overcome by using *complex moments*

$$c_{pq} = \int_{-\infty}^{\infty}\int_{-\infty}^{\infty}(x+iy)^p(x-iy)^q f(x,y)\mathrm{d}x\mathrm{d}y. \tag{8}$$

The complex moments change under the inner rotation by angle α simply as

$$c'_{pq} = e^{-i(p-q)\alpha}c_{pq} \tag{9}$$

(see [30] for the proof). Under a total rotation of a vector field, $c^{(\mathbf{f})}_{pq}$ fulfills

$$c^{(\mathbf{f}')}_{pq} = e^{-i\alpha}e^{-i(p-q)\alpha}\cdot c^{(\mathbf{f})}_{pq} = e^{-i(p-q+1)\alpha}\cdot c^{(\mathbf{f})}_{pq}. \tag{10}$$

The link between the geometric and the complex moments [30] (which is the same both for scalar and vector images)

$$c_{pq} = \sum_{k=0}^{p}\sum_{j=0}^{q}\binom{p}{k}\binom{q}{j}(-1)^{q-j}i^{p+q-k-j}m_{k+j,p+q-k-j} \tag{11}$$

yields the possibility of applying the Yang's theorem. When replacing the c_{pq}'s by the corresponding functions of the GH moments

$$d_{pq} = \sum_{k=0}^{p}\sum_{j=0}^{q}\binom{p}{k}\binom{q}{j}(-1)^{q-j}i^{p+q-k-j}\hat{\eta}_{k+j,p+q-k-j}, \tag{12}$$

the behavior under a total rotation must be preserved, which leads to

$$d^{(\mathbf{f}')}_{pq} = e^{-i(p-q+1)\alpha}\cdot d^{(\mathbf{f})}_{pq}. \tag{13}$$

Now we can cancel the rotation parameter by multiplication of proper powers of the d_{pq}'s. Let $\ell \geq 1$ and further let k_i, p_i, and q_i $(i = 1, \ldots, \ell)$ be non-negative integers such that

$$\sum_{i=1}^{\ell} k_i(p_i - q_i + 1) = 0.$$

Then,

$$I = \prod_{i=1}^{\ell} d_{p_iq_i}^{k_i} \tag{14}$$

is invariant with respect to total rotation of a vector field.

Eq. (14) may generate an infinite number of rotation invariants. It is desirable to work with an independent and complete subset (basis). The simplest possible basis can be obtained by

$$\Phi(p,q) \equiv d_{pq}d_{q_0p_0}^{p-q+1}, \tag{15}$$

where $p_0 - q_0 = 2$ and $d_{q_0p_0} \neq 0$. To get a complete system, we set by definition $\Phi(q_0, p_0) \equiv |d_{q_0p_0}|$ (note that $\Phi(q_0, p_0)$, if calculated from Eq. (15), would always equal one).

The choice of the basis is not unique and it is determined by the choice of $d_{q_0p_0}$, which is sometimes called the basic moment or the *normalizer*. The normalizer must be nonzero for all vector fields in the given experiment. If this condition was not fulfilled, the basis would lose its discrimination power. The construction of the basis requires special care if the fields in question exhibit certain symmetry, as we will see in the next section.

3.1. Symmetry issues

In moment-based pattern recognition, symmetric objects require special care when we define the invariants. Many moments are zero on objects that exhibit a certain symmetry. If they were used as a factor in a product, the invariant would become trivial on any object with the given type of symmetry. Trivial invariants do not provide any discriminability and only increase the dimensionality of the feature space, which may lead to a drop in performance. When we want to recognize different symmetric objects, the vanishing moments must be identified in advance and the trivial invariants need to be discarded from the system.

For rotation invariants of scalar images, the systematic analysis of this phenomenon was first presented in [31], where the authors showed the solution based on complex moments for objects with N-fold rotation symmetry. Vanishing of Gaussian–Hermite moments was studied later in [29], where the basis construction that prevents the use of the vanishing moments was proposed. The most general choice of the non-vanishing invariants of complex moments was proposed by Bujack [32], who introduced so-called flexible basis.

The problem of vanishing moments appears in case of vector fields, too. Unlike scalar images, the symmetry we have to investigate in the case of vector fields is that one which is related to the *total* rotation of the field. Let us define the notion of *total N-fold rotation symmetry*. The vector field $\mathbf{f}$ is said to be totally N-fold symmetric if it holds, for $\alpha = 2\pi/N$,

$$\mathbf{f}'(\mathbf{x}) \equiv \mathbf{R}_\alpha\mathbf{f}(\mathbf{R}_{-\alpha}\cdot\mathbf{x}) = \mathbf{f}(\mathbf{x}).$$

We may extend this definition also to $N = \infty$; then the equality must hold for any α.

If a vector field $\mathbf{f}$ is totally N-fold symmetric, then $d^{(\mathbf{f})}_{pq} = 0$ for any index pair p, q such that $(p-q+1)/N$ is *not* an integer. This can be observed immediately from Eq. (13) if we set $\alpha = 2\pi/N$. Then, due to the symmetry of field $\mathbf{f}$, we get $d^{(\mathbf{f}')}_{pq} = d^{(\mathbf{f})}_{pq}$. This equality can be fulfilled only if $d^{(\mathbf{f})}_{pq} = 0$ or if $(p-q+1)/N$ is integer.

We should take this proposition into account when designing invariants that are supposed to discriminate two vector fields with the same total N-fold symmetry. Instead of the basic invariants $\Phi(p, q)$ from Eq. (15), which may vanish, we create a non-trivial basis composed of the invariants

$$\Phi_N(p,q) \equiv d_{pq}d_{q_0p_0}^{\frac{p-q+1}{N}}, \tag{16}$$

where $(p-q+1)/N$ is an integer and $p_0 - q_0 = N + 1$.

When considering a total radial symmetry $N{=}\infty$, the only non-vanishing invariants are

$$\Phi_\infty(p, p+1) \equiv d_{p,p+1}. \tag{17}$$

The described problem of invariants of symmetric fields is not marginal as many specific templates we search for often exhibit symmetry with respect to a total rotation. The symmetry must be identified in advance and the invariant basis should be chosen according to (16) or (17).

3.2. Flexible basis

However, in practice, symmetric patterns may not be exactly symmetric due to sampling errors. Even if we do not detect any zero moments, certain moments may be very close to zero. This may happen also for some non-symmetric patterns. If we choose such a numerically zero moment as a basic moment in (15), the resulting invariants may be unstable and vulnerable to noise. To overcome that, we may construct a so-called *flexible invariant basis* as follows. We relax the constraint given earlier on the indices

p_0 and q_0 by only requiring $p_0 - q_0 + 1 \neq 0$. We look for a "significantly non-zero" moment $d_{q_0 p_0}$ satisfying this constraint by calculating the average magnitude of all d_{pq}'s up to the given order. The lowest-order moment whose magnitude exceeds the average is then taken as the normalizer $d_{q_0 p_0}$ and the basis is constructed via

$$\Phi_{flex}(p,q) \equiv d_{pq} d_{q_0 p_0}^{\frac{p-q+1}{p_0-q_0-1}}. \tag{18}$$

There are $|p_0 - q_0 - 1|$ complex roots, so $\Phi_{flex}(p, q)$ is defined with a $|p_0 - q_0 - 1|$-ambiguity. Since all these solutions are dependent, it is sufficient to store a single value only (all of them should be, however, taken into account when comparing two patterns). To avoid working with the multiple roots, we can alternatively use the powers

$$\Pi(p,q) \equiv \Phi_{flex}(p,q)^{p_0-q_0-1} = d_{pq}^{p_0-q_0-1} d_{q_0 p_0}^{p-q+1}, \tag{19}$$

which are defined unambiguously.

The flexible basis avoids using close-to-zero moments but does not require a prior analysis of the symmetry. It may be used in any case; however for common non-symmetric and non-singular patterns the flexible basis provides the same discrimination power as the basis (15) (in many cases the chosen normalizer is exactly the same as in (15)).

4. Zernike rotation invariants of vector fields

Zernike polynomials were originally proposed to describe the diffracted wavefront in phase contrast imaging [33] and have found numerous applications in mathematics, optics, and imaging. Zernike moments (ZMs) [5] have become very popular in image analysis. They belong to the family of *radial moments*, along with the Pseudo–Zernike, Fourier–Mellin, Jacobi–Fourier, Chebyshev–Fourier, and other moments (see [2] for a survey)). Their main advantage comes from the fact that they are orthogonal on the unit disk, they keep their magnitude constant under an image rotation, and their phase change is simple and easy to eliminate. The latter property ensures a theoretically easy construction of rotation invariants of scalar images [6].

Zernike moment of degree n with repetition ℓ of vector field $\mathbf{f}$ is defined as

$$A_{n\ell} = \frac{n+1}{\pi} \int_0^{2\pi} \int_0^1 V_{n\ell}^*(r,\theta) \mathbf{f}(r,\theta) r \, \mathrm{d}r\mathrm{d}\theta, \tag{20}$$

where $n = 0, 1, 2, \ldots$, $\ell = -n, -n+2, \ldots, n$ and $V_{n\ell}(r, \theta)$ is the respective Zernike polynomial (see for instance [2] for its complete definition).

Under a total rotation of the field by α, ZMs are transformed as

$$A'_{n\ell} = A_{n\ell} \, e^{-i(\ell-1)\alpha}. \tag{21}$$

The rotation invariants of vector fields are then obtained by phase cancellation as

$$Z_{n\ell} = A_{n\ell} (A_{n_0 \ell_0})^{-(\ell-1)/(\ell_0-1)}, \tag{22}$$

where the normalizer should be chosen such that $\ell_0 \neq 1$ and $A_{n_0\ell_0} \neq 0$. If we choose $\ell_0 = 0$ or $\ell_0 = 2$, we avoid the complex roots and end up with simpler invariants

$$Z_{n\ell} = A_{n\ell} (A_{n_0 \ell_0})^{\pm(\ell-1)}. \tag{23}$$

5. Experiments

The goal of the experimental section is to compare the proposed orthogonal invariants of vector fields (both GH and ZM) to their competitors – the invariants composed of geometric/complex moments [2]. These invariants are formally defined by the same equation as (15), but complex moments c_{pq} are used in place of d_{pq}:

$$\Psi(p,q) \equiv c_{pq} c_{q_0 p_0}^{p-q+1} \tag{24}$$

and $\Psi(q_0, p_0) \equiv |c_{q_0 p_0}|$. A few special cases of the invariants (24) of low orders, without mentioning the general formula, were used in [8] and in the follow-up papers mentioned in the introduction. In fact, they perform the only method for template matching in vector fields published so far.

In the remainder of this paper, we will refer to the invariants given by Eq. (24) as the *geometric* invariants.[2]

In the first experiment, we demonstrate the main advantage of the orthogonal invariants – high numerical stability and low precision loss even for high-order invariants. The second and third experiments illustrate the application of the GH invariants in template matching in real vector fields.

5.1. Numerical precision

In this experiment, we evaluated numerical properties of GH, ZM and geometric moment invariants up to the order $p + q = 160$. It can be expected that high-order geometric moment invariants lose precision because they comprise very high and very low numbers. Since the GH moments can be calculated by the recurrence relation (2), the overflow and underflow effects should be less significant or even not present at all. The same is true for the Zernike moments. Due to their popularity, great effort has been made to develop efficient and numerically stable algorithms for their calculation [34–40]. In this experiment, we used an implementation of the recurrent *Kintner method* [2,34], which is like a gold standard in the ZM computation.

The evaluation is done by measuring the relative error of each invariant. We took a 365×451 vector field (obtained as a gradient field of the image of a hair, see Fig. 5), rotated it by $\pi/4$ using the total rotation, and calculated the relative error in percents as

$$\varepsilon_\Gamma(p,q) = 100 \cdot \frac{|\Gamma(p,q) - \Gamma'(p,q)|}{\Gamma(p,q)},$$

where $\Gamma(p, q)$ stands for the geometric/GH/ZM invariant and $\Gamma'(p, q)$ denotes the same invariant of the rotated field. Theoretically it should hold $\varepsilon = 0$ for any p, q, and Γ; the non-zero values are caused by the field resampling and by numerical errors of the moment calculations. This is why we used the rotation by $\pi/4$ – the relative errors are greater than for any other angle and allow to observe the differences between the three types of the invariants clearly.

The relative errors of the geometric invariants are visualized in Fig. 6 using the color map on the right. It is worth noting that the invariants are well defined only in a strip along the diagonal $p = q$. Outside the colored area, the Matlab code yielded NaN values when calculating the invariants. This illustrates the limited possibility of working with the geometric invariants if $p - q > 20$ and $p, q > 80$ (the particular numbers depend on the given vector field).

The relative errors of the GH invariants and the ZM invariants are visualized in the same way in Fig. 7 and in Fig. 8, respectively. The main difference, which is apparent at first sight, is that all investigated invariants are valid, there have been no NaN's in the

[2] This terminology originates from the fact that the complex moments are simple functions of geometric moments, the most elementary moments. Sometimes they are called *monomial* invariants because they are based on the monomial basis functions.

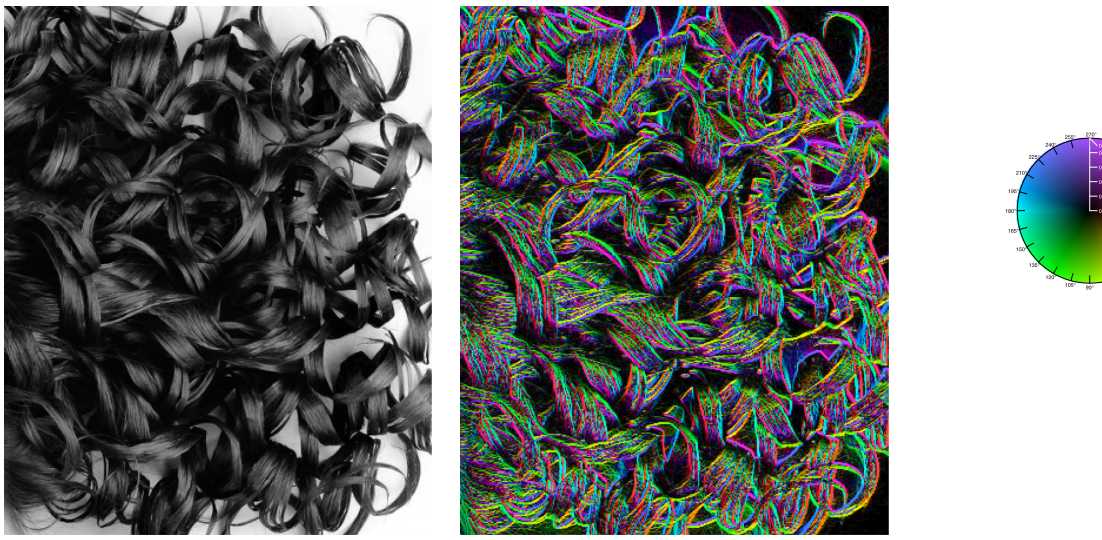

(a) (b) (c)

Fig. 5. Hair image: (a) the original, (b) the gradient field, and (c) the colormap for gradient visualization. The brightness corresponds to the magnitude and the hue to the direction of the gradient.

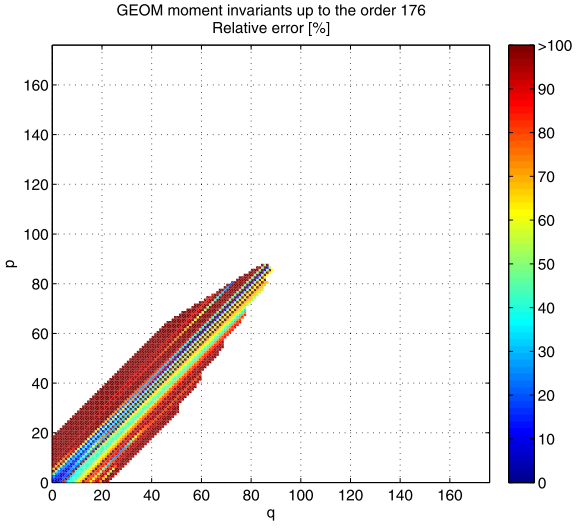

Fig. 6. Relative errors of the geometric invariants. White area corresponds to NaN values of the invariants.

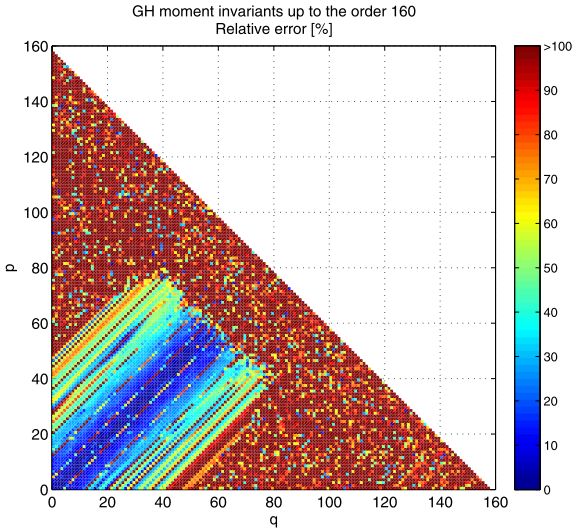

Fig. 7. Relative errors of the Gaussian–Hermite invariants.

calculations. To compare the relative errors in the valid region, we calculated element-wise the ratios

$$\varrho_1(p,q) = \frac{\varepsilon(geometric)}{\varepsilon(GH)},$$

$$\varrho_2(p,q) = \frac{\varepsilon(geometric)}{\varepsilon(ZM)},$$

and

$$\varrho_3(p,q) = \frac{\varepsilon(GH)}{\varepsilon(ZM)}.$$

They are visualized in Figs. 9–11. While the calculation of ϱ_1 is straightforward, the definition of ϱ_2 and ϱ_3 may not be unique, because the second index of the Zernike moment expresses the angular repetition factor while both indices of the geometric/GH moments are the degrees of the basis polynomials. A reasonable way, which we employed here, of comparing the geometric/GH moments to the ZMs, is to link the indices p, q of geometric/GH moments to the indices $p+q$, $p-q$ of the ZMs. The yellow-red color map is used for $\varrho > 1$, light green is neutral ($\varrho = 1$) and green-blue stands for $\varrho < 1$ (to keep the same range on both sides, the values of $\varrho > 1$ were displayed as $2 - 1/\varrho$). The vast majority of indices

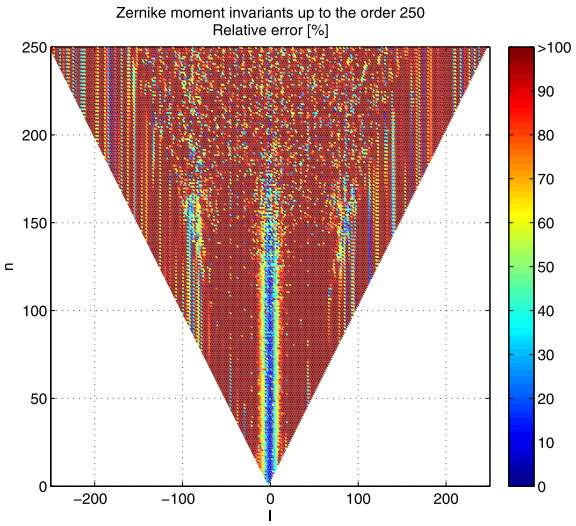

Fig. 8. Relative errors of the Zernike moment invariants.

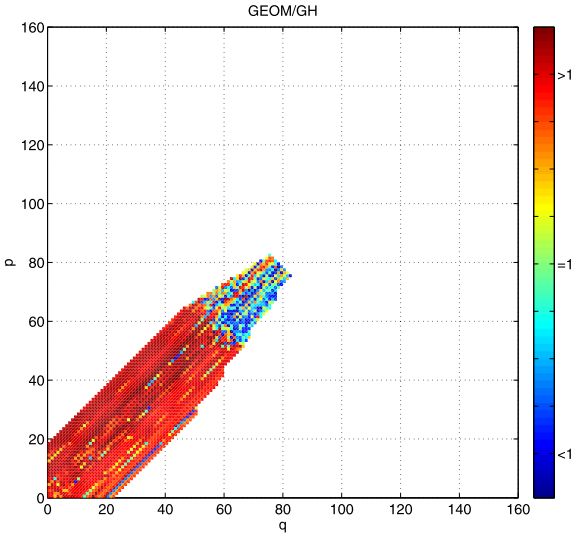

Fig. 9. The ratio of the relative errors ϱ_1.

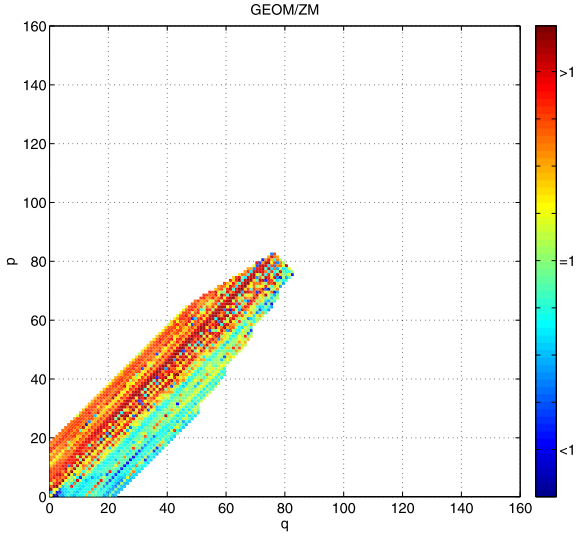

Fig. 10. The ratio of the relative errors ϱ_2.

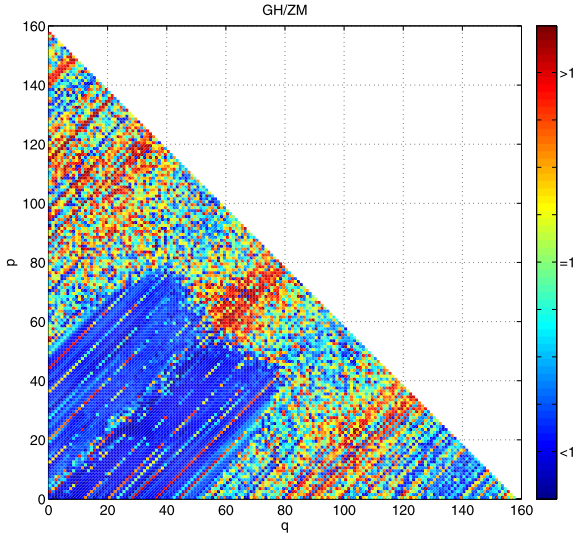

Fig. 11. The ratio of the relative errors ϱ_3.

(p, q) (precisely in 85%), satisfies $\varrho_1 > 1$, which means the relative error of the geometric invariants is higher than that of the GH invariants. The mean value of ϱ_1 is 7.3 and the median equals 4.3, which clearly illustrates the higher stability of the GH invariants. The behavior of ϱ_2 is similar, although the dominance of the ZMs is not as prominent.

The quantitative comparison between the GH and ZM invariants is expressed by ϱ_3. In the central strip area, the GH invariants are more stable (the mean value of ϱ_3 is 0.8, the median is 0.65). Outside this area, ϱ_3 looks like a close-to-zero-mean random noise, which shows there is no significant difference between the GH and ZM invariants in this range of the indices.

5.2. Template matching in a gradient field

In this experiment we demonstrate the use of the GH invariants for template matching, i.e. in the task they have been designed for and where they are supposed to be applied in practice. As the test vector field, we again used the gradient of the hair image, see Fig. 5. We chose this particular photograph to make the matching challenging. On one hand, the picture is rich in edges so there are no large regions of a constant gradient; on the other hand there are many patches similar to each other, which makes the matching non-trivial.

We randomly extracted 1000 circular templates of the radius 20 pixels from the gradient field, rotated them by random angles, and matched them against the original field. The matching was carried out by searching for the minimum ℓ_2-distance in the space

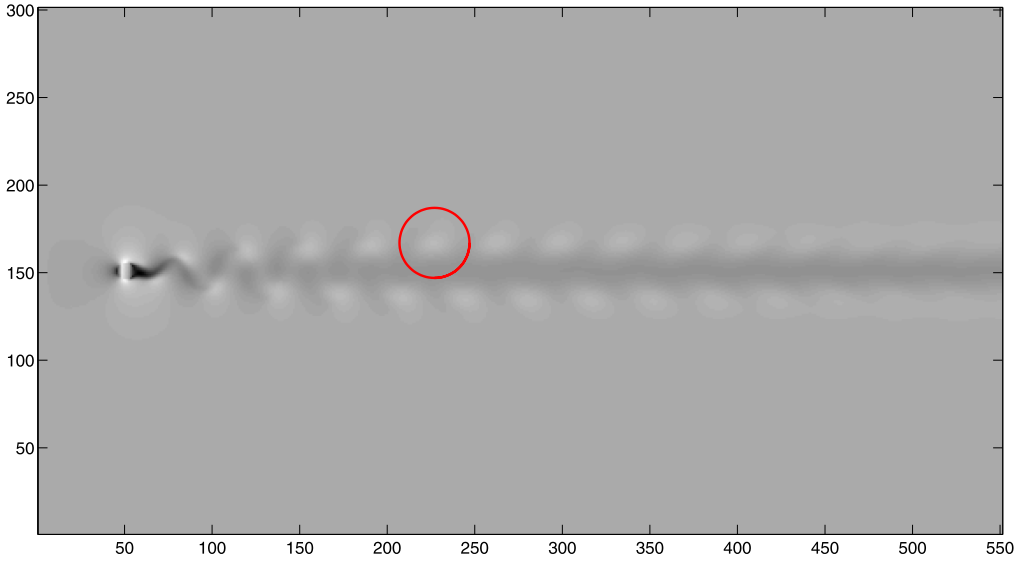

Fig. 12. The Kármán vortex street with the selected template.

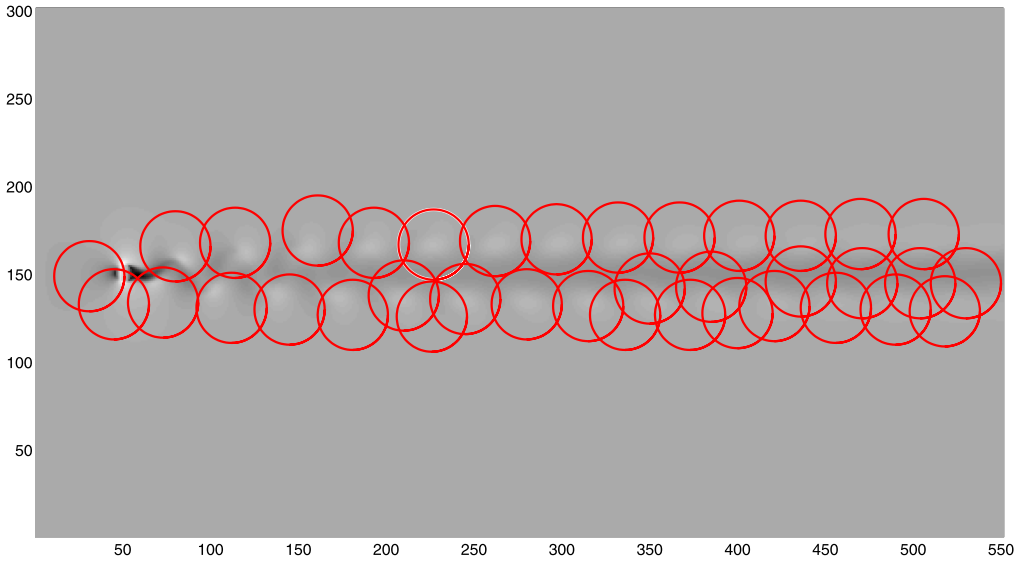

Fig. 13. The matching vortices when only the GH invariants up to the fourth order have been employed.

of the invariants between the template and all field patches of the same size. We encountered two kinds of errors which we call "small" and "gross". An error is considered "small" if it is less than 10 pixels (measured as the Euclidean distance from the ground-truth location). These errors are governed by a Rayleigh distribution $R(x;\sigma)$ [41] (provided that the errors in horizontal and vertical directions are independent, normally distributed random variables with the same variance), whose density is

$$R(x;\sigma) = \frac{x}{\sigma^2} e^{-\frac{x^2}{2\sigma^2}}. \tag{25}$$

The mean value of the distribution, which we used to quantify the small errors, is $\sigma\sqrt{\pi/2}$.

The "gross" error means the template was found at a completely wrong place, usually because there was a similar patch at that position. Since in most applications the errors are considered equally serious if they are, let us say, 50 or 500 pixels (in both cases, the location found is totally wrong and the position cannot be refined by searching within a neighborhood), we only count the number of these gross errors to evaluate the matching.

We matched each template by eight different invariants for comparison. We used the vector-field GH invariants up to the orders four and six to illustrate the contribution of higher orders. To show the differences in numerical stability, we did the same with the vector-field invariants composed of complex (geometric) moments [2]. Finally, we converted the vector values to magnitudes

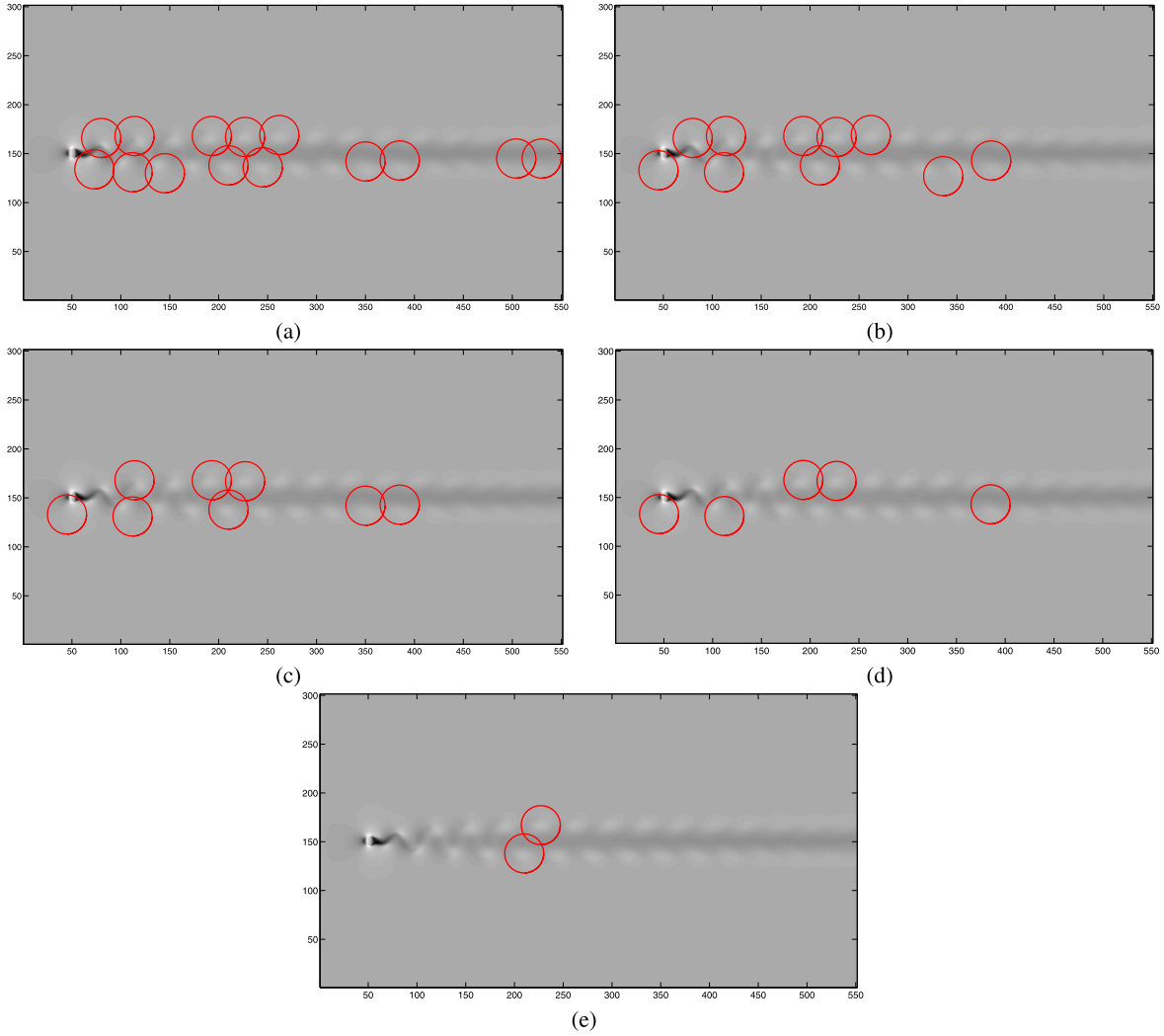

Fig. 14. The matching vortices when also higher-order GH invariants have been used. The higher orders obviously yield less matching results: (a) fifth order, (b) seventh order, (c) ninth order, (d) eleventh order, and (e) thirteenth order.

Table 1
The number of gross errors (NGE) and the mean small errors (MSE) out of 1000 trials in the experiment with the template matching in the gradient field.

Features	4th order		6th order	
	NGE	MSE	NGE	MSE
GH vector	114	0.504	75	0.401
CM vector	360	1.157	282	0.836
GH scalar	391	0.748	176	0.624
CM scalar	745	1.497	647	1.070

and used traditional scalar image invariants (both GH and CM) acting on magnitudes only to match the templates. This shows that the vector field template matching cannot be reduced to scalar image matching without a loss of performance. The results are summarized in Table 1. It can be seen clearly, that the vector field GH invariants outperform the other three methods significantly, both in the number of gross errors as well as in the mean value of the small ones. At the same time, we can observe an improvement of the performance of all methods when the 6-th order moments were used.

5.3. Template matching in a fluid flow field

In this experiment, we demonstrate the applicability of the proposed technique in an important problem from fluid dynamics engineering – vortex detection in a fluid flow vector field. We used the field showing the Kármán vortex street, which is a repeating pattern of swirling vortices caused by the flow of a fluid around blunt bodies. In the Kármán pattern, we can see several vortices arranged into two rows. The orientation of the “street” is given by the main flow direction and is generally not known a priori. A patch with a typical vortex is used as a template. In this task we used a vortex from the upper row (see Fig. 12), but generally, the template may be extracted from another similar field. To sim-

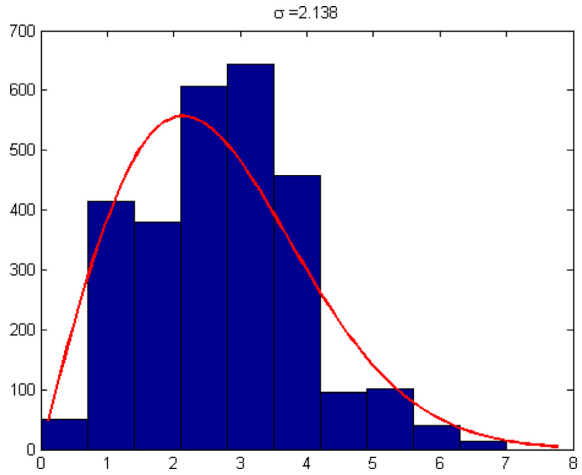

Fig. 15. The histogram of absolute errors (in pixels) of the vortex localization (the bar graph) with the fitted Rayleigh distribution superimposed (the curve).

ulate this, we rotated the template by 30 degrees. The task is to find all vortices of a similar shape regardless of their orientation. The search is performed in the space of the rotation invariants. Unlike the previous experiment, we search for all local minima of ℓ_2-distance below a user-defined threshold.

Such a task definition is rather "soft", because it specifies neither the significance of the vortices to be detected nor the required degree of similarity with the template. As we can see, the results may be controlled by the number/order of the invariants we use.[3]

In Fig. 13, we can see the matching results when only the invariants up to the fourth order have been employed. Almost all vortices, existing in the field, were detected. The detection of the vortices in the bottom row requires special care, because they are flipped comparing to the upper row. The GH invariants are transformed under a mirroring w.r.t. an arbitrary line as

$$\tilde{\Phi}(p,q) = \Phi(p,q)^*. \tag{26}$$

Hence, the real part of $\Phi(p, q)$ keeps its value, but the imaginary part should be taken with an opposite sign. If we want to detect both kinds, the absolute value of the imaginary part should be used.

As we increased the order of the invariants, we identified only those vortices, which are more similar to the template (see Fig. 14). Note that the results does not necessarily form a nested sequence because the degree of similarity may not be monotonic with the order. This process terminated at the order 14, where only a single vortex, the one identical with the template, was found.

The previous experiment was carried out on a single vector field with a few templates. In order to perform an objective error analysis, we used a 300-frame video, showing the time-development simulation of the Kármán street. We used the same vortex template as before and matched it to each frame individually. To ensure independency, no information from the previous frames was used. We employed the GH invariants up to the fourth order. In each frame, the algorithm identified 21 or 22 vortices, which are similar to the template. The video with the vortex tracking is at [42]. To evaluate the accuracy, we measured the localization error of each vortex in each frame. The ground truth positions were deduced from the fluid mechanics theory, which guarantees (under ideal conditions) the equidistant placement of the vortices (this assumption, however, works only in the first half of the street; the second half behaves differently and the ground-truth positions could not be estimated there). The ground-truth positions of the first two vortices were detected manually. We measured the absolute localization errors of all templates in the first half of each frame, so we obtained about 3000 random values, which should exhibit a Rayleigh distribution. We estimated its parameter σ and, consequently, the mean of the absolute errors (see Fig. 15 for the error histogram fitted with the Rayleigh curve). We obtained $\sigma = 2.138$, which yields the mean $m = \sigma\sqrt{\pi/2} = 2.68$. The actual mean localization error is probably even smaller because our Kármán street does not behave exactly as the ideal one and the error we have measured contains not only the localization error but also the error between the ideal and actual Kármán street.

[3] The number of matches may be influenced also by the choice of the threshold. To eliminate this influence, we used thresholds of the same significance in each moment order and the same thresholds in each run of the experiment.

6. Conclusion

The paper introduced rotation invariants of vector fields, which are functions of orthogonal moments. Vector fields behave differently from graylevel and color images under spatial transformations and traditional scalar invariants cannot be efficiently used for recognition.

Although vector-field invariants can be from simple geometric moments [2], in this paper we demonstrated that the use of orthogonal moments provides significantly higher numerical stability than the stability of geometric/complex moment invariants. We tested two popular kinds of orthogonal moments – Gaussian–Hermite and Zernike moments. Although they are distinct from one another in their nature (the GH moments are orthogonal on a square, while the Zernike moments are orthogonal on a disk), both can be employed as the building blocks of the invariants. The stability of the GH invariants was slightly better in our experiments, but the difference was not significant and each kind has its own pros and cons, implied by their different areas of orthogonality. We demonstrated their performance in template matching in a gradient field and in a vortex detection in a fluid flow vector field. Comparing to vector-field invariants from non-orthogonal moments and to scalar image invariants, the proposed technique achieved significantly better results.

The paper was focused solely on rotational invariance. Translational invariance is irrelevant in template matching (it could be ensured by using central moments if needed). Invariance to total scaling of the vector field is formally not difficult to achieve – we can just follow the idea of *variable modulation* of the GH moments, which was proposed for scalar images by Yang et al. [43] and which can be modified for vector fields easily. Dealing with scaled templates brings, however, another problem. Since it is not clear how large the corresponding neighborhood should be, one has to test several sizes in a reasonable interval, which increases the computational time.

Acknowledgments

This work was supported by the National Natural Science Foundation of China (Grant No. 61502389), by the Fundamental Research Funds for the Central Universities (Grant No. 3102015ZY047), by Science Foundation of Ministry of Education (Grant No. G2016001 and No. X2017016), and by Scientific and Technological Project in Shaanxi Province (Grant No. 2016GY-070). It was also supported by the Czech Science Foundation (Grant No. GA15-16928S), and by the Grant Agency of the Czech Technical University (Grant No. SGS15/214/OHK4/3T/14). This work is published under LA-UR-17-26797. It was supported by the National

Nuclear Security Administration (NNSA) Advanced Simulation and Computing (ASC) Program.

We thank Professor Mario Hlawitschka for providing the Kármán vortex street data.

Access to computing and storage facilities owned by parties and projects contributing to the National Grid Infrastructure MetaCentrum provided under the programme "Projects of Large Research, Development, and Innovations Infrastructures" (CESNET LM2015042), is greatly appreciated.

References

[1] A. Goshtasby, Template matching in rotated images, IEEE Trans. Pattern Anal. Mach. Intell. 7 (3) (1985) 338–344.
[2] J. Flusser, T. Suk, B. Zitová, 2D and 3D Image Analysis by Moments, Wiley, Chichester, U.K., 2016.
[3] J. Flusser, On the independence of rotation moment invariants, Pattern Recognit. 33 (9) (2000) 1405–1410.
[4] B. Yang, T. Suk, M. Dai, J. Flusser, 2D and 3D image analysis by Gaussian-Hermite moments, in: G.A. Papakostas (Ed.), Moments and Moment Invariants - Theory and Applications, Gate to Computer Science and Research, Vol. 1, Science Gate Publishing, 2014, pp. 143–173, doi:10.15579/gcsr.vol1.
[5] M.R. Teague, Image analysis via the general theory of moments, J. Opt. Soc. Am. 70 (8) (1980) 920–930.
[6] Å. Wallin, O. Kübler, Complete sets of complex Zernike moment invariants and the role of the pseudoinvariants, IEEE Trans. Pattern Anal. Mach. Intell. 17 (11) (1995) 1106–1110.
[7] P.-T. Yap, X. Jiang, A.C. Kot, Two-dimensional polar harmonic transforms for invariant image representation, IEEE Trans. Pattern Anal. Mach. Intell. 32 (7) (2010) 1259–1270.
[8] M. Schlemmer, M. Heringer, F. Morr, I. Hotz, M.-H. Bertram, C. Garth, W. Kollmann, B. Hamann, H. Hagen, Moment invariants for the analysis of 2D flow fields, IEEE Trans. Vis. Comput. Graph 13 (6) (2007) 1743–1750.
[9] Y.S. Abu-Mostafa, D. Psaltis, Recognitive aspects of moment invariants, IEEE Trans. Pattern Anal. Mach. Intell. 6 (6) (1984) 698–706.
[10] J. Flusser, On the inverse problem of rotation moment invariants, Pattern Recognit. 35 (12) (2002) 3015–3017.
[11] W. Liu, E. Ribeiro, Detecting singular patterns in 2-D vector fields using weighted Laurent polynomial, Pattern Recognit. 45 (11) (2012) 3912–3925.
[12] M. Liu, P.-T. Yap, Invariant representation of orientation fields for fingerprint indexing, Pattern Recognit. 45 (7) (2012) 2532–2542.
[13] R. Bujack, I. Hotz, G. Scheuermann, E. Hitzer, Moment invariants for 2D flow fields using normalization, in: Pacific Visualization Symposium, PacificVis'14, IEEE, 2014, pp. 41–48.
[14] R. Bujack, M. Hlawitschka, G. Scheuermann, E. Hitzer, Customized TRS invariants for 2D vector fields via moment normalization, Pattern Recognit. Lett. 46 (1) (2014) 46–59.
[15] C. Hermite, Sur un nouveau développement en série des fonctions, Vol. 58, Gauthier-Villars, 1864. (in French)
[16] J. Shen, Orthogonal Gaussian-Hermite moments for image characterization, in: D.P. Casasent (Ed.), Intelligent Robots and Computer Vision XVI: Algorithms, Techniques, Active Vision, and Materials Handling, 3208, SPIE, 1997, pp. 224–233.
[17] J. Shen, W. Shen, D. Shen, On geometric and orthogonal moments, Int. J. Pattern Recognit. Artif. Intell. 14 (7) (2000) 875–894.
[18] L. Wang, Y. Wu, M. Dai, Some aspects of Gaussian-Hermite moments in image analysis, in: L.P. Suresh, S.S. Dash, B.K. Panigrahi (Eds.), Third International Conference on Natural Computation ICNC'07, Advances in Intelligent Systems and Computing, Vol. 2, IEEE, 2007, pp. 450–454.
[19] J. Shen, W. Shen, D. Shen, On geometric and orthogonal moments, in: J. Shen, P.S.P. Wang, T. Zhang (Eds.), Multispectral Image Processing and Pattern Recognition, Machine Perception Artificial Intelligence, Vol. 44, World Scientific Publishing, 2001, pp. 17–36.
[20] Y. Wu, J. Shen, Properties of orthogonal Gaussian-Hermite moments and their applications, EURASIP J. Appl. Signal Process. (4) (2005) 588–599.
[21] X. Ma, R. Pan, L. Wang, License plate character recognition based on Gaussian-Hermite moments, in: Second International Workshop on Education Technology and Computer Science ETCS'10, 3, IEEE, 2010, pp. 11–14.
[22] L. Wang, M. Dai, Application of a new type of singular points in fingerprint classification, Pattern Recognit. Lett. 28 (13) (2007) 1640–1650.
[23] S. Farokhi, U.U. Sheikh, J. Flusser, B. Yang, Near infrared face recognition using Zernike moments and Hermite kernels, Inf. Sci. (Ny) 316 (2015) 234–245.
[24] N. Belghini, A. Zarghili, J. Kharroubi, 3D face recognition using Gaussian–Hermite moments, Int. J. Comput. Appl. Special Issue Softw. Eng. Databases Expert Syst. SEDEX (1) (2012) 1–4.
[25] B. Yang, J. Flusser, T. Suk, 3D rotation invariants of Gaussian–Hermite moments, Pattern Recognit. Lett. 54 (1) (2015) 18–26.
[26] B. Yang, J. Flusser, T. Suk, Steerability of Hermite kernel, Int. J. Pattern Recognit. Artif. Intell. 27 (4) (2013) 1–25.
[27] B. Yang, M. Dai, Image analysis by Gaussian–Hermite moments, Signal Process. 91 (10) (2011) 2290–2303.
[28] B. Yang, G. Li, H. Zhang, M. Dai, Rotation and translation invariants of Gaussian-Hermite moments, Pattern Recognit. Lett. 32 (2) (2011) 1283–1298.
[29] B. Yang, J. Flusser, T. Suk, Design of high-order rotation invariants from Gaussian–Hermite moments, Signal Process. 113 (1) (2015) 61–67.
[30] J. Flusser, T. Suk, B. Zitová, Moments and Moment Invariants in Pattern Recognition, Wiley, Chichester, U.K., 2009.
[31] J. Flusser, T. Suk, Rotation moment invariants for recognition of symmetric objects, IEEE Trans. Image Process. 15 (12) (2006) 3784–3790.
[32] R. Bujack, J. Flusser, Flexible basis of rotation moment invariants, in: V. Skala (Ed.), International Conferences in Central Europe on Computer Graphics, Visualization and Computer Vision WSCG'17, 2017.
[33] F. Zernike, Beugungstheorie des Schneidenverfarhens und seiner verbesserten Form, der Phasenkontrastmethode, Physica 1 (7) (1934) 689–704. (in German)
[34] E.C. Kintner, On the mathematical properties of Zernike polynomials, J. Mod. Opt. 23 (8) (1976) 679–680.
[35] A. Prata, W.V.T. Rusch, Algorithm for computation of Zernike polynomials expansion coefficients, Appl. Opt. 28 (4) (1989) 749–754.
[36] S.-K. Hwang, W.-Y. Kim, A novel approach to the fast computation of Zernike moments, Pattern Recognit. 39 (11) (2006) 2065–2076.
[37] J. Gu, H.Z. Shu, C. Toumoulin, L.M. Luo, A novel algorithm for fast computation of Zernike moments, Pattern Recognit. 35 (12) (2002) 2905–2911.
[38] C.-W. Chong, P. Raveendran, R. Mukundan, An efficient algorithm for fast computation of pseudo-Zernike moments, Int. J. Pattern Recognit. Artif. Intell. 17 (06) (2003) 1011–1023.
[39] S.O. Belkasim, M. Ahmadi, M. Shridhar, Efficient algorithm or fast computation of Zernike moments, J. Franklin Inst. 333(B) (4) (1996) 577–581.
[40] K.M. Hosny, Fast computation of accurate Zernike moments, J. Real-Time Image Process. 3 (1) (2010) 97–107.
[41] Wikipedia, https://en.wikipedia.org/wiki/Rayleigh_distribution#cite_note-1 last watch 2017.
[42] B. Yang, J. Kostková, J. Flusser, T. Suk, R. Bujack, 2017a https://drive.google.com/drive/folders/0B7eg_EHhe-jSOHlvWnRLYThhYjg.
[43] B. Yang, J. Kostková, J. Flusser, T. Suk, Scale invariants from Gaussian–Hermite moments, Signal Process. 132 (2017) 77–84.

Bo Yang received the M.Sc. degree in Control Science and Engineering from the Northwestern Polytechnical University, Xi'an, China in 2007, his Ph.D. degree in Image Science from the University of Bordeaux 3, France, in 2012. He was a post-doctoral at the Institute of Information Theory and Automation, Prague, in Czech Republic from 2012 to 2014. Currently, he works as a lecturer in the Northwestern Polytechnical University at Xi'an. His research interests include image processing and pattern recognition with a particular focus on applications of orthogonal polynomials.

Jitka Kostkova received the M.Sc. degree in Applied Mathematical Stochastic Methods from the Czech Technical University, Faculty of Nuclear Science and Physical Engineering, Prague, Czech Republic, in 2015. Currently, she is a PhD student in Mathematical Engineering and tutors undergraduate courses on mathematical analysis at the same university. Jitka Kostkova's research interest is focused on moments and moment invariants.

Jan Flusser received the M.Sc. degree in mathematical engineering from the Czech Technical University, Prague, Czech Republic, in 1985, the Ph.D degree in computer science from the Czechoslovak Academy of Sciences in 1990, and the DrSc. degree in technical cybernetics in 2001. Since 1985 he has been with the Institute of Information Theory and Automation, Czech Academy of Sciences, Prague. In 1995–2007, he was holding the position of a head of Department of Image Processing. Since 2007 he has been a Director of the Institute. He is a full professor of computer science at the Czech Technical University, Faculty of Nuclear Science and Physical Engineering, and at the Charles University, Faculty of Mathematics and Physics, Prague, Czech Republic, where he gives undergraduate and graduate courses on Digital Image Processing, Pattern Recognition, and Moment Invariants and Wavelets. Jan Flusser's research interest covers moments and moment invariants, image registration, image fusion, multichannel blind deconvolution, and super-resolution imaging. He has authored and coauthored more than 200 research publications in these areas, including the monographs *Moments and Moment Invariants in Pattern Recognition* (Wiley, 2009) and *2D and 3D Image Analysis by Moments* (Wiley, 2016). In 2007 Jan Flusser received the Award of the Chairman of the Czech Science Foundation for the best research project and won the Prize of the Academy of Sciences of the Czech Republic for the contribution to image fusion theory. In 2010, he was awarded by the SCOPUS 1000 Award. He received the Felber Medal of the Czech Technical University for excellent contribution to research and education in 2015 and the Academic Premium of the Czech Academy of Sciences for outstanding researchers in 2017.

Tomas Suk received the M.Sc. degree in electrical engineering from the Czech Technical University, Faculty of Electrical Engineering, Prague, Czech Republic, in 1987 and the Ph.D degree in computer science from the Czechoslovak Academy of Sciences in 1992. Since 1991 he has been a researcher with the Institute of Information Theory and Automation, Czech Academy of Sciences, Prague. He has authored 15 journal papers and more than 30 conference papers. Tomas Suk's research interests include digital image processing, pattern recognition, image filtering, invariant features, moment-based and point-based invariants, spatial transformations of images, and applications in remote sensing, astronomy, botany, medicine, and computer vision. In 2002 Tomas Suk received the Otto Wichterle Premium of the Czech Academy of Sciences for excellent young scientists.

Roxana Bujack graduated as M.Sc. in mathematics at Leipzig University in Germany in 2010. Then, she received her B.Sc. and her Ph.D. in computer science in the Image and Signal Processing Group at Leipzig University. She worked as a postdoctoral researcher at IDAV at the University of California, Davis in the USA and at the Computer Graphics and HCI Group at the Technical University Kaiserslautern. Currently, she is a staff scientist in the Data Science at Scale Team at Los Alamos National Laboratory. Her research interests include visualization, pattern recognition, vector fields, moment invariants, Lagrangian flow representations, image processing, big data, and Clifford analysis.

Affine Invariants of Vector Fields

Jitka Kostková, Tomáš Suk, and Jan Flusser, *Senior Member, IEEE*

***Abstract*—Vector fields are a special kind of multidimensional data, which are in a certain sense similar to digital color images, but are distinct from them in several aspects. In each pixel, the field is assigned to a vector that shows the direction and the magnitude of the quantity, which has been measured. To detect the patterns of interest in the field, special matching methods must be developed. In this paper, we propose a method for the description and matching of vector field patterns under an unknown affine transformation of the field. Unlike digital images, transformations of vector fields act not only on the spatial coordinates but also on the field values, which makes the detection different from the image case. To measure the similarity between the template and the field patch, we propose original invariants with respect to total affine transformation. They are designed from the vector field moments. It is demonstrated by experiments on real data from fluid mechanics that they perform significantly better than potential competitors.**

***Index Terms*—Vector field, total affine transformation, affine invariants, template matching, vector field moments.**

I. Introduction

ANALYSIS of *vector fields* has been attracting an increasing attention in last ten years. Vector fields are special kind of multidimensional data, that appear in numerous scientific and engineering areas, such as in mechanical engineering, fluid dynamics, medicine, computer vision, and meteorology. They describe particle velocity, wind velocity, optical/motion flow, image gradient, and other phenomena.

In fluid mechanics, flow fields and their mathematical models (mostly based on Navier-Stokes equations) have been studied for centuries. However, in connection with new devices/techniques producing vector or even tensor field data, such as diffusion tensor imaging, the tasks appeared which seem to be better resolved by signal-processing approach rather than by traditional fluid mechanics.

A typical example of such task is the detection of various patterns of interest. It comprises not only detection of singularities such as vortices, saddle points, vortex-saddle combinations, and double vortices (these could be found by traditional techniques as well), but also detection of arbitrary patterns, which are similar to the patterns stored in the pattern-of-interest database (these patterns may be extracted from similar fields or obtained as a result of a simulation). Since the patterns of interest may not have any special mathematical properties, their detection by traditional tools is questionable or even impossible.

The detection of these patterns can be accomplished by *template matching*, which is a technique widely applied in image processing but relatively new in vector field analysis. The search algorithm evaluates the similarity between the template and a field patch and must be primarily *invariant* with respect to all possible pattern deformations, which might be present (for instance, the template stored in the database may depict a circular vortex, but we want to find also all elliptic vortices of arbitrary size and orientation, which may appear near obstacles and boundaries). Fig. 1 schematically shows the pattern matching in a vector field.

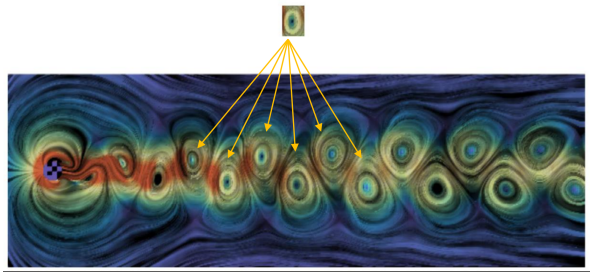

Fig. 1. Vortex detection in a swirling fluid by template matching. The detection method must be invariant to the template deformation.

The main contribution of this paper is the derivation of a new class of vector-field invariants, which are suitable for template matching. We assume the template deformations can be modeled by so called *total affine transformation* (TAFT – see Section II for mathematical description). This assumption is realistic and the underlaying model is reasonably general, but still possible to be handled thanks to its linearity. This problem formulation is original and we are not aware of any other paper, which would come up with a formulation and/or a solution of a similar task. We also introduce *multilayer graphs*, which can represent the invariants and can be employed for their automatic generation and for studying their properties. Showing the connection between the invariants and the multilayer graphs is another significant theoretical contribution of the paper.

The paper is structured as follows. After giving a survey of relevant literature in Section III, we introduce vector field invariants w.r.t. TAFT, composed of the moments of the field, in Section IV. In Section V, we introduce the notion of a multi-layer graph and establish the connection between the invariants and the multi-layer graphs, which helps to understand the structure of the set of invariants. Section VI presents algorithms for generating all graphs that represent the invariants. Since such set is highly redundant, we propose a selection of complete and independent set in Section VII. Finally, in Section VIII we demonstrate the performance and the advantages of these invariants in affine-invariant template matching on simulated and real data.

Jitka Kostková, Tomáš Suk, and Jan Flusser are with the Czech Academy of Sciences, Institute of Information Theory and Automation, Pod vodárenskou věží 4, 182 08 Praha 8, Czech Republic, e-mails: kostkova@utia.cas.cz, suk@utia.cas.cz, flusser@utia.cas.cz

Manuscript received ...; revised .....

II. Vector fields and their transformations

In this section, we formally define a vector field, introduce the notion of its *total transformation* and show how the transformations of "traditional" images and vector fields differ from one another, even if both can be understood as particular cases of total transformations.

Definition 1. A 2D vector field $\mathbf{f}(\mathbf{x})$ is an ordered pair of scalar fields $\mathbf{f}(\mathbf{x}) = (f_1(\mathbf{x}), f_2(\mathbf{x}))$.

At each point $\mathbf{x} = (x, y)$, the value of $\mathbf{f}(\mathbf{x})$ shows the orientation and the magnitude of the measured vector. The scalar field $f_i(\mathbf{x})$ can be understood as a graylevel image which may contain also negative values.[1]

By a total transformation we understand any transformation in the vector field space, which acts simultaneously in spatial and function domains. Even if this definition can be used for arbitrary (non-linear) transformations, in this paper we restrict to linear ones.

Definition 2. Let A and B be regular matrices and $\mathbf{f}$ be a vector field. The transformation $\mathbf{f} \to \mathbf{f}'$, where

$$\mathbf{f}'(\mathbf{x}) = B\mathbf{f}(A^{-1}\mathbf{x}) \tag{1}$$

is called *independent total affine transformation* of the field $\mathbf{f}$. Matrix A is called *inner* transformation matrix (or just inner transformation for short), while matrix B is called *outer* transformation matrix.

The above transformation model does not contain a shift, which is basically for two reasons. The shift in the outer part might occur as a basic flow in the background and can be removed by subtracting the background flow from the entire field. The shift in the inner part, which is independent of the outer shift, may appear in some applications and captures the translation of the field in the plane. In such a case, $A^{-1}\mathbf{x}$ is replaced with $A^{-1}\mathbf{x} + \mathbf{t}$ in the model. However, for pattern detection via template matching it is irrelevant to include the shift into the deformation model, because the shift is the key parameter we want to detect. If, in some other applications, incorporating the shift was desirable, it would be sufficient to replace the moments in the invariants (see Section IV) with central moments related to a properly defined field centroid and we automatically obtain invariants to inner translation.

In reality, vector fields are mostly transformed by a slightly simpler transformation than (1) in which $A = B$. Such a model is called *special total affine transformation* and captures one of the basic properties of vector fields – if the field is transformed in the space domain, the function domain (i.e. the vector values) are transformed *by the same transformation*. The scenarios where $A \neq B$ are rare, but may happen as well if, for instance, the measuring device exhibits different calibrations for inner and outer part. The special transformation can be understood intuitively. Let us imagine the vector field as an array of arrows. If we deform spatially the array, the absolute orientation and length of the arrows must be changed accordingly such that their relative orientation and length is preserved (see Fig. 2 for an example).

This is the principal difference between "true" vector fields and images. Traditional images can be viewed as particular cases of vector fields, where the number of components equals the number of the spectral bands. Most often, they are transformed with $B = I$, where I is an identity matrix, and the transformation is purely spatial. The total transformation model can also capture the spatial transformation accompanied by contrast changes of individual channels (when B is diagonal different from I) or by spectral mixing (when B is not diagonal). However, the situations when B is not diagonal are rare for traditional images and in any case, there is absolutely no reason why B should be the same as A.

In the theory of invariants, it is well known that the set of all admissible transformations, with respect to which we want to design invariants, must form a *group* or at least a *semi-group* (see, for instance, [1] or [2] for explanation). In particular, the transformations must exhibit the *closure property* – the composition of two arbitrary transformations must be again a transformation within the given set. The set of all independent total affine transformations is closed under composition. To see this, consider two such transformations given by matrices $A_i, B_i; i = 1, 2$, which have been applied consecutively to a vector field. The result is equivalent to applying a single independent total affine transformations with matrices $A = A_2A_1$ and $B = B_2B_1$. The closure property is preserved, if we consider special total affine transformations only. Both transformations are invertible and contain a unit element (identity transformation). Hence, both sets are groups (but not Abelian groups as matrix multiplication is not commutative).

III. Literature survey

Although affine invariants of vector fields have never been studied, we still found several inspiring papers that formed the background of our current work. They fall basically into two categories: papers on rotation invariants of vector fields and papers on affine invariants of scalar and color images.

The problem of finding vector field invariants to total rotation was raised for the first time relatively recently by Schlemmer et al. [3], who adapted the scalar moment invariants proposed by Mostafa and Psaltis [4] and Flusser [5], [6] and designed invariants composed of geometric complex moments of the field. Schlemmer et al. used these invariants to detect specific patterns in a turbulent swirling jet flow. Rotation invariants from geometric complex moments have found several applications. Liu and Ribeiro [7] used them, along with a local approximation of the vector field by a polynomial, to detect singularities on meteorological satellite images showing wind velocity. Basically the same kind of rotation invariants were used by Liu and Yap [8] for the indexing and recognition of fingerprint images. A generalization to more than two dimensions using tensor contraction was proposed by Langbein and Hagen [9]. Bujack et al. [10], [11] studied the invariants of complex moments thoroughly, generalized the previous works, and showed that the invariants can be derived also by means

[1] Apart from 2D vector fields, there exist also 3D vector fields, matrix fields, and tensor fields. The study of these more general fields is beyond the scope of this paper.

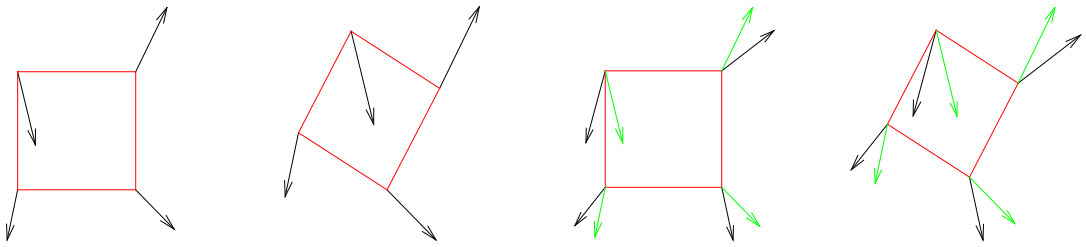

Fig. 2. Vector field transformations: (a) an original vector field, (b) its inner affine transformation, (c) its outer affine transformation, (d) its special total affine transformation. The green arrows in (c) and (d) show the vector field without the outer transformation.

of the field normalization approach. Yang et al. improved the numerical stability of the invariants by using orthogonal Gaussian-Hermite [12] and Zernike [13] moments instead of the geometric ones. Most recently, Bujack [14] introduced so-called flexible basis of the invariants to avoid moments that vanish on the given templates. In all these papers, the authors considered the total rotation model only. The gap between total rotation and total affine transformation is so big that almost nothing from the referenced papers can be used or adapted to derive invariants w.r.t. total affine transformation.

Apart of the above methods, which all were more or less inspired by signal processing and approached a vector field as a specific multi-valued image, we can find several "non-image methods in flow analysis for detecting singularities. Comparing to the signal-based methods, they suffer from several limitations. The most serious one is that they were designed for detection of singularities only and cannot detect arbitrary templates. Majority of the existing methods concerns with the detection of vortices, other methods are able to detect foci, stable points or nodes. Vortex detection methods mostly compute the curl of the flow field, which characterizes vortices. Almost all methods for detection of other singularities calculate the gradient of the flow velocity and locally calculate the eigenvalues of the underlying tensor. The criterion "vortex/focus/node/..." is evaluated from these eigenvalues, differently in each individual method. They are not affine-invariant and cannot be easily generalized to this invariance, because intrinsically assume circular shape of the vortices. Some of those methods assume (at least implicitly) that the flow is ruled by Navier-Stokes equations. This is, however, not generally true for gradient fields and optical flow fields. Many methods of this kind can be found in the literature. A good survey of vorticity measures based on the determinant and trace of the flow velocity gradient tensor is given in [15], where the method of helicity [16], swirl parameter method [17], λ_2 method [18], Predictor-Corrector method [19], parallel vectors method [20], and streamline method [21] are reviewed and compared. Chen [22] describes various criteria (vorticity measures) for detection of vortices and their simplification in planar flow – Delta-criterion, λ_{ci} criterion, Q criterion, and λ_2 criterion (we use this method in the experimental section for comparison).

Comparing to the above group of papers on vector field rotation invariants, *affine moment invariants* (AMIs) of graylevel images have been studied in hundreds of papers and books in the last 100 years.[2] They can be traced back to the end of the 19th century, to the times when neither computers nor automatic object recognition existed. Probably the first one who systematically studied invariants to affine transformation was the famous German mathematician David Hilbert. He did not work explicitly with moments but studied so called *algebraic invariants* [23]. The algebraic invariants are polynomials of coefficients of a binary form, which are invariant w.r.t. an affine transformation. Hilbert had many followers, who elaborated the traditional theory of algebraic invariants in the late 19th and early 20th century, see for instance [24]–[28]. The algebraic invariants are closely linked with the AMIs through the *Fundamental theorem of the AMIs*, formulated (unfortunately incorrectly) by Hu [29] in 1962. Through this link, the core of the Hilbert's work can be adapted to moments in a relatively straightforward way. The Fundamental theorem of the AMIs was later corrected by Reiss [30] and Flusser and Suk [31]. Since then, several new methods of deriving AMIs have appeared. They differ from each other in the mathematical tools used. One may use graph theory as was proposed in [32], [33], tensor algebra [34], direct solution of proper partial differential equations [35], transvectants [36], and derivation via image normalization [37]. The resulting AMIs achieved by all these approaches are theoretically equivalent, because there exists a polynomial one-to-one mapping between any two AMI sets. However, differences can be found in complexity of the derivation and in numerical properties of the respective AMI's.

Special AMIs were proposed for color images [38]–[42], where the between-channel bond and various kinds of linear color changes were considered together with the spatial affine transformation.

IV. Construction of VFAMIs

In this section, we propose *vector field moment invariants w.r.t. total affine transformation* (VFAMIs). The invariants, which we are going to construct, are functions of geometric moments of the field. In case of a 2D vector field $\mathbf{f}$ with the

[2]There exist also many affine invariants, which are not based on moments, but they are irrelevant for this work, so we do not mention them here.

components f_1 and f_2 we may use standard geometric scalar moments [1], [2] given as

$$m_{pq}^{(i)} = \int_{-\infty}^{\infty}\int_{-\infty}^{\infty} x^p y^q f_i(x,y)\,\mathrm{d}x\,\mathrm{d}y\,. \tag{2}$$

Let us for simplicity assume that $\mathbf{f}$ is compactly supported and both f_i are piecewise continuous. Under these assumptions, all moments $m_{pq}^{(i)}$ of indices $p, q = 0, 1, 2, \ldots$ are well-defined and completely characterize the field $\mathbf{f}$.

A. Invariants to inner transformation

Let us first construct the VFAMIs for the particular case of $B = I$ (this is essentially the problem of AMIs for two-band images). We start by constructing the AMIs for components f_1 and f_2 separately. To do so, we use the method proposed in [32] and further elaborated in [33], which guarantees to produce a complete set.

Let us consider two arbitrary points $\mathbf{x}_1 = (x_1, y_1)$, $\mathbf{x}_2 = (x_2, y_2)$ from the support of $\mathbf{f}$. Let us denote the "cross-product" of these points as C_{12}:

$$C_{12} = x_1 y_2 - x_2 y_1\,.$$

Geometric meaning of C_{12} is the oriented double area of the triangle, whose vertices are (x_1, y_1), (x_2, y_2), and $(0, 0)$. After an affine transformation $\mathbf{x}' = A\mathbf{x}$ has been applied, the cross-product is transformed as $C'_{12} = J_A \cdot C_{12}$, where $J_A = \det(A)$ is the Jacobian of the transformation. This proves that C_{12} is a relative invariant with respect to inner transformation A. Now we consider various numbers of points (x_i, y_i) and we integrate their cross-products (or some integer powers of their cross-products) over the support of $\mathbf{f}$. These integrals can be expressed in terms of moments and, after eliminating the Jacobian by a proper normalization, they yield absolute affine invariants.

More precisely, having $r > 1$ distinct points (x_1, y_1), $\cdots$, (x_r, y_r), we define functional I of scalar f depending on r and on non-negative integers n_{kj} as

$$I(f) = \int_{-\infty}^{\infty}\cdots\int_{-\infty}^{\infty} \prod_{k,j=1}^{r} C_{kj}^{n_{kj}} \cdot \prod_{i=1}^{r} f(x_i, y_i)\,\mathrm{d}x_i\,\mathrm{d}y_i\,. \tag{3}$$

Note that it is meaningful to consider only $j > k$, because $C_{kj} = -C_{jk}$ and $C_{kk} = 0$.

After an inner affine transformation we have $f'(\mathbf{x}) = f(A^{-1}\mathbf{x})$ and $I(f')$ becomes

$$\begin{aligned} I(f') &= \int_{-\infty}^{\infty}\cdots\int_{-\infty}^{\infty} \prod_{k,j=1}^{r} C_{kj}^{n_{kj}} \cdot \prod_{i=1}^{r} f(A^{-1}\mathbf{x}_i)\,\mathrm{d}x_i\,\mathrm{d}y_i = \\ &= \int_{-\infty}^{\infty}\cdots\int_{-\infty}^{\infty} \prod_{k,j=1}^{r} (C_{kj}^{n_{kj}})' \cdot \prod_{i=1}^{r} f(x_i, y_i)|J_A|^r\,\mathrm{d}x_i\,\mathrm{d}y_i = \\ &= J_A^w |J_A|^r \cdot I(f)\,, \end{aligned} \tag{4}$$

where $w = \sum_{k,j} n_{kj}$ is the *weight* of the invariant and r is its *degree*. Hence, $I(f)$ is a relative affine invariant, too. If $I(f)$ is normalized by m_{00}^{w+r}, we obtain a desirable absolute affine invariant

$$\left(\frac{I(f)}{m_{00}^{w+r}}\right)' = \left(\frac{I(f)}{m_{00}^{w+r}}\right) \tag{5}$$

(if w is odd and $J < 0$ the sign change occurs in Eq. (5)). If we expand the integrand in Eq. (3) and integrate term-wise, we obtain an expression of I in terms of geometric moments of f. Varying r and n_{kj}, we can generate infinitely many invariants of all orders. Such a set is complete but highly redundant. The process of eliminating reducible invariants is described in [33].

The invariants from Eq. (5) can be derived separately for both field components f_1 and f_2. In addition to that, we can further employ the fact that transformation A is the same for both components, which brings a possibility of constructing *joint invariants* (i.e. those containing moments of both f_1 and f_2 at the same invariant). This idea was proposed in [38] in the context of invariants for color images and slightly increases the number of independent invariants.

For the sake of completeness, it should be mentioned that Eq. (3) may be formulated in a more general way as

$$I(f) = \int_{-\infty}^{\infty}\cdots\int_{-\infty}^{\infty} \prod_{k,j=1}^{r} C_{kj}^{n_{kj}} \cdot \prod_{i=1}^{r} f^{v_i}(x_i, y_i)\,\mathrm{d}x_i\,\mathrm{d}y_i\,, \tag{6}$$

where v_i are arbitrary powers. Eqs. (4) and (5) still hold (note that the normalization in (5) does not depend on v_i). However, the integration of (3) does not lead to moments of f but generally to moments of f^{v_i}. This is highly redundant, because the *moment uniqueness theorem* (see [2] for instance) assures that all moments of any f^{v_i} can be calculated from the moments of f. Hence, using $v_i \neq 1$ in (3) is generally useless and we do not follow that approach in this paper (it might be justifiable only if we confine ourselves to a few low moment orders, where the redundancy is weak, as for instance did the authors in [39], [40]).

B. Invariants to outer transformation

If $B \neq I$, it is not easy to extend the "inner" invariants from the previous section. The exception is when B is diagonal, so the components f_1 and f_2 are not mixed together. This is not realistic for "true" vector fields, but this model was studied in the connection with color images of indoor scenes, underlaying photometric transformation due to a varying illumination [43], [44]. If B is diagonal, the invariants (3) of the component f_i are just multiplied by B_{ii}^r. This multiplication factor can be eliminated by taking a ratio of two invariants of the same r or by a ratios of proper powers of two arbitrary invariants.

Now let us consider arbitrary regular B, but assume for simplicity that $A = I$, so only an outer transformation of the vector field is effective. We proceed analogously to the previous section. The role of C_{kj} has been taken over by "component cross-products" F_{kj}

$$F_{kj} = f_1(x_k, y_k) f_2(x_j, y_j) - f_1(x_j, y_j) f_2(x_k, y_k)\,.$$

F_{kj} is a relative invariant w.r.t. outer affine transformation as

$$F'_{kj} = J_B \cdot F_{kj}\,,$$

where $J_B = \det(B)$ (see Appendix A for the proof). The simplest moment invariants are given as

$$O_{pqst}(\mathbf{f}) = \int_{-\infty}^{\infty} \cdots \int_{-\infty}^{\infty} x_1^p y_1^q x_2^s y_2^t F_{12}\, \mathrm{d}x_1\, \mathrm{d}x_2\, \mathrm{d}y_1\, \mathrm{d}y_2\,, \quad (7)$$

which yields, after the term-wise integration, the moment form

$$O_{pqst}(\mathbf{f}) = m_{pq}^{(1)} m_{st}^{(2)} - m_{st}^{(1)} m_{pq}^{(2)}\,. \quad (8)$$

The relative invariance property $O_{pqst}(\mathbf{f'}) = J_B \cdot O_{pqst}(\mathbf{f})$ follows immediately from the same of F_{12}. Eq. (8) yields a non-trivial invariant for arbitrary combinations of indexes except $(p,q) = (s,t)$ (note that $O_{pqpq}(\mathbf{f}) = 0$ for any p, q, and $\mathbf{f}$). Swapping of the indexes $(p,q) \leftrightarrow (s,t)$ just changes the sign as $O_{pqst}(\mathbf{f}) = -O_{stpq}(\mathbf{f})$ and does not yield an independent invariant. Hence, using all non-trivial configurations of indexes p, q, s, t up to the given order R, we obtain $R(R+1)(R+2)(R+3)/8$ invariants of the form(8). Since there exist only $(R+1)(R+2)$ moments, it is clear that the set of invariants is redundant and must contain dependent invariants. Since the outer transformation has four degrees of freedom, the number of independent invariants is at most $(R+1)(R+2)-4$. Although the number of the invariants (8)) is higher for any $R > 0$, it is not automatically guaranteed that they are complete.

To prove the completeness, we show that from the knowledge of all invariants of the form (8) we can recover all moment values, except four freely chosen moments the value of which may be arbitrary. Let us assume there exists at least one invariant such that $O_{pqst} \neq 0$ (if this is not the case, then $f_1 = \alpha f_2$, all invariants (8) vanish, and $\mathbf{f}$ is called a *coupled field*). Choose indexes a, b arbitrary such that $(a,b) \neq (p,q)$ and $(a,b) \neq (s,t)$ and solve the system

$$\begin{aligned} m_{pq}^{(2)} m_{ab}^{(1)} - m_{pq}^{(1)} m_{ab}^{(2)} &= O_{abpq} \\ m_{st}^{(2)} m_{ab}^{(1)} - m_{st}^{(1)} m_{ab}^{(2)} &= O_{abst} \end{aligned} \quad (9)$$

for $m_{ab}^{(1)}$ and $m_{ab}^{(2)}$. The determinant of the system equals O_{pqst}, which means the system is regular and unambiguously solvable, regardless of particular values of $m_{pq}^{(1)}, m_{pq}^{(2)}, m_{st}^{(1)}$, and $m_{st}^{(2)}$, which may be chosen freely. Keeping their choice fixed, this process is repeated for all admissible couples (a,b). In this way we recover all moments of the field from its invariants, up to the four degrees of freedom due to the transformation matrix B.

Invariants to outer transformation of a field can also be obtained in a general form analogous to Eq. (6) as

$$O(f) = \int_{-\infty}^{\infty} \cdots \int_{-\infty}^{\infty} \prod_{k,j=1}^{r} F_{kj}^{v_{kj}} \cdot \prod_{i=1}^{r} x_i^{p_i} y_i^{q_i}\, \mathrm{d}x_i\, \mathrm{d}y_i\,, \quad (10)$$

which leads to relative invariants given by

$$O(\mathbf{f'}) = J_B^v \cdot O(\mathbf{f})\,,$$

where $v = \sum v_{kj}$. However, in the case of pure outer transformation this is useless. Since Eq. (8) generates a complete set of invariants by itself, any additional invariant designed by Eq. (10) is a function of them and does not carry any independent information.

Summarizing this section, we proved that Eq. (8) constitutes relative invariants w.r.t. outer transformation of a vector field. We proved they form a complete system. Absolute invariants are obtained as a ratio of any two non-trivial relative invariants (8). We also showed that the only vector fields laying in the joint null-space of the invariants are coupled fields, which must be handled separately and described by other invariants.

C. Invariants to total transformation

In this section, we go to the core of the problem. We show how to put the inner and outer invariants together and we propose vector field invariants w.r.t. total affine transformation. The key definition, analogous to (6) and (10), is now

$$V(\mathbf{f}) = \int_{-\infty}^{\infty} \cdots \int_{-\infty}^{\infty} \prod_{k,j=1}^{r} C_{kj}^{n_{kj}} \cdot F_{kj}^{v_{kj}} \cdot \prod_{i=1}^{r} \mathrm{d}x_i\, \mathrm{d}y_i\,. \quad (11)$$

$V(\mathbf{f})$ is a relative invariant as

$$V(\mathbf{f'}) = J_B^v J_A^w |J_A|^r V(\mathbf{f})\,. \quad (12)$$

To eliminate J_A and J_B and obtain an absolute invariant, we have to normalize the relative invariant (11) by proper powers of other two relative invariants such that both Jacobians get canceled[3].

If used extensively with many various parameters, Eq. (11) yields a huge number of redundant invariants. The first step to eliminate the redundancy is to fulfill the constraint that $V(\mathbf{f})$ must be composed solely of moments of the field $\mathbf{f}$. This is equivalent to the constraints imposed on the powers v_{kj}. Considering all possible index pairs (k,j), each of the points $(x_1, y_1), \ldots, (x_r, y_r)$ must be involved just once in all F_{kj}'s used. Hence, any v_{kj} can only equal 0 or 1, $v = r/2$ (which immediately implies that r must be even), and $v_{kj} = 0$ for all $k \geq j$ (this constraint is because $F_{kj} = -F_{jk}$ and $F_{kk} = 0$, so it would be useless to include them into the invariant). If $v_{kj} = 1$, then $v_{mj} = v_{jm} = v_{km} = v_{mk} = 0$ for all index pairs different from (k,j).

We may notice, that generating VFAMIs from Eq. (11), even if the choice of v_{kj} has been constrained as mentioned above, leads to many invariants, which are identically zero or which are somehow dependent on the other invariants that have been obtained from Eq. (11)) with other settings of the parameters. For instance, the simplest ever choice of $r = 2, v_{12} = 1$ and $n_{12} = 0$ yields a vanishing invariant; the same is true for $r = 2, v_{12} = 1, n_{12} = 2$ and for many other choices with higher r (the setting of $r = 4, v_{14} = v_{23} = 1$ and $n_{12} = n_{13} = n_{24} = n_{34} = 1, n_{kj} = 0$ otherwise, is an example leading to another vanishing invariant). As an example of a simple dependency, we may choose $r = 4, v_{12} = v_{34} = 1, n_{12} = n_{34} = 1, n_{kj} = 0$ otherwise, which leads to invariant $V(\mathbf{f}) = V_a^2$. Another example is the setting $r = 4, v_{12} = v_{34} = 1, n_{12} = 3, n_{34} = 1, n_{kj} = 0$ otherwise, which yields $V(\mathbf{f}) = V_a V_b$ (see below for explicit forms of V_a and V_b). Dependent invariants do not

[3]Unlike scalar AMIs, we cannot normalize by a power of m_{00} because m_{00} is not a relative invariant w.r.t. the total affine transformation.

contribute to the recognition power of the system and only increase the dimensionality of the invariant set. It is highly desirable to identify them and exclude them from the set. An algorithm for detection of dependent invariants is proposed in Section VII.

As an example, we show four simple VFAMIs in explicit forms below; hundreds of other invariants generated from Eq. (11) can be found on our webpage zoi.utia.cas.cz/affine-vector-fields.

The simplest non-trivial choice is $r = 2$ and $n_{12} = v_{12} = 1$, which yields

$$V_a = m_{10}^{(1)} m_{01}^{(2)} - m_{10}^{(2)} m_{01}^{(1)} .$$

The choice of $r = 2, v_{12} = 1$ and $n_{12} = 3$ yields

$$V_b = m_{30}^{(1)} m_{03}^{(2)} - 3m_{21}^{(1)} m_{12}^{(2)} + 3m_{12}^{(1)} m_{21}^{(2)} - m_{03}^{(1)} m_{30}^{(2)} .$$

The parameters $r = 2$, $v_{12} = 1$ and $n_{12} = 5$ lead to the invariant

$$\begin{aligned} V_c \;=\; & m_{50}^{(1)} m_{05}^{(2)} - 5m_{41}^{(1)} m_{14}^{(2)} + 10m_{32}^{(1)} m_{23}^{(2)} \\ & -10m_{23}^{(1)} m_{32}^{(2)} + 5m_{14}^{(1)} m_{41}^{(2)} - m_{05}^{(1)} m_{50}^{(2)} . \end{aligned}$$

If we choose $r = 4$, $v_{12} = v_{34} = 1$ and $n_{12} = n_{13} = n_{24} = n_{34} = 1$, $n_{kj} = 0$ otherwise, we obtain

$$\begin{aligned} V_d \;=\; & -(m_{20}^{(1)})^2 (m_{02}^{(2)})^2 + 4m_{20}^{(1)} m_{11}^{(1)} m_{11}^{(2)} m_{02}^{(2)} \\ & +2m_{20}^{(1)} m_{02}^{(1)} m_{20}^{(2)} m_{02}^{(2)} - 4m_{20}^{(1)} m_{02}^{(1)} (m_{11}^{(2)})^2 \\ & -4(m_{11}^{(1)})^2 m_{20}^{(2)} m_{02}^{(2)} + 4m_{11}^{(1)} m_{02}^{(1)} m_{20}^{(2)} m_{11}^{(2)} - \\ & (m_{02}^{(1)})^2 (m_{20}^{(2)})^2 . \end{aligned}$$

If the vector field in question is a coupled field, all invariants generated from Eq. (11) obviously vanish. In such a case, we use only the first component of the field and treat it as a scalar image undergoing spatial affine transformation and contrast stretching. Any ratio of absolute scalar AMIs (5) of the same degree r and weight w yields a desired invariant.

D. Invariants to special total transformation

As we already explained, the inner and outer transformations of a vector field are often the same, i.e. $A = B$ and Eq. (12) is simplified to the form

$$V(\mathbf{f}') = J_A^{w+r/2} |J_A|^r V(\mathbf{f}) . \tag{13}$$

The normalization can be accomplished just by one invariant, while the other one, which was needed to cancel J_B before, can be saved for recognition. This is, however, not the only difference. Since the number of degrees of freedom of the transformation has been reduced from eight to four, one may expect the existence of four additional independent invariants.

For a special total transformation, there exists yet another possibility how to generate invariants. We can replace the "intensity cross-product" F_{kj} by the "mixed cross-product"

$$D_{kj} = y_j f_1(x_k, y_k) - x_j f_2(x_k, y_k) .$$

D_{kj} is a relative invariant w.r.t. special total transformation as

$$D'_{kj} = J_A \cdot D_{kj}$$

(see Appendix B for the proof). Unlike the previous case, here generally D_{kj} and D_{jk} are independent, and $D_{kk} \neq 0$.

Similarly to Eq. (11), we define functional

$$W(\mathbf{f}) = \int_{-\infty}^{\infty} \cdots \int_{-\infty}^{\infty} \prod_{k,j=1}^{r} C_{kj}^{n_{kj}} \cdot D_{kj}^{u_{kj}} \cdot \prod_{i=1}^{r} \mathrm{d}x_i \, \mathrm{d}y_i , \tag{14}$$

which is a relative invariant because

$$W(\mathbf{f}') = J_A^{w+u} |J_A|^r W(\mathbf{f}) . \tag{15}$$

Eq. (14) leads to moments only under certain restrictions, imposed on exponents u_{kj}. Each of the points $(x_1, y_1), \ldots, (x_r, y_r)$ must be involved just once as a field argument in all D_{kj}'s used. Hence, any u_{kj} can only equal 0 or 1 and $u \equiv \sum u_{kj} = r$.

We may go even further and generate invariants of the form

$$Z(\mathbf{f}) = \int_{-\infty}^{\infty} \cdots \int_{-\infty}^{\infty} \prod_{k,j=1}^{r} C_{kj}^{n_{kj}} \cdot F_{kj}^{v_{kj}} \cdot D_{kj}^{u_{kj}} \cdot \prod_{i=1}^{r} \mathrm{d}x_i \, \mathrm{d}y_i . \tag{16}$$

In this case, however, the constraints on v and u are different from the previous cases and are linked together. It still holds that each point (x_i, y_i) must appear just once as a field argument in the integrand. Hence, $2v+u = r$. Any v_{kj} and u_{kj} can only equal 0 or 1 as before, but they are further constrained as follows. If $v_{kj} = 1$, then $v_{mj} = v_{jm} = v_{km} = v_{mk} = 0$ for all index pairs except (k, j) and $u_{km} = u_{jm} = 0$ for any m. If $u_{kj} = 1$, then $u_{km} = 0$ for any $m \neq j$ and $v_{km} = v_{mk} = 0$ for any m.

Z is again a relative invariant, since

$$Z(\mathbf{f}') = J_A^{w+v+u} |J_A|^r Z(\mathbf{f}) . \tag{17}$$

It should be, however, noted, that each of the sets generated by Eqs. (11), (14), and (16) is highly redundant even on its own, and this redundancy increases, if two or all three sets are used together. Actually, the invariants obtained from Eqs. (11) and (14) are nothing but a subset of those obtained from Eq. (16). Careful selection of independent (or at least irreducible) invariants is highly recommended for practical applications. Section VII presents a selection algorithm.

V. VFAMIs and multi-layer graphs

In this section, we establish the correspondence between VFAMIs generated by Eqs. (11), Eq. (14) and (16) and *multi-layer graphs*. The representation by multi-layer graphs helps to understand the structure of the VFAMIs and is also useful for elimination of reducible invariants. We start with the definition of multi-layer graphs.

Definition 3. Let $\mathcal{V}$ be a set of vertices (nodes) and $E_1, E_2, \ldots, E_m$ be sets of edges. An ordered $(m+1)$-tuple $G = (\mathcal{V}; E_1, E_2, \ldots, E_m)$ is called a *multi-layer graph* on $\mathcal{V}$. Graph $G_k = (\mathcal{V}; E_k)$ is called the *k-th layer* of graph G. If $m = 2$, G is called a *bi-layer graph*. If there exists a layer G_k, which is a multigraph (i.e. which contains multiple edges), then G is called *multi-layer multigraph*.

Definition 4. Let $G = (\mathcal{V}; E_1, E_2, \ldots, E_m)$ be a multi-layer (multi)graph. Ordinary (multi)graph $U_G = (\mathcal{V}; E_1 \cup E_2 \cup \ldots \cup$

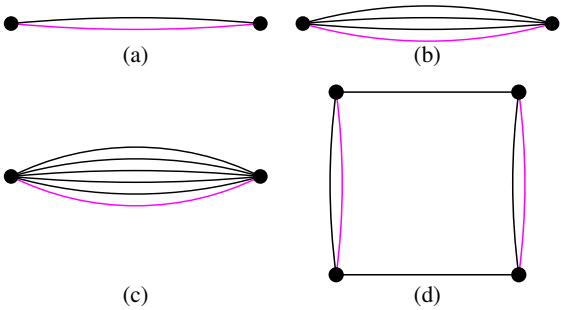

Fig. 3. The graphs representing invariants V_a, V_b, V_c, and V_d. The edges belonging to E_1 are shown in black, magenta edges belong to E_2.

E_m) is called a *union* of G. G is called *connected multi-layer graph* if U_G is a connected graph.

Multi-layer graphs serve in many areas for modelling different network layers on the same set of nodes. The edges of different layers may be totally independent or there may be a kind of band among them.

An arbitrary invariant generated by Eq. (11) can be represented by a bi-layer graph as follows. Each point (x_k, y_k) corresponds to a graph node, so we have r nodes. Each cross-product C_{kj} corresponds to n_{kj} edges of the first layer connecting the kth and jth nodes (generally, the first layer is a multigraph). The second layer is constructed in a similar way – each intensity cross-product F_{kj} corresponds to v_{kj} edges (note that v_{kj} can only be zero or one). In Fig. 3, we can see the graphs representing invariants V_a, V_b, V_c, and V_d from Section IV.C. More examples of representation graphs can be found in Appendix C.

We can immediately make several simple statements about the bi-layer graphs than represent VFAMIs from Eq. (11).

1) The number of nodes is even.
2) In G_2, all nodes have degree one. If $r > 2$, then G_2 is not a connected graph.
3) Neither layer is a directed graph.
4) Neither layer contains self-loops.
5) If G is not connected, then the corresponding invariant is a product of several simpler invariants, which correspond to each connected component of G.
6) Any invariant of the form (11) is in fact a sum, where each term is a product of r moments. The order of the moments is preserved in all terms (for instance in V_4, there are always four moments of the second order in each term). The moment orders contained in a single term are the same as the degrees of all vertices in G_1.

The proof of all above statements follows immediately from Eq. (11) and from the definition of the corresponding graphs. We can see that the problem of generating all invariants is equivalent to finding all connected bi-layer graphs, satisfying the constraints 1–4.

Now let us assume the affine transformation is special one and consider the mixed invariants generated by Eq. (16). They can be represented by *three-layer graphs*, where the first two layers correspond to cross-products C_{kj} and F_{kj}, respectively, as before. The third layer G_3 corresponds to mixed cross-products D_{kj}. G_3 is a *directed* graph because D_{kj} and D_{jk} are different and we have to distinguish between them. We define the "direction" of the edge corresponding to D_{kj} as from (x_k, y_k) to (x_j, y_j). It is easy to prove the following simple statements, they follow from Eq. (16) and from the way how the graph has been constructed.

1) The number of nodes may be arbitrary.
2) G_3 may contain loops, self-loops and double edges (with reverse direction).
3) In G_3, we define the *outdegree* of the vertex as the number of "tail" edge ends adjacent to this vertex. The *indegree* is the number of "head" edge ends adjacent to the vertex. The outdegree of any vertex is less or equal one. The indegree of any vertex may be arbitrary from zero to u.
4) Consider graph $(\mathcal{V}; E_2 \cup E_3)$. For each vertex, the sum of its degree in E_2 and its outdegree in E_3 is called the *cumulative degree*. The cumulative degree always equals one.
5) If there are two or more edges in E_2, then $(\mathcal{V}; E_2 \cup E_3)$ is not a connected graph. If there is one or no edge in E_2, then $(\mathcal{V}; E_2 \cup E_3)$ may or may not be connected.

Examples of representation graphs of this kind can be found in Appendix D.

The established correspondence between the invariants and the graphs can be efficiently used to generate the invariants. Instead of working directly with Eqs. (11) and (16) all trying all possible point pairs and parameter combinations, it is sufficient to generate all multi-layer graphs satisfying the constraints presented above. In the next section, we present an algorithm for a systematic graph generation.

VI. Generating the Representation Multi-Layer Graphs

The algorithms for generating the graphs, which represent invariants V_i (11) and Z_i (16) are similar in main principles and differ from one another in details (yet important ones) only. We start with an algorithm that generates invariants V_i (11).

The task is to generate all bi-layer graphs satisfying the constraints. Each layer is generated separately. The graph nodes are numbered from 1 to r. The main idea is to begin with a graph that have the node labels as low as possible and then successively increase the node labels until the last possible graph has been reached.

To generate all possible first layers with w edges, we start with the graph on two nodes with a w-multiple edge connecting them. Matrix representation of such graph is

$$\begin{pmatrix} 1 & 1 & \dots & 1 & 1 \\ 2 & 2 & \dots & 2 & 2 \end{pmatrix}, \tag{18}$$

where the column $\begin{matrix} 1 \\ 2 \end{matrix}$ means an edge connecting the nodes 1 and 2. The "last" graph, on which the algorithm should stop, is

$$\begin{pmatrix} 1 & 2 & 3 & 4 & \dots & w-2 & w-1 & w-1 \\ 2 & 3 & 4 & 5 & \dots & w-1 & w & w \end{pmatrix}. \tag{19}$$

Starting from the first graph, we iterate the algorithm shown in Fig. 4.

To generate the second layer, we proceed analogically with some modifications. The first graph is now

$$\begin{pmatrix} 1 & 3 & \dots & r-3 & r-1 \\ 2 & 4 & \dots & r-2 & r \end{pmatrix}, \tag{20}$$

As we already explained, r must be even and the representation matrix has $r/2$ columns. The inner loop of the algorithm must be modified, too. The criterion, if a matrix element can be increased, is not its comparison with the final graph, but the test, if there is a non-used node.

1) Set k to $r-1$, it is the last but one edge.
2) Test the second node of the kth edge. If there is a node with higher label, set it; otherwise decrease k by one.
3) If k is zero, no other graph can be generated. Stop.
4) Assign the free nodes to the edges behind k.
5) got to 2).

The generating algorithm of Z_i is in principle analogical to the previous one. Modifications are required when generating E_3 edges because the third layer is a directed graph, self-loops are allowed and there is a strong constraint on a cumulative $E_2 - E_3$ degree of each vertex. Since these modifications are rather technical ones, we do not describe this algorithm in detail.

A complete description of the algorithms for generating of both V_i and Z_i, including commented codes, can be found on http://zoi.utia.cas.cz/affine-vector-fields. On the same website, the reader may find extensive collections of the invariants (explicit formulas along with the representation graphs) – 6323 invariants of type Z_i and 1890 invariants of type V_i. On http://zoi.utia.cas.cz/Afintensors, we made available the software by means of which these invariants were generated. The software is in C++, has a user-friendly GUI and a detailed manual, so the readers may generate their own collections of the invariants with various parameters.

VII. Selection of a complete and independent set of the invariants

In an ideal case, any feature set for object recognition should be complete and independent. The completeness means that the object can be precisely reconstructed (modulo the intra-class transformation group) from the values of the invariants and guarantees the maximum possible discrimination power. The independence ensures that the invariants do not contain any redundant information. The features are called dependent, if some of them is a function of the others; otherwise they are independent. While the independence is always desirable to keep the feature space dimensionality low, the completeness may not be necessary. In most practical cases, the objects in question can be discriminated from each other by a small incomplete subset.

Both the invariants V_i (11) and Z_i (16) form theoretically complete sets, if all possible parameter settings have been used. In reality, when the invariants are generated by the algorithms described in the previous section, we are always limited by the maximum number of edges w and that of nodes r, which leads to an incomplete set. This is, however, not a principal problem in practice. For any given database of sampled and quantized objects, we can find finite w and r such that the objects are distinguishable.

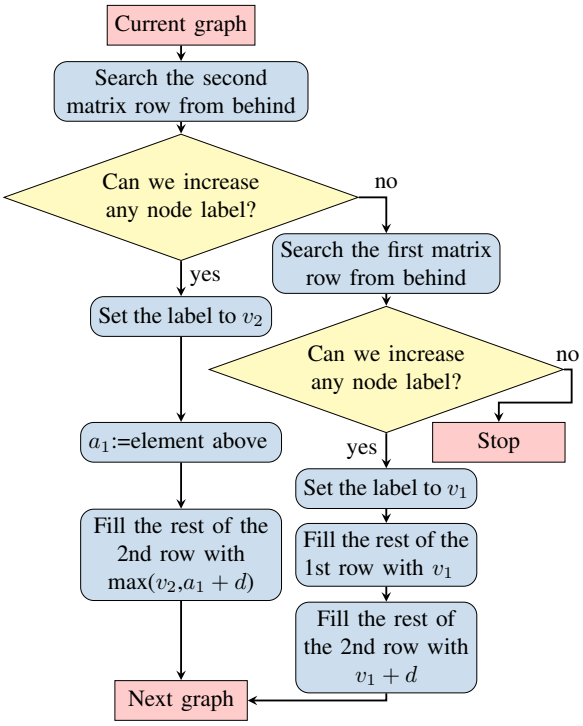

Fig. 4. Algorithm for the next graph generation. $d = 1$ for invariants V_i and $d = 0$ for invariants Z_i.

If used extensively, the algorithm generates a huge number of dependent invariants. We distinguish two kinds of dependencies among the invariants. The "simple" ones, which comprise linear combinations and products, can be found in the same way as in the case of graylevel AMIs (see [2], Chapter 5). The main idea is that a linear dependency may occur among invariants, whose representation graphs have the same numbers of nodes and the same numbers of edges going from individual nodes. We assemble a matrix of coefficients of all invariants generated by these graphs; the dependent invariants can be identified by singular value decomposition of this matrix. The eliminated invariants are called *reducible*, the remaining linearly and product independent invariants are called *irreducible*.

After the reducible invariants have been eliminated, there may still be polynomial dependencies among remaining invariants. The only method, which guarantees identifying all these dependencies is a kind of full search, but it is not computationally feasible. Instead, we propose two heuristics. No one guarantees to find all polynomial dependencies, but both are close to this optimum.

The first heuristics is based on the idea that the number of independent invariants n_i should equal the number of

independent variables (moments) n_m minus the number of free parameters of the transformation group n_p (which is 8 for invariants V_i (11) and 4 for Z_i (16), if no translation is considered; otherwise it increases by two). We can take the generated irreducible invariants order by order, calculate the number n_i for each order separately and throw away all the invariants above this number. This method is very fast. As the result, we get the correct number of invariants, but there still might exist polynomial dependencies among them.

The second method is inspired by [36], it can also be found in [9]. If we have a dependent set of n_k invariants, there must exist function F such that

$$F(I_1, I_2, \ldots, I_{n_k}) = 0\,. \tag{21}$$

It must hold, for its derivatives with respect to an arbitrary moment (the proof is in [45])

$$\frac{\partial F(I_1, I_2, \ldots, I_{n_k})}{\partial m_{pq}^{(s)}} = 0\,. \tag{22}$$

Let us sort somehow the moments $m_{pq}^{(s)}$ and change their labels to m_j, where $j = 1, 2, \ldots, n_m$. We can decompose Eq. (22) to the form

$$\frac{\partial F(I_1, I_2, \ldots, I_{n_k})}{\partial m_j} = \sum_{\ell=1}^{n_k} \frac{\partial F(I_1, I_2, \ldots, I_{n_k})}{\partial I_\ell} \frac{\partial I_\ell}{\partial m_j} = 0\,, \tag{23}$$

where again $j = 1, 2, \ldots, n_m$.

The invariants as the functions of the moments are known, so the factor $\dfrac{\partial I_\ell}{\partial m_j}$ can be evaluated for specific values of the moments. The factor $\dfrac{\partial F(I_1, I_2, \ldots, I_{n_k})}{\partial I_\ell}$ is unknown, but it is the same for all j, it depends only on ℓ. Equation (23) can be understood as a system of linear equations with the matrix of elements $a_{j\ell} = \dfrac{\partial I_\ell}{\partial m_j}$ of size $n_k \times n_m$ and the vector of unknown coefficients $b_\ell = \dfrac{\partial F(I_1, I_2, \ldots, I_{n_k})}{\partial I_\ell}$ of the size n_k. If the invariants are independent, the system can only have one solution with $b_\ell = 0$ for all ℓ. Then the matrix $(a_{j\ell})$ must have full rank n_k (it also means $n_k \leq n_m$). If the rank n_r is less than n_k, then only n_r invariants are independent (in this case n_k can be greater than n_m).

The above idea is clear and correct. However, when implementing it, we encounter some problems in computing the rank n_r of matrix $(a_{j\ell})$. It cannot be determined by symbolic computation. We should calculate $(a_{j\ell})$ on a representative set of objects and set n_r as the maximum particular rank. This would be impractical and time-consuming. Instead, we generate randomly five sets of moment values[4] and calculate the rank of the matrices via SVD using the Matlab in-built function `rank`. Then we estimate n_r as the maximum of these five particular ranks.

If we end up with $n_r \ll n_k$, we must somehow select n_r invariants out of n_k such that they are independent. We apply a sequential incremental procedure. First, we select the simplest invariant available. As soon as a subset of invariants has been selected, we add a new one such that the rank of $(a_{j\ell})$ increases by one. We iterate this process until the number n_r of the chosen invariants has been reached. Theoretically, this algorithm may select a dependent set due to the nesting effect. To improve it, we could implement a kind of backtracking, but this is actually a borderline problem that need not be solved in this case.

As we already pointed out, the graph generation algorithm is limited by the maximum number of edges. We run it for $w = 9$ at most. After eliminating the reducible invariants, we obtained 1890 irreducible invariants of the type (11) and 6323 irreducible invariants of the type (16) in explicit form. The selection algorithm based on the rank of $(a_{j\ell})$ yielded 76 and 77 independent invariants, respectively. They are listed on http://zoi.utia.cas.cz/affine-vector-fields. This process took 50 hours on a computer with the processor Intel Core i7-2600K CPU 3.4 GHz and 16 GB operational memory. It might seem too long, but note that this process is applied only once and does not depend on any data. As soon as the invariant sets have been created, we can apply them to any vector field without the necessity of their re-generation.

VIII. Numerical Experiments

A. Verification of the invariance

In the first experiment, we verified the invariance property under simulated conditions. We transformed a vector field (which had been obtained as a gradient field of a grayscale Lena image, see Fig. 5) by 100 randomly generated independent TAFTs (i.e. transformations of the type (1), where A and B were independent) and calculated five invariants of V-type and five ones of Z-type. Theoretically, all V_k should be exactly invariant, while some Z_k may change since they are generally not invariant. The experiment confirmed this expectation (see Fig. 6 for visualization of the results). The small fluctuations of the V_k values appear due to the field resampling and interpolation, while the fluctuations of the Z_k values are really significant. If we constrain the transformation such that $B = A$, invariants Z_k become really invariant, as can be seen in Fig. 6c.

When we relaxed the perfect conditions, the invariance property became violated, but still the invariants exhibit a good robustness. We repeated the previous experiment, but we had added Gaussian noise independently to both field components before the field was transformed. We can observe the behavior of one selected invariant in Fig. 7, the others behave similarly. If SNR > 10dB, the relative error is under 5%, which is fully acceptable.

B. Template matching in a gradient field

In this experiment, we demonstrate the performance in template matching, for the present again in a controlled environment to be able to evaluate the results quantitatively. We calculated a gradient field of a real photograph and randomly selected 100 circular templates (see Fig. 8), the coordinates of which were drawn from a uniform distribution. Then we

[4]Moment values of a vector field could be almost arbitrary, the only constraint is so-called complete monotonicity [2].

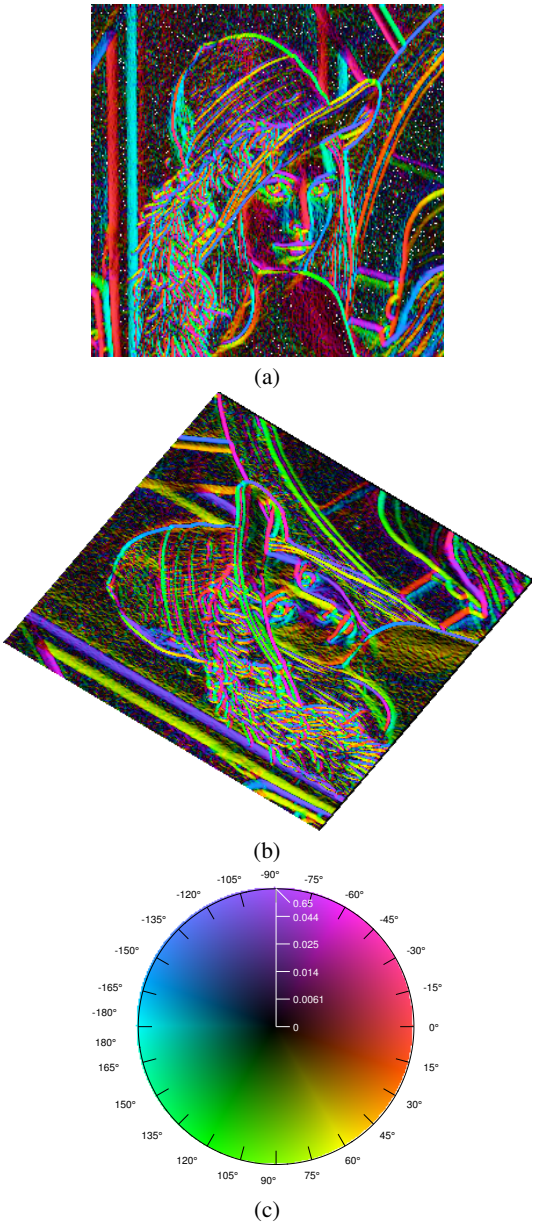

Fig. 5. (a) Gradient field of a grayscale image, which served as a test vector field in the synthetic experiments, (b) an example of the vector field transformed by a randomly generated TAFT, (c) colormap for gradient visualization, where the brightness corresponds to the magnitude and the hue to the direction of the gradient.

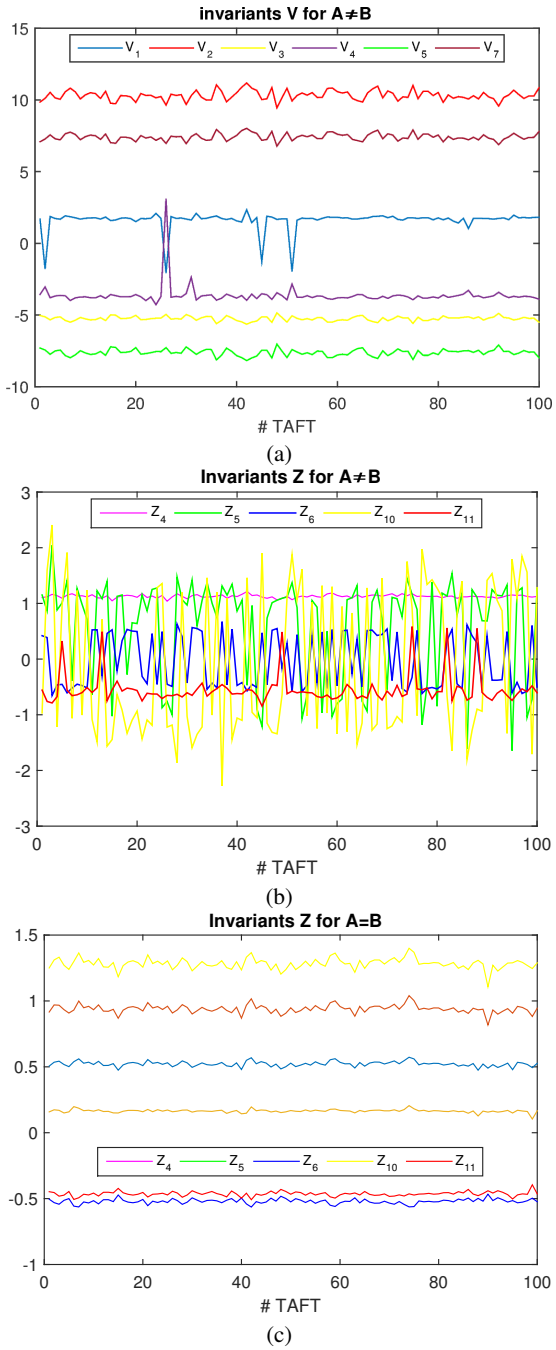

Fig. 6. The values of the invariants over 100 randomly generated total affine transformations. (a) - Five selected invariants of the V-type exhibit very good invariance (except a few cases when the transformation is close to singular), (b) - Invariants of the Z-type are not really invariant under these conditions, (c) - The same invariants of the Z-type when the transformations were constrained such that $B = A$.

transformed the gradient field by a TAFT transformation and tried to localize the templates in the deformed field.

The matching was implemented as a search of all possible template locations and the matching position is determined as that one which minimizes ℓ_2-distance in the space of 33 invariants. If the localization error was less or equal than two pixels, the match was considered correct, and false otherwise.

We run this experiment ten times for various deformations and various template sets. The success rate in each run depends on the significance (structure) of the selected templates and also on the particular deformation. It ranged from 100% to

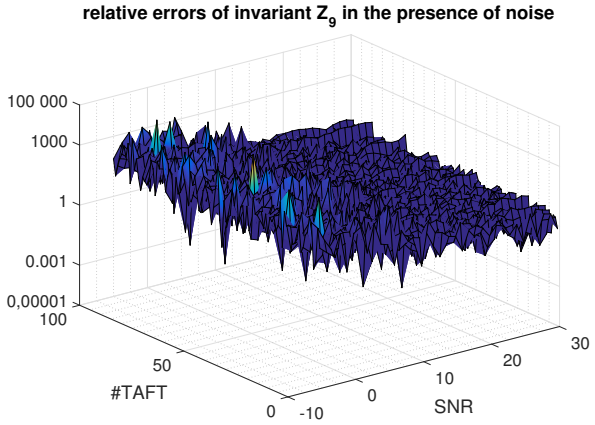

Fig. 7. The relative error of the invariant Z_9 over 100 randomly generated total affine transformations and SNR ranging from 30 dB to -5 dB. The robustness is very good for SNR $>$ 10dB. Only the ratio of the "noisy" and original value is visualized.

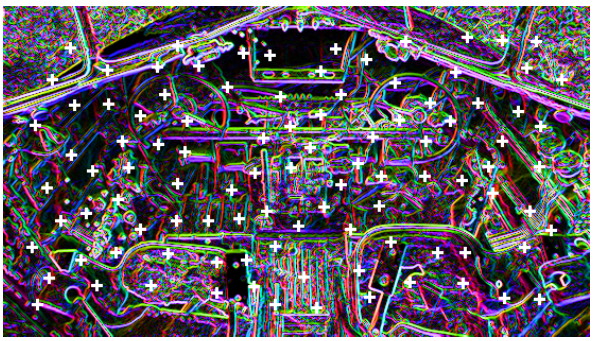

Fig. 8. Gradient field with 100 randomly selected templates used in a single run of the experiment. The colormap is the same as in Fig. 5.

75%, being almost uniformly distributed between 95% and 80%. For a comparison, we applied in each run also rotation vector field invariants from [13]. Their success rate never exceeded 10%, which clearly illustrates the advantage of the affine invariants over the rotational ones if a true affine deformation is present.

C. Template matching in a fluid flow field

In this experiment, we demonstrate the applicability of the proposed invariants in an important problem from fluid dynamics engineering – vortex detection in a fluid flow vector field. We used the field showing the Kármán vortex street, which is a repeating pattern of swirling vortices caused by the flow of a fluid around blunt bodies. In the Kármán pattern, we can see several vortices arranged into two rows. The orientation of the "street" is given by the main flow direction and is generally not known a priori. The data used in this experiment come from a computer simulation, not from a real physical measurement. The simulation resulted in a 300-frame video, showing the time-development of the Kármán street.

In the initial frame, we selected a template with a typical vortex, see Fig. 9. Then we deformed the video by two different TAFTs, which comprised anisotropic scaling with a factor of 5/4 and 7/4, respectively. The task is to find all vortices of a similar shape modulo TAFT in each frame of the deformed video. The search is performed in the space of invariants Z_k. We search for all local minima of ℓ_2-distance below a user-defined threshold. Such a task definition is rather "soft", because it specifies neither the significance of the vortices to be detected nor the required degree of similarity with the template. The results may be controlled by the number/order of the invariants we use[5].

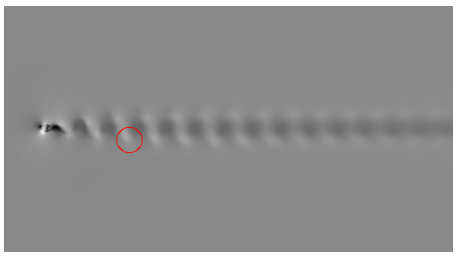

Fig. 9. The Kármán vortex street with the selected template (the first frame of the video).

We matched the template to each frame individually. We repeated the experiment for various maximum invariant order. So, we matched the templates in ten videos, which means we processed 3000 frames altogether. The resulting videos showing the vortex tracking can be found at zoi.utia.cas.cz/Experiment-with-Karman-Street. Two sample frames, one for each deformation, can be seen in Fig. 10.

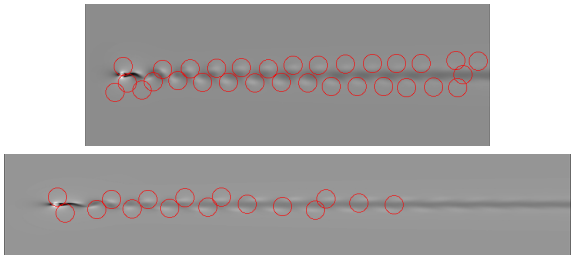

Fig. 10. The detected vortices in the deformed field when invariants Z_i up to 7th order were employed. The deformation comprised anisotropic scaling with factors 5/4 (top) and 7/4 (bottom). The full videos can be found at zoi.utia.cas.cz/Experiment-with-Karman-Street .

Since the ground truth is not known in this experiment, the matching accuracy cannot be evaluated quantitatively. However, visual inspection of the videos provide a good insight into the performance of the method. Most of the vortices were correctly found, but we can also observe some gross errors. They arose most probably because the neighborhood, the invariants were calculated from, was always circular and of

[5]The number of matches may be influenced also by the choice of the threshold. To eliminate this influence, we used thresholds of the same significance in each moment order.

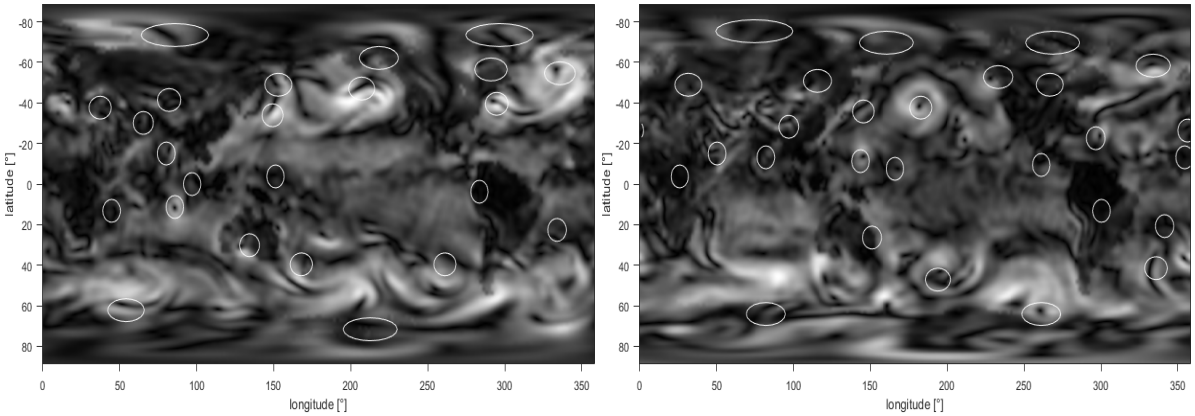

Fig. 11. Vortex detection in NOAA images by means of the invariants. The images display the wind magnitude only but the orientation is available as well and was used for the detection.

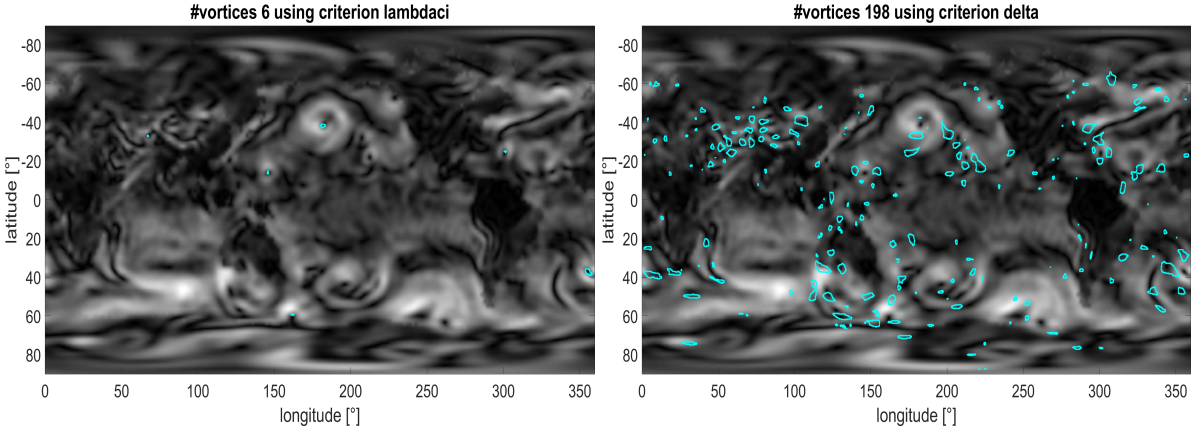

Fig. 12. Vortex detection by λ_{ci} (left) and Delta method (right) from [22]. The first method missed many vortices, the second one exhibits numerous false positives.

the same size as the original template. To comply with all theoretical assumptions, the neighborhood should be transformed according to the inner transformation into an ellipse. However, we did not follow this approach in order to simulate real-world conditions (in practice, the transformation is unknown).

D. Vortex detection in NOAA data

In this experiment, we show on real data how our method can be used for vortex detection in weather satellite images and we also compare the results with two of "non-image" vortex detection methods [22]. We used the world wind maps from the NOAA satellite [46], which are publicly available through www.esrl.noaa.gov/psd/. We used 18 frames from different days. We extracted three typical circular templates of a wind vortex of the same size (two from the northern and one from the southern hemisphere). Then we tried to locate vortices of the same shape in the other frames. The results achieved by the invariants in two sample frames are shown in Fig. 11. For the template matching, we used 35 independent invariants up to the order five (both types V_i and Z_i were included). Since there is no measurable ground truth, we are left to a visual evaluation. We can see the detection works quite well. Thanks to the affine invariance, also some vortices that exhibit an elongated shape due to data resampling in polar areas were detected (when searching the polar areas, the templates were not resampled, only the underlaying patch in the image was taken elliptical rather than circular). The method missed some vortices which look similar to the templates in magnitudes but their structure is different.

Then we applied the method from [22], which is a typical representative of "non-image" methods. It calculates the vorticity measure locally in each pixel from the gradient of the wind velocity. A vortex is a connected region where the vorticity measure exceeds a given threshold. We used two vorticity measures proposed in [22] – λ_{ci} and Delta criterion, respectively. The results for one frame are shown in Fig. 12. We can see that the sensitivity of the λ_{ci} method is low and only few vortices were found. On the other hand, the Delta method has higher sensitivity but low specificity, which leads to many false positives (as soon as the wind

trajectory is curved enough, the area is considered to be a vortex). Both algorithms were applied with the parameter setting recommended in [22].

IX. Conclusion

This paper introduced invariants of vector fields w.r.t. total affine transformation based on the moments of the vector field. The behavior of VFs under TAFT is significantly different from scalar and color images under standard affine transformation and the traditional techniques cannot be used. We derived new invariants in explicit closed form and showed that they can be represented by multilayer graphs. We also proposed the algorithm for selection of a maximal independent set of the invariants and use it to derive irreducible and independent invariants up to the weight nine. We demonstrated the performance of the invariants in template matching on gradient fields, on simulated data from fluid dynamics, and on real data from NOAA satellite. The comparison to rotation invariants and two "non-image" vortex detection methods showed the advantages of the proposed affine invariants.

Appendix A

Let $B = (B_{mn})$ be a regular outer transformation matrix. Then

$$\begin{aligned}
F'_{kj} &= f'_1(x_k, y_k) f'_2(x_j, y_j) - f'_1(x_j, y_j) f'_2(x_k, y_k) = \\
&= [B_{11} f_1(x_k, y_k) + B_{12} f_2(x_k, y_k)]\, [B_{21} f_1(x_j, y_j) \\
&\quad + B_{22} f_2(x_j, y_j)] - [B_{11} f_1(x_j, y_j) + B_{12} f_2(x_j, y_j)] \\
&\quad [B_{21} f_1(x_k, y_k) + B_{22} f_2(x_k, y_k)] = \\
&= B_{11} B_{21} f_1(x_j, y_j) f_1(x_k, y_k) \\
&\quad + B_{11} B_{22} f_1(x_k, y_k) f_2(x_j, y_j) \\
&\quad + B_{12} B_{21} f_2(x_k, y_k) f_1(x_j, y_j) \\
&\quad + B_{12} B_{22} f_2(x_k, y_k) f_2(x_j, y_j) \\
&\quad - B_{11} B_{21} f_1(x_j, y_j) f_1(x_k, y_k) \\
&\quad - B_{11} B_{22} f_1(x_j, y_j) f_2(x_k, y_k) \\
&\quad - B_{12} B_{21} f_2(x_j, y_j) f_1(x_k, y_k) \\
&\quad - B_{12} B_{22} f_2(x_j, y_j) f_2(x_k, y_k) = \\
&= (B_{11} B_{22} - B_{12} B_{21})\, [f_1(x_k, y_k) f_2(x_j, y_j) \\
&\quad - f_2(x_k, y_k) f_1(x_j, y_j)] = J_B \cdot F_{kj}\,.
\end{aligned}$$

Appendix B

Let $A = (A_{mn})$ be a regular outer and inner transformation matrix. Then

$$\begin{aligned}
D'_{kj} &= y'_j f'_1(x'_k, y'_k) - x'_j f'_2(x'_k, y'_k) = \\
&= (A_{21} x_j + A_{22} y_j)\, [A_{11} f_1(x_k, y_k) + A_{12} f_2(x_k, y_k)] \\
&\quad - (A_{11} x_j + A_{12} y_j)\, [A_{21} f_1(x_k, y_k) + A_{22} f_2(x_k, y_k)] = \\
&= A_{21} A_{11} x_j f_1(x_k, y_k) + A_{21} A_{12} x_j f_2(x_k, y_k) \\
&\quad + A_{22} A_{11} y_j f_1(x_k, y_k) + A_{22} A_{12} y_j f_2(x_k, y_k) \\
&\quad - A_{11} A_{21} x_j f_1(x_k, y_k) - A_{11} A_{22} x_j f_2(x_k, y_k) \\
&\quad - A_{12} A_{21} y_j f_1(x_k, y_k) - A_{12} A_{22} y_j f_2(x_k, y_k) = \\
&= (A_{11} A_{22} - A_{12} A_{21})\, [y_j f_1(x_k, y_k) - x_j f_2(x_k, y_k)] = \\
&= J_A \cdot D_{kj}\,.
\end{aligned}$$

Appendix C

In this appendix, we present the multilayer graphs representing the invariants $V(\mathbf{f})$ (11). The black edges belong to E_1 and the magenta edges belong to E_2. The invariants $V_1, V_2, \ldots, V_8$ shown here were selected from the set of the irreducible invariants http://zoi.utia.cas.cz/affine-vector-fields, where they are labeled as $V_{r1}, V_{r2}, V_{r4}, V_{r7}, V_{r15}, V_{r18}, V_{r3}$, and V_{r19} respectively. The invariants $V_1, V_2, \ldots, V_8$ create a complete and independent set of the second and third-order VFAMIs. The invariants V_1 and V_2 are shown also in their explicit forms. For explicit formulas of all other invariants, please visit the website http://zoi.utia.cas.cz/affine-vector-fields.

$$\begin{aligned}
V_1 &= -(\mu^{(1)}_{20})^2 (\mu^{(2)}_{02})^2 + 4\mu^{(1)}_{20}\mu^{(1)}_{11}\mu^{(2)}_{11}\mu^{(2)}_{02} \\
&\quad + 2\mu^{(1)}_{20}\mu^{(1)}_{02}\mu^{(2)}_{20}\mu^{(2)}_{02} - 4\mu^{(1)}_{20}\mu^{(1)}_{02}(\mu^{(2)}_{11})^2 \\
&\quad - 4(\mu^{(1)}_{11})^2\mu^{(2)}_{20}\mu^{(2)}_{02} + 4\mu^{(1)}_{11}\mu^{(1)}_{02}\mu^{(2)}_{20}\mu^{(2)}_{11} - (\mu^{(1)}_{02})^2(\mu^{(2)}_{20})^2
\end{aligned}$$

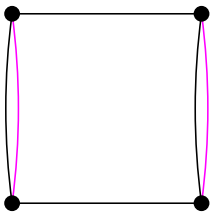

$$V_2 = \mu^{(1)}_{30}\mu^{(2)}_{03} - 3\mu^{(1)}_{21}\mu^{(2)}_{12} + 3\mu^{(1)}_{12}\mu^{(2)}_{21} - \mu^{(1)}_{03}\mu^{(2)}_{30}$$

V_3

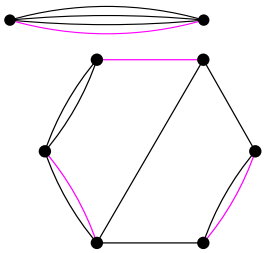

V_4

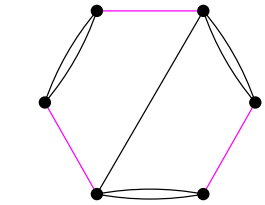

V_5

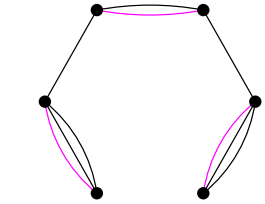

V_6

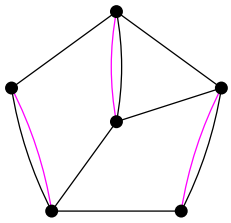

V_7

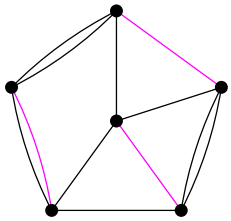

V_8

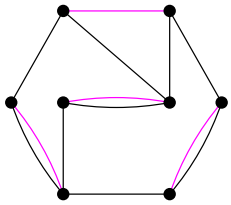

APPENDIX D

In this appendix, we present the multilayer graphs representing the invariants w.r.t. special total transformation $Z(\mathbf{f})$ (16). The black edges belong to E_1, the magenta edges belong to E_2, and the black-magenta edges depict the layer E_3 (the head-end of the edge is black). The invariants $Z_1, Z_2, \ldots, Z_{10}$ shown here were selected from the set of the irreducible invariants http://zoi.utia.cas.cz/affine-vector-fields, where they are labeled as $Z_{r3}, Z_{r4}, Z_{r6}, Z_{r8}, Z_{r9}, Z_{r19}, Z_{r20}, Z_{r21}, Z_{r11}$, and Z_{r13} respectively. The invariants $Z_1, Z_2, \ldots, Z_{10}$ create a complete and independent set of the second and third order. For higher-order invariants please visit the website http://zoi.utia.cas.cz/affine-vector-fields.

$$
\begin{aligned}
Z_1 = &-(\mu_{20}^{(1)})^2(\mu_{02}^{(2)})^2 + 4\mu_{20}^{(1)}\mu_{11}^{(1)}\mu_{11}^{(2)}\mu_{02}^{(2)} \\
&+ 2\mu_{20}^{(1)}\mu_{02}^{(1)}\mu_{20}^{(2)}\mu_{02}^{(2)} - 4\mu_{20}^{(1)}\mu_{02}^{(1)}(\mu_{11}^{(2)})^2 - 4(\mu_{11}^{(1)})^2\mu_{20}^{(2)}\mu_{02}^{(2)} \\
&+ 4\mu_{11}^{(1)}\mu_{02}^{(1)}\mu_{20}^{(2)}\mu_{11}^{(2)} - (\mu_{02}^{(1)})^2(\mu_{20}^{(2)})^2
\end{aligned}
$$

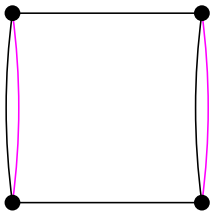

$$
\begin{aligned}
Z_2 = &\, 2\mu_{20}^{(1)}\mu_{20}^{(2)}\mu_{11}^{(2)}\mu_{02}^{(2)} - (\mu_{20}^{(1)})^2(\mu_{02}^{(2)})^2 - 2\mu_{20}^{(1)}(\mu_{11}^{(2)})^3 \\
&+ 2\mu_{20}^{(1)}\mu_{11}^{(1)}\mu_{11}^{(2)}\mu_{02}^{(2)} + 2\mu_{20}^{(1)}\mu_{11}^{(1)}\mu_{02}^{(1)}\mu_{02}^{(2)} - 2\mu_{20}^{(1)}(\mu_{02}^{(1)})^2\mu_{11}^{(2)} \\
&- 2\mu_{11}^{(1)}(\mu_{20}^{(2)})^2\mu_{02}^{(2)} + 2\mu_{11}^{(1)}\mu_{20}^{(2)}(\mu_{11}^{(2)})^2 - 2(\mu_{11}^{(1)})^3\mu_{02}^{(2)} \\
&+ 2(\mu_{11}^{(1)})^2\mu_{02}^{(1)}\mu_{11}^{(2)} - 2\mu_{11}^{(1)}\mu_{02}^{(1)}\mu_{20}^{(2)}\mu_{11}^{(2)} + (\mu_{02}^{(1)})^2(\mu_{20}^{(2)})^2
\end{aligned}
$$

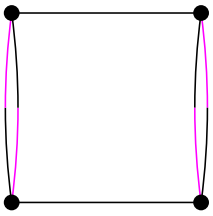

$$
\begin{aligned}
Z_3 = &\, (\mu_{20}^{(2)})^3\mu_{02}^{(2)} - (\mu_{20}^{(2)})^2(\mu_{11}^{(2)})^2 - \mu_{20}^{(1)}(\mu_{11}^{(2)})^3 \\
&+ 3\mu_{20}^{(1)}\mu_{02}^{(1)}(\mu_{11}^{(2)})^2 - 3\mu_{20}^{(1)}(\mu_{02}^{(1)})^2\mu_{11}^{(2)} + \mu_{20}^{(1)}(\mu_{02}^{(1)})^3 \\
&- 3\mu_{11}^{(1)}(\mu_{20}^{(2)})^2\mu_{02}^{(2)} + 5\mu_{11}^{(1)}\mu_{20}^{(2)}(\mu_{11}^{(2)})^2 + 3(\mu_{11}^{(1)})^2\mu_{20}^{(2)}\mu_{02}^{(2)} \\
&- 4(\mu_{11}^{(1)})^2(\mu_{11}^{(2)})^2 - (\mu_{11}^{(1)})^3\mu_{02}^{(2)} + 5(\mu_{11}^{(1)})^2\mu_{02}^{(1)}\mu_{11}^{(2)} \\
&- (\mu_{11}^{(1)})^2(\mu_{02}^{(1)})^2 - 4\mu_{11}^{(1)}\mu_{02}^{(1)}\mu_{20}^{(2)}\mu_{11}^{(2)} - \mu_{11}^{(1)}(\mu_{02}^{(1)})^2\mu_{20}^{(2)} \\
&- \mu_{02}^{(1)}(\mu_{20}^{(2)})^2\mu_{11}^{(2)} + 2(\mu_{02}^{(1)})^2(\mu_{20}^{(2)})^2
\end{aligned}
$$

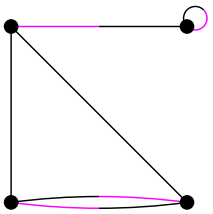

$$
Z_4 = \mu_{30}^{(1)}\mu_{03}^{(2)} - 3\mu_{21}^{(1)}\mu_{12}^{(2)} + 3\mu_{12}^{(1)}\mu_{21}^{(2)} - \mu_{03}^{(1)}\mu_{30}^{(2)}
$$

$$
\begin{aligned}
Z_5 = &-\mu_{30}^{(2)}\mu_{12}^{(2)} + \mu_{30}^{(1)}\mu_{03}^{(2)} + (\mu_{21}^{(2)})^2 - 2\mu_{21}^{(1)}\mu_{12}^{(2)} - \mu_{21}^{(1)}\mu_{03}^{(1)} \\
&+ \mu_{12}^{(1)}\mu_{21}^{(2)} + (\mu_{12}^{(1)})^2
\end{aligned}
$$

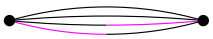

$$
\begin{aligned}
Z_6 = &-\mu_{20}^{(1)}\mu_{11}^{(2)}\mu_{12}^{(2)} - \mu_{20}^{(1)}\mu_{12}^{(1)}\mu_{02}^{(2)} + \mu_{20}^{(1)}\mu_{02}^{(2)}\mu_{21}^{(2)} \\
&+ \mu_{20}^{(1)}\mu_{03}^{(1)}\mu_{11}^{(2)} + \mu_{11}^{(1)}\mu_{20}^{(2)}\mu_{12}^{(2)} + \mu_{11}^{(1)}\mu_{21}^{(1)}\mu_{02}^{(2)} \\
&- \mu_{11}^{(1)}\mu_{02}^{(2)}\mu_{30}^{(2)} - \mu_{11}^{(1)}\mu_{03}^{(1)}\mu_{20}^{(2)} - \mu_{02}^{(1)}\mu_{20}^{(2)}\mu_{21}^{(2)} \\
&- \mu_{02}^{(1)}\mu_{21}^{(1)}\mu_{11}^{(2)} + \mu_{02}^{(1)}\mu_{11}^{(2)}\mu_{30}^{(2)} + \mu_{02}^{(1)}\mu_{12}^{(1)}\mu_{20}^{(2)}
\end{aligned}
$$

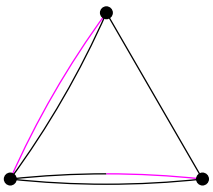

$$
\begin{aligned}
Z_7 = &\, \mu_{21}^{(1)}\mu_{20}^{(2)}\mu_{02}^{(2)} - \mu_{21}^{(1)}(\mu_{11}^{(2)})^2 - \mu_{20}^{(1)}\mu_{12}^{(1)}\mu_{02}^{(2)} \\
&- \mu_{20}^{(2)}\mu_{02}^{(2)}\mu_{30}^{(2)} + \mu_{20}^{(1)}\mu_{02}^{(2)}\mu_{21}^{(2)} - \mu_{20}^{(1)}\mu_{02}^{(1)}\mu_{12}^{(2)} \\
&+ \mu_{20}^{(1)}\mu_{02}^{(1)}\mu_{03}^{(1)} + (\mu_{11}^{(2)})^2\mu_{30}^{(2)} - 2\mu_{11}^{(1)}\mu_{11}^{(2)}\mu_{21}^{(2)}
\end{aligned}
$$

$$+ 2\mu_{11}^{(1)}\mu_{12}^{(1)}\mu_{11}^{(2)} + (\mu_{11}^{(1)})^2\mu_{12}^{(2)} - (\mu_{11}^{(1)})^2\mu_{03}^{(1)} + \mu_{02}^{(1)}\mu_{20}^{(2)}\mu_{21}^{(2)} - \mu_{02}^{(1)}\mu_{12}^{(1)}\mu_{20}^{(2)}$$

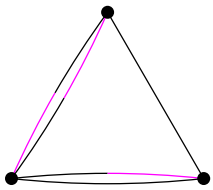

$$\begin{aligned} Z_8 = {} & -\mu_{30}^{(1)}\mu_{11}^{(2)}\mu_{02}^{(2)} + \mu_{21}^{(1)}\mu_{20}^{(2)}\mu_{02}^{(2)} - \mu_{20}^{(1)}\mu_{20}^{(2)}\mu_{03}^{(2)} \\ & + 2\mu_{21}^{(1)}(\mu_{11}^{(2)})^2 + \mu_{20}^{(1)}\mu_{11}^{(2)}\mu_{12}^{(2)} + \mu_{20}^{(1)}\mu_{11}^{(1)}\mu_{03}^{(2)} \\ & - \mu_{20}^{(1)}\mu_{02}^{(1)}\mu_{12}^{(2)} - 3\mu_{12}^{(1)}\mu_{20}^{(2)}\mu_{11}^{(2)} + 2\mu_{11}^{(1)}\mu_{20}^{(2)}\mu_{12}^{(2)} \\ & - \mu_{11}^{(1)}\mu_{21}^{(1)}\mu_{02}^{(2)} - 2\mu_{11}^{(1)}\mu_{11}^{(2)}\mu_{21}^{(2)} + 2\mu_{11}^{(1)}\mu_{12}^{(1)}\mu_{11}^{(2)} \\ & - 2(\mu_{11}^{(1)})^2\mu_{12}^{(2)} - \mu_{11}^{(1)}\mu_{03}^{(1)}\mu_{20}^{(2)} + 3\mu_{11}^{(1)}\mu_{02}^{(1)}\mu_{21}^{(2)} \\ & + \mu_{02}^{(1)}\mu_{30}^{(1)}\mu_{02}^{(2)} + \mu_{03}^{(1)}(\mu_{20}^{(2)})^2 - \mu_{02}^{(1)}\mu_{20}^{(2)}\mu_{21}^{(2)} \\ & - 2\mu_{02}^{(1)}\mu_{21}^{(1)}\mu_{11}^{(2)} + \mu_{02}^{(1)}\mu_{11}^{(2)}\mu_{30}^{(2)} + \mu_{02}^{(1)}\mu_{12}^{(1)}\mu_{20}^{(2)} \\ & - (\mu_{02}^{(1)})^2\mu_{30}^{(2)} \end{aligned}$$

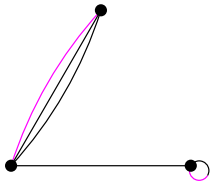

$$\begin{aligned} Z_9 = {} & \mu_{30}^{(1)}\mu_{21}^{(2)}\mu_{03}^{(2)} - \mu_{30}^{(1)}(\mu_{12}^{(2)})^2 + \mu_{30}^{(1)}\mu_{12}^{(1)}\mu_{03}^{(2)} \\ & - \mu_{30}^{(1)}\mu_{03}^{(1)}\mu_{12}^{(2)} - \mu_{21}^{(1)}\mu_{30}^{(2)}\mu_{03}^{(2)} + \mu_{21}^{(1)}\mu_{21}^{(2)}\mu_{12}^{(2)} - (\mu_{21}^{(1)})^2\mu_{03}^{(2)} \\ & + \mu_{21}^{(1)}\mu_{12}^{(1)}\mu_{12}^{(2)} + \mu_{21}^{(1)}\mu_{03}^{(1)}\mu_{21}^{(2)} + \mu_{12}^{(1)}\mu_{30}^{(2)}\mu_{12}^{(2)} - \mu_{12}^{(1)}(\mu_{21}^{(2)})^2 \\ & - (\mu_{12}^{(1)})^2\mu_{21}^{(2)} \end{aligned}$$

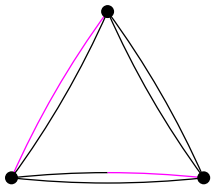

$$\begin{aligned} Z_{10} = {} & -(\mu_{30}^{(2)})^2\mu_{03}^{(2)} + 3\mu_{30}^{(2)}\mu_{21}^{(2)}\mu_{12}^{(2)} - \mu_{30}^{(1)}(\mu_{12}^{(2)})^2 \\ & + 2\mu_{30}^{(1)}\mu_{03}^{(1)}\mu_{12}^{(2)} - \mu_{30}^{(1)}(\mu_{03}^{(1)})^2 + 2\mu_{21}^{(1)}\mu_{30}^{(2)}\mu_{03}^{(2)} \\ & - 2(\mu_{21}^{(2)})^3 + \mu_{21}^{(1)}\mu_{21}^{(2)}\mu_{12}^{(2)} - (\mu_{21}^{(1)})^2\mu_{03}^{(2)} + \mu_{21}^{(1)}\mu_{12}^{(1)}\mu_{12}^{(2)} \\ & + 3\mu_{21}^{(1)}\mu_{12}^{(1)}\mu_{03}^{(1)} - 5\mu_{21}^{(1)}\mu_{03}^{(1)}\mu_{21}^{(2)} - 5\mu_{12}^{(1)}\mu_{30}^{(2)}\mu_{12}^{(2)} \\ & + 2\mu_{12}^{(1)}(\mu_{21}^{(2)})^2 + 2(\mu_{12}^{(1)})^2\mu_{21}^{(2)} - 2(\mu_{12}^{(1)})^3 \\ & + \mu_{12}^{(1)}\mu_{03}^{(1)}\mu_{30}^{(2)} + \mu_{03}^{(1)}\mu_{30}^{(2)}\mu_{21}^{(2)} \end{aligned}$$

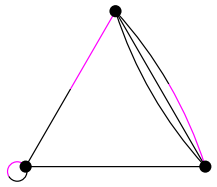

ACKNOWLEDGMENTS

This work has been supported by the Czech Science Foundation under the grant No. GA18-07247S, by the Grant SGS18/188/OHK4/3T/14 provided by the Ministry of Education, Youth, and Sports of the Czech Republic (MŠMT ČR), and by the *Praemium Academiae*. We also thank Prof. Mario Hlawitschka and Dr. Roxana Bujack for providing the Karman vortex street data, and the NOAA ESRL Physical Sciences Division, Boulder, Colorado, for providing the wind maps.

REFERENCES

[1] J. Flusser, T. Suk, and B. Zitová, *Moments and Moment Invariants in Pattern Recognition*. Chichester, U.K.: Wiley, 2009.

[2] ——, *2D and 3D Image Analysis by Moments*. Chichester, U.K.: Wiley, 2016.

[3] M. Schlemmer, M. Heringer, F. Morr, I. Hotz, M.-H. Bertram, C. Garth, W. Kollmann, B. Hamann, and H. Hagen, "Moment invariants for the analysis of 2D flow fields," *IEEE Transactions on Visualization and Computer Graphics*, vol. 13, no. 6, pp. 1743–1750, 2007.

[4] Y. S. Abu-Mostafa and D. Psaltis, "Recognitive aspects of moment invariants," *IEEE Transactions on Pattern Analysis and Machine Intelligence*, vol. 6, no. 6, pp. 698–706, 1984.

[5] J. Flusser, "On the independence of rotation moment invariants," *Pattern Recognition*, vol. 33, no. 9, pp. 1405–1410, 2000.

[6] ——, "On the inverse problem of rotation moment invariants," *Pattern Recognition*, vol. 35, no. 12, pp. 3015–3017, 2002.

[7] W. Liu and E. Ribeiro, "Detecting singular patterns in 2-D vector fields using weighted Laurent polynomial," *Pattern Recognition*, vol. 45, no. 11, pp. 3912–3925, 2012.

[8] M. Liu and P.-T. Yap, "Invariant representation of orientation fields for fingerprint indexing," *Pattern Recognition*, vol. 45, no. 7, pp. 2532–2542, 2012.

[9] M. Langbein and H. Hagen, "A generalization of moment invariants on 2D vector fields to tensor fields of arbitrary order and dimension," in *Proceedings of 5th International Symposium Advances in Visual Computing, ISVC'09, Part II*, ser. Lecture Notes in Computer Science, vol. 5876. Springer, 2009, pp. 1151–1160.

[10] R. Bujack, I. Hotz, G. Scheuermann, and E. Hitzer, "Moment invariants for 2D flow fields using normalization," in *Pacific Visualization Symposium, PacificVis'14*. IEEE, March 2014, pp. 41–48.

[11] R. Bujack, M. Hlawitschka, G. Scheuermann, and E. Hitzer, "Customized TRS invariants for 2D vector fields via moment normalization," *Pattern Recognition Letters*, vol. 46, no. 1, pp. 46–59, 2014.

[12] B. Yang, J. Kostková, T. Suk, J. Flusser, and R. Bujack, "Recognition of patterns in vector fields by Gaussian–Hermite invariants," in *International Conference on Image Processing ICIP'17*, J. Luo, W. Zeng, and Y.-J. Zhang, Eds. IEEE, 2017, pp. 2350–2363.

[13] B. Yang, J. Kostková, J. Flusser, T. Suk, and R. Bujack, "Rotation invariants of vector fields from orthogonal moments," *Pattern Recognition*, vol. 74, pp. 110–121, 2018.

[14] R. Bujack and J. Flusser, "Flexible basis of rotation moment invariants," in *International Conferences in Central Europe on Computer Graphics, Visualization and Computer Vision WSCG'17*, V. Skala, Ed., 2017, pp. 11–20.

[15] M. Jiang, R. Machiraju, and D. Thompson, *Visualization Handbook*. Elsevier Science, 2011, ch. Detection and visualization of vortices, pp. 295–312.

[16] D. Degani, A. Seginer, and Y. Levy, "Graphical visualization of vortical flows by means of helicity," *AIAA journal*, vol. 28, no. 8, pp. 1347–1352, 1990.

[17] C. Berdahl and D. Thompson, "Eduction of swirling structure using the velocity gradient tensor," *AIAA journal*, vol. 31, no. 1, pp. 97–103, 1993.

[18] J. Jeong and F. Hussain, "On the identification of a vortex," *Journal of fluid mechanics*, vol. 285, pp. 69–94, 1995.
[19] D. C. Banks and B. A. Singer, "A predictor-corrector technique for visualizing unsteady flow," *IEEE Transactions on Visualization and Computer Graphics*, vol. 1, no. 2, pp. 151–163, 1995.
[20] M. Roth and R. Peikert, "A higher-order method for finding vortex core lines," in *Proceedings Visualization'98 (Cat. No. 98CB36276)*. IEEE, 1998, pp. 143–150.
[21] I. A. Sadarjoen, F. H. Post, B. Ma, D. C. Banks, and H.-G. Pagendarm, "Selective visualization of vortices in hydrodynamic flows," in *Proceedings Visualization'98 (Cat. No. 98CB36276)*. IEEE, 1998, pp. 419–422.
[22] Q. Chen, Q. Zhong, M. Qi, and X. Wang, "Comparison of vortex identification criteria for planar velocity fields in wall turbulence," *Physics of Fluids*, vol. 27, no. 8, p. 085101, 2015.
[23] D. Hilbert, *Theory of Algebraic Invariants*. Cambridge, U.K.: Cambridge University Press, 1993.
[24] J. H. Grace and A. Young, *The Algebra of Invariants*. Cambridge, U.K.: Cambridge University Press, 1903.
[25] J. J. Sylvester assisted by F. Franklin, "Tables of the generating functions and groundforms for the binary quantics of the first ten orders," *American Journal of Mathematics*, vol. 2, pp. 223–251, 1879.
[26] ——, "Tables of the generating functions and groundforms for simultaneous binary quantics of the first four orders taken two and two together," *American Journal of Mathematics*, vol. 2, pp. 293–306, 324–329, 1879.
[27] I. Schur, *Vorlesungen über Invariantentheorie*. Berlin, Germany: Springer, 1968, in German.
[28] G. B. Gurevich, *Foundations of the Theory of Algebraic Invariants*. Groningen, The Netherlands: Nordhoff, 1964.
[29] M.-K. Hu, "Visual pattern recognition by moment invariants," *IRE Transactions on Information Theory*, vol. 8, no. 2, pp. 179–187, 1962.
[30] T. H. Reiss, "The revised fundamental theorem of moment invariants," *IEEE Transactions on Pattern Analysis and Machine Intelligence*, vol. 13, no. 8, pp. 830–834, 1991.
[31] J. Flusser and T. Suk, "Pattern recognition by affine moment invariants," *Pattern Recognition*, vol. 26, no. 1, pp. 167–174, 1993.
[32] T. Suk and J. Flusser, "Graph method for generating affine moment invariants," in *Proceedings of the 17th International Conference on Pattern Recognition ICPR'04*. IEEE Computer Society, 2004, pp. 192–195.
[33] ——, "Affine moment invariants generated by graph method," *Pattern Recognition*, vol. 44, no. 9, pp. 2047–2056, 2011.
[34] T. H. Reiss, *Recognizing Planar Objects Using Invariant Image Features*, ser. LNCS. Berlin, Germany: Springer, 1993, vol. 676.
[35] T. Suk and J. Flusser, "Affine moment invariants generated by automated solution of the equations," in *Proceedings of the 19th International Conference on Pattern Recognition ICPR'08*. IEEE Computer Society, 2008.
[36] M. S. Hickman, "Geometric moments and their invariants," *Journal of Mathematical Imaging and Vision*, vol. 44, no. 3, pp. 223–235, 2012.
[37] I. Rothe, H. Süsse, and K. Voss, "The method of normalization to determine invariants," *IEEE Transactions on Pattern Analysis and Machine Intelligence*, vol. 18, no. 4, pp. 366–376, 1996.
[38] T. Suk and J. Flusser, "Affine moment invariants of color images," in *Computer Analysis of Images and Patterns CAIP'09*, X. Jiang and N. Petkov, Eds., vol. LNCS 5702. Springer, September 2009, pp. 334–341.
[39] F. Mindru, T. Moons, and L. V. Gool, "Color-based moment invariants for viewpoint and illumination independent recognition of planar color patterns," in *International Conference on Advances in Pattern Recognition ICAPR'98*. Springer, 1998, pp. 113–122.
[40] F. Mindru, T. Tuytelaars, L. V. Gool, and T. Moons, "Moment invariants for recognition under changing viewpoint and illumination," *Computer Vision and Image Understanding*, vol. 94, no. 1–3, pp. 3–27, 2004.
[41] M. Gong, Y. Hao, H. Mo, and H. Li, "Naturally combined shape-color moment invariants under affine transformations," *Computer Vision and Image Understanding*, vol. 162, pp. 46–56, 2017.
[42] J. Kostková and J. Flusser, "On the null-space of the shape-color moment invariants," in *International Conference on Computer Analysis of Images and Patterns CAIP'19*, vol. LNCS 11678. Springer, 2019, pp. 402–408.
[43] G. Finlayson, M. Drew, and B. Funt, "Color constancy: generalized diagonal transforms suffice," *Journal of the Optical Society of America A*, vol. 11, no. 11, pp. 3011–3019, 1994.
[44] T. Gevers and A. Smeulders, "A comparative study of several color models for color image invariant retrieval," in *Proceedings of the First International Workshop on Image Database and Multimedia Search, IDB-MMS'96*. IAPR, 1996, pp. 17–23.
[45] A. B. Brown, "Functional dependence," *Transactions of the American Mathematical Society*, vol. 38, no. 2, pp. 379–394, 1935.
[46] E. Kalnay, M. Kanamitsu, R. Kistler, W. Collins, D. Deaven, L. Gandin, M. Iredell, S. Saha, G. White, J. Woollen *et al.*, "The NCEP/NCAR 40-year reanalysis project," *Bulletin of the American Meteorological Society*, vol. 77, no. 3, pp. 437–472, 1996.

Jitka Kostková received the M.Sc. degree in Applied Mathematical Stochastic Methods from the Czech Technical University, Faculty of Nuclear Science and Physical Engineering, Prague, Czech Republic, in 2015. Currently, she is a PhD. student in Mathematical Engineering and tutors undergraduate courses on mathematical analysis at the same university. Jitka Kostková's research interest is focused on moments and moment invariants.

Tomáš Suk received the M.Sc. degree in electrical engineering from the Czech Technical University, Faculty of Electrical Engineering, Prague, Czech Republic, in 1987, the Ph.D degree in computer science from the Czechoslovak Academy of Sciences in 1992 and DSc. degree from the Czech Academy of Sciences in 2018. Since 1991 he has been a researcher with the Institute of Information Theory and Automation, Czech Academy of Sciences, Prague. He has authored more than 35 journal papers, more than 50 conference papers and coauthored the monographs Moments and Moment Invariants in Pattern Recognition (Wiley, 2009) and 2D and 3D Image Analysis by Moments (Wiley, 2016). Tomáš Suk's research interests include digital image processing, pattern recognition, image filtering, invariant features, moment-based and point-based invariants, spatial transformations of images, and applications in remote sensing, astronomy, botany, medicine, and computer vision. In 2002 Tomáš Suk received the Otto Wichterle Premium of the Czech Academy of Sciences for excellent young scientists.

Jan Flusser received the M.Sc. degree in mathematical engineering from the Czech Technical University, Prague, Czech Republic, in 1985, the Ph.D degree in computer science from the Czechoslovak Academy of Sciences in 1990, and the DrSc. degree in technical cybernetics in 2001. Since 1985 he has been with the Institute of Information Theory and Automation, Czech Academy of Sciences, Prague. In 1995–2007, he was holding the position of a head of Department of Image Processing. Since 2007 he has been a Director of the Institute. He is a full professor of computer science at the Czech Technical University, Faculty of Nuclear Science and Physical Engineering, and at the Charles University, Faculty of Mathematics and Physics, Prague, Czech Republic, where he gives undergraduate and graduate courses on Digital Image Processing, Pattern Recognition, and Moment Invariants and Wavelets. Jan Flussers research interest covers moments and moment invariants, image registration, image fusion, multichannel blind deconvolution, and super-resolution imaging. He has authored and coauthored more than 200 research publications in these areas, including the monographs Moments and Moment Invariants in Pattern Recognition (Wiley, 2009) and 2D and 3D Image Analysis by Moments (Wiley, 2016). In 2007 Jan Flusser received the Award of the Chairman of the Czech Science Foundation for the best research project and won the Prize of the Academy of Sciences of the Czech Republic for the contribution to image fusion theory. In 2010, he was awarded by the SCOPUS 1000 Award. He received the Felber Medal of the Czech Technical University for excellent contribution to research and education in 2015 and the *Praemium Academiae* of the Czech Academy of Sciences for outstanding researchers in 2017.

Pattern Recognition 103 (2020) 107264

Contents lists available at ScienceDirect

Pattern Recognition

journal homepage: www.elsevier.com/locate/patcog

Handling Gaussian blur without deconvolution

Jitka Kostková[a], Jan Flusser[a,*], Matěj Lébl[a], Matteo Pedone[b]

[a] Czech Academy of Sciences, Institute of Information Theory and Automation, Pod vodárenskou věží 4, 182 08 Prague 8, Czech Republic
[b] Center for Machine Vision Research, Department of Computer Science and Engineering, University of Oulu, Oulu FI-90014, Finland

ARTICLE INFO

Article history:
Received 30 July 2019
Revised 22 November 2019
Accepted 5 February 2020
Available online 15 February 2020

Keywords:
Gaussian blur
Semi-group
Projection operator
Blur invariants
Image moments
Affine transformation
Combined invariants

ABSTRACT

The paper presents a new theory of invariants to Gaussian blur. Unlike earlier methods, the blur kernel may be arbitrary oriented, scaled and elongated. Such blurring is a semi-group action in the image space, where the orbits are classes of blur-equivalent images. We propose a non-linear projection operator which extracts blur-insensitive component of the image. The invariants are then formally defined as moments of this component but can be computed directly from the blurred image without an explicit construction of the projections. Image description by the new invariants does not require any prior knowledge of the blur kernel parameters and does not include any deconvolution. The invariance property could be extended also to linear transformation of the image coordinates and combined affine-blur invariants can be constructed. Experimental comparison to three other blur-invariant methods is given. Potential applications of the new invariants are in blur/position invariant image recognition and in robust template matching.

1. Introduction

In image processing and analysis, we often have to deal with images which are degraded versions of the original scene. One of the most common degradations is *blur*, which usually appears as a smoothing or suppression of high-frequency details of the image. Capturing an ideal scene f by an imaging device with the point-spread function (PSF) h, the observed image g can be modeled as a convolution of both

$$g(\mathbf{x}) = (f * h)(\mathbf{x}). \tag{1}$$

This linear image formation model, even if it is very simple, is a reasonably accurate approximation of many imaging devices and acquisition scenarios. In this paper, we concentrate our attention to the case when the PSF is a Gaussian function with unknown parameters.

Gaussian blur appears whenever the image has been acquired through a turbulent medium and the acquisition/exposure time is by far longer than the period of Brownian motion of the particles in the medium. Random fluctuations of the refractive index perturb the phase of the light and blur the acquired image. Ground-based astronomical imaging through the atmosphere, long-distance aerial and satellite surveillance, taking pictures through a haze, underwater imaging, and fluorescence microscopy are typical examples of such situation (in some cases, the blur may be coupled with a contrast decrease). Gaussian blur is also introduced into the images as the sensor blur which is due to a finite size of the sampling pulse. It may be sometimes applied intentionally as a low-pass filter for noise suppression, as a graphic tool to soften the image, and as a preprocessing when building the scale-space image pyramid to prevent aliasing artifacts. Few examples of Gaussian-blurred images can be seen in Fig. 1.

Eq. (1) is an example of an *inverse problem*, where we want to estimate f from its degraded version g, while the PSF may be partially known or unknown. This task is ill posed. Without additional constraints, infinitely many solutions satisfying Eq. (1) may exist. Solving of (1) has been known in image processing literature as *image restoration* and can be traced back to1960's. Despite of its long history, it has not been fully resolved. Although some of the current image restoration and deconvolution methods yield good results, they rely on prior knowledge incorporated into regularization terms or in other constraints. If such prior knowledge is not available, the methods may diverge or converge to a solution which is far from the ground truth. In case of a Gaussian blur, the parametric shape of the PSF can be used as a prior but another specific problem appears. Since any Gaussian function is infinitely divisible (it can be expressed as a convolution of arbitrary number of Gaussians) and since the convolution is an associative operation, the deconvolution may eliminate only a part of the actual blur, while the rest of the blur may be mistakenly considered as a part of the

* Corresponding author.
E-mail addresses: kostkova@utia.cas.cz (J. Kostková), flusser@utia.cas.cz (J. Flusser), lebl@utia.cas.cz (M. Lébl), matped@ee.oulu.fi (M. Pedone).

https://doi.org/10.1016/j.patcog.2020.107264
0031-3203/

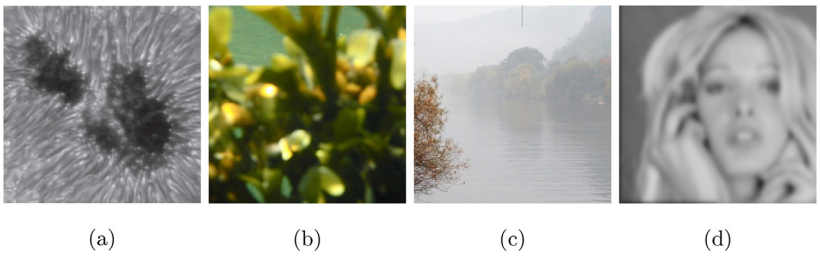

Fig. 1. Examples of the Gaussian blur: (a) a sunspot blurred by atmospheric turbulence, (b) underwater photo blurred by light dispersion, (c) a picture taken through haze, (d) a digitally low-pass filtered image.

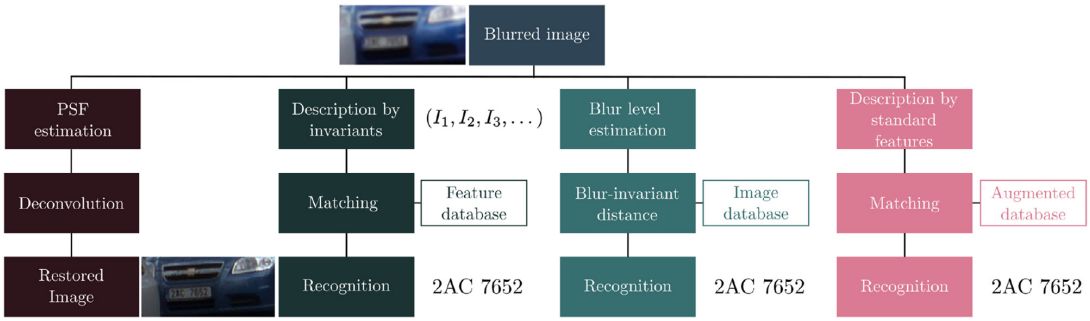

Fig. 2. Four approaches to analysis of blurred images. Image restoration via deconvolution (first branch), description and recognition by blur invariants (second branch), matching by minimum blur-invariant distance (third branch), and brute-force searching an augmented database (last branch).

original image. From a purely mathematical point of view, there is in principle no chance to avoid these formally correct but actually false solutions if no other prior information is available.

In 1990′s, some researchers not only realized all the above-mentioned difficulties connected with the solving of Eq. (1) but also found out that in many applications a complete restoration of f is not necessary and can be avoided, provided that an appropriate image representation is used. A typical example is a recognition of objects in blurred images, where a blur-robust object description forms a sufficient input for the classifier. This led to introducing the idea of *blur invariants*. Roughly speaking, blur invariant I is a functional fulfilling the constraint $I(f) = I(f * h)$ for any h from a certain set S of admissible PSF's. Many systems of blur invariants have been proposed so far. They differ from one another by the assumptions on the PSF, by the mathematical tools used for invariant construction, by the domain in which the invariants are defined, and by the application area which the invariants were designed for (see [1], Chapter 6, for a survey of blur invariants and further references).

Instead of constructing blur invariants of an individual image, in a few papers the authors proposed rather to use *blur-invariant distance* to measure the similarity between a blurred query image and clear database elements. This may help for such PSF's for which the invariants $I(f)$ are difficult to design or expensive to calculate.

The last group of methods replaces the theoretical construction of blur invariants with a brute-force search of an augmented database, which contains numerous samples of artificially generated blurred versions of each clear database image.

Fig. 2 illustrates the differences between these four approaches. Relevant work of all these categories are reviewed in Section 2.

All current methods dealing with Gaussian blur, regardless of the category they belong to, suffer from two serious limitations. The first one is that they were designed for *circular* Gaussian blur only and cannot handle more general scenarios. The assumption of the circular symmetry of the blur is an intrinsic aspect of most methods. The generalization from circular to anisotropic arbitrary oriented Gaussian blur is non-trivial and requires completely new approaches. The second limitation, which is partially connected with the first one, is that almost all current methods cannot handle simultaneously the blur and geometric transformations, such as rotation, scaling and affine transformation. They either cannot be adapted to handle spatial transformations at all (this is true namely for the invariant distances) or the possibility of the adaptation is coupled with the assumption of circular blur, which must not be violated under the spatial transformation (which is not the case of an affine transform). Since in practical applications the template rotation/scaling/affine transform may be present quite often, this is a serious drawback. One might think that an anisotropic Gaussian blur does not appear often in practice but the opposite is true. If the sensor has different resolution in horizontal and vertical direction then, even if the ground-truth PSF is circular, the image is blurred differently in x and y. If, moreover, the sensor parameters are not adjusted w.r.t. the database images, we face the problem of recognition of rotated/scaled/skewed and blurred images by an arbitrary-shaped Gaussian. An anisotropic Gaussian blur appears also if the turbulence in the medium, we are taking the picture through, is in certain direction more significant (due to wind for instance) than in the others. All this is a clear call for a discovery of more advanced invariants.

The main novel contribution of this paper is the design of the *combined invariants* to Gaussian blur and spatial affine transformation. This problem has not been tackled in the literature so far. This is accomplished through a derivation of the invariants w.r.t. blurring with a general (anisotropic) Gaussian kernel. The new blur invariants are defined by means of non-linear projection operators and are able to handle much more general scenarios than any other existing method, as we demonstrate by experiments. This brings immediate practical benefits. When applying the earlier

invariants, we should first check whether or not the Gaussian blurring PSF is circularly symmetric, which is almost impossible to verify from the blurred image itself. If this constraint has not been met, the method fails. The new invariants presented in this paper can be applied directly and do not require any prior estimation of the blurring PSF. The proposed combination with a rotation/affine invariance is based on the *Substitution Theorem*, which crowns the paper.

The paper is structured as follows. After the literature survey given in the next Section, we introduce the mathematical background of Gaussian blur in Section 3. Blur invariants in Fourier domain are proposed in Section 4 and their counterparts in image domain, moment-based blur invariants, are presented in Section 5. In Section 6, we formulate the Substitution Theorem, which allows to construct combined blur-affine invariants. Section 7 presents several recognition experiments on real real images and video.

2. Related work

State-of-the-art methods, dealing with the model (1) and with Gaussian blur, can be categorized into four main groups. In the sequel, we give a brief overview of each of them.

2.1. Restoration methods

Several image restoration methods specifically designed for Gaussian blur have been published. They try to estimate the size (variance) of the blur and perform a non-blind deconvolution. Honarvar et al. [2] proposed to perform the deconvolution in the moment domain but that algorithm contains a time-consuming search in the parametric space and is sensitive to overestimation of the Gaussian variance. The APEX method [3] estimated the blur variance by fitting the image spectrum in the Fourier domain. There exist also several local methods that estimate the blur size by investigating the response on a point source or on an ideal edge [4,5]. A common weakness of these methods is their sensitivity to noise and the necessity of the prior knowledge where an ideal point or edge is located. Xue and Blu [6] proposed to estimate the blur variance by minimizing a proper functional and then to apply a non-blind Wiener filtering. As in the previous cases, the method is sensitive to the variance overestimation and relatively time consuming. Numerous other methods were developed specially for atmospheric turbulence restoration [7] and most of the general blind-deconvolution algorithms (see, for instance, [8] for a survey and further references) can be used for Gaussian blur restoration as well with average results.

Restoration methods are not direct competitors of the proposed invariant-based technique. They were primarily designed to yield an estimation of the ideal image for visual interpretation. When used for recognition purposes, they serve as a pre-processing of the query image which is then described by some standard features. Such approach is, however, slow and unstable due to the restoration artifacts.

2.2. Brute force and convolution neural networks

A brute-force approach to recognition of degraded images relies on high computational power of current super-computers. To avoid both inversion of the degradation model as well as the design of the invariants, the training set is extended with all assumable degradations (using a proper sampling of the parametric space) of the training images. This process is called *data augmentation* and is popular especially in the connection with deep convolution neural networks (CNNs) where it may improve the recognition rate, see for instance [9]. Large-scale data augmentation is, however, time and memory consuming. In our case, the augmentation would require to generate blurred and spatially deformed versions of each training image with Gaussian kernels and transformation parameters from a certain range, and a consequent massive training. Since this would enlarge the training set by several orders, it is clear that this is not a feasible solution for databases containing many classes. Without data augmentation, even the state-of-the-art CNNs that perform excellently on clear images fail frequently when recognizing blurred inputs. As shown experimentally in [10], their performance drops when they are used to recognize degraded images while they have been trained on clear images only [10].

2.3. Blur-invariant distances

The idea of blur-invariant distance was firstly proposed by Zhang et al. [11] and has found several successors. All algorithms of this kind try to define a distance between two images, which fulfills the constrain $d(f_1, f_2) = d(f_1 * h, f_2)$ for any admissible h.

Zhang et al. [11,12] assumed circular Gaussian blur, estimated the blur level of the images to be compared (the authors took the integral of the image Laplacian as the blur estimator) and brought the images to the same blur level by blurring of the one which was less blurred. The distance $d(f_1, f_2)$ is then defined either as a weighted L_2-distance between the images of the same blur level [11] or as a geodesic distance on the surface of the manifold which contains the images of the same blur level [12]. The advantage of the Zhang's method is its simplicity. It does not contain any deblurring, minimization and iterations. However, the proposed estimation of the blur level is questionable for two images with different amount of high-frequency information.

Gopalan et al. [13] derived another blur-invariant distance measure without assuming the knowledge of the blur shape but they imposed a limitation on the blur support size. The authors showed that all blurred versions of the given image create a linear subspace, which can be understood as a point on Grassmann manifold. The blur-invariant distance between two images is then defined as the Riemannian distance between two points on the manifold. At the same time, this can be equivalently understood as measuring the angle between two subspaces. Although the Gopalan's method does not explicitly use the parametric shape of the blur, it performs well on Gaussian blur. However, the method suffers from two major drawbacks – the absence of any constraints imposed on the blur (except the support size) admits physically non-realistic blurs with negative values and the calculation of the Riemannian distance is very time-consuming.

The Gopalan's method was improved by Vageeswaran et al. [14], who introduced the positivity and energy-preserving constraints into the Gopalan's method. Under these constraints, blur-equivalent images form a convex set in the image space. The blur-invariant distance between the query image and the template is defined as the distance between the point, representing the query image, and its projection onto the convex set containing all blurred versions of the template. Most recently, essentially the same idea was independently proposed by Lébl et al. [15] who also presented an efficient algorithm for distance calculation by quadratic programming.

Fig. 3 visualizes, in a simplified way, the differences between the above mentioned distance measures. All three measures are compared to the proposed method in the experiments in Section 7.

2.4. Explicit blur invariants

Invariants w.r.t. blur were originally proposed in the work by Flusser et al. [16,17]. The first blur invariants were invariant w.r.t. any centrosymmetric PSF, without taking into account its parametric form. In 2015, Flusser et al. proposed a general theory of linear

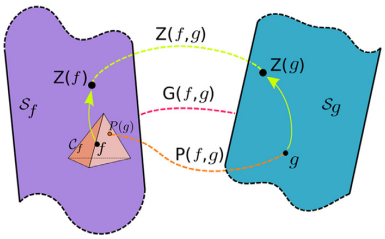

Fig. 3. Illustration of three blur invariant distances: Zhang's (Z) "image to image", Gopalan's (G) "subspace to subspace" and Lébl's and Vageeswaran's (P) "image to a convex set".

projection operators [18], which allowed to design specific blur invariants w.r.t. arbitrary N-fold symmetric blur, which led to an increase of their discriminability. The literature on blur invariants is relatively rich. Below we review only those methods, that were designed specifically for Gaussian blur. If a parametric Gaussian form of the blur kernel is assumed, the general invariants from [18] and similar can be still used but do not provide the optimal discrimination power.

Liu and Zhang [19] realized that the complex moments of the image, one index of which is zero, are invariant to Gaussian blur. Xiao [20] seemingly derived invariants to Gaussian blur but in fact he only employed the symmetry of the Gaussian rather than its parametric form. Höschl proposed invariants to Gaussian convolution in 1D and applied them to image histograms [21]. Flusser et al. [22] introduced a complete set of moment-based Gaussian blur invariants for the case that the Gaussian PSF is circularly symmetric. The experimental evaluation in [22] shows that these invariants, thanks to their specificity, outperform in template-matching experiments general methods such as cross-correlation, local phase quantization (LPQ) [23] and centrosymmetric blur invariants [17]. They even performed better than the Zhang's distance [12].

Serious weakness of all above mentioned Gaussian-blur invariant methods is that they assume circularly symmetric Gaussian blur only. Some of them, such as [12] and [22], could be generalized to work with elongated Gaussian blur in axial position (i.e. with a diagonal covariance matrix) but it is not possible to go beyond this limitation. This is also the reason why these methods cannot combine the invariance to blur with the invariance to image rotation and/or affine transformation, which is a critical limitation for practical usage.

Most recently, Kostková et al. [24] published the first paper ever on invariants w.r.t. Gaussian blur with a non-diagonal covariance matrix. In this paper, we adopt some preliminary results published in [24]. However, the idea of the combined invariants was not mentioned in [24].

3. Gaussian blur

In this section, we establish the necessary mathematical background which will be later used for designing the invariants.

By d-dimensional *image function* (or just image for short) $f(\mathbf{x})$ we understand any function from $L_1\left(\mathbb{R}^d\right)$, the integral of which is nonzero. For the sake of generality, we do not constraint it to be non-negative. In this paper, we are mostly dealing with 2D images, but many conclusions are valid or can be readily extended to arbitrary d.

By d-dimensional Gaussian G_Σ we understand the function

$$G_\Sigma(\mathbf{x}) = \frac{1}{(2\pi)^{d/2}\sqrt{|\Sigma|}} \exp\left(-\frac{1}{2}\mathbf{x}^T\Sigma^{-1}\mathbf{x}\right), \tag{2}$$

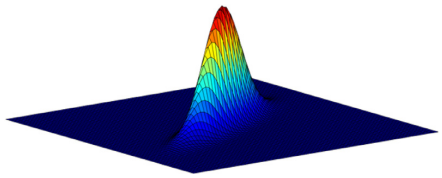

Fig. 4. 2D general Gaussian function with the principal eigenvector oriented in approx 30 degrees and with the eigenvalue ratio 6.

where $\mathbf{x} \equiv (x_1, x_2, \ldots, x_d)^T$ and Σ is a $d \times d$ regular covariance matrix. Since the covariance matrix is positive definite, we have, for its determinant, $|\Sigma| > 0$. We consider centralized Gaussians only (convolution with a non-centralized PSF just introduces an extra shift of the image).

The covariance matrix determines the shape of the Gaussian. If it is a multiple of a unitary matrix, then we get a circularly symmetric function. If it is diagonal but not unitary, we obtain an "elongated" Gaussian with elliptical contours in the axial position (in that case, d-dimensional Gaussian can be factorized into a product of d one-dimensional Gaussians). Generally, the Gaussian may be arbitrary oriented and elongated. The eigenvectors of Σ define the axes of the Gaussian and the eigenvalues determine its elongation (see Fig. 4).

The set S of all Gaussian blurring kernels is

$$S = \{aG_\Sigma | a > 0, \Sigma \text{ positive definite}\}. \tag{3}$$

Note that S is not a linear vector space because the sum of two different Gaussians is not a Gaussian. For the sake of generality, we consider un-normalized kernels to be able to model also a change of the image contrast. The basic properties of the set S are listed below. The *closure properties* play the most important role in deriving invariants.

Proposition 1 (Integrability). *$S \subset L_1$ since $\int aG_\Sigma = a$.*

Proposition 2 (Convolution closure). *S is closed under convolution as*

$$a_1G_{\Sigma_1} * a_2G_{\Sigma_2} = a_1a_2G_{\Sigma_1+\Sigma_2}.$$

Proposition 3 (Multiplication closure). *S is closed under point-wise multiplication as*

$$a_1G_{\Sigma_1} \cdot a_2G_{\Sigma_2} = aG_\Sigma,$$

where

$$a = \frac{a_1a_2}{(2\pi)^{d/2}\sqrt{|\Sigma_1 + \Sigma_2|}}$$

and $\Sigma = \left(\Sigma_1^{-1} + \Sigma_2^{-1}\right)^{-1}$.

Proposition 4 (Fourier transform closure). *Fourier transform of a function from S always exists, lies in S and is given by*

$$\mathcal{F}(aG_\Sigma) = \frac{a}{(2\pi)^{d/2}\sqrt{|\Sigma|}} G_{\Sigma_1},$$

where

$$\Sigma_1 = \frac{1}{4\pi^2}\Sigma^{-1}.$$

Proposition 5 (Coordinate transform closure). *Let A be a regular $d \times d$ matrix describing a linear transform of the coordinates. Then S turns to itself under the transform $\mathbf{x}' = A\mathbf{x}$. This follows from the fact that*

$$aG_\Sigma(A\mathbf{x}) = \frac{a}{\|A\|} G_{A^{-1}\Sigma A^{-T}}(\mathbf{x}),$$

where $\|A\|$ *means the absolute value of the determinant of* A *and* $A^{-T} \equiv (A^T)^{-1} = (A^{-1})^T$.

In the sequel, we use a slightly extended definition of S with Dirac δ-function being incorporated

$$S = \{aG_\Sigma | a > 0, \Sigma \text{ positive definite}\} \cup \{a\delta\}\,. \tag{4}$$

Proposition 2, along with the associativity of convolution, says that $(S, *)$ is a *semi-group* (it is not a group since convolution is not invertible within S). Hence, convolution with a function from S is a *semi-group action* on L_1.

The image space L_1 is factorized into *blur-equivalent classes* by the following relation. We say that the images f and g are Gaussian blur equivalent ($f \sim g$), if and only if there exist $h_1, h_2 \in S$ such that $h_1 * f = h_2 * g$. Thanks to Proposition 2 and to the commutativity of convolution, this relation is transitive, while symmetry and reflexivity are obvious. At the same time, the equivalence classes of $L_1/_\sim$ are related to the *orbits* of the above mentioned semi-group action. An orbit, originating from image f, is the set of all images that can be obtained from f as the result of the semi-group action. We will later show that the classes of $L_1/_\sim$ are exactly the same as the orbits generated by certain special images (this assertion will be formulated as Theorem 2 in Section 4).

The main idea of this paper is the following. We are going to find these "origins" of the orbits (we will call them *primordial images*) and describe them by means of properly chosen descriptors – *invariants* of the orbits. For instance, the set S itself forms an orbit with δ being its primordial image. The invariants stay constant within each equivalence class, while should distinguish any two images belonging to different classes. The invariance in question is in fact the invariance w.r.t. arbitrary Gaussian blur. The main trick, which makes this theory practically applicable, is that the invariants can be calculated from the given blurred image without explicitly constructing the primordial image.

In Section 4, we define a *projection operator* that "projects" each image onto S. The primordial images and, consequently, Gaussian blur invariants are constructed by means of this projection operator.

4. Projection operators and blur invariants

In linear algebra, projection operators onto linear subspaces are a well-established tool to decompose the given space into a direct sum of two subspaces, which usually have distinct properties. The idea of projecting the image space onto proper subspaces and then to define the image invariants in one of them was originally proposed by Flusser et al. in [18], where the invariants w.r.t. convolution with a symmetric non-parametric kernel were proposed. The authors constructed the projection onto the kernel subspace and defined the invariants in the complementary subspace.

In this paper, we face an analogous situation – we may try to construct the image projection onto the set S, eliminate somehow this Gaussian component of the image and define the invariants in the complement. However, there is a significant difference from the mathematical point of view. While in [18], linear projections onto linear, mutually orthogonal, subspaces were sufficient to resolve the problem, here we have to find a projection onto the set S of Gaussian kernels, which is not a linear subspace. Clearly, the respective projection operator cannot be linear and must be constructed in a different way than the operators proposed in [18].

Let us define the projection operator P such that it projects an image f onto the nearest un-normalized Gaussian, where the term "nearest" means the Gaussian having the same integral and covariance matrix as the image f itself. So, for $d = 2$ we define

$$Pf = m_{00} G_C\,, \tag{5}$$

where

$$C = \frac{1}{m_{00}} \begin{pmatrix} m_{20} & m_{11} \\ m_{11} & m_{02} \end{pmatrix},$$

and m_{pq} is the centralized image moment

$$m_{pq} = \int\int (x - c_1)^p (y - c_2)^q f(x, y)\, \mathrm{d}x\, \mathrm{d}y \tag{6}$$

with (c_1, c_2) being the image centroid.

Clearly, P is well defined for all "common" images[1] and actually if Pf exists, then always $Pf \in S$. Although P is not linear, it can still be called projection operator, because it is idempotent, i.e. $P^2 = P$. In particular, $P(aG_\Sigma) = aG_\Sigma$. Pf can be understood as a Gaussian component of f. Note, that the Gaussian component depends both on the image content and on the Gaussian blur (if any). Both factors contribute jointly to Pf. So, Pf is not an estimate of the actual blur kernel.

The key property of P, which will be later used for construction of the invariants, is that it commutes with a convolution with a Gaussian kernel, as shown in the following lemma.

Lemma 1. *Let* P *be the above-defined projector,* $f \in L_1$ *be an image function such that* Pf *exists and let* $G_\Sigma \in S$. *Then it holds*

$$P(f * G_\Sigma) = Pf * G_\Sigma\,. \tag{7}$$

Proof. To prove this lemma, we first recall how the image central moments are transformed under convolution. For arbitrary f and h we have

$$\begin{aligned}
m_{00}^{(f*h)} &= m_{00}^{(f)} m_{00}^{(h)}\,,\\
m_{20}^{(f*h)} &= m_{20}^{(f)} m_{00}^{(h)} + m_{00}^{(f)} m_{20}^{(h)}\,,\\
m_{11}^{(f*h)} &= m_{11}^{(f)} m_{00}^{(h)} + m_{00}^{(f)} m_{11}^{(h)}\,,\\
m_{02}^{(f*h)} &= m_{02}^{(f)} m_{00}^{(h)} + m_{00}^{(f)} m_{02}^{(h)}\,.
\end{aligned}$$

Considering the projection of $f * G_\Sigma$, it must have a form $P(f * G_\Sigma) = aG_K$, where $a = m_{00}^{(f*G_\Sigma)} = m_{00}^{(f)}$ and

$$K = \frac{1}{m_{00}} \begin{pmatrix} m_{20} + m_{00}\Sigma_{20} & m_{11} + m_{00}\Sigma_{11} \\ m_{11} + m_{00}\Sigma_{11} & m_{02} + m_{00}\Sigma_{02} \end{pmatrix}.$$

All moments m_{pq} in the above equation are related to f. Hence, $K = C + \Sigma$. On the other hand, we have

$$Pf * G_\Sigma = m_{00} G_C * G_\Sigma = m_{00} G_{C+\Sigma}\,.$$

The last equality follows from Proposition 2. □

Now we can formulate the Fundamental theorem on blur invariants.

Theorem 1. *Let* P *be the above-defined projector and let* f *be an image function such that* Pf *exists. Then*

$$I(f) = \frac{\mathcal{F}(f)}{\mathcal{F}(Pf)} \tag{8}$$

is an invariant to Gaussian blur, i.e. $I(f) = I(f * h)$ *for any* $h \in S$.

Proof. The proof follows immediately from Lemma 1.

$$I(f * h) = \frac{\mathcal{F}(f * h)}{\mathcal{F}(P(f * h))} = \frac{\mathcal{F}(f)\mathcal{F}(h)}{\mathcal{F}(Pf * h)} = \frac{\mathcal{F}(f)\mathcal{F}(h)}{\mathcal{F}(Pf)\mathcal{F}(h)} = \frac{\mathcal{F}(f)}{\mathcal{F}(Pf)} = I(f)$$

□

Note that if Pf exists, then $I(f)$ is well defined on all frequencies because the denominator $\mathcal{F}(Pf)$ is a Gaussian and hence non-zero everywhere.

[1] If $m_{00} = 0$ or if C is not positive definite or if some second-order moment(s) are infinite, then Pf is undefined. Although such functions exist in L_1, they do not describe real-life images and we do not consider them in this paper.

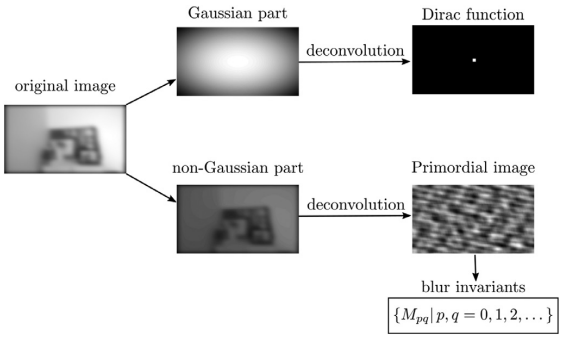

Fig. 5. Visualization of the main idea: The image is projected onto a set of Gaussians and this projection (i.e. the Gaussian part of the image) is used to "deconvolve" the image in Fourier domain. Blur-invariant primordial image is obtained as the result of this operation. Moments of the primordial image are blur invariants introduced in Eq. (15).

The following Theorem says that the invariant $I(f)$ is *complete*, which means the equality $I(f_1) = I(f_2)$ occurs if and only if f_1 and f_2 belong to the same equivalence class.

Theorem 2. *Let f_1 and f_2 be two image functions and $I(f)$ be the invariant defined in Theorem 1. Then $I(f_1) = I(f_2)$ if and only if there exist $h_1, h_2 \in S$ such that $h_1 * f_1 = h_2 * f_2$.*

The proof is straightforward by setting $h_1 = Pf_2$ and $h_2 = Pf_1$. The completeness guarantees that $I(f)$ discriminates between the images from different equivalence classes, while stays constant inside each class due to the invariance property. This assertion not only shows the limitations (the images belonging to the same equivalence class can never be discriminated) but also explains why these invariants outperform general blur invariants if Gaussian blur is present (equivalence classes w.r.t. a general blur are larger than those w.r.t. Gaussian blur).

Invariant $I(f)$ is a ratio of two Fourier transforms which may be interpreted as a deconvolution in frequency domain. Having an image f, we seemingly "deconvolve" it by the kernel Pf. This deconvolution always sends the Gaussian component of f to δ-function. We call the result of this seeming deconvolution the *primordial image*

$$f_r = \mathcal{F}^{-1}(I(f)) .$$

Hence, $I(f)$ can be viewed as Fourier transform of f_r. Note that f_r is actually the "maximally possible" deconvolved image f, which creates the origin of the respective orbit (see Fig. 5 for schematic illustration). Primordial image can be also understood as a kind of normalization (or canonical form) of f w.r.t. arbitrary Gaussian blurring.

It should be noted, that the primordial image is a useful theoretical concept of blur invariants but it is not actually constructed in the implementation of the method. It may lie outside L_1 or may even not exist but it does not matter – the existence of its Fourier transform, the invariants are obtained from, is guaranteed.

5. Invariants in the image domain

Although $I(f)$ itself could serve as an image descriptor, its direct usage brings certain difficulties and disadvantages. On high frequencies, we divide by small numbers which may lead to precision loss. This effect is even more severe if f is noisy. This problem could be overcome by suppressing high frequencies by a low-pass filter, but such a procedure would introduce a user-defined parameter (the cut-off frequency) which should be set up with respect to the particular noise level. Another disadvantage is that we would have to actually construct $\mathcal{F}(Pf)$ in order to calculate $I(f)$. That is why we prefer to work directly in the image domain, where moment-based invariants equivalent to $I(f)$ can be constructed and evaluated without an explicit calculation of Pf.

First of all, we recall that geometric moments of an image are Taylor coefficients (up to a constant factor) of its Fourier transform[2]

$$\mathcal{F}(f)(\mathbf{u}) = \sum_{\mathbf{p}\geq\mathbf{0}} \frac{(-2\pi i)^{|\mathbf{p}|}}{\mathbf{p}!} m_{\mathbf{p}}^{(f)} \mathbf{u}^{\mathbf{p}} \tag{9}$$

(for simplicity, and also to show the independence of the dimension d, we use the multi-index notation).

Theorem 1 can be rewritten as

$$\mathcal{F}(Pf)(\mathbf{u}) \cdot I(f)(\mathbf{u}) = \mathcal{F}(f)(\mathbf{u}) .$$

All these three Fourier transforms can be expanded similarly to (9) into absolutely convergent Taylor series

$$\sum_{\mathbf{p}\geq\mathbf{0}} \frac{(-2\pi i)^{|\mathbf{p}|}}{\mathbf{p}!} m_{\mathbf{p}}^{(Pf)} \mathbf{u}^{\mathbf{p}} \cdot \sum_{\mathbf{p}\geq\mathbf{0}} \frac{(-2\pi i)^{|\mathbf{p}|}}{\mathbf{p}!} M_{\mathbf{p}} \mathbf{u}^{\mathbf{p}} = \sum_{\mathbf{p}\geq\mathbf{0}} \frac{(-2\pi i)^{|\mathbf{p}|}}{\mathbf{p}!} m_{\mathbf{p}}^{(f)} \mathbf{u}^{\mathbf{p}} , \tag{10}$$

where by $M_{\mathbf{p}}$ we denote the Taylor coefficient of $I(f)$ (we will show later that $M_{\mathbf{p}}$ is in fact the moment of the primordial image).

Comparing the coefficients of the same powers of $\mathbf{u}$ we obtain, for any $\mathbf{p}$,

$$\sum_{\mathbf{k}\leq\mathbf{p}} \frac{(-2\pi i)^{|\mathbf{k}|}}{\mathbf{k}!} \frac{(-2\pi i)^{|\mathbf{p}-\mathbf{k}|}}{(\mathbf{p}-\mathbf{k})!} m_{\mathbf{k}}^{(Pf)} M_{\mathbf{p}-\mathbf{k}} = \frac{(-2\pi i)^{|\mathbf{p}|}}{\mathbf{p}!} m_{\mathbf{p}}^{(f)} , \tag{11}$$

which can be read as

$$\sum_{\mathbf{k}\leq\mathbf{p}} \binom{\mathbf{p}}{\mathbf{k}} m_{\mathbf{k}}^{(Pf)} M_{\mathbf{p}-\mathbf{k}} = m_{\mathbf{p}}^{(f)} . \tag{12}$$

In 2D, Eq. (12) reads as

$$\sum_{m=0}^{p} \sum_{n=0}^{q} \binom{p}{m} \binom{q}{n} m_{mn}^{(Pf)} M_{p-m,q-n} = m_{pq}^{(f)} . \tag{13}$$

Since $Pf = m_{00}^{(f)} G_C$, where C is given by the second-order moments of f, we can express its moments $m_{mn}^{(Pf)}$ without actually constructing the projection Pf. Clearly, $m_{mn}^{(Pf)} = 0$ for any odd $m+n$ due to the centrosymmetry of G_C. For any even $m+n$, $m_{mn}^{(Pf)}$ can be expressed in terms of the moments of f as

$$\begin{aligned} m_{mn}^{(Pf)} &= m_{00}^{(f)} m_{mn}^{(G_C)} \\ &= m_{00}^{(f)} \sum_{\substack{i=0 \\ j\geq\frac{m-n}{2}}}^{\lfloor\frac{m}{2}\rfloor} \sum_{j=0}^{i} (-1)^{i-j} \binom{m}{2i} \binom{i}{j} (m+n-2i-1)!! \cdot \\ &\quad \cdot (2i-1)!! \left(\frac{m_{11}}{m_{00}}\right)^{m-2j} \left(\frac{m_{20}}{m_{00}}\right)^{j} \left(\frac{m_{02}}{m_{00}}\right)^{\frac{n-m}{2}+j} . \end{aligned} \tag{14}$$

The above expression was obtained by substituting our particular C into the formula for moments of a 2D Gaussian. (The moment formula for a diagonal covariance matrix is well known. For a general covariance matrix, it is not commonly cited in the literature. It can be either deduced from the papers presenting general approaches to moment calculation [25,26] or obtained directly from the definition by integration.)

[2] We assume that all moments are finite, which is guaranteed for all images with bounded support.

Now we can isolate M_{pq} on the left-hand side and obtain the recurrence

$$M_{pq} = \frac{m^{(f)}_{pq}}{m_{00}} - \sum_{\substack{l=0\\ l+k\neq 0,\\ l+k \text{ even}}}^{p}\sum_{k=0}^{q}\binom{p}{l}\binom{q}{k}\sum_{\substack{i=0\\ j\geq\frac{k-l}{2}}}^{\lfloor\frac{k}{2}\rfloor}\sum_{j=0}^{i}(-1)^{i-j}\binom{k}{2i}\binom{i}{j}(l+k-2i-1)!!\cdot$$

$$\cdot(2i-1)!!\left(\frac{m_{11}}{m_{00}}\right)^{k-2j}\left(\frac{m_{20}}{m_{00}}\right)^{\frac{l-k}{2}+j}\left(\frac{m_{02}}{m_{00}}\right)^{j}M_{p-l,q-k}\,. \tag{15}$$

This recurrence formula defines Gaussian blur invariants in the image domain. Since $I(f)$ has been proven to be invariant to Gaussian blur, all coefficients M_{pq} must also be blur invariants. The M_{pq}'s can be understood as the moments of the primordial image f_r. The power of Eq. (15) lies in the fact that we can calculate them directly from the moments of f, without constructing the primordial image explicitly either in frequency or in the spatial domain and also without any prior knowledge of the blurring kernel orientation. Thanks to the uniqueness of Fourier transform, the set of all M_{pq}'s carries the same information about the function f as $I(f)$ itself, so the cumulative discrimination power of all M_{pq}'s equals to that of $I(f)$.

Some of the invariants (15) are always trivial. Regardless of f, we have $M_{00}=1$, $M_{10}=M_{01}=0$ because we work in centralized coordinates, and $M_{20}=M_{11}=M_{02}=0$ since these three moments were already used for the definition of *Pf*. Note that the joint nullspace of all M_{pq}'s except M_{00} equals the set S, which is implied by the fact that $P(aG_\Sigma)=aG_\Sigma$ and the corresponding primordial image $f_r^{(S)}=\delta$.

Eq. (15) can be turned to an equivalent non-recursive form

$$M_{pq}=\frac{1}{m_{00}}\sum_{\substack{l=0\\ l+k \text{ even}}}^{p}\sum_{k=0}^{q}(-1)^{\frac{k+l}{2}}\binom{p}{l}\binom{q}{k}\sum_{\substack{i=0\\ j\geq\frac{k+l}{2}}}^{\lfloor\frac{k}{2}\rfloor}\sum_{j=0}^{i}(-1)^{i-j}\binom{k}{2i}\binom{i}{j}(l+k-2i-1)!!\cdot$$

$$\cdot(2i-1)!!\left(\frac{m_{11}}{m_{00}}\right)^{k-2j}\left(\frac{m_{20}}{m_{00}}\right)^{\frac{l-k}{2}+j}\left(\frac{m_{02}}{m_{00}}\right)^{j}m^{(f)}_{p-l,q-k}\,. \tag{16}$$

While the recursive formula is efficient if we want to calculate all invariants up to a certain order, the non-recursive one is useful for calculating a single invariant of higher order.

6. Combined invariants

One of the main benefits of the assumption that the covariance matrix is not constrained to be diagonal is the existence of *combined invariants* to blur and affine transformation of the coordinates. If the blurring Gaussian kernel was assumed in the axial position and hence C was constrained to be diagonal, we could never combine blur with an affine transformation or rotation, because it would violate the assumption. This is why the combined invariants have not been constructed yet (except a very special case of a unitary covariance matrix and rotation, see [22]).

The key idea of designing the combined invariants follows from the observation how the primordial image is transformed if the original image has undergone an affine transformation $f'(\mathbf{x})=f(A\mathbf{x})$. By means of Propositions 3–5, it is easy to show that

$$I\big(f'\big)(\mathbf{u}) = I(f)\big(A^{-T}\mathbf{u}\big)\,.$$

Applying inverse Fourier transform, we get

$$f'_r(\mathbf{x}) = \|A\|\,f_r(A\mathbf{x})\,,$$

where f'_r is the primordial image of f'. This relation tells us that the primordial image is transformed by *the same* coordinate transformation as the original image.

Since the invariants M_{pq} in Eq. (15) are in a fact moments of f_r, we can simply substitute them into any affine or rotation moment invariant (we only should avoid those containing second-order moments because they would lead to trivial invariants) and we end up with the combined invariant. The theory of both affine and rotation moment invariants has been well elaborated and several complete and independent invariant sets are available, see for instance [1,27–31]. Since blur invariants M_{pq} also form a complete and independent set (see Theorem 2), we get in this way a complete and independent set of combined invariants. This strong result is summarized in the following Theorem.

Theorem 3 (Substitution Theorem)**.** *Let f be an image function and let M_{pq} be invariants w.r.t. Gaussian blur defined by Eq. (15). Let $f'(\mathbf{x})=f(A\mathbf{x})$, A being a regular 2×2 matrix. Let $J(m_{pq}|\,p,q=0,\dots,r)$ be an absolute invariant of image moments w.r.t. A, i.e. $J(m'_{pq}|\,p,q=0,\dots,r)=J(m_{pq}|\,p,q=0,\dots,r)$. Then $J(M_{pq}|\,p,q=0,\dots,r)$ is a relative invariant w.r.t. both A and Gaussian blur as*

$$\|A\|^w J(M'_{pq}|\,p,q=0,\dots,r) = J(M_{pq}|\,p,q=0,\dots,r)\,,$$

where w is the weight[3] of invariant $J(m_{pq}|\,p,q=0,\dots,r)$.

Proof. Since $f'_r(\mathbf{x})=\|A\|f_r(A\mathbf{x})$, the moments M'_{pq} of $f'_r(\mathbf{x})$ are related to the moments $\tilde{M}_{pq}$ of $f_r(A\mathbf{x})$ as $M'_{pq}=\|A\|\tilde{M}_{pq}$ for any p and q. In the theory of affine moment invariants [1,29], it is well known that any absolute invariant $J(m_{pq}|\,p,q=0,\dots,r)$ must have a form of a finite sum, where all terms are products of K moments (K is called the *degree* of the invariant) divided by $(K+w)$-th power of m_{00}. The statement of Theorem 3 follows immediately from this fact. Note that the invariance of $J(M_{pq}|\,p,q=0,\dots,r)$ w.r.t. Gaussian blur is obvious and does not depend on the order in which the blurring and the coordinate transformation A have been applied. They are commutative in the sense that $(f*h)'=1/\|A\|(f'*h')$ and still $h'\in S$ thanks to Proposition 5. □

Since A is usually unknown in practice, absolute invariants are more convenient image descriptors than the relative ones. An absolute combined invariant can be obtained as a ratio of two relative invariants of the same weight or, more generally, as a ratio of any two products of various relative invariants such that the factor $\|A\|$ is cancelled.

7. Experiments

Numerical experiments presented in this section aim to illustrate the properties of the proposed invariants, namely to evaluate the invariance w.r.t. arbitrary Gaussian blur, the recognition power and the robustness to additive noise. First, we prove the invariance on static images and also on a real video, where the Gaussian blur model is not exactly valid. As sample applications, we show how the blur invariants can be used for object tracking in a video and for recognition of blurred faces. A comparison to other state-of-the-art methods is given. Finally, we show the performance of the combined affine-blur invariants in digit recognition.

7.1. Invariance verification on public datasets

This basic experiment is a verification of the invariance of functionals M_{pq} from Eq. (15). We used two public-domain image databases, which contain series of Gaussian-blurred images (see Fig. 6 for two examples). We used 30 series (original and five blurred instances of various extent of the blur) from the CID:IQ dataset [32] and 23 series from the CSIQ dataset [33]. For each of them, we calculated the invariants up to the 9th order. The relative error of all invariants on each image series was always between 10^{-4} and 10^{-3}, which illustrates a perfect invariance. The fluctuation within a single series is so small that in no way diminishes

[3] The term *weight of an invariant has been commonly used in the theory of algebraic invariants, see for instance* [1], [29] for the definition. For any given invariant, its weight is known and follows from the way how the invariant has been constructed.

Fig. 6. Two examples of the Gaussian-blurred image series from the CSIQ database.

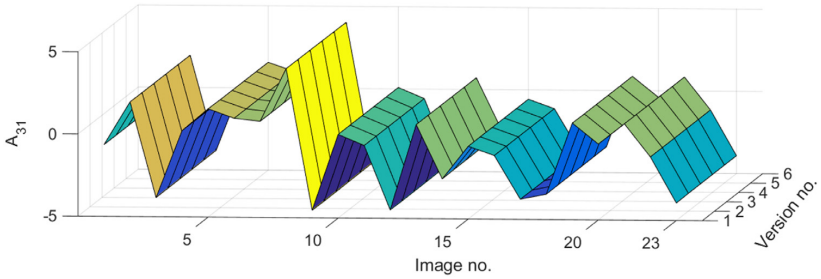

Fig. 7. The values of a single invariant calculated over 23 series (from left to right) consisting of six blurred instances of the originals (from front to back). The value is always almost constant within each individual series while significantly different for distinct images.

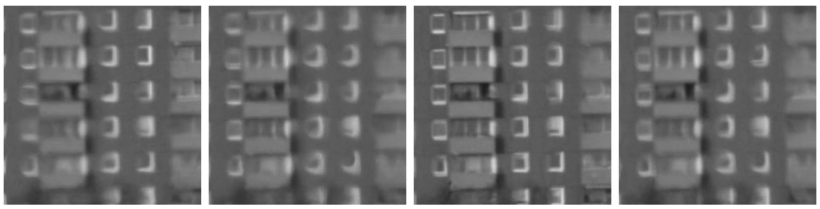

Fig. 8. Four sample frames of a video blurred due to the hot air turbulence.

the ability to discriminate two different originals, as is illustrated in Fig. 7.

7.2. Verification on a real video

In this experiment, we used publicly accessible video[4] from [7] showing a static scene (front side of a building) captured intentionally through a turbulent hot air. Due to the turbulence, the video is degraded by a time-varying blur, which is, according to [7], expected to be approximately Gaussian. Four sample frames of the sequence are shown in Fig. 8.

Similarly to the previous experiment, we calculated the blur invariants M_{pq} from Eq. (15) up to the 8th order for each frame. The graph in Fig. 9 summarizes the results. It is worth noting that the invariants exhibit a perfect stability even if the real blur is probably not exactly Gaussian.

7.3. Tracking in a video

The proposed blur invariants can be used also for tracking objects in a blurred video. We took an indoor video that starts with a clear frame. Then the video becomes more and more blurred. The blur is Gaussian with a time-varying covariance matrix. In the first frame, we chose the template of interest that we track by invariant template matching in the rest of the video.

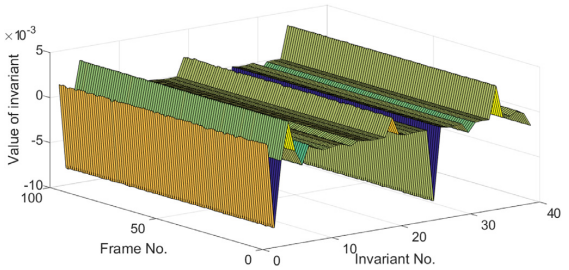

Fig. 9. The values of the invariants up to the 8th order calculated over 99 frames of a video corrupted by a real turbulence blur. The value of each invariant is always almost constant on all frames.

To show the strength of the method, each frame was processed independently (in reality, the motion information could be used to speed up and stabilize the tracking but here we wanted to demonstrate solely the performance of the invariants). We can evaluate visually that the tracking is reasonably stable and accurate and actually follows the real motion of the template. Sample frames with the detected template are shown in Fig. 10.[5]

[4] http://alumni.soe.ucsc.edu/~xzhu/doc/turbulence.html.

[5] The full video is available at http://zoi.utia.cas.cz/files/Tracking_changing_blur_5th_order.gif.

Fig. 10. Tracking in a blurred video. The initial clear image with the template (top left), sample frames of the blurred video with the template detected.

Table 1
The recognition rate [%] of the tested methods for Gaussian blur of various size.

Blur size (Gaussian)	Invariants	Zhang	Lébl	Gopalan
7 × 7	100	100	100	74
11 × 11	100	86	100	25
15 × 15	100	48	100	5

7.4. Recognition of blurred faces

In this experiment we show the performance of the proposed invariants in face recognition applied on blurred photographs. We compare the proposed method with the blur-invariant distances proposed by Gopalan et al. [13], Zhang et al. [11], and Lébl et al. [15] (see Section 2.3 for a brief description of these competitors). We calculated also the standard ℓ_2-distance, which does not take the blur into account at all, but it expectedly failed completely so we did not include it in the tables.

We used 38 distinct human faces from the Extended Yale Face Database B [34] (the same database was used in [13]). This database contains clear faces only, so we created the blurred and noisy query images artificially (see Fig. 11 for some examples). In all tests, moment invariants up to the 9th order were used.

First, we tested the recognition rate as a function of the blur size. The blurred, noise-free query image was always classified against the clear 38-image database. While moment invariants and the Lébl's method are 100% successful even for relatively large blurs, the Gopalan's method surprisingly does not reach comparable results. Its success rate drops very rapidly with the increasing blur size, even if we provided the correct blur size as the input parameter of the algorithm. The Zhang's method performs well for small blurs (see Table 1). It should be pointed out, that the reported 100% success rate of the invariants was achieved thanks to a controlled noise-free environment, where the Gaussian convolution model held perfectly. In the next two experiments, these ideal conditions will be relaxed and we will monitor the impact on the method performance.

If we apply a significantly non-Gaussian blur (we used a directional motion blur in this experiment), we observe a drop of the performance of the invariants, while the other methods perform more or less the same as in the case of Gaussian blur (see Table 2). This is not surprising, because the derivation of the invariants was inherently based on the assumption of a Gaussian blur while the Gopalan's and Lébl's methods assume only the knowledge of the blur size, which was fulfilled in this experiment. The invariants are relatively sensitive to the violation of the Gaussian blur shape.

Then, we tested the noise robustness of all methods. We corrupted the query images with an additive white normally distributed noise of SNR from 20 dB to 0 dB. The success rate of the invariants as well as of the Lébl's method remains very high even for heavy noise, while the other two methods appear to be vulnerable. Table 3 summarizes the results. High robustness of the invariants can be explained by the fact that the moments, being integral features, average-out the noise.

Table 2
The recognition rate [%] of the tested methods for a motion blur of various size.

Blur size (motion)	Invariants	Zhang	Lébl	Gopalan
7 × 7	87	100	100	99
11 × 11	71	72	100	76
15 × 15	45	17	100	40

Table 3
Noise robustness test: The recognition rate [%] achieved for various SNR.

SNR [dB]	Invariants	Zhang	Lébl	Gopalan	OG Invariants
20	100	100	100	76	100
10	100	55	100	51	100
5	99	44	99	37	99
2	97	37	87	27	97
0	92	32	79	26	95

Many papers on moments have shown experimentally that orthogonal (OG) moments are more robust to numerical errors and also to noise. This is due to the fact that OG moments can be calculated indirectly using recurrent formulas, which avoids working with very high and very low numbers. For this reason, various OG moments have been implemented in moment invariants, where they replace traditional geometric moments (see [1], Chapter 7, for a survey of OG moments). In the context of blur invariants (but not to Gaussian blur), this approach was applied for instance in [35–41].[6] We tested the use of Legendre moments in the proposed Gaussian blur invariants. We expressed geometric moments as functions of Legendre moments, substituted these functions into (15) and obtained in this way blur invariants in terms of Legendre moments. We applied these invariants on the same noisy facial images as above. The results are shown in the rightmost column of Table 3. The recognition rate is the same as for the invariants from geometric moments except SNR = 0 dB, where a slightly better robustness of OG moments appears.

Finally, we compared the speed of all methods. We evaluated it as a function of the image size. The results are shown in Fig. 12. The time refers to a single query and does not comprise any precalculations on the database images.

The proposed invariants work with a highly-compressed image representation (only the moments up to the 9th order were used). All other methods use a complete pixel-wise representation, however with various time-efficiency. The Lébl's method is the most efficient for small images. As the image size increases, moment invariants become more time efficient. They outperform the Lébl's method for images larger than approximately 600 × 600 pixels. It should be noted, that the complexity of calculation of the invariants is determined solely by the complexity of moment computation. For a graylevel $N \times N$ image, this is typically $O(N^2)$ and does not depend on the actual blur size (unlike the Zhang's and Gopalan's methods). Although some faster algorithms exist for moment computation [43], we did not use them here because they are efficient for special types of images only.

[6] It should be noted that the use of OG moments in blur invariants is solely because of their favorable numerical properties. As proved by Kautsky [42], blur invariants in any two distinct polynomial bases are theoretically equivalent.

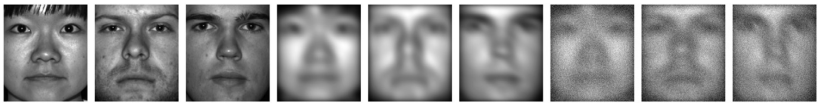

Fig. 11. Sample face images used in the experiments: clear database faces (images 1–3), blurred (images 4–6) and noisy (images 7–9) query images.

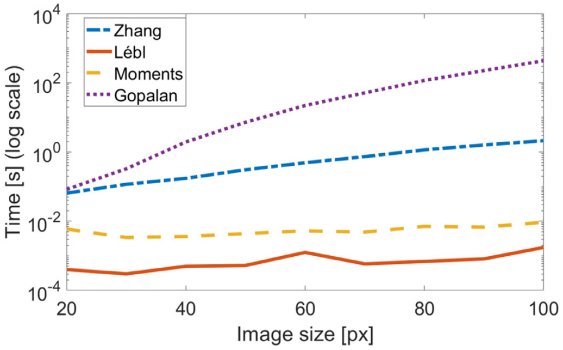

Fig. 12. Time [s] needed to compare a query image to a single database image as a function of the image size. The blur size was fixed at 15 × 15 pixels. The time axis is shown in a logarithmic scale.

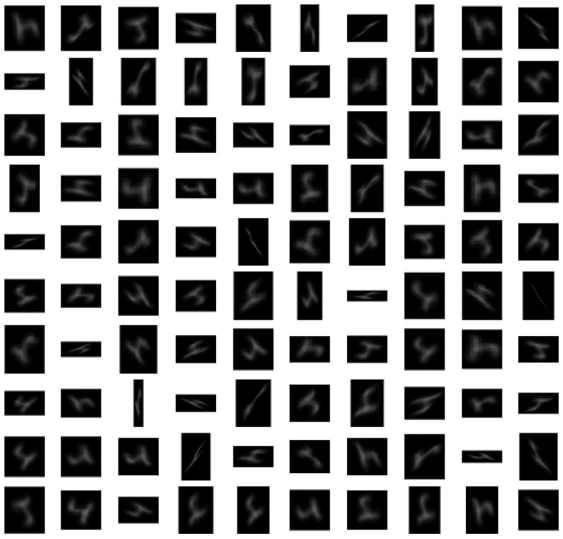

Fig. 13. 100 randomly blurred and affinely deformed pictures of digit 4.

7.5. Recognition of blurred and affinely deformed objects

In the last experiment, we demonstrate the power of the combined affine-blur invariants proposed in Section 6. For this test, we used the popular MNIST dataset of handwritten digits [44]. For each digit $0, 1, \ldots, 9$ we randomly generated 100 blurred and affinely deformed samples (see Fig. 13 showing the test set of the digit 4) and classified them against the original dataset. The affine-blur invariants used in this test were constructed according to the Substitution Theorem (Theorem 3), where we used the well-established Affine moment invariants (AMIs) [29] as $J(m_{pq})$.

To illustrate the advantage of the combined invariants, we compared them both to "pure" AMIs [29] and to "pure" Gaussian blur invariants (15). The combined invariants yielded the overall recognition rate 98.5 %, while the AMIs only 20 % and the blur invariants performed even worse yielding 15.6 % success rate. This clearly shows that the Substitution Theorem brings invariants of a new quality.

The comparison to the Gopalan's, Zhang's, and Lébl's invariant distances as in the face recognition experiment does not make sense here because all those methods require the images to be precisely geometrically aligned and collapse completely in case of spatial misalignment.

8. Conclusion

Blur invariants w.r.t. blur kernels which are defined by certain generic properties rather than by their parametric form were already discovered for centrosymmetric [17], radial [45], N-fold rotational symmetric [18,46], and N-fold dihedral [47] blurs, respectively. In this paper, we focused on parametric kernels since they allow to derive more specific invariants which yields a better discrimination power. We proposed new invariants w.r.t. Gaussian blur. Unlike all earlier works on Gaussian blur, our method does not require the Gaussian blurring kernel to be circularly symmetric and works with arbitrary Gaussians. We found a non-linear projection operator by means of which the invariants are defined in the Fourier domain. Equivalently, the invariants can be calculated directly in the image domain, without an explicit construction of the projections. We showed that the new invariants can be made invariant also to a linear transformation of the coordinates thanks to the Substitution Theorem, which was not possible in case of earlier Gaussian-blur invariants. Experimental evaluation and comparison to alternative approaches (namely to various blur-invariant distances) showed a superior performance in most scenarios in terms of the recognition rate and speed.

In a future work, it would be interesting to couple the proposed blur-invariant representation with the CNNs in order to make the CNNs blur-invariant without any data augmentation. CNNs probably cannot be fed directly with the moment invariant (15). Instead, we envisage to use the Fourier-domain invariants (8) for this purpose. However, since the distinctive patterns in spectral domain are totally different from those in the image domain, one probably cannot use any publicly available pre-trained network and will have to train (and maybe also to design) the network by himself.

Declaration of Competing Interest

None.

Acknowledgments

This work has been supported by the Czech Science Foundation under the grant no. GA18-07247S, by the grant SGS18/188/OHK4/3T/14 provided by the Ministry of Education, Youth, and Sports of the Czech Republic (MŠMT ČR), and by the *Praemium Academiae*.

References

[1] J. Flusser, T. Suk, B. Zitová, 2D and 3D Image Analysis by Moments, Wiley, Chichester, U.K., 2016.
[2] B. Honarvar, R. Paramesran, C.-L. Lim, Image reconstruction from a complete set of geometric and complex moments, Signal Processing 98 (2014) 224–232.
[3] A.S. Carasso, The APEX method in image sharpening and the use of low exponent Lévy stable laws, SIAM J. Appl. Math. 63 (2) (2003) 593–618.
[4] J.H. Elder, S.W. Zucker, Local scale control for edge detection and blur estimation, IEEE Trans Pattern Anal Mach Intell 20 (7) (1998) 699–716.

[5] W. Zhang, W.-K. Cham, Single-image refocusing and defocusing, IEEE Trans. Image Process. 21 (2) (2012) 873–882.
[6] F. Xue, T. Blu, A novel SURE-based criterion for parametric PSF estimation, IEEE Trans. Image Process. 24 (2) (2015) 595–607.
[7] X. Zhu, P. Milanfar, Removing atmospheric turbulence via space-invariant deconvolution, IEEE Trans. Pattern Anal. Mach. Intell. 35 (1) (2013) 157–170.
[8] P. Campisi, K. Egiazarian, Blind Image Deconvolution: Theory and Applications, CRC, 2007.
[9] L. Taylor, G. Nitschke, Improving deep learning using generic data augmentation, arXiv preprint arXiv:1708.06020 (2017).
[10] Y. Pei, Y. Huang, Q. Zou, X. Zhang, S. Wang, Effects of image degradation and degradation removal to CNN-based image classification, IEEE Trans. Pattern Anal. Mach. Intell. (2019), doi:10.1109/TPAMI.2019.2950923.
[11] Z. Zhang, E. Klassen, A. Srivastava, P. Turaga, R. Chellappa, Blurring-invariant Riemannian metrics for comparing signals and images, in: IEEE International Conference on Computer Vision, ICCV'11, 2011, pp. 1770–1775.
[12] Z. Zhang, E. Klassen, A. Srivastava, Gaussian blurring-invariant comparison of signals and images, IEEE Trans. Image Process. 22 (8) (2013) 3145–3157.
[13] R. Gopalan, P. Turaga, R. Chellappa, A blur-robust descriptor with applications to face recognition, IEEE Trans. Pattern Anal. Mach. Intell. 34 (6) (2012) 1220–1226.
[14] P. Vageeswaran, K. Mitra, R. Chellappa, Blur and illumination robust face recognition via set-theoretic characterization, IEEE Trans. Image Process. 22 (4) (2013) 1362–1372.
[15] M. Lébl, F. Šroubek, J. Kautský, J. Flusser, Blur invariant template matching using projection onto convex sets, in: Proc. 18th Int'l. Conf. Computer Analysis of Images and Patterns CAIP'19, 2019, pp. 351–362.
[16] J. Flusser, T. Suk, S. Saic, Recognition of blurred images by the method of moments, IEEE Trans. Image Process. 5 (3) (1996) 533–538.
[17] J. Flusser, T. Suk, Degraded image analysis: an invariant approach, IEEE Trans. Pattern Anal. Mach. Intell. 20 (6) (1998) 590–603.
[18] J. Flusser, T. Suk, J. Boldyš, B. Zitová, Projection operators and moment invariants to image blurring, IEEE Trans. Pattern Anal. Mach. Intell. 37 (4) (2015) 786–802.
[19] J. Liu, T. Zhang, Recognition of the blurred image by complex moment invariants, Pattern Recognit. Lett. 26 (8) (2005) 1128–1138.
[20] B. Xiao, J.-F. Ma, J.-T. Cui, Combined blur, translation, scale and rotation invariant image recognition by Radon and pseudo-Fourier-Mellin transforms, Pattern Recognit. 45 (2012) 314–321.
[21] C. Höschl IV, J. Flusser, Robust histogram-based image retrieval, Pattern Recognit. Lett. 69 (1) (2016) 72–81.
[22] J. Flusser, S. Farokhi, C. Höschl IV, T. Suk, B. Zitová, M. Pedone, Recognition of images degraded by Gaussian blur, IEEE Trans. Image Process. 25 (2) (2016) 790–806.
[23] V. Ojansivu, J. Heikkilä, Blur insensitive texture classification using local phase quantization, in: A. Elmoataz, O. Lezoray, F. Nouboud, D. Mammass (Eds.), Image and Signal Processing ICISP'08, Lecture Notes in Computer Science, 5099, Springer, Berlin, Heidelberg, Germany, 2008, pp. 236–243.
[24] J. Kostková, J. Flusser, M. Lébl, M. Pedone, Image invariants to anisotropic Gaussian blur, in: Proceedings of the Scandinavian Conf. Image Analysis SCIA'19, LNCS 11482, Springer, 2019, pp. 140â–151.
[25] L. Isserlis, On a formula for the product-moment coefficient of any order of a normal frequency distribution in any number of variables, Biometrika 12 (1/2) (1918) 134–139.
[26] D. von Rosen, Moments for matrix normal variables, Statistics: J. Theoret. Appl.Stat. 19 (4) (1988) 575–583.
[27] J. Flusser, On the independence of rotation moment invariants, Pattern Recognit. 33 (9) (2000) 1405–1410.
[28] T.H. Reiss, The revised fundamental theorem of moment invariants, IEEE Trans. Pattern Anal. Mach. Intell. 13 (8) (1991) 830–834.
[29] T. Suk, J. Flusser, Affine moment invariants generated by graph method, Pattern Recognit. 44 (9) (2011) 2047–2056.
[30] B. Xiao, J.-T. Cui, H.-X. Qin, W.-S. Li, G.-Y. Wang, Moments and moment invariants in the Radon space, Pattern Recognit. 48 (9) (2015) 2772–2784.
[31] B. Xiao, L. Li, Y. Li, W. Li, G. Wang, Image analysis by fractional-order orthogonal moments, Inf. Sci. 382 (2017) 135–149.
[32] X. Liu, M. Pedersen, J.Y. Hardeberg, CID: IQ–a new image quality database, in: International Conference on Image and Signal Processing, Springer, 2014, pp. 193–202.
[33] E.C. Larson, D.M. Chandler, Most apparent distortion: full-reference image quality assessment and the role of strategy, J. Electron Imaging 19 (1) (2010) 11006.
[34] A.S. Georghiades, P.N. Belhumeur, D.J. Kriegman, From few to many: illumination cone models for face recognition under variable lighting and pose, IEEE Trans. Pattern Anal. Mach. Intell. 23 (6) (2001) 643–660.
[35] H. Zhang, H. Shu, G.-N. Han, G. Coatrieux, L. Luo, J.L. Coatrieux, Blurred image recognition by Legendre moment invariants, IEEE Trans. Image Process. 19 (3) (2010) 596–611.
[36] C.-Y. Wee, R. Paramesran, Derivation of blur-invariant features using orthogonal Legendre moments, IET Comput. Vision 1 (2) (2007) 66–77.
[37] H. Zhu, M. Liu, H. Ji, Y. Li, Combined invariants to blur and rotation using Zernike moment descriptors, Pattern Anal. Appl. 3 (13) (2010) 309–319.
[38] B. Chen, H. Shu, H. Zhang, G. Coatrieux, L. Luo, J.L. Coatrieux, Combined invariants to similarity transformation and to blur using orthogonal Zernike moments, IEEE Trans. Image Process. 20 (2) (2011) 345–360.
[39] H. Ji, H. Zhu, Degraded image analysis using Zernike moment invariants, in: Proceedings of the International Conference on Acoustics, Speech and Signal Processing ICASSP'09, 2009, pp. 1941–1944.
[40] X. Dai, T. Liu, H. Shu, L. Luo, Pseudo-Zernike moment invariants to blur degradation and their use in image recognition, in: J. Yang, F. Fang, C. Sun (Eds.), Intelligent Science and Intelligent Data Engineering IScIDE'12, Lecture Notes in Computer Science, 7751, Springer, 2013, pp. 90–97.
[41] Q. Liu, H. Zhu, Q. Li, Image recognition by combined affine and blur Tchebichef moment invariants, in: Proceedings of 4th International Conference on Image and Signal Processing (CISP), 2011, pp. 1517–1521.
[42] J. Kautsky, J. Flusser, Blur invariants constructed from arbitrary moments, IEEE Trans. Image Process. 20 (12) (2011) 3606–3611.
[43] T. Suk, C. Höschl IV, J. Flusser, Decomposition of binary images – a survey and comparison, Pattern Recognit. 45 (12) (2012) 4279–4291.
[44] Y. LeCun, C. Cortes, MNIST handwritten digit database, 2010, http://yann.lecun.com/exdb/mnist/.
[45] J. Flusser, B. Zitová, Invariants to convolution with circularly symmetric PSF, in: Proceedings of the 17th International Conference on Pattern Recognition ICPR'04, IEEE Computer Society, 2004, pp. 11–14.
[46] M. Pedone, J. Flusser, J. Heikkilä, Blur invariant translational image registration for *N*-fold symmetric blurs, IEEE Trans. Image Process. 22 (9) (2013) 3676–3689.
[47] M. Pedone, J. Flusser, J. Heikkilä, Registration of images with *N*-fold dihedral blur, IEEE Trans. Image Process. 24 (3) (2015) 1036–1045.

Jitka Kostková received the M.Sc. degree in Applied Mathematical Stochastic Methods from the Czech Technical University, Faculty of Nuclear Science and Physical Engineering, Prague, Czech Republic, in 2015. Currently, she is a Ph.D. student in Mathematical Engineering and tutors undergraduate courses on mathematical analysis at the same university. Jitka Kostková's research interest is focused on moments and moment invariants.

Jan Flusser received the M.Sc. degree in mathematical engineering from the Czech Technical University, Prague, Czech Republic, in 1985, the Ph.D. degree in computer science from the Czechoslovak Academy of Sciences in 1990, and the DrSc. degree in technical cybernetics in 2001. Since 1985 he has been with the Institute of Information Theory and Automation, Czech Academy of Sciences, Prague. In 1995–2007, he was holding the position of a head of Department of Image Processing. Since 2007 he has been a Director of the Institute. He is a full professor of computer science at the Czech Technical University, Faculty of Nuclear Science and Physical Engineering, and at the Charles University, Faculty of Mathematics and Physics, Prague, Czech Republic, where he gives undergraduate and graduate courses on Digital Image Processing, Pattern Recognition, and Moment Invariants and Wavelets. Jan Flusser's research interest covers moments and moment invariants, image registration, image fusion, multichannel blind deconvolution, and super-resolution imaging. He has authored and coauthored more than 200 research publications in these areas, including the monographs *Moments and Moment Invariants in Pattern Recognition* (Wiley, 2009) and *2D and 3D Image Analysis by Moments* (Wiley, 2016). In 2007 Jan Flusser received the Award of the Chairman of the Czech Science Foundation for the best research project and won the Prize of the Academy of Sciences of the Czech Republic for the contribution to image fusion theory. In 2010, he was awarded by the SCOPUS 1000 Award. He received the Felber Medal of the Czech Technical University for excellent contribution to research and education in 2015 and the Academic Premium of the Czech Academy of Sciences for outstanding researchers in 2017.

Matteo Pedone received the M.Sc. degree in computer science from "La Sapienza" University of Rome, Italy, in 2007, and the Doctor of Technology (Ph.D.) degree in computer science from the University of Oulu, Finland, in 2015. He is currently a post-doctoral researcher at the Center for Machine Vision Research, University of Oulu, Finland. His research interests include computer vision, computational photography, invariant theory, statistical signal processing, differential geometry, and Clifford algebra.

Matěj Lébl received the M.Sc. degree in Numerical and Computational Mathematics from the Charles University, Faculty of Mathematics and Physics, Prague, Czech Republic, in 2017. Currently, he is a Ph.D. student in Informatics.

Multidimensional Systems and Signal Processing (2020) 31:1113–1143
https://doi.org/10.1007/s11045-020-00702-7

Robust multivariate density estimation under Gaussian noise

Jitka Kostková[1] · **Jan Flusser**[1,2]

Received: 17 June 2019 / Revised: 13 January 2020 / Accepted: 20 January 2020 /
Published online: 30 January 2020

Abstract
Observation of random variables is often corrupted by additive Gaussian noise. Noise-reducing data processing is time-consuming and may introduce unwanted artifacts. In this paper, a novel approach to description of random variables insensitive with respect to Gaussian noise is presented. The proposed quantities represent the probability density function of the variable to be observed, while noise estimation, deconvolution or denoising are avoided. Projection operators are constructed, that divide the probability density function into a non-Gaussian and a Gaussian part. The Gaussian part is subsequently removed by modifying the characteristic function to ensure the invariance. The descriptors are based on the moments of the probability density function of the noisy random variable. The invariance property and the performance of the proposed method are demonstrated on real image data.

Keywords Multivariate density · Gaussian additive noise · Noise-robust estimation · Moments · Invariant characteristics

1 Introduction

Observation of random variables in a real-world environment is often corrupted by numerous degradation factors, among which an additive random noise is one of the most frequent ones. The noise may be introduced by measurement device imperfection, by storing and transmitting, and also due to the precision loss when pre-processing the data.

This work has been supported by the Czech Science Foundation (Grant No. GA18-07247S), by the Grant SGS18/188/OHK4/3T/14 provided by the Ministry of Education, Youth, and Sports of the Czech Republic (MŠMT ČR), by *Praemium Academiae*, and by the Joint Laboratory SALOME2. Thanks to Dr. Cyril Höschl IV for kind providing the test images used in the experiments in Section 8.2.

Jitka Kostková
kostkova@utia.cas.cz

Jan Flusser
flusser@utia.cas.cz

1 Institute of Information Theory and Automation, Czech Academy of Sciences, Pod vodárenskou věží 4, 182 08 Prague 8, Czech Republic

2 Faculty of Management, University of Economics, Jarosovska 1117/II, 377 01 Jindrichuv Hradec, Czech Republic

Let X be the multivariate random variable to be observed and let N be an additive noise. As a result of the measurement, we actually observe realizations of a random variable $Z = X + N$ instead of X, which is observed only indirectly. If the signal-to-noise ratio is low, the corruption is so heavy that it is very difficult to deduce anything about the observed variable X from the sample data Z. This situation occurs frequently in many application areas such as signal and image processing, econometrics, experimental physics, geoscience, and many others.

A large amount of effort has been spent to develop methods that decrease the impact of the noise and allow to estimate either the entire X or at least some of its discriminative characteristics. These methods can be categorized into three main groups – denoising, deconvolution, and robust estimators.

Denoising methods aim to suppress the noise in the data and are usually based on linear or non-linear filtering of high-frequency components and data smoothing. The advantage of denoising methods is that they provide a complete estimate of X while the common disadvantage however may be artifacts and deformation or loss of high-frequency information contained in original X.

Deconvolution methods try to recover the *probability density function* (PDF) f_X of random variable X from the estimated PDF of the observed Z. Assuming the noise is independent of the data, it is well known that the PDF of the sum of two independent random variables is a convolution of the densities of the summands, i.e. in our case

$$f_Z(x) = (f_X * f_N)(x) = \int f_X(x - s) f_N(s)\, \mathrm{d}s. \tag{1}$$

Deconvolution methods could theoretically yield an accurate estimate of f_X but in reality they suffer from several drawbacks. Blind deconvolution methods, which do not require any prior knowledge of the noise density f_N, are numerically unstable, may converge to an incorrect solution and are very time-consuming. Non-blind methods are better in that sense but obtaining a good estimate of f_N may be in practice difficult or even impossible.

Robust estimators try to estimate certain characteristics of X such as mean value, variance, skewness and higher-order moments directly from the observed samples of Z. Standard formulas for sample moments do not perform well on noisy data. This is why some authors proposed not to resolve Eq. (1) but only to find some characteristics which are not affected by convolution. Such characteristics, called *convolution invariants*, must be the same for both f_Z and f_X and should be calculated directly from sample observations of Z. This modern approach [it was firstly proposed in Höschl IV and Flusser (2016)] may be very efficient whenever a complete knowledge of f_X is not necessary, typically in noisy signal classification and signal/image retrieval. In this paper, we develop this idea substantially.

The main idea of this paper is as follows. We assume that noise N is a multivariate Gaussian random variable with zero mean and a general covariance matrix, which is unknown. We introduce *projection operators*, acting on the space of all PDF's, that divide each PDF into two components. Based on the known parametric form of f_N, we show that one of the components can be used to compute quantities, which are invariant with respect to convolution in Eq. (1). These quantities can be used directly to characterize f_X without any noise estimation, denoising and deconvolution. Unlike Höschl IV and Flusser (2016), where the idea of invariant descriptors was used heuristically for univariate densities only, we present here a consistent theory for multivariate densities.

After providing the state-of-the-art review in Sect. 2, we formulate the problem formally in Sect. 3. Section 4 is dedicated to the construction of a projection operator and its relation to invariants. This theory is then used for the construction of moment-based invariants

descriptors in r dimensions (r-D) in Sect. 5. In Sect. 6, one and two-dimensional cases are analyzed in detail and explicit invariant formula is derived. Finally, the experimental section verifies the theory on simulated as well as real data from image processing area and shows a potential application in image retrieval.

2 Literature review

2.1 Denoising methods

Majority of the articles on denoising comes from signal processing area, such as Motwani et al. (2004), Buades et al. (2005b). These methods often lead to subjective improvement but they can cause the loss of important information, the formation of artifacts, smoothing of the signal, etc. The simplest way of removing noise from the signal is a linear filtering, when the corrupted signal is convolved with some low-pass filter. This method, however, leads to deformation of the high-frequency components of the signal. Non-linear filtering methods, such as median filter and the anisotropic filter designed by Perona and Malik (1990), attempt to avoid the effect of signal blurring. One of the state-of-the-art methods is the *Non-Local Means* algorithm based on the self-similarity of signal patches (Buades et al. 2005a). Various methods rely on a transform domain filtering, e.g. wavelet-based denoising (Chen et al. 2013; Cho and Bui 2005), ridgelet- and curvelet-based denoising (Starck et al. 2002), and Fourier Wiener filtering (Khireddine et al. 2007). Other methods make use of minimization of some functionals, e.g. a total variation method (Chambolle and Lions 1997) and a method using higher order statistics (Teuber et al. 2012).

2.2 Deconvolution methods

Many books and papers dedicated to this topic have been published. The tutorial article (De Brabanter and De Moor 2012) and the book (Meister 2009) gave an introduction to deconvolution problems in non-parametric statistics (density estimation based on contaminated data, errors-in-variables regression, and image reconstruction). One of the approaches is to estimate the density of Z in the non-parametric form by a kernel estimator and then to use Fourier transform to recover the distribution of X (Carroll and Hall 1988; Stefanski and Carroll 1990; Fan 1992); another is Bayesian approach (Efron 2014) and wavelet approach (Pensky et al. 1999). The paper (Butucea et al. 2009) tries to estimate $\mathbb{E}[\psi(X)]$, where ψ is a known integrable function and the distribution of N is known. In Johannes et al. (2009), the authors deal with the estimation of deconvolution, when only an estimate of the distribution of N is available. The authors of Comte and Lacour (2011) suppose that the distribution of N is unknown and present an adaptive estimator. The goal of Kappus et al. (2014) is analogous, but they do not impose any assumption on the shape of the characteristic function of noise.

2.3 Convolution invariants

The use of convolution invariants for a noise-robust PDF estimation was firstly proposed in the paper Höschl IV and Flusser (2016), which was motivated by histogram-based image retrieval. The authors presented invariants defined for univariate densities only. Their invariants were based on moments of a histogram of the noisy graylevel image. However, the results

of Höschl IV and Flusser (2016) cannot be easily extended to multidimensional signals and multivariate PDF's. It should be noted that convolution invariants have been thoroughly studied in a different context and domains (Flusser and Suk 1998; Flusser et al. 2003; Galigekere and Swamy 2006; Ojansivu and Heikkilä 2007; Zhang et al. 2010; Gopalan et al. 2012; Makaremi and Ahmadi 2012; Pedone et al. 2013; Flusser et al. 2015) but those results are not suitable for noisy PDF estimation due to a very specific convolution kernel shapes, that do not correspond to real-life noise PDFs.

3 Problem formulation

Let X and N be two r-D independent random variables with probability density functions f_X and f_N, respectively, where $N \sim \mathcal{N}(\mathbf{0}, \Sigma)$ is a normally distributed zero-mean random variable with a regular covariance matrix Σ. Then f_N has the well-known Gaussian shape

$$f_N(\mathbf{x}) = \frac{1}{\sqrt{(2\pi)^r |\Sigma|}} \exp\left\{-\frac{1}{2}\mathbf{x}^T \Sigma^{-1}\mathbf{x}\right\}, \tag{2}$$

where $\mathbf{x} = (x_1, \ldots, x_r)^T$. Most frequently, but not necessarily, X is the multivariate random variable which represents the original non-corrupted data and N is an additive Gaussian noise.

Under the above assumptions, the PDF of the sum of these variables

$$Z = X + N \tag{3}$$

exists and is given by

$$f_Z = f_X * f_N. \tag{4}$$

Our aim is to design a functional (descriptor) I, which is invariant with respect to the noise. Since we construct this functional on the space of the PDFs, we require

$$I(f_X) = I(f_Z) = I(f_X * f_N) \tag{5}$$

for any normally distributed zero-mean random variable N with arbitrary (unknown) covariance matrix Σ.

To comply with Eq. (5) is, however, not the only desirable property of I. At the same time, I must be *discriminable*, which means

$$I(f_X) \neq I(f_Y) \tag{6}$$

for any X and Y such that they are not linked as $Y = X + N$ for any Gaussian N.

If we design such invariant I, it maps the original data as well as all its corrupted versions into a single point in an abstract feature space, while any two distinct data are mapped into distinct points regardless of their potential corruption. Such invariant feature space can be efficiently used for data description and classification.

4 Construction of the invariant

The main idea of constructing invariants to Gaussian convolution is based on projections of a PDF onto the set of all Gaussian functions. In this way, we extract the Gaussian component of the random variable. We will show that the ratio of the characteristic functions of the original

random variable and of its Gaussian component possesses the desired invariant property. In the sequel, we introduce the necessary mathematical background.

Let us denote the set of all probability density functions with finite second-order central moments as $\mathcal{D}$ and the set of all zero-mean Gaussian probability density functions

$$\mathcal{S} = \{f_N | \Sigma \triangleright 0\}, \tag{7}$$

where $\Sigma \triangleright 0$ denotes the positive-definiteness of covariance matrix Σ. The set $\mathcal{S}$ exhibits the following basic properties.

Lemma 1 *$\mathcal{S}$ is closed under convolution.*

It holds for any two Gaussian PDFs f_{N_1} and f_{N_2} with covariance matrices Σ_1 and Σ_2 that the result of convolution

$$f_{N_1} * f_{N_2} = f_N$$

is again a Gaussian PDF with covariance matrix $\Sigma = \Sigma_1 + \Sigma_2$.

Let us define projection operator P that projects an arbitrary $f \in \mathcal{D}$ on the "nearest" Gaussian PDF in the sense of having the same covariance matrix. In particular, $P : \mathcal{D} \mapsto \mathcal{S}$ is defined as

$$Pf = f_N, \tag{8}$$

where f_N has the same covariance matrix as f. The operator P is well defined for all PDFs with a regular covariance matrix[1] and is idempotent, i.e. $P^2 = P$. Note that P is not linear, so it is not a projector in the common sense known from linear algebra.

For our purposes, the crucial property of operator P is that it commutes with the convolution with functions from $\mathcal{S}$. This property is necessary for the construction of the invariant descriptors.

Lemma 2 *Let $f \in \mathcal{D}$ and $g \in \mathcal{S}$. Then*

$$P(f * g) = Pf * g. \tag{9}$$

Proof First, we investigate the right-hand side, where we have a convolution of two Gaussians with covariance matrices Σ_f and Σ_g, respectively. Thanks to Lemma 1, this is also a Gaussian with covariance matrix $\Sigma = \Sigma_f + \Sigma_g$.

On the left-hand side, $P(f * g)$ is by definition a Gaussian with covariance matrix Σ_{f*g}. It is well known that central second-order moments of any PDF, which is a convolution of two other PDFs, are sums of the same moments of the factors. The same is true for entire covariance matrix. Hence, we have $\Sigma_{f*g} = \Sigma_f + \Sigma_g = \Sigma$, which completes the proof. □

Now we formulate the principal theorem of the paper that introduces the invariant descriptor of a probability density function as a ratio of certain characteristic functions.

Theorem 1 *Let $f \in \mathcal{D}$ and let P be the projection operator defined above. Then the ratio of characteristic functions Φ of the densities f and Pf*

$$I(f) = \frac{\Phi(f)}{\Phi(Pf)} \tag{10}$$

is an invariant to convolution with a Gaussian probability density function, i.e. $I(f) = I(f * f_N)$ for any $f_N \in \mathcal{S}$.

[1] It is possible to extend this definition also to singular covariance matrices by admitting degenerated Gaussian densities in $\mathcal{S}$.

Proof First, note that I is well defined. Both characteristic functions always exist (they actually equal to the Fourier transform of the respective PDF) and the denominator is non-zero everywhere. The rest of the proof follows from the fact that P commutes with the Gaussian convolution (see Lemma 2). If $f_N \in \mathcal{S}$, then

$$I(f * f_N) = \frac{\Phi(f * f_N)}{\Phi(P(f * f_N))} = \frac{\Phi(f * f_N)}{\Phi(Pf * f_N)} = \frac{\Phi(f)\Phi(f_N)}{\Phi(Pf)\Phi(f_N)} = \frac{\Phi(f)}{\Phi(Pf)} = I(f).$$

□

The following Theorem claims that the invariant I is a complete description of f modulo convolution with a Gaussian.

Theorem 2 *Let f_1 and f_2 be two probability density functions and $I(f)$ be the invariant defined in Theorem 1. Then $I(f_1) = I(f_2)$ if and only if there exist $f_{N_1}, f_{N_2} \in \mathcal{S}$ such that $f_{N_1} * f_1 = f_{N_2} * f_2$.*

Proof Let us prove the forward implication first.

$$\begin{aligned} I(f_1) = I(f_2) \Rightarrow \frac{\Phi(f_1)}{\Phi(Pf_1)} = \frac{\Phi(f_2)}{\Phi(Pf_2)} \Rightarrow \Phi(f_1)\Phi(Pf_2) = \Phi(f_2)\Phi(Pf_1) \\ \Rightarrow \Phi(f_1 * Pf_2) = \Phi(f_2 * Pf_1) \Rightarrow f_1 * Pf_2 = f_2 * Pf_1. \end{aligned}$$

So, we have found $f_{N_1} = Pf_2$ and $f_{N_2} = Pf_1$. The backward implication follows directly from Theorem 1. □

In 1D, Theorem 2 can be formulated in a stronger way. $I(f_1) = I(f_2)$ if and only if there exists $f_N \in \mathcal{S}$ such that $f_N * f_1 = f_2$ or $f_N * f_2 = f_1$. This statement follows from the divisibility of 1D Gaussian functions but it cannot be extended into the multidimensional case.

Theorems 1 and 2 show that invariant I entirely and uniquely describes any PDF modulo convolution with a Gaussian. In particular, for any $f \in \mathcal{S}$ we have $I(f) = 1$.

5 Invariants from moments

Although theoretically the invariant $I(f)$ fully describes f, several problems can occur when dealing with finite-precision arithmetic. The division by small numbers leads to the precision loss. To speed up the computation, it would be better to avoid the explicit construction of $\Phi(f)$ and $\Phi(Pf)$. In this Section, we show that it can be accomplished by constructing moment-based invariants equivalent to $I(f)$.

We can rewrite Eq. (10) as

$$\Phi(Pf) \cdot I(f) = \Phi(f). \tag{11}$$

If the 1D characteristic function is n-times differentiable, then its k-th derivative ($k \leq n$) is the moment m_k of the PDF up to a multiplicative constant. The same is true in multidimensional case. If the characteristic function $\Phi(f)$ has a Taylor expansion, then we can write, using a multi-index notation,

$$\sum_{\substack{\mathbf{k}=\mathbf{0} \\ |\mathbf{k}|\neq 0,\ \text{even}}}^{\infty} \frac{\mathrm{i}^{|\mathbf{k}|}}{\mathbf{k}!} m_{\mathbf{k}}^{(Pf)} \mathbf{u}^{\mathbf{k}} \cdot \sum_{\mathbf{p}=\mathbf{0}}^{\infty} \frac{\mathrm{i}^{|\mathbf{p}|}}{\mathbf{p}!} A_{\mathbf{p}} \mathbf{u}^{\mathbf{p}} = \sum_{\mathbf{q}=\mathbf{0}}^{\infty} \frac{\mathrm{i}^{|\mathbf{q}|}}{\mathbf{q}!} m_{\mathbf{q}}^{(f)} \mathbf{u}^{\mathbf{q}}. \tag{12}$$

where the $A_{\mathbf{k}}$'s are Taylor coefficients of $I(f)$. By equating the coefficients of the same power of $\mathbf{u}$ we get

$$\sum_{\substack{\mathbf{l}=\mathbf{0} \\ |\mathbf{l}| \text{ even}}}^{\mathbf{k}} \frac{\mathrm{i}^{|\mathbf{l}|}}{\mathbf{l}!} m_{\mathbf{l}}^{(Pf)} \frac{\mathrm{i}^{|\mathbf{k}|-|\mathbf{l}|}}{(\mathbf{k}-\mathbf{l})!} A_{\mathbf{k}-\mathbf{l}} = \frac{\mathrm{i}^{|\mathbf{k}|}}{\mathbf{k}!} m_{\mathbf{k}}^{(f)}, \tag{13}$$

which is equivalent to

$$\sum_{\substack{\mathbf{l}=\mathbf{0} \\ |\mathbf{l}| \text{ even}}}^{\mathbf{k}} \binom{\mathbf{k}}{\mathbf{l}} m_{\mathbf{l}}^{(Pf)} A_{\mathbf{k}-\mathbf{l}} = m_{\mathbf{k}}^{(f)}. \tag{14}$$

Since $I(f)$ is an invariant, each $A_{\mathbf{k}}$ must be an invariant, too. Re-arranging the previous equation, we obtain a recursive formula for $A_{\mathbf{k}}$

$$A_{\mathbf{k}} = m_{\mathbf{k}}^{(f)} - \sum_{\substack{\mathbf{l}=\mathbf{0} \\ |\mathbf{l}|\neq 0, \text{ even}}}^{\mathbf{k}} \binom{\mathbf{k}}{\mathbf{l}} m_{\mathbf{l}}^{(Pf)} A_{\mathbf{k}-\mathbf{l}}. \tag{15}$$

For characteristic functions that do not possess a complete Taylor expansion, we may use the Taylor's Theorem. If the characteristic function has continuous derivatives up to the order $n+1$, then one can write the characteristic function as the Taylor expansion up to the n-th order plus the remainder. Consequently, the invariants up to the order n exist and follow Formula (15).

An intuitive meaning of the invariants $A_{\mathbf{k}}$ is the following one. They could be understood as moments of a "mother function" f_m, which is a function that has no Gaussian component and that "generates" f in the sense that there exist $g \in \mathcal{S}$ such that $f = g * f_m$. In general, f_m lies outside $\mathcal{D}$ or may not even exist but the invariants $A_{\mathbf{k}}$ can be, however, still applied correctly.

Another noteworthy point is that generally we have to calculate moments of both f and Pf in order to evaluate Eq. (15). In the next Section, we show how the construction of Pf and calculation of its moments can be avoided in one and two dimensions.

6 Invariants in one and two dimensions

In many practical applications, especially in signal and image processing, the PDFs we want to characterize are one dimensional or two dimensional functions. In this Section, we show how Eq. (15) can be further simplified in those cases.

In 1D, the recursive form of invariants (15) obtains the form

$$A_p = m_p^{(f)} - \sum_{\substack{k=2 \\ k \text{ even}}}^{p} \binom{p}{k} (k-1)!!\, m_2^{k/2} A_{p-k}. \tag{16}$$

This simplification follows from the fact that the odd-order moments of a 1D Gaussian with standard deviation σ vanish and the even-order ones are given as $m_p = \sigma^p (p-1)!!$. Furthermore, $\sigma^2 \equiv m_2^{(Pf)} = m_2^{(f)}$ which allows us to express all moments of Pf in terms of

those of f. Thanks to this, Eq. (16) can be equivalently rewritten in a non-recursive form as

$$A_p = \sum_{\substack{k=0 \\ k \text{ even}}}^{p} (-1)^{k/2} \binom{p}{k} (k-1)!!\, m_2^{k/2} m_{p-k}^{(f)}. \tag{17}$$

In 2D, simplification of Eq. (15) is much more difficult. First, we need to express the moments of 2D Gaussian PDF explicitly. If we assume that the two components of our random variable N are independent, then we can constraint the covariance matrix of Pf to be diagonal. Then the general moment of Pf is simply

$$m_{pq}^{(Pf)} = (p-1)!!(q-1)!! m_{20}^{p} m_{02}^{q} \tag{18}$$

and we obtain similar formulas as in 1D case

$$A_{mn} = m_{mn}^{(f)} - \sum_{\substack{l=0 \\ l+k \neq 0, \\ l+k \text{ even}}}^{m} \sum_{k=0}^{n} \binom{m}{l} \binom{n}{k} (l-1)!!(k-1)!!\, m_{20}^{l/2} m_{02}^{k/2} A_{m-l,n-k} \tag{19}$$

in the recursive form and

$$A_{mn} = \sum_{\substack{l=0 \\ l+k \text{ even}}}^{m} \sum_{k=0}^{n} (-1)^{\frac{k+l}{2}} \binom{m}{l} \binom{n}{k} (l-1)!!(k-1)!!\, m_{20}^{l/2} m_{02}^{k/2} m_{m-l,n-k}^{(f)} \tag{20}$$

in the explicit form.

However, the assumption of independent components and hence of the diagonal covariance matrix is not realistic in practice. We illustrate this by real data from signal processing. The signal was captured in two spectral bands, both corrupted by a thermal noise of the sensor. This noise can be approximatively modelled as an additive Gaussian noise. In Fig. 1, we can see the 2D histogram of the noise extracted from a real image by means of denoising algorithm and subtracting from the original. The normalized histogram is a sampled PDF of the noise. It is clearly apparent that there is a strong correlation between the noise in red and green channels. So, to make our method applicable in practice, we have to assume a general covariance matrix of Pf.

For a general covariance matrix, the formula for moments of a 2D Gaussian is much more complicated and is not commonly cited in the literature. It can be either deduced, after some manipulations, from the papers presenting general approaches to moment calculation (Isserlis 1918; Bar and Dittrich 1971; Von Rosen 1988; Blacher 2003; Schott 2003; Triantafyllopoulos 2003; Song and Lee 2015) or obtained directly from the definition by integration as shown in "Appendix A".

The moments of 2D Gaussian PDF are given as

$$\mathrm{m}_{mn}^{(Pf)} = \sum_{\substack{i=0 \\ j \geq \frac{m-n}{2}}}^{\lfloor \frac{m}{2} \rfloor} \sum_{j=0}^{i} (-1)^{i-j} \binom{m}{2i} \binom{i}{j} (m+n-2i-1)!!(2i-1)!! m_{11}^{m-2j} m_{20}^{j} m_{02}^{\frac{n-m}{2}+j}. \tag{21}$$

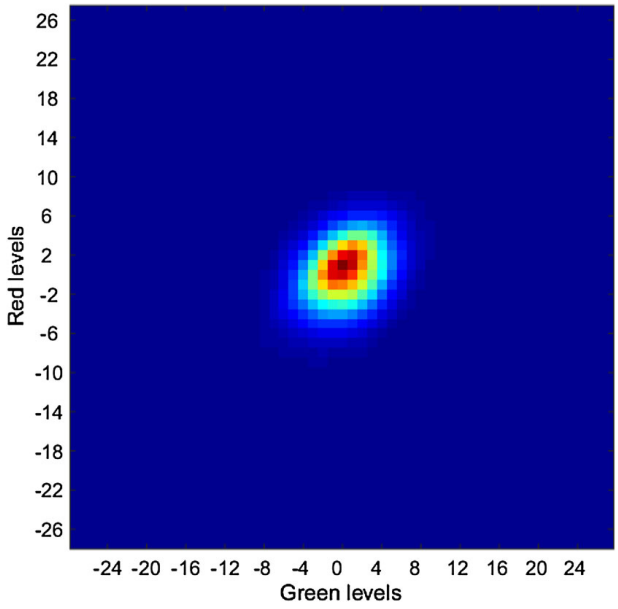

Fig. 1 2D histogram of the noise extracted from red and green channels of a real digital image. The on-chip postprocessing introduces a correlation about 0.33 between the noise in individual channels (Color figure online)

If we use Formula (21), the general recursive definition of the invariants (15) turns to the form

$$\begin{aligned} A_{mn} =& m^{(f)}_{mn} - \sum_{\substack{l=0\\ l+k\neq 0,\\ l+k \text{ even}}}^{m}\sum_{k=0}^{n}\binom{m}{l}\binom{n}{k}\sum_{\substack{i=0\\ j\geq\frac{k-l}{2}}}^{\lfloor\frac{k}{2}\rfloor}\sum_{j=0}^{i}(-1)^{i-j}\binom{k}{2i}\binom{i}{j}(l+k-2i-1)!! \\ & \cdot (2i-1)!!\, m_{11}^{k-2j} m_{20}^{\frac{l-k}{2}+j} m_{02}^{j} A_{m-l,n-k}, \end{aligned} \tag{22}$$

which can again be rewritten into a non-recursive formula

$$\begin{aligned} A_{mn} =& \sum_{\substack{l=0\\ l+k \text{ even}}}^{m}\sum_{k=0}^{n}(-1)^{\frac{k+l}{2}}\binom{m}{l}\binom{n}{k}\sum_{\substack{i=0\\ j\geq\frac{k-l}{2}}}^{\lfloor\frac{k}{2}\rfloor}\sum_{j=0}^{i}(-1)^{i-j}\binom{k}{2i}\binom{i}{j}(l+k-2i-1)!! \\ & \cdot (2i-1)!!\, m_{11}^{k-2j} m_{20}^{\frac{l-k}{2}+j} m_{02}^{j} m^{(f)}_{m-l,n-k}. \end{aligned} \tag{23}$$

The proof of equivalence of (22) and (23) can be found in "Appendix B".

7 Implementation

The formulas (22) and (23) are both efficient in the sense that they contain only the moments of f, which is the PDF of the observed noisy random variable. As we will see in the next section, in practice the theoretical PDF is often replaced with a normalized multidimensional histogram, which is in fact a sampled PDF and is easy to compute directly from the observed values. Neither the characteristic function $\Phi(f)$ nor the projection Pf are necessary to be constructed. This is the main advantage of the moment approach over the direct use of $I(f)$. Hence, in numerical implementation, we always use the moment-based invariants A_{mn} instead of $I(f)$.

The value of A_{mn} can be calculated either from (22) or (23). Since they are theoretically equivalent, the choice depends on the particular task. If all invariants up to a certain order are to be computed, the recursive formula is recommended. Formula (23) is more efficient if we want to compute a single invariant only. The complexity of both depends mainly on our ability to compute the moments of the PDF efficiently. Since the PDF may be of arbitrary shape, we calculate the moments from definition without any speed-up tricks.

In Eqs. (22) and (23), we may use either general or central moments, depending on the nature of the random variable we observe. If there is a systematic shift of the values, which is not important in our application, we use central moments that are not influenced by this shift. Regardless of what moments we employ, some invariants are trivial. $A_{00} = 1$ and $A_{20} = A_{02} = A_{11} = 0$ because of the normalization constraints. If we use central moments, then also $A_{10} = A_{01} = 0$. Trivial invariants are useless for the PDF description and should be removed from the feature vector to reduce its dimensionality.

When calculating the moments of a large-scale histogram, we face a threat of a precision loss due to rounding or even a floating-point overflow. This may happen particularly for higher-order moments and degrade the calculation of the invariants. However, in practice we usually obtain a sufficient characterization of the PDF from the invariants A_{mn} of reasonably low orders (in our experiments in the next section, the maximum order was 25) and we do not encounter any significant precision loss, but one has to be aware of this danger.

8 Experiments

In this section, we demonstrate the invariance property and performance of the proposed method on real data from image processing.

We can view an image as a realization of a random variable, the dimension of which is given by the number of spectral/color bands. Its normalized multidimensional histogram plays the role of a sampled multivariate PDF. The image has been corrupted by an additive Gaussian noise in all bands, which is assumed to be independent of the image content.

8.1 Invariance to simulated noise

In this experiment, we show the invariance property if the noise exactly follows the Gaussian model. We used real color photographs as the test data and we corrupted them by an artificial Gaussian noise generated from the PDF (2). We did not cut off the values below zero and above 255 in order to fulfill the assumption of normal distribution. We used two families of noise, each represented by 100 realizations. Medium noise (SNR about 32 dB) was generated such that the eigenvalues of the correlation matrix were set $\lambda_1 = 6$, $\lambda_2 = 3.5$ and the correlation coefficient was random. Heavy noise (SNR about 28) was generated in the same way using $\lambda_1 = 15$ and $\lambda_2 = 8$. To get 2D histograms, we used the RGB channels pairwise.

In Fig. 2, we can see the first test image. Figure 3 shows a segment of the original and noisy images, respectively, to illustrate the visual appearance of the noise. Figure 4 shows the 2D histogram of blue and green channels and the histogram of the same channels of the noisy image.

We calculated more than 300 invariants using Eq. (22) of a histogram of each noisy image and took the mean value of each invariant (separately for medium noise and heavy noise). Then we calculated relative errors between this mean value and the invariants calculated from the original "clear" histogram. The relative errors of all invariants are visualized in Fig. 5

Fig. 2 The original image of a meadow

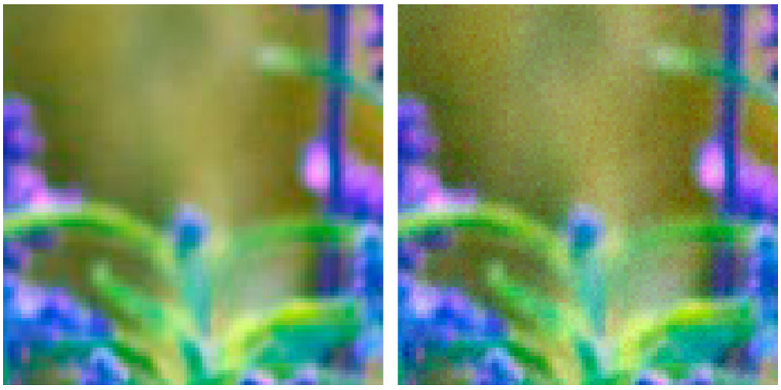

Fig. 3 The segment of the original image (left) and of the noisy image (right). The noise is visually apparent

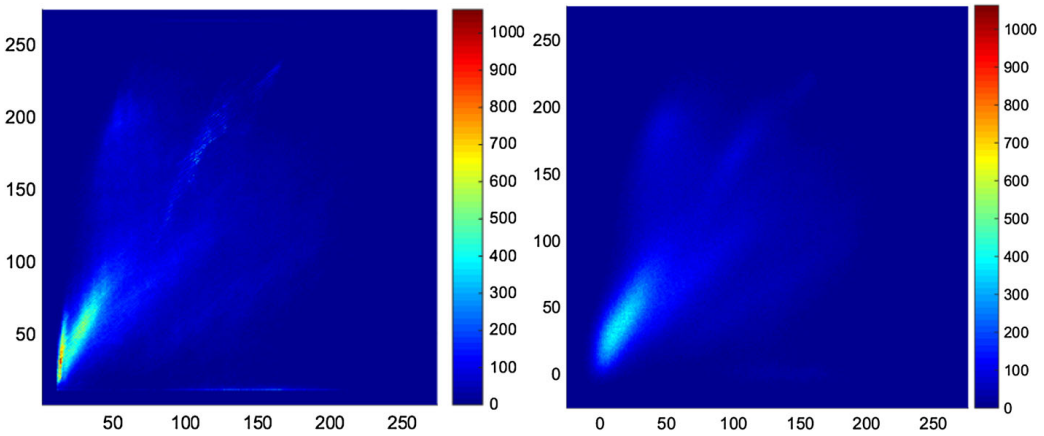

Fig. 4 2D histogram of the blue and green channels of the original clear image (left) and of the same image corrupted by an additive Gaussian noise (right). Note that the "noisy" histogram is actually a smoothed version of the original histogram

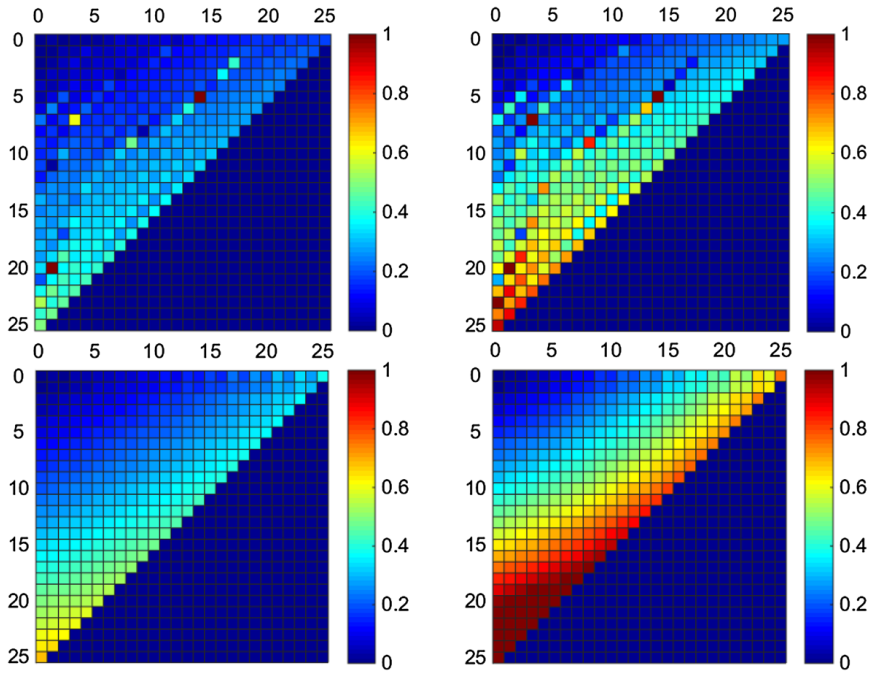

Fig. 5 Mean relative errors of the invariants (top) and of the moments (bottom) up to the order 25. The 25×25 matrix contains the color-encoded values of the mean errors of individual invariants/moments. Only the upper left triangle of the matrix is valid. Top left matrix shows invariants calculated from 100 instances of medium noise (see the text for the details on noise generation), top right matrix shows the same for heavy noise. The bottom matrices display the same for the moments (Color figure online)

(top). We can see that almost all errors are reasonably low. Relative errors higher than 1% appear only for heavy noise in case of few invariants of orders between 20 and 25. To show the advantage of the proposed invariants over the plain moments, we calculated the same for the moments of the histograms, see Fig. 5 bottom. Comparing the corresponding values, we can see the errors of the moments are by one order higher since the moments do not posses the invariance property and are heavily influenced by noise. The errors of the invariants are, however, not zero as one could expect from the theory. Especially for higher-order invariants, we face precision loss in calculations. Another source of errors is that the theory assumes continuous Gaussian convolution kernel while in the discrete domain we work with sampled and truncated Gaussian.

We repeated this experiment on other test images and with various color band pairs. In most cases, the results were fully comparable to those described above (see Figs. 6, 7 and 8 for three other examples). However, we found a few examples where the relative errors of the invariants are significantly higher, even for medium noise. This occurs when the histogram is extremely sparse. In such a case, the sampling errors are more significant and the invariants properties derived in a continuous domain are violated (see Fig. 9 for an example).

8.2 Invariance on real pictures

In the second experiment, we tested the invariance on real noisy images captured by a compact camera. The noise comes mainly due to physical processes on the CCD chip and has several components. Photon shot noise, thermal noise, readout noise and background noise are the main ones. An additive noise component can be reasonably modelled by a Gaussian random

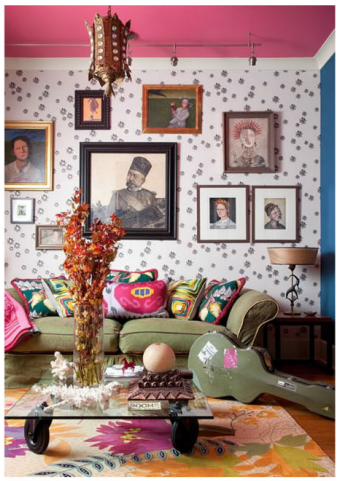

(a) The original image of a living room.

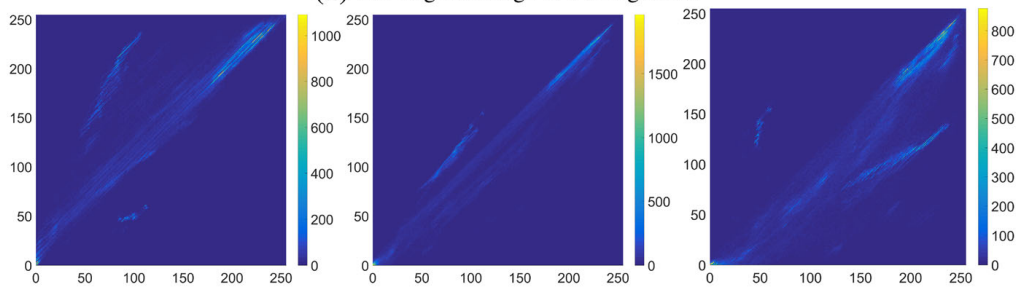

(b) 2D histograms of the original image - red-green (left), blue-green (middle), red-blue (right).

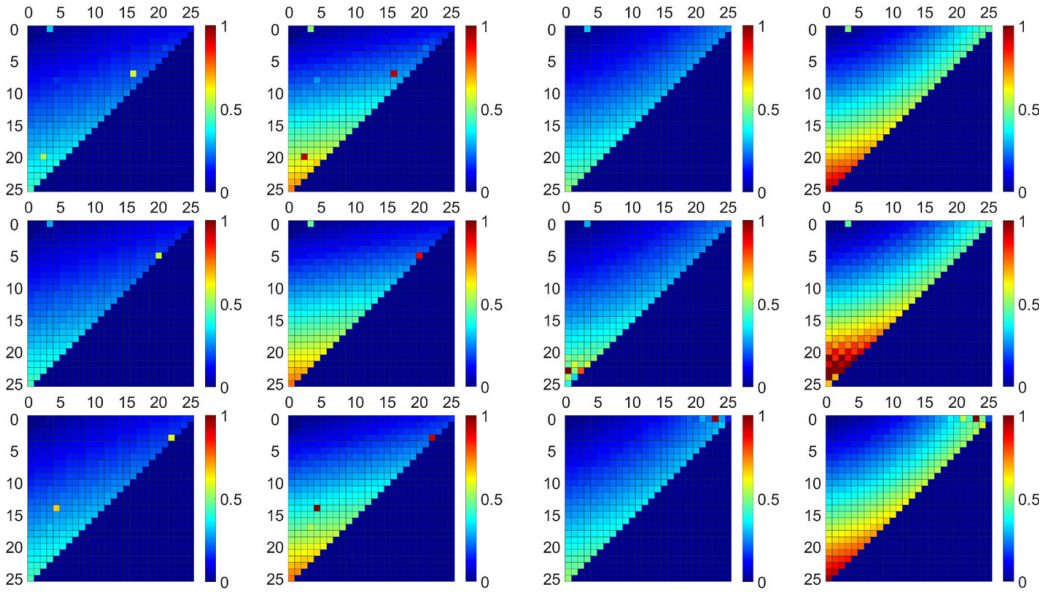

(c) MRE of the invariants. **(d)** MRE of the moments.

Fig. 6 Picture of a living room **a** with its 2D histograms **b** and mean relative errors (**c**, **d**). Mean relative errors of the invariants for medium noise (first column) and heavy noise (second column), and of the moments for the same noise (third and fourth column, respectively). Histograms of red–green (first row), blue–green (second row) and red–blue (third row) channels were used (Color figure online)

(a) The original image of a couple.

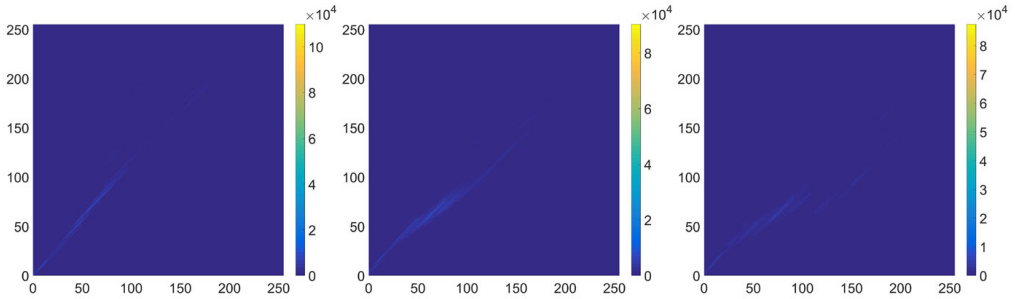

(b) 2D histograms of the original image - red-green (left), blue-green (middle), red-blue (right).

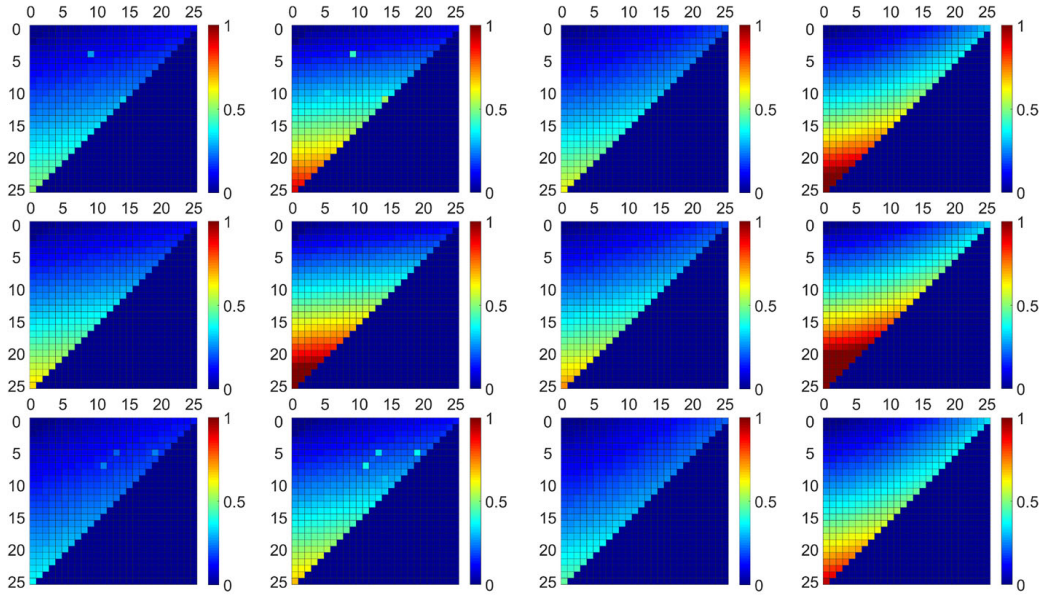

(c) MRE of the invariants.

(d) MRE of the moments.

Fig. 7 Picture of a couple **a** with its 2D histograms **b** and mean relative errors (**c**, **d**). Mean relative errors of the invariants for medium noise (first column) and heavy noise (second column), and of the moments for the same noise (third and fourth column, respectively). Histograms of red–green (first row), blue–green (second row) and red–blue (third row) channels were used (Color figure online)

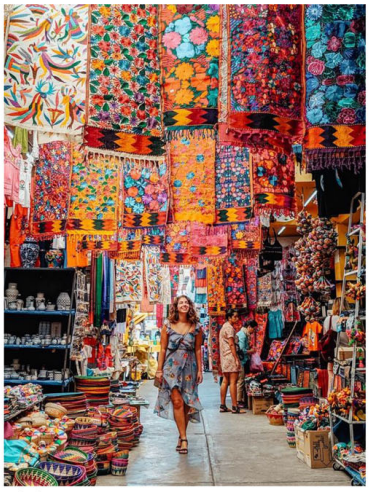

(a) The original image of a market.

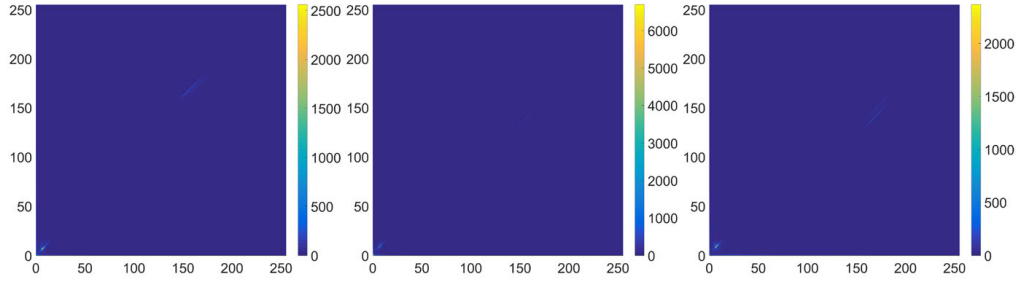

(b) 2D histograms of the original image - red-green (left), blue-green (middle), red-blue (right).

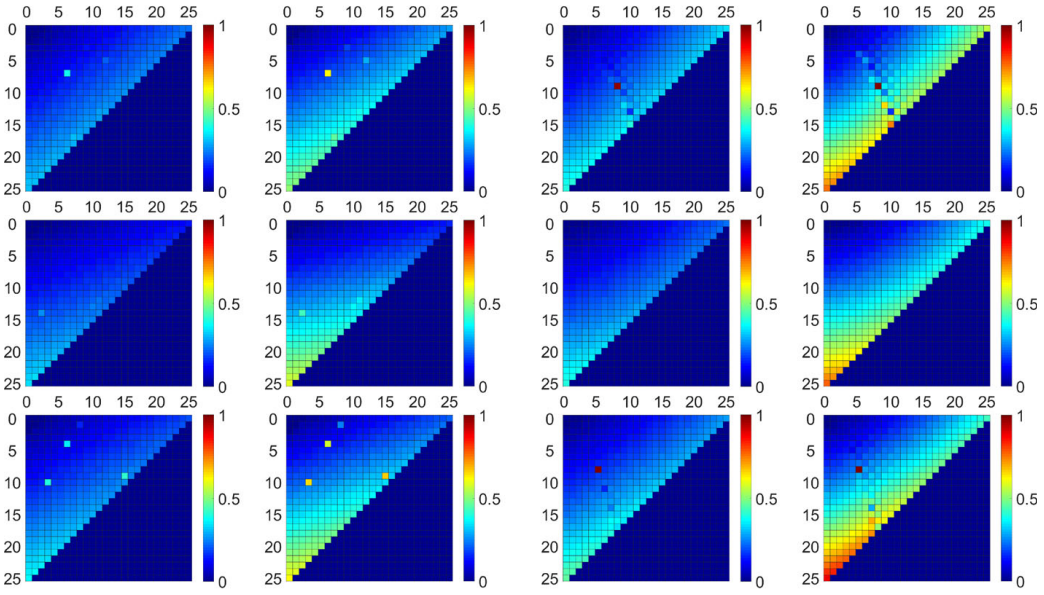

(c) MRE of the invariants. **(d)** MRE of the moments.

Fig. 8 Picture of a market **a** with its 2D histograms **b** and mean relative errors (**c**, **d**). Mean relative errors of the invariants for medium noise (first column) and heavy noise (second column), and of the moments for the same noise (third and fourth column, respectively). Histograms of red–green (first row), blue–green (second row) and red–blue (third row) channels were used (Color figure online)

(a) The original image of a mountain.

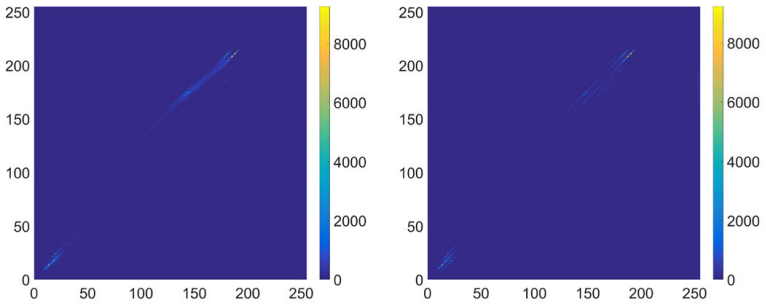

(b) 2D histograms of the original image - blue-green (left), red-blue (right).

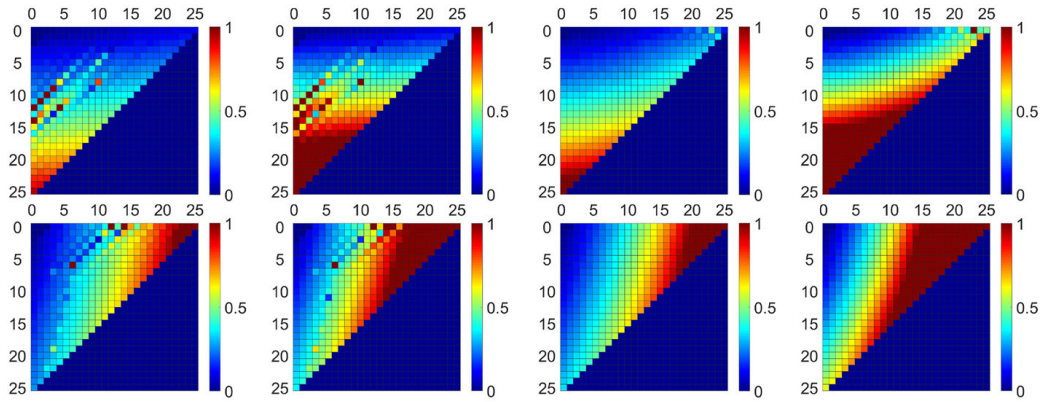

(c) MRE of the invariants. **(d)** MRE of the moments.

Fig. 9 Picture of a mountain **a** with its 2D histograms **b** and mean relative errors (**c**, **d**). Mean relative errors of the invariants for medium noise (first column) and heavy noise (second column), and of the moments for the same noise (third and fourth column, respectively). Histograms of blue–green (first row) and red–blue (second row) channels were used (Color figure online)

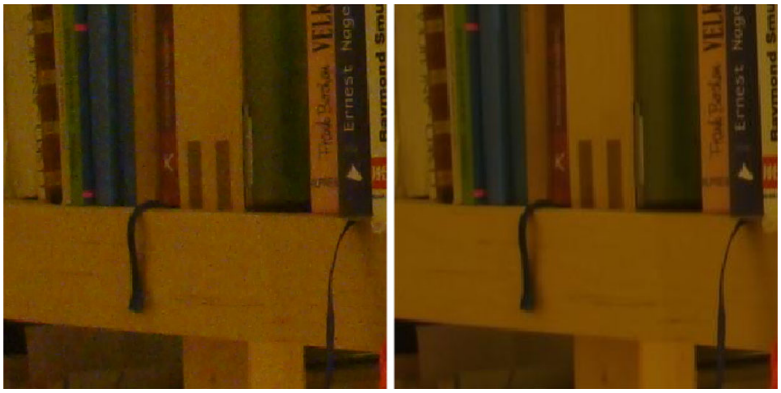

Fig. 10 A patch of a real noisy picture (left) and the same patch with the noise suppressed by time averaging over 10 images (right)

variable uncorrelated with the image values while the signal-dependent component (which is less significant here) follows Poisson distribution and cannot be handled by the proposed method. The main difference from the synthetic case is that the pixel values are always between 0 and 255, which cuts off the tails of the noise distribution and makes the PDF different from a Gaussian.

To obtain test images with visually apparent noise, we deliberately took pictures of the same scene in a dark environment using low exposure and high ISO. Such setup amplifies the noise, see Fig. 10 left for an example. Since it was not possible to capture the reference clear image directly, we estimated it by a time-averaging of twenty noisy images of the same scene, see Fig. 10 right.

We calculated three 2D histograms (R–G, R–B, and G–B) of each noisy image and the denoised image and computed the invariants. The ratio between the invariants is plotted in Fig. 11. Ideally, it should be close to one. We can, however, observe some oscillations around this theoretical value. This is caused by several factors. The actual noise distribution is not exactly normal (the normality hypothesis was in all cases rejected by the Pearson's test) and the convolution model between the clear and noisy histogram is not valid in boundary regions of the color space. Still, the invariants are relatively stable (especially comparing to moments and other common PDF characteristics) and provide a noise-robust description of the histogram, which can be used for instance in histogram-based image retrieval systems.

8.3 Application in image retrieval

The previous experiments indicated that one of the potential application areas of the proposed convolution invariants could be a content-based image retrieval (CBIR). CBIR methods often relies on histograms, because two images with similar histograms are mostly perceived as similar by humans (Pass and Zabih 1996; Wang and Healey 1998; Swain and Ballard 1991). Another attractive property of the histogram is that it does not depend on image translation, rotation and (if normalized to the image size) on scaling. Simple preprocessing can also make the histogram insensitive to linear changes of the contrast and brightness of the image. Current CBIR methods based on comparing histograms are sensitive to noise in the images. We already demonstrated that an additive noise leads to a histogram smoothing, which results in a drop of the retrieval performance because different histograms tend to be more and more similar to each other.

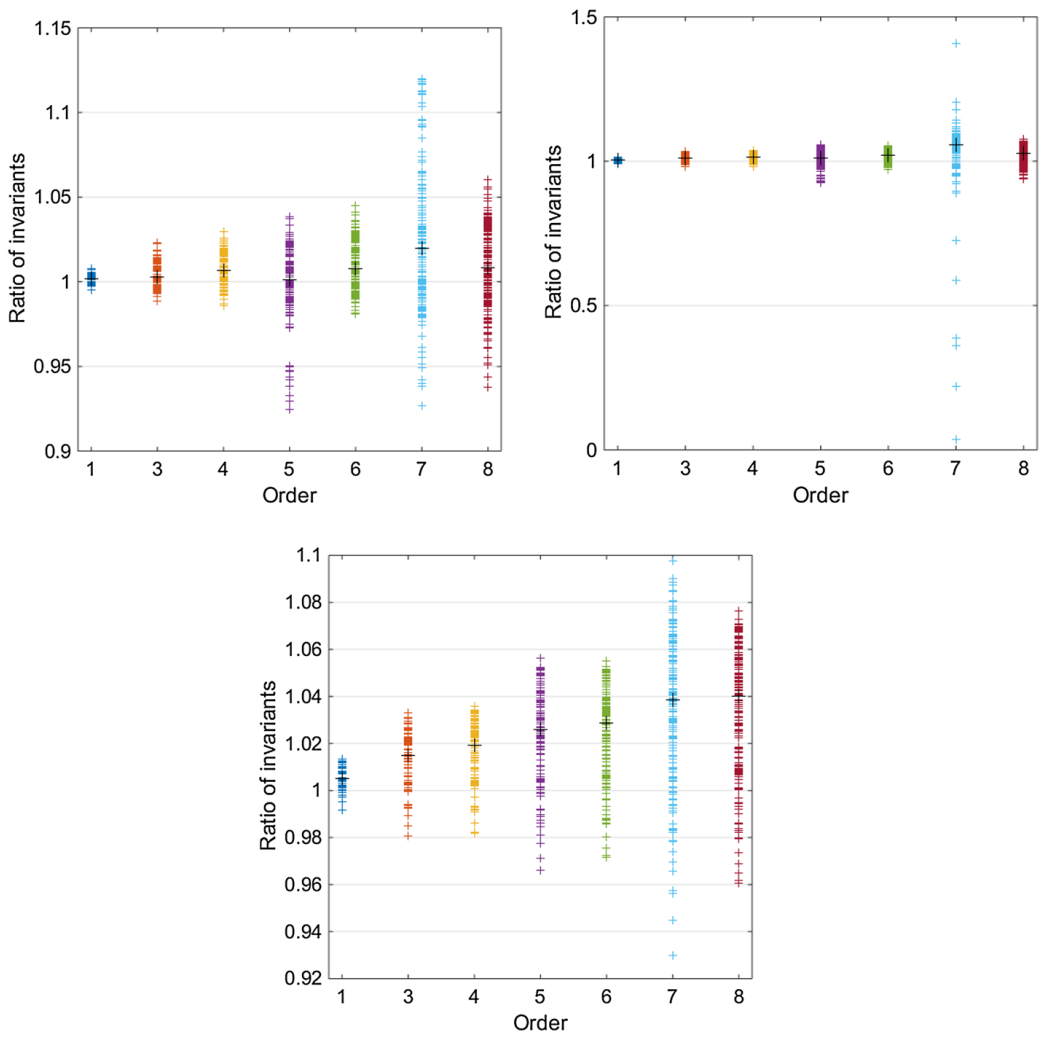

Fig. 11 The ratio of the invariants up to the order 8 of noisy and clear images for histogram of red and blue channels (left), red and green channels (right) and green and blue channels (bottom), respectively. Black crosses denote the median of the invariants (Color figure online)

We envisage the use of the proposed invariants as noise-robust descriptors of multidimensional histograms, similarly as the authors of Höschl IV and Flusser (2016) used the 1D convolution invariants for graylevel histogram recognition. The new invariants could be helpful in the case of noisy database and/or noisy query images (see Fig. 12 for the proposed method outline).

9 Conclusion

We proposed a new method for description of random variables, which is robust to an additive Gaussian noise. The method is based on the fact that the PDF of the noisy variable is a convolution of the PDF of the original unobservable variable and the PDF of the noise.

We constructed a projection operator onto the set of all Gaussian probability density functions, removed the Gaussian part of the functions and described the complement by

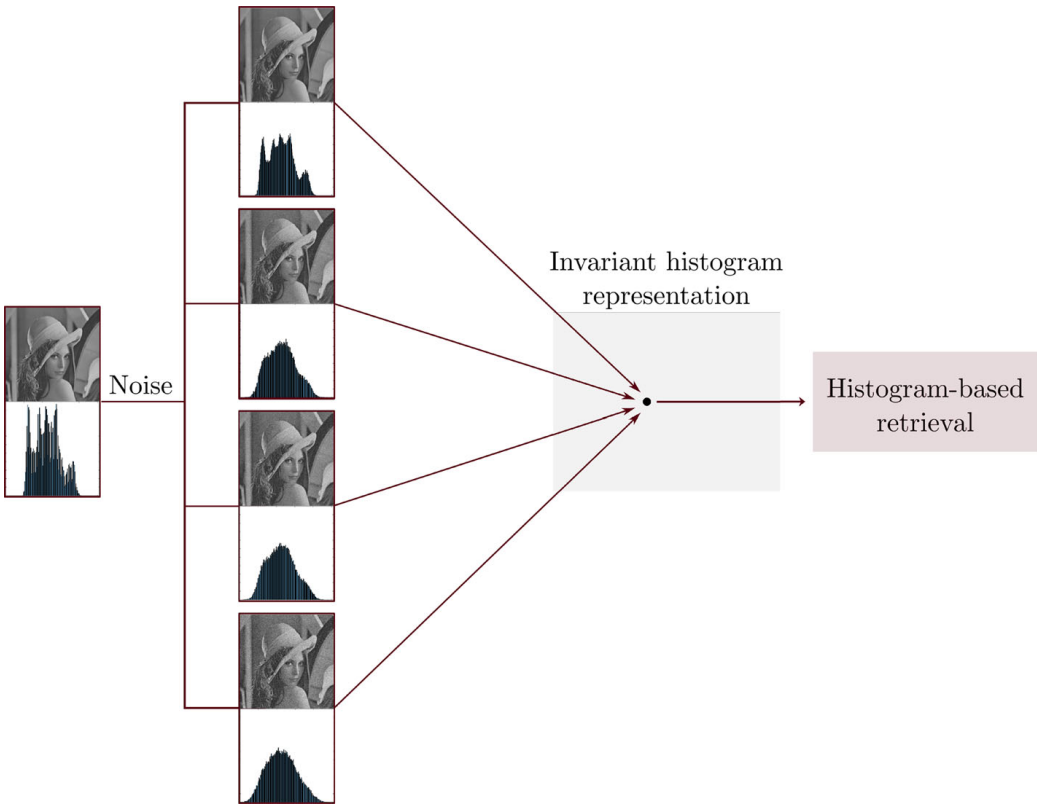

Fig. 12 Noise-robust CBIR. From left to right: original image and its histogram, noisy images with smoothed histograms, representation of the histograms by the proposed convolution invariants, image retrieval based on histogram similarity measured by the invariants. The actual implementation works with color images and multidimensional histograms

invariants composed of moments. The method does not require any estimation of the noise parameters, which makes it attractive for practical usage The 2D case was discussed in more details because of its importance in applications. The invariance property was demonstrated on experiments from image processing area.

A Explicit formula for Gaussian moments in two dimensions

In this Appendix, we present the derivation of the explicit formula for 2D central moments of the Gaussian probability density function $f_N(\mathbf{x})$ with the covariance matrix

$$\Sigma = \begin{pmatrix} \sigma_1 & \rho \\ \rho & \sigma_2 \end{pmatrix}.$$

It holds for the inverse matrix Σ^{-1} and its determinant

$$\Sigma^{-1} = \frac{1}{|\Sigma|}\begin{pmatrix} \sigma_2 & -\rho \\ -\rho & \sigma_1 \end{pmatrix} \equiv \begin{pmatrix} a & b \\ b & c \end{pmatrix}, \quad |\Sigma^{-1}| = ac - b^2 = \frac{1}{|\Sigma|}.$$

If $m + n$ is odd, the moments vanish due to the symmetry

$$\mathrm{m}_{mn}^{(f_N)} = 0.$$

For $m+n$ even we have

$$\begin{aligned}
\mathrm{m}_{mn}^{(f_N)} &= \frac{1}{2\pi\sqrt{|\Sigma|}} \iint\limits_{\mathbb{R}^2} x^m y^n \mathrm{e}^{-\frac{1}{2}(ax^2+2bxy+cy^2)}\,\mathrm{d}x\,\mathrm{d}y \\
&= \frac{1}{2\pi\sqrt{|\Sigma|}} \iint\limits_{\mathbb{R}^2} x^m \mathrm{e}^{-\frac{1}{2}x^2\left(a-\frac{b^2}{c}\right)} y^n \mathrm{e}^{-\frac{1}{2}\left(y+\frac{b}{c}x\right)^2 c}\,\mathrm{d}x\,\mathrm{d}y = \\
&= \left|\begin{array}{rl} y+\frac{b}{c}x &= u \\ x &= v \end{array}\right| = \frac{1}{2\pi\sqrt{|\Sigma|}} \iint\limits_{\mathbb{R}^2} v^m \mathrm{e}^{-\frac{1}{2}v^2\left(a-\frac{b^2}{c}\right)} \left(u-\frac{b}{c}v\right)^n \mathrm{e}^{-\frac{1}{2}u^2 c}\,\mathrm{d}u\,\mathrm{d}v.
\end{aligned}$$

We can separate the integrals and use the formula for 1D moments of Gaussian function:

$$\begin{aligned}
&= \frac{1}{2\pi\sqrt{|\Sigma|}} \sum_{k=0}^{n} \binom{n}{k} \left(-\frac{b}{c}\right)^{n-k} \int\limits_{\mathbb{R}} u^k \mathrm{e}^{-\frac{1}{2}u^2 c}\,\mathrm{d}u \int\limits_{\mathbb{R}} v^{m+n-k} \mathrm{e}^{-\frac{1}{2}v^2\left(a-\frac{b^2}{c}\right)}\,\mathrm{d}v \\
&= \frac{1}{\sqrt{|\Sigma|}} \sum_{\substack{k=0,\\ k \text{ even}}}^{n} \binom{n}{k} \left(\frac{-b}{c}\right)^{n-k} \left(\frac{1}{a-\frac{b^2}{c}}\right)^{\frac{m+n-k+1}{2}} (m+n-k-1)!! \left(\frac{1}{c}\right)^{\frac{k+1}{2}} (k-1)!! \\
&= \sum_{\substack{k=0,\\ k \text{ even}}}^{n} \binom{n}{k} \left(\frac{-b}{|\Sigma^{-1}|}\right)^{n-k} \left(\frac{c}{|\Sigma^{-1}|}\right)^{\frac{m-n}{2}} |\Sigma|^{k/2} (m+n-k-1)!!(k-1)!! \\
&= \sum_{i=0}^{\lfloor \frac{n}{2} \rfloor} \binom{n}{2i} \rho^{n-2i} \sigma_1^{\frac{m-n}{2}} \left(\sigma_1\sigma_2-\rho^2\right)^i (m+n-2i-1)!!(2i-1)!! \\
&= \sum_{i=0}^{\lfloor \frac{n}{2} \rfloor} \sum_{j=0}^{i} (-1)^{i-j} \binom{n}{2i} \binom{i}{k} (m+n-2i-1)!!(2i-1)!! \rho^{n-2j} \sigma_1^{\frac{m-n}{2}+j} \sigma_2^j. \qquad (24)
\end{aligned}$$

We may reduce the quadratic form in the exponent to a sum of squares in the following way

$$\frac{1}{2\pi\sqrt{|\Sigma|}} \iint\limits_{\mathbb{R}^2} y^n \mathrm{e}^{-\frac{1}{2}y^2\left(c-\frac{b^2}{a}\right)} x^m \mathrm{e}^{-\frac{1}{2}\left(x+\frac{b}{a}y\right)^2 a}\,\mathrm{d}x\,\mathrm{d}y.$$

Then using the substitution

$$\begin{aligned} x+\frac{b}{a}y &= u \\ y &= v \end{aligned}$$

another formula for moments of bivariate Gaussian distribution is obtained

$$\mathrm{m}_{mn}^{(f_N)} = \sum_{i=0}^{\lfloor \frac{m}{2} \rfloor} \sum_{j=0}^{i} (-1)^{i-j} \binom{m}{2i} \binom{i}{j} (m+n-2i-1)!!(2i-1)!! \rho^{m-2j} \sigma_1^j \sigma_2^{\frac{n-m}{2}+j}. \qquad (25)$$

When we compare these two results, it is obvious that the coefficients of negative powers must be zero. Hence, moments are composed of positive powers of the elements of covariance

matrix only

$$\mathrm{m}_{mn}^{(f_N)} = \sum_{\substack{i=0 \\ j\geq \frac{m-n}{2}}}^{\lfloor \frac{m}{2} \rfloor} \sum_{j=0}^{i} (-1)^{i-j} \binom{m}{2i} \binom{i}{j} (m+n-2i-1)!!\rho^{m-2j} \sigma_1^j \sigma_2^{\frac{n-m}{2}+j}. \tag{26}$$

B Proof of the equivalence

Let us show that Formulas (22) and (23) for convolution invariants are equivalent. The proof is done by induction.

Proof $A_{00} = 1$ in Formula (22) as well as in Formula (23).

Let us assume (m, n), $m + n > 0$. From the induction assumption, the explicit formula is valid for all indices (p, q), where $p \leq m$, $q \leq n$ and $(p, q) \neq (m, n)$.

$$\begin{aligned}
A_{mn} &= m_{mn} - \sum_{\substack{l=0 \\ l+k\neq 0, \\ l+k \text{ even}}}^{m} \sum_{k=0}^{n} \binom{m}{l} \binom{n}{k} \sum_{\substack{i=0 \\ j\geq \frac{k-l}{2}}}^{\lfloor \frac{k}{2} \rfloor} \sum_{j=0}^{i} (-1)^{i-j} \binom{k}{2i} \binom{i}{j} (l+k-2i-1)!!(2i-1)!! \\
&\quad \cdot m_{11}^{k-2j} m_{20}^{\frac{l-k}{2}+j} m_{02}^{j} A_{m-l,n-k} = \\
&= m_{mn} - \sum_{\substack{l=0 \\ l+k\neq 0, \\ l+k \text{ even}}}^{m} \sum_{k=0}^{n} \binom{m}{l} \binom{n}{k} \sum_{\substack{i=0 \\ j\geq \frac{k-l}{2}}}^{\lfloor \frac{k}{2} \rfloor} \sum_{j=0}^{i} (-1)^{i-j} \binom{k}{2i} \binom{i}{j} \\
&\quad \cdot (l+k-2i-1)!!(2i-1)!! \, m_{11}^{k-2j} m_{20}^{\frac{l-k}{2}+j} m_{02}^{j} \\
&\quad \cdot \sum_{\substack{s=0 \\ s+t \text{ even}}}^{n-k} \sum_{t=0}^{m-l} (-1)^{\frac{s+t}{2}} \binom{m-l}{t} \binom{n-k}{s} \sum_{\substack{\alpha=0 \\ \beta\geq \frac{s-t}{2}}}^{\lfloor \frac{s}{2} \rfloor} \sum_{\beta=0}^{\alpha} (-1)^{\alpha-\beta} \binom{s}{2\alpha} \binom{\alpha}{\beta} \\
&\quad (2\alpha-1)!!(s+t-2\alpha-1)!! \\
&\quad \cdot m_{11}^{s-2\beta} m_{20}^{\frac{t-s}{2}+\beta} m_{02}^{\beta} m_{m-l-t,n-k-s} = \\
&= m_{mn} - \sum_{\substack{l=0 \\ l+k\neq 0, \\ l+k \text{ even}}}^{m} \sum_{k=0}^{n} \frac{m!}{l!(m-l)!} \frac{n!}{k!(n-k)!} \sum_{\substack{i=0 \\ j\geq \frac{k-l}{2}}}^{\lfloor \frac{k}{2} \rfloor} \sum_{j=0}^{i} (-1)^{i-j} \binom{k}{2i} \binom{i}{j} (2i-1)!! \\
&\quad \cdot (l+k-2i-1)!! \\
&\quad \cdot m_{11}^{k-2j} m_{20}^{\frac{l-k}{2}+j} m_{02}^{j} \sum_{\substack{s=0 \\ s+t \text{ even}}}^{n-k} \sum_{t=0}^{m-l} (-1)^{\frac{s+t}{2}} \frac{(m-l)!}{t!(m-l-t)!} \frac{(n-k)!}{s!(n-k-s)!}
\end{aligned}$$

$$\cdot \sum_{\substack{\alpha=0 \\ \beta \geq \frac{s-t}{2}}}^{\lfloor \frac{s}{2} \rfloor} \sum_{\beta=0}^{\alpha} (-1)^{\alpha-\beta} \binom{s}{2\alpha} \binom{\alpha}{\beta} (2\alpha-1)!!(s+t-2\alpha-1)!! m_{11}^{s-2\beta} m_{20}^{\frac{t-s}{2}+\beta}$$

$$\cdot m_{02}^{\beta} m_{m-l-t,n-k-s}$$

$$= \left| \begin{matrix} p=k+s \\ q=t+l \end{matrix} \right| = m_{mn} - \sum_{\substack{l=0 \\ l+k \neq 0, \\ l+k \text{ even}}}^{m} \sum_{k=0}^{n} \frac{m!}{l!} \frac{n!}{k!} \sum_{\substack{i=0 \\ j \geq \frac{k-l}{2}}}^{\lfloor \frac{k}{2} \rfloor} \sum_{j=0}^{i} (-1)^{i-j} \binom{k}{2i} \binom{i}{j}$$

$$\cdot (l+k-2i-1)!!(2i-1)!!$$

$$\cdot m_{11}^{k-2j} m_{20}^{\frac{l-k}{2}+j} m_{02}^{j} \sum_{\substack{p=k \\ p+q \text{ even}}}^{n} \sum_{\substack{q=l \\ p+q \text{ even}}}^{m} \frac{(-1)^{\frac{p+q-k-l}{2}}}{(q-l)!(m-q)!} \frac{1}{(p-k)!(n-p)!} \sum_{\substack{\alpha=0 \\ \beta \geq \frac{p-q+l-k}{2}}}^{\lfloor \frac{p-k}{2} \rfloor} \sum_{\beta=0}^{\alpha} (-1)^{\alpha-\beta}$$

$$\cdot \binom{p-k}{2\alpha} \binom{\alpha}{\beta} (2\alpha-1)!!$$

$$\cdot (p+q-k-l-2\alpha-1)!! m_{11}^{p-k-2\beta} m_{20}^{\frac{q-p+k-l}{2}+\beta} m_{02}^{\beta} m_{m-q,n-p} =$$

$$= m_{mn} - \sum_{\substack{l=0 \\ l+k \neq 0, \\ l+k \text{ even}}}^{m} \sum_{k=0}^{n} \sum_{\substack{p=k \\ p+q \text{ even}}}^{n} \sum_{\substack{q=l \\ p+q \text{ even}}}^{m} \binom{m}{q} \binom{q}{l} \binom{n}{p} \binom{p}{k} (-1)^{\frac{p+q-k-l}{2}} m_{m-q,n-p}$$

$$\cdot \sum_{\substack{i=0 \\ j \geq \frac{k-l}{2}}}^{\lfloor \frac{k}{2} \rfloor} \sum_{j=0}^{i} (-1)^{i-j} \binom{k}{2i} \binom{i}{j}$$

$$\cdot (l+k-2i-1)!!(2i-1)!! \sum_{\substack{\alpha=0 \\ \beta \geq \frac{p-q+l-k}{2}}}^{\lfloor \frac{p-k}{2} \rfloor} \sum_{\beta=0}^{\alpha} (-1)^{\alpha-\beta} \binom{p-k}{2\alpha} \binom{\alpha}{\beta}$$

$$\cdot (2\alpha-1)!!(p+q-k-l-2\alpha-1)!!$$

$$\cdot m_{11}^{p-2j-2\beta} m_{20}^{\frac{q-p}{2}+j+\beta} m_{02}^{j+\beta} =$$

$$= m_{mn} - \sum_{\substack{p=0 \\ l+k \neq 0, p+q \neq 0 \\ l+k \text{ even}, p+q \text{ even}}}^{n} \sum_{k=0}^{p} \sum_{\substack{q=0 \\ p+q \neq 0 \\ p+q \text{ even}}}^{m} \sum_{l=0}^{q} \binom{m}{q} \binom{q}{l} \binom{n}{p} \binom{p}{k} (-1)^{\frac{p+q-k-l}{2}} m_{m-q,n-p}$$

$$\cdot \sum_{\substack{i=0 \\ j \geq \frac{k-l}{2}}}^{\lfloor \frac{k}{2} \rfloor} \sum_{j=0}^{i} (-1)^{i-j} \binom{k}{2i} \binom{i}{j}$$

$$\cdot (l+k-2i-1)!!(2i-1)!! \sum_{\substack{\alpha=0 \\ \beta \geq \frac{p-q+l-k}{2}}}^{\lfloor \frac{p-k}{2} \rfloor} \sum_{\beta=0}^{\alpha} (-1)^{\alpha-\beta} \binom{p-k}{2\alpha} \binom{\alpha}{\beta} (2\alpha-1)!!$$

$$\cdot (p+q-k-l-2\alpha-1)!!$$

$$\cdot m_{11}^{p-2j-2\beta} m_{20}^{\frac{q-p}{2}+j+\beta} m_{02}^{j+\beta} =$$

$$= m_{mn} - \sum_{\substack{p=0 \\ p+q \neq 0, \\ p+q \text{ even}}}^{n} \sum_{q=0}^{m} (-1)^{\frac{p+q}{2}} \binom{m}{q} \binom{n}{p} m_{m-q,n-p} \sum_{\substack{k=0 \\ k+l \text{ even} \\ k+l \neq 0}}^{p} \sum_{l=0}^{q} (-1)^{\frac{k+l}{2}} \binom{q}{l} \binom{p}{k}$$

$$\cdot \sum_{\substack{i=0 \\ j \geq \frac{k-l}{2}}}^{\lfloor \frac{k}{2} \rfloor} \sum_{j=0}^{i} (-1)^{i-j} \binom{k}{2i} \binom{i}{j}$$

$$\cdot (2i-1)!!(l+k-2i-1)!! m_{11}^{k-2j} m_{20}^{\frac{l-k}{2}+j} m_{02}^{j} \sum_{\substack{\alpha=0 \\ \beta \geq \frac{p-q-k+l}{2}}}^{\lfloor \frac{p-k}{2} \rfloor} \sum_{\beta=0}^{\alpha} (-1)^{\alpha-\beta} \binom{p-k}{2\alpha} \binom{\alpha}{\beta}$$

$$\cdot (2\alpha-1)!!(p+q-k-l-2\alpha-1)!! m_{11}^{p-k-2\beta} m_{20}^{\frac{q-p+k-l}{2}+\beta} m_{02}^{\beta} =$$

$$= m_{mn} - \sum_{\substack{p=0 \\ p+q \neq 0, \\ p+q \text{ even}}}^{n} \sum_{q=0}^{m} (-1)^{\frac{p+q}{2}} \binom{m}{q} \binom{n}{p} m_{m-q,n-p}$$

$$\cdot \Bigg[\sum_{\substack{k=0 \\ k+l \text{ even}}}^{p} \sum_{l=0}^{q} (-1)^{\frac{k+l}{2}} \binom{p}{k} \binom{q}{l} m_{l,k}^{(G)} m_{q-l,p-k}^{(G)}$$

$$- \sum_{\substack{\alpha=0 \\ \beta \geq \frac{p-q}{2}}}^{\lfloor \frac{p}{2} \rfloor} \sum_{\beta=0}^{\alpha} (-1)^{\alpha-\beta} \binom{p}{2\alpha} \binom{\alpha}{\beta} (2\alpha-1)!!(p+q-2\alpha-1)!! m_{11}^{p-2\beta} m_{20}^{\frac{q-p}{2}+\beta} m_{02}^{\beta} \Bigg] =$$

$$= \sum_{\substack{l=0 \\ l+k \text{ even}}}^{m} \sum_{k=0}^{n} (-1)^{\frac{k+l}{2}} \binom{m}{l} \binom{n}{k} \sum_{\substack{i=0 \\ j \geq \frac{k-l}{2}}}^{\lfloor \frac{k}{2} \rfloor} \sum_{j=0}^{i} (-1)^{i-j} \binom{k}{2i} \binom{i}{j} (l+k-2i-1)!!(2i-1)!!$$

$$\cdot m_{11}^{k-2j} m_{20}^{\frac{l-k}{2}+j} m_{02}^{j} m_{m-l,n-k}.$$

It remains to prove that for $p+q > 0,\ p+q$ even, it holds

$$\sum_{\substack{k=0 \\ k+l \text{ even}}}^{p} \sum_{l=0}^{q} (-1)^{\frac{k+l}{2}} \binom{p}{k} \binom{q}{l} m_{l,k}^{(f_N)} m_{q-l,p-k}^{(f_N)} = 0. \tag{27}$$

For $\frac{p+q}{2}$ being odd, the proof is trivial because every combination is present twice with the opposite signs. Thus, all terms vanish.

$$\begin{aligned} k=a, l=b \Rightarrow \quad & (-1)^{\frac{a+b}{2}}\binom{p}{a}\binom{q}{b}m_{b,a}m_{q-b,p-a} \\ k=p-a, l=q-b \Rightarrow \quad & (-1)^{\frac{p+q-(a+b)}{2}}\binom{p}{p-a}\binom{q}{q-b}m_{q-b,p-a}m_{b,a} = \\ & -\left[(-1)^{\frac{a+b}{2}}\binom{p}{a}\binom{q}{b}m_{b,a}m_{q-b,p-a}\right] \end{aligned}$$

For $\frac{p+q}{2}$ even we have

$$\sum_{\substack{k=0\\ k+l \text{ even}}}^{p}\sum_{l=0}^{q}(-1)^{\frac{k+l}{2}}\binom{p}{k}\binom{q}{l}m_{l,k}^{(f_N)}m_{q-l,p-k}^{(f_N)} =$$

$$= \sum_{\substack{k=0\\ k+l \text{ even}}}^{p}\sum_{l=0}^{q}(-1)^{\frac{k+l}{2}}\binom{p}{k}\binom{q}{l}\sum_{\substack{i=0\\ t\geq\frac{k-l}{2}}}^{\lfloor\frac{k}{2}\rfloor}\sum_{t=0}^{i}(-1)^{i-t}\binom{k}{2i}\binom{i}{t}(l+k-2i-1)!!$$

$$\cdot (2i-1)!!\, m_{11}^{k-2t}m_{20}^{\frac{l-k}{2}+t}m_{02}^{t}$$

$$\cdot \sum_{\substack{s=0\\ r\geq\frac{p-q-k+l}{2}}}^{\lfloor\frac{p-k}{2}\rfloor}\sum_{r=0}^{s}(-1)^{s-r}\binom{p-k}{2s}\binom{s}{r}(p+q-l-k-2s-1)!!$$

$$\cdot (2s-1)!!\, m_{11}^{p-k-2r}m_{20}^{\frac{q-l-p+k}{2}+r}m_{02}^{r} =$$

$$= \sum_{\substack{k=0\\ k+l \text{ even}\ \wedge\ t\geq\frac{k-l}{2}\ \wedge\ r\geq\frac{p-q-k+l}{2}}}^{p}\sum_{l=0}^{q}\sum_{i=0}^{\lfloor\frac{k}{2}\rfloor}\sum_{t=0}^{i}\sum_{s=0}^{\lfloor\frac{p-k}{2}\rfloor}\sum_{r=0}^{s}\binom{p}{k}\binom{q}{l}\binom{k}{2i}\binom{i}{t}\binom{p-k}{2s}\binom{s}{r}(2i-1)!!(2s-1)!!$$

$$\cdot (l+k-2i-1)!!(p+q-l-k-2s-1)!!(-1)^{\frac{k+l}{2}+i-t+s-r}$$

$$\cdot m_{11}^{p-2t-2r}m_{20}^{\frac{q-p}{2}+r+t}m_{02}^{r+t}$$

$$= \sum_{\substack{k=0\\ k+l \text{ even}\ \wedge\ t\geq\frac{k-l}{2}\ \wedge\ r\geq\frac{p-q-k+l}{2}}}^{p}\sum_{l=0}^{q}\sum_{t=0}^{\lfloor\frac{k}{2}\rfloor}\sum_{i=t}^{\lfloor\frac{k}{2}\rfloor}\sum_{s=0}^{\lfloor\frac{p-k}{2}\rfloor}\sum_{r=0}^{s}\binom{p}{k}\binom{q}{l}\binom{k}{2i}\binom{i}{t}\binom{p-k}{2s}\binom{s}{r}(2i-1)!!(2s-1)!!$$

$$\cdot (l+k-2i-1)!!(p+q-l-k-2s-1)!!(-1)^{\frac{k+l}{2}+i-t+s-r}m_{11}^{p-2t-2r}m_{20}^{\frac{q-p}{2}+r+t}m_{02}^{r+t}$$

$$= \left|\begin{matrix} k=0:p,\ t=0:\lfloor\frac{k}{2}\rfloor \Rightarrow \\ t=0:\lfloor\frac{p}{2}\rfloor,\ k=2t:p \end{matrix}\right| \left|\begin{matrix} s=0:\lfloor\frac{p-k}{2}\rfloor,\ r=0:s \Rightarrow \\ r=0:\lfloor\frac{p-k}{2}\rfloor,\ s=r:\lfloor\frac{p-k}{2}\rfloor \end{matrix}\right| =$$

$$= \sum_{t=0}^{\lfloor \frac{p}{2} \rfloor} \sum_{k=2t}^{p} \sum_{l=0}^{q} \sum_{i=t}^{\lfloor \frac{k}{2} \rfloor} \sum_{r=0}^{\lfloor \frac{p-k}{2} \rfloor} \sum_{s=r}^{\lfloor \frac{p-k}{2} \rfloor} \binom{p}{k}\binom{q}{l}\binom{k}{2i}\binom{i}{t}\binom{p-k}{2s}\binom{s}{r}(2i-1)!!(2s-1)!!$$
$$k+l \text{ even} \wedge t \geq \frac{k-l}{2} \wedge r \geq \frac{p-q-k+l}{2}$$
$$\cdot (l+k-2i-1)!!(p+q-l-k-2s-1)!!(-1)^{\frac{k+l}{2}+i-t+s-r} m_{11}^{p-2t-2r}$$
$$\cdot m_{20}^{\frac{q-p}{2}+r+t} m_{02}^{r+t}$$
$$= \left| \begin{matrix} k = 2t : p,\ r = 0 : \lfloor \frac{p-k}{2} \rfloor \Rightarrow \\ r = 0 : \lfloor \frac{p-2t}{2} \rfloor,\ k = 2t : p-2r \end{matrix} \right| =$$
$$= \sum_{t=0}^{\lfloor \frac{p}{2} \rfloor} \sum_{r=0}^{\lfloor \frac{p-2t}{2} \rfloor} \sum_{k=2t}^{p-2r} \sum_{l=0}^{q} \sum_{i=t}^{\lfloor \frac{k}{2} \rfloor} \sum_{s=r}^{\lfloor \frac{p-k}{2} \rfloor} \binom{p}{k}\binom{q}{l}\binom{k}{2i}\binom{i}{t}\binom{p-k}{2s}\binom{s}{r}(2i-1)!!(2s-1)!!$$
$$k+l \text{ even} \wedge t \geq \frac{k-l}{2} \wedge r \geq \frac{p-q-k+l}{2}$$
$$\cdot (l+k-2i-1)!!(p+q-l-k-2s-1)!!(-1)^{\frac{k+l}{2}+i-t+s-r} m_{11}^{p-2t-2r}$$
$$\cdot m_{20}^{\frac{q-p}{2}+r+t} m_{02}^{r+t}$$
$$= \sum_{t=0}^{\lfloor \frac{p}{2} \rfloor} \sum_{r=0}^{\lfloor \frac{p-2t}{2} \rfloor} m_{11}^{p-2t-2r} m_{20}^{\frac{q-p}{2}+r+t} m_{02}^{r+t} \sum_{k=2t}^{p-2r} \sum_{l=0}^{q} \sum_{i=t}^{\lfloor \frac{k}{2} \rfloor} \sum_{s=r}^{\lfloor \frac{p-k}{2} \rfloor} (-1)^{\frac{k+l}{2}+i-t+s-r} \binom{p}{k}\binom{q}{l}$$
$$k+l \text{ even} \wedge t \geq \frac{k-l}{2} \wedge r \geq \frac{p-q-k+l}{2}$$
$$\cdot \binom{k}{2i}\binom{i}{t}\binom{p-k}{2s}\binom{s}{r}(2i-1)!!(2s-1)!!(l+k-2i-1)!!(p+q-l-k-2s-1)!!$$
$$= \left| \begin{matrix} t + r = N \Rightarrow r = N - t \\ t = 0 : \lfloor \frac{p}{2} \rfloor \Rightarrow \\ N = t : \lfloor \frac{p}{2} \rfloor \end{matrix} \right| =$$

$$= \sum_{t=0}^{\lfloor \frac{p}{2} \rfloor} \sum_{N=t}^{\lfloor \frac{p}{2} \rfloor} m_{11}^{p-2N} m_{20}^{\frac{q-p}{2}+N} m_{02}^{N} \sum_{k=2t}^{p-2N+2t} \sum_{l=0}^{q} \sum_{i=t}^{\lfloor \frac{k}{2} \rfloor} \sum_{s=N-t}^{\lfloor \frac{p-k}{2} \rfloor} (-1)^{\frac{k+l}{2}+i+s-N} \binom{p}{k}\binom{q}{l}\binom{k}{2i}\binom{i}{t}$$
$$k+l \text{ even} \wedge N - \frac{p-k-q+l}{2} \geq t \geq \frac{k-l}{2}$$
$$\cdot \binom{p-k}{2s}\binom{s}{N-t}(2i-1)!!(2s-1)!!(l+k-2i-1)!!(p+q-l-k-2s-1)!!$$
$$= \left| \begin{matrix} t = 0 : \lfloor \frac{p}{2} \rfloor, N = t : \lfloor \frac{p}{2} \rfloor \Rightarrow \\ N = 0 : \lfloor \frac{p}{2} \rfloor, t = 0 : N \end{matrix} \right| =$$
$$= \sum_{N=0}^{\lfloor \frac{p}{2} \rfloor} \sum_{t=0}^{N} m_{11}^{p-2N} m_{20}^{\frac{q-p}{2}+N} m_{02}^{N} \sum_{k=2t}^{p-2N+2t} \sum_{l=0}^{q} \sum_{i=t}^{\lfloor \frac{k}{2} \rfloor} \sum_{s=N-t}^{\lfloor \frac{p-k}{2} \rfloor} (-1)^{\frac{k+l}{2}+i+s-N} \binom{p}{k}\binom{q}{l}\binom{i}{t}$$
$$k+l \text{ even} \wedge N - \frac{p-k-q+l}{2} \geq t \geq \frac{k-l}{2}$$
$$\cdot \binom{k}{2i}\binom{p-k}{2s}\binom{s}{N-t}(2i-1)!!(2s-1)!!(l+k-2i-1)!!(p+q-l-k-2s-1)!! =$$
$$= \left| \begin{matrix} k - 2t = m \Rightarrow k = m + 2t \\ k = 2t : p - 2N + 2t \Rightarrow \\ m = 0 : p - 2N \end{matrix} \right| =$$

$$= \sum_{N=0}^{\lfloor \frac{p}{2} \rfloor} m_{11}^{p-2N} m_{20}^{\frac{q-p}{2}+N} m_{02}^{N} \sum_{t=0}^{N} \sum_{m=0}^{p-2N} \sum_{l=0}^{q} \sum_{i=t}^{\lfloor \frac{m+2t}{2} \rfloor} \sum_{s=N-t}^{\lfloor \frac{p-m-2t}{2} \rfloor} (-1)^{\frac{m+l}{2}+t+i+s-N}$$
$$m+l \text{ even} \wedge N-\tfrac{p-q}{2} \geq \tfrac{l-m}{2} \geq 0$$
$$\cdot \binom{p}{m+2t}\binom{q}{l}\binom{m+2t}{2i}\binom{i}{t}$$
$$\cdot \binom{s}{N-t}\binom{p-m-2t}{2s}(2i-1)!!(2s-1)!!$$
$$\cdot (l+m+2t-2i-1)!!(p+q-l-m-2t-2s-1)!!$$
$$= \left| \begin{array}{c} i-t=j \Rightarrow i=j+t \\ i=t:\lfloor \frac{m+2t}{2} \rfloor \Rightarrow \\ j=0:\lfloor \frac{m}{2} \rfloor \end{array} \right| =$$

$$= \sum_{N=0}^{\lfloor \frac{p}{2} \rfloor} m_{11}^{p-2N} m_{20}^{\frac{q-p}{2}+N} m_{02}^{N} \sum_{t=0}^{N} \sum_{m=0}^{p-2N} \sum_{l=0}^{q} \sum_{j=0}^{\lfloor \frac{m}{2} \rfloor} \sum_{s=N-t}^{\lfloor \frac{p-m-2t}{2} \rfloor} (-1)^{\frac{m+l}{2}+j+2t+s-N}$$
$$m+l \text{ even} \wedge N-\tfrac{p-q}{2} \geq \tfrac{l-m}{2} \geq 0$$
$$\cdot \binom{p}{m+2t}\binom{q}{l}\binom{m+2t}{2j+2t}\binom{j+t}{t}$$
$$\cdot \binom{s}{N-t}\binom{p-m-2t}{2s}(2j+2t-1)!!(2s-1)!!(l+m-2j-1)!!$$
$$\cdot (p+q-l-m-2t-2s-1)!!$$
$$= \left| \begin{array}{c} s-N+t=k \Rightarrow s=N-t+k \\ s=N-t:\lfloor \frac{p-2m-2t}{2} \rfloor \Rightarrow \\ k=0:\lfloor \frac{p-2m-2N}{2} \rfloor \end{array} \right| =$$

$$= \sum_{N=0}^{\lfloor \frac{p}{2} \rfloor} m_{11}^{p-2N} m_{20}^{\frac{q-p}{2}+N} m_{02}^{N} \sum_{t=0}^{N} \sum_{m=0}^{p-2N} \sum_{l=0}^{q} \sum_{j=0}^{\lfloor \frac{m}{2} \rfloor} \sum_{k=0}^{\lfloor \frac{p-m-2N}{2} \rfloor} (-1)^{\frac{m+l}{2}+j+k+t} \binom{p}{m+2t}\binom{q}{l}$$
$$m+l \text{ even} \wedge N-\tfrac{p-q}{2} \geq \tfrac{l-m}{2} \geq 0$$
$$\cdot \binom{m+2t}{2j+2t}\binom{j+t}{t}\binom{N-t+k}{N-t}\binom{p-m-2t}{2N-2t+2k}(2j+2t-1)!!(2N-2t+2k-1)!!$$
$$\cdot (l+m-2j-1)!!(p+q-l-m-2N-2k-1)!!$$
$$= \sum_{N=0}^{\lfloor \frac{p}{2} \rfloor} m_{11}^{p-2N} m_{20}^{\frac{q-p}{2}+N} m_{02}^{N} \sum_{t=0}^{N} \sum_{m=0}^{p-2N} \sum_{l=0}^{q} \sum_{j=0}^{\lfloor \frac{m}{2} \rfloor} \sum_{k=0}^{\lfloor \frac{p-m-2N}{2} \rfloor} (-1)^{\frac{m+l}{2}+j+k+t} \binom{q}{l} p!$$
$$m+l \text{ even} \wedge N-\tfrac{p-q}{2} \geq \tfrac{l-m}{2} \geq 0$$
$$\cdot \frac{(2j+2t-1)!!}{(2j+2t)!(m-2j)!}\frac{(j+t)!}{t!j!}\frac{(N-t+k)!}{(N-t)!k!}\frac{(2N-2t+2k-1)!!}{(2N-2t+2k)!(p-m-2N-2k)!}$$
$$\cdot (l+m-2j-1)!!(p+q-l-m-2N-2k-1)!!$$
$$= \sum_{N=0}^{\lfloor \frac{p}{2} \rfloor} m_{11}^{p-2N} m_{20}^{\frac{q-p}{2}+N} m_{02}^{N} \sum_{t=0}^{N} \sum_{m=0}^{p-2N} \sum_{l=0}^{q} \sum_{j=0}^{\lfloor \frac{m}{2} \rfloor} \sum_{k=0}^{\lfloor \frac{p-m-2N}{2} \rfloor} (-1)^{\frac{m+l}{2}+j+k+t} \binom{q}{l} p!$$
$$m+l \text{ even} \wedge N-\tfrac{p-q}{2} \geq \tfrac{l-m}{2} \geq 0$$

$$\cdot \frac{1}{(2j+2t)!!(m-2j)!}\frac{(j+t)!}{t!j!}\frac{(N-t+k)!}{(N-t)!k!}\frac{1}{(2N-2t+2k)!!(p-m-2N-2k)!}$$

$$\cdot (l+m-2j-1)!!(p+q-l-m-2N-2k-1)!!$$

$$= \sum_{N=0}^{\lfloor \frac{p}{2} \rfloor} m_{11}^{p-2N} m_{20}^{\frac{q-p}{2}+N} m_{02}^{N} \sum_{t=0}^{N}\sum_{m=0}^{p-2N}\sum_{l=0}^{q}\sum_{j=0}^{\lfloor \frac{m}{2} \rfloor}\sum_{k=0}^{\lfloor \frac{p-m-2N}{2} \rfloor} (-1)^{\frac{m+l}{2}+j+k+t}\binom{q}{l}p!$$
$$m+l \text{ even} \wedge N-\frac{p-q}{2} \geq \frac{l-m}{2} \geq 0$$

$$\cdot \frac{1}{2^{j+t}(j+t)!(m-2j)!}\frac{(j+t)!}{t!j!}\frac{(N-t+k)!}{(N-t)!k!}\frac{1}{2^{N-t+k}(N-t+k)!(p-m-2N-2k)!}$$

$$\cdot (l+m-2j-1)!!(p+q-l-m-2N-2k-1)!!$$

$$= \sum_{N=0}^{\lfloor \frac{p}{2} \rfloor} m_{11}^{p-2N} m_{20}^{\frac{q-p}{2}+N} m_{02}^{N} \sum_{t=0}^{N}\sum_{m=0}^{p-2N}\sum_{l=0}^{q}\sum_{j=0}^{\lfloor \frac{m}{2} \rfloor}\sum_{k=0}^{\lfloor \frac{p-m-2N}{2} \rfloor} (-1)^{\frac{m+l}{2}+j+k+t}\binom{q}{l}p!$$
$$m+l \text{ even} \wedge N-\frac{p-q}{2} \geq \frac{l-m}{2} \geq 0$$

$$\cdot \frac{1}{2^j j!(m-2j)!}\frac{1}{2^{N+k}k!(p-m-2N-2k)!}\frac{1}{t!(N-t)!}$$

$$\cdot (l+m-2j-1)!!(p+q-l-m-2N-2k-1)!!$$

$$= \sum_{N=0}^{\lfloor \frac{p}{2} \rfloor} m_{11}^{p-2N} m_{20}^{\frac{q-p}{2}+N} m_{02}^{N} \sum_{m=0}^{p-2N}\sum_{l=0}^{q}\sum_{j=0}^{\lfloor \frac{m}{2} \rfloor}\sum_{k=0}^{\lfloor \frac{p-m-2N}{2} \rfloor} (-1)^{\frac{m+l}{2}+j+k}\binom{q}{l}p!$$
$$m+l \text{ even} \wedge N-\frac{p-q}{2} \geq \frac{l-m}{2} \geq 0$$

$$\cdot \frac{1}{(2j)!!(m-2j)!}\frac{1}{(2k)!!(p-m-2N-2k)!2^N N!}$$

$$\cdot (l+m-2j-1)!!(p+q-l-m-2N-2k-1)!!\sum_{t=0}^{N}(-1)^t\binom{N}{t} = \tag{28}$$

$$= \sum_{N=0}^{\lfloor \frac{p}{2} \rfloor} m_{11}^{p-2N} m_{20}^{\frac{q-p}{2}+N} m_{02}^{N} \sum_{m=0}^{p-2N}\sum_{l=0}^{q}\sum_{j=0}^{\lfloor \frac{m}{2} \rfloor}\sum_{k=0}^{\lfloor \frac{p-m-2N}{2} \rfloor} (-1)^{\frac{m+l}{2}+j+k}\binom{q}{l}p!$$
$$m+l \text{ even} \wedge N-\frac{p-q}{2} \geq \frac{l-m}{2} \geq 0$$

$$\cdot \frac{(2j-1)!!}{(2j)!(m-2j)!}\frac{(2k-1)!!}{(2k)!(p-m-2N-2k)!(2N)!!}$$

$$\cdot (l+m-2j-1)!!(p+q-l-m-2N-2k-1)!!(1-1)^N. \tag{29}$$

All the terms of (29) are zero if $N > 0$. If $N = 0$, there remains the last term only

$$\sum_{m=0}^{p}\sum_{l=0}^{q}\sum_{j=0}^{\lfloor \frac{m}{2} \rfloor}\sum_{k=0}^{\lfloor \frac{p-m}{2} \rfloor} (-1)^{\frac{m+l}{2}+j+k}\binom{p}{m}\binom{q}{l}\binom{m}{2j}\binom{p-m}{2k}$$
$$m+l \text{ even} \wedge q-p \geq l-m \geq 0$$
$$\cdot (2j-1)!!(2k-1)!!(l+m-2j-1)!!(p+q-l-m-2k-1)!!. \tag{30}$$

Now we prove that this term is zero as well. This term is equivalent to

$$\sum_{\substack{m=0 \\ m+l \text{ even} \\ q-p\geq l-m\geq 0}}^{p}\sum_{l=0}^{q}(-1)^{\frac{m+l}{2}}\binom{p}{m}\binom{q}{l}\sum_{j=0}^{\lfloor\frac{m}{2}\rfloor}(-1)^{j}\binom{m}{2j}(l+m-2j-1)!!(2j-1)!!$$
$$\cdot\sum_{k=0}^{\lfloor\frac{p-m}{2}\rfloor}(-1)^{k}\binom{p-m}{2k}(p+q-l-m-2k-1)!!(2k-1)!!=\Xi. \tag{31}$$

It can be shown for $l\geq m$ using the method of generating functions described in Gould and Quaintance (2012) that

$$\sum_{j=0}^{\lfloor\frac{m}{2}\rfloor}(-1)^{j}\binom{m}{2j}(l+m-2j-1)!!(2j-1)!!=\frac{l!}{(l-m)!!}. \tag{32}$$

We adopt the notation from Gould and Quaintance (2012) for double factorial binomial coefficients and we recall $(p+q)/2$ is even. The previous expression can be rewritten

$$\Xi=\sum_{\substack{m=0 \\ m+l \text{ even} \\ q-p\geq l-m\geq 0}}^{p}\sum_{l=0}^{q}(-1)^{\frac{m+l}{2}}\binom{p}{m}\binom{q}{l}\frac{l!}{(l-m)!!}\frac{(q-l)!}{(q-l-p+m)!!}=$$
$$=\frac{q!}{(q-p)!!}\sum_{\substack{m=0 \\ m+l \text{ even} \\ q-p\geq l-m\geq 0}}^{p}\sum_{l=m}^{q-p+m}(-1)^{\frac{m+l}{2}}\binom{p}{m}\left(\!\binom{q-p}{l-m}\!\right)=\left|\begin{matrix}l-m=2j\\ j=0:\frac{q-p}{2}\end{matrix}\right|=$$
$$=\frac{q!}{(q-p)!!}\sum_{m=0}^{p}\sum_{j=0}^{\frac{q-p}{2}}(-1)^{j+m}\binom{p}{m}\left(\!\binom{q-p}{2j}\!\right)=$$
$$=\frac{q!}{(q-p)!!}\sum_{m=0}^{p}(-1)^{m}\binom{p}{m}\sum_{j=0}^{\frac{q-p}{2}}(-1)^{j}\left(\!\binom{q-p}{2j}\!\right) \tag{33}$$

The inner sum is zero if $q>p$

$$\sum_{j=0}^{\frac{q-p}{2}}(-1)^{j}\left(\!\binom{q-p}{2j}\!\right)=\sum_{j=0}^{\frac{q-p}{2}}(-1)^{j}\frac{(q-p)!!}{(2j)!!(q-p-2j)!!}$$
$$=\sum_{j=0}^{\frac{q-p}{2}}(-1)^{j}\binom{\frac{q-p}{2}}{j}=(1-1)^{\frac{q-p}{2}}=0. \tag{34}$$

For the case $q=p$ ($q-p$ must be non-negative) the inner sum equals 1 and the expression (33) is

$$p!\sum_{m=0}^{p}(-1)^{m}\binom{p}{m}=p!(1-1)^{p} \tag{35}$$

which completes the proof because it is zero whenever $p>0$.

The formula

$$\sum_{\substack{k=0\\ k+l \text{ even}}}^{p}\sum_{l=0}^{q}(-1)^{\frac{k+l}{2}}\binom{p}{k}\binom{q}{l}m_{l,k}^{(f_N)}m_{q-l,p-k}^{(f_N)}=0 \tag{36}$$

holds not only for $p+q$ even but for all p and q. If $p+q$ is odd, then $m_{q-l,p-k}^{(f_N)}$ is Gaussian moment of the odd order and all the terms in summation are zero. □

References

Bar, W., & Dittrich, F. (1971). Useful formula or moment computation of normal random variables with nonzero means. *IEEE Transactions on Automatic Control*, *16*(3), 263–265.

Blacher, R. (2003). Multivariate quadratic forms of random vectors. *Journal of Multivariate Analysis*, *87*(1), 2–23.

Buades, A., Coll, B., & Morel, J. M. (2005a). A non-local algorithm for image denoising. In *IEEE computer society conference on computer vision and pattern recognition, 2005, CVPR 2005* (Vol. 2, pp. 60–65). IEEE.

Buades, A., Coll, B., & Morel, J. M. (2005b). A review of image denoising algorithms, with a new one. *Multiscale Modeling and Simulation*, *4*(2), 490–530.

Butucea, C., Comte, F., et al. (2009). Adaptive estimation of linear functionals in the convolution model and applications. *Bernoulli*, *15*(1), 69–98.

Carroll, R. J., & Hall, P. (1988). Optimal rates of convergence for deconvolving a density. *Journal of the American Statistical Association*, *83*(404), 1184–1186.

Chambolle, A., & Lions, P. L. (1997). Image recovery via total variation minimization and related problems. *Numerische Mathematik*, *76*(2), 167–188.

Chen, G., Xie, W., & Zhao, Y. (2013). Wavelet-based denoising: A brief review. In *2013 fourth international conference on intelligent control and information processing (ICICIP)* (pp. 570–574). IEEE.

Cho, D., & Bui, T. D. (2005). Multivariate statistical approach for image denoising. In *IEEE International conference on acoustics, speech, and signal processing, 2005. Proceedings (ICASSP'05)* (Vol. 4, pp. 4–589). IEEE.

Comte, F., & Lacour, C. (2011). Data-driven density estimation in the presence of additive noise with unknown distribution. *Journal of the Royal Statistical Society: Series B (Statistical Methodology)*, *73*(4), 601–627.

De Brabanter, K., & De Moor, B. (2012). Deconvolution in nonparametric statistics. In *ESANN*.

Efron, B. (2014). *The Bayes deconvolution problem*. Stanford: Division of Biostatistics, Stanford University.

Fan, J. (1992). Deconvolution with supersmooth distributions. *Canadian Journal of Statistics*, *20*(2), 155–169.

Flusser, J., Boldyš, J., & Zitová, B. (2003). Moment forms invariant to rotation and blur in arbitrary number of dimensions. *IEEE Transactions on Pattern Analysis and Machine Intelligence*, *25*(2), 234–246.

Flusser, J., & Suk, T. (1998). Degraded image analysis: An invariant approach. *IEEE Transactions on Pattern Analysis and Machine Intelligence*, *20*(6), 590–603.

Flusser, J., Suk, T., Boldyš, J., & Zitová, B. (2015). Projection operators and moment invariants to image blurring. *IEEE Transactions on Pattern Analysis and Machine Intelligence*, *37*(4), 786–802.

Galigekere, R. R., & Swamy, M. N. S. (2006). Moment patterns in the Radon space: Invariance to blur. *Optical Engineering*, *45*(7), 0770036.

Gopalan, R., Turaga, P., & Chellappa, R. (2012). A blur-robust descriptor with applications to face recognition. *IEEE Transactions on Pattern Analysis and Machine Intelligence*, *34*(6), 1220–1226.

Gould, H., & Quaintance, J. (2012). Double fun with double factorials. *Mathematics Magazine*, *85*(3), 177–192.

Höschl, C, I. V., & Flusser, J. (2016). Robust histogram-based image retrieval. *Pattern Recognition Letters*, *69*(1), 72–81.

Isserlis, L. (1918). On a formula for the product-moment coefficient of any order of a normal frequency distribution in any number of variables. *Biometrika*, *12*(1/2), 134–139.

Johannes, J., et al. (2009). Deconvolution with unknown error distribution. *The Annals of Statistics*, *37*(5A), 2301–2323.

Kappus, J., Mabon, G., et al. (2014). Adaptive density estimation in deconvolution problems with unknown error distribution. *Electronic Journal of Statistics*, *8*(2), 2879–2904.

Khireddine, A., Benmahammed, K., & Puech, W. (2007). Digital image restoration by Wiener filter in 2D case. *Advances in Engineering Software*, *38*(7), 513–516.

Makaremi, I., & Ahmadi, M. (2012). Wavelet domain blur invariants for image analysis. *IEEE Transactions on Image Processing*, *21*(3), 996–1006.
Meister, A. (2009). *Deconvolution problems in nonparametric statistics. Lecture notes in statistics* (Vol. 193). Berlin: Springer.
Motwani, M. C., Gadiya, M. C., Motwani, R. C., & Harris, F. C. (2004). Survey of image denoising techniques. In *Proceedings of GSPX* (pp. 27–30).
Ojansivu, V., & Heikkilä, J. (2007). Image registration using blur-invariant phase correlation. *IEEE Signal Processing Letters*, *14*(7), 449–452.
Pass, G., & Zabih, R. (1996). Histogram refinement for content-based image retrieval. In *Proceedings 3rd IEEE workshop on applications of computer vision WACV'96* (pp. 96–102). IEEE.
Pedone, M., Flusser, J., & Heikkilä, J. (2013). Blur invariant translational image registration for N-fold symmetric blurs. *IEEE Transactions on Image Processing*, *22*(9), 3676–3689.
Pensky, M., Vidakovic, B., et al. (1999). Adaptive wavelet estimator for nonparametric density deconvolution. *The Annals of Statistics*, *27*(6), 2033–2053.
Perona, P., & Malik, J. (1990). Scale-space and edge detection using anisotropic diffusion. *IEEE Transactions on Pattern Analysis and Machine Intelligence*, *12*(7), 629–639.
Schott, J. R. (2003). Kronecker product permutation matrices and their application to moment matrices of the normal distribution. *Journal of Multivariate analysis*, *87*(1), 177–190.
Song, I., & Lee, S. (2015). Explicit formulae for product moments of multivariate Gaussian random variables. *Statistics and Probability Letters*, *100*, 27–34.
Starck, J. L., Candès, E. J., & Donoho, D. L. (2002). The curvelet transform for image denoising. *IEEE Transactions on Image Processing*, *11*(6), 670–684.
Stefanski, L. A., & Carroll, R. J. (1990). Deconvolving kernel density estimators. *Statistics*, *21*(2), 169–184.
Swain, M. J., & Ballard, D. H. (1991). Color indexing. *International Journal of Computer Vision*, *7*(1), 11–32.
Teuber, T., Remmele, S., Hesser, J., & Steidl, G. (2012). Denoising by second order statistics. *Signal Processing*, *92*(12), 2837–2847.
Triantafyllopoulos, K. (2003). On the central moments of the multidimensional Gaussian distribution. *Mathematical Scientist*, *28*(2), 125–128.
Von Rosen, D. (1988). Moments for matrix normal variables. *Statistics: A Journal of Theoretical and Applied Statistics*, *19*(4), 575–583.
Wang, L., & Healey, G. (1998). Using Zernike moments for the illumination and geometry invariant classification of multispectral texture. *IEEE Transactions on Image Processing*, *7*(2), 196–203.
Zhang, H., Shu, H., Han, G. N., Coatrieux, G., Luo, L., & Coatrieux, J. L. (2010). Blurred image recognition by Legendre moment invariants. *IEEE Transactions on Image Processing*, *19*(3), 596–611.

Jitka Kostková received the M.Sc. degree in Applied Mathematical Stochastic Methods from the Czech Technical University, Faculty of Nuclear Sciences and Physical Engineering, Prague, Czech Republic, in 2015. Currently, she is a Ph.D. student in Mathematical Engineering and tutors undergraduate courses on mathematical analysis at the same university. Jitka Kostková's research interest is focused on moments and moment invariants.

Jan Flusser received the M.Sc. degree in mathematical engineering from the Czech Technical University, Prague, Czech Republic, in 1985, the Ph.D. degree in computer science from the Czechoslovak Academy of Sciences in 1990, and the DrSc. degree in technical cybernetics in 2001. Since 1985 he has been with the Institute of Information Theory and Automation, Czech Academy of Sciences, Prague. In 1995–2007, he was holding the position of a head of Department of Image Processing. Since 2007 he has been a Director of the Institute. He is a full professor of computer science at the Czech Technical University, Faculty of Nuclear Sciences and Physical Engineering, and at the Charles University, Faculty of Mathematics and Physics, Prague, Czech Republic, where he gives undergraduate and graduate courses on Digital Image Processing, Pattern Recognition, and Moment Invariants and Wavelets. Jan Flusser's research interest covers moments and moment invariants, image registration, image fusion, multichannel blind deconvolution, and super-resolution imaging. He has authored and coauthored more than 200 research publications in these areas, including the monographs Moments and Moment Invariants in Pattern Recognition (Wiley, 2009) and 2D and 3D Image Analysis by Moments (Wiley, 2016). In 2007 Jan Flusser received the Award of the Chairman of the Czech Science Foundation for the best research project and won the Prize of the Academy of Sciences of the Czech Republic for the contribution toimage fusion theory. In 2010, he was awarded by the SCOPUS 1000 Award. He received the Felber Medal of the Czech Technical University for excellent contribution to research and education in 2015 and the Praemium Academiae of the Czech Academy of Sciences for outstanding researchers in 2017.

In this Appendix, we will complete the proof from the paper [2]. This part of the proof was not included in the original paper because of the page limit. We use the method of generating functions described in [165] to prove Equation (32), i.e.

$$\sum_{j=0}^{\lfloor \frac{m}{2} \rfloor} (-1)^j \binom{m}{2j} (l+m-2j-1)!!(2j-1)!! = \\ = m! \sum_{j=0}^{\lfloor \frac{m}{2} \rfloor} (-1)^j \frac{(2j-1)!!}{(2j)!} \frac{(l+m-2j-1)!!}{(m-2j)!} = \frac{l!}{(l-m)!!}\,. \tag{5}$$

Proof. We are looking for such series $\sum_{n=0}^{+\infty} a_n x^n$, $\sum_{n=0}^{+\infty} b_n x^n$, $\sum_{n=0}^{+\infty} c_n x^n$ that

$$\sum_{n=0}^{+\infty} c_n x^n = \left(\sum_{n=0}^{+\infty} a_n x^n \right) \cdot \left(\sum_{n=0}^{+\infty} b_n x^n \right) = \sum_{n=0}^{+\infty} \left(\sum_{j=0}^{n} a_j b_{n-j} \right) x^n \,.$$

Then it holds for the coefficients

$$c_n = \sum_{k=0}^{n} a_k b_{n-k}\,.$$

We can divide the proof into two parts to get rid of the floor of $m/2$.

1. If $m = 2n$ is even then $l = 2N$ is even and we can simplify Eq. (5) to

   $$\sum_{j=0}^{\lfloor \frac{m}{2} \rfloor} (-1)^j \frac{(2j-1)!!}{(2j)!} \frac{(l+m-2j-1)!!}{(m-2j)!} = \sum_{j=0}^{n} (-1)^j \frac{(2j-1)!!}{(2j)!} \frac{(2N+2n-2j-1)!!}{(2n-2j)!}\,.$$

   Clearly, the coefficient a_k is

   $$a_k = (-1)^k \frac{(2k-1)!!}{(2k)!}\,. \tag{6}$$

   Hence, the power series becomes

   $$\sum_{n=0}^{+\infty} a_n x^n = \sum_{n=0}^{+\infty} (-1)^n \frac{(2n-1)!!}{(2n)!} x^n = \sum_{n=0}^{+\infty} (-1)^n \frac{(2n-1)!!}{(2n)!!(2n-1)!!} x^n = \\ = \sum_{n=0}^{+\infty} (-1)^n \frac{1}{2^n n!} x^n = \sum_{n=0}^{+\infty} \frac{\left(-\frac{x}{2}\right)^n}{n!} = \mathrm{e}^{-x/2}\,.$$

   In the case of the second power series, the process will be more complicated

   $$\sum_{n=0}^{+\infty} b_n x^n = \sum_{n=0}^{+\infty} \frac{(2N+2n-1)!!}{(2n)!} x^n =$$

$$= \sum_{n=0}^{+\infty} (2N+2n-1)\cdot(2N+2n-3)\cdots(2n+1)\cdot\frac{(2n-1)!!}{(2n)!}x^n \equiv s(x)\,.$$

Let us define new series

$$f_0(x) \equiv s\left(x^2\right) = \sum_{n=0}^{+\infty} (2N+2n-1)\cdot(2N+2n-3)\cdots(2n+1)\cdot\frac{(2n-1)!!}{(2n)!}x^{2n}\,. \tag{7}$$

We will find the sum of the power series $f_0(x)$ by means of termwise integration

$$\begin{aligned}
F_0(x) &= \int f_0(x)\,\mathrm{d}x = \\
&= \sum_{n=0}^{+\infty} (2N+2n-1)\cdot(2N+2n-3)\cdots(2n+3)\cdot\frac{(2n-1)!!}{(2n)!}x^{2n+1} \\
f_1(x) &= xF_0(x) = \\
&= \sum_{n=0}^{+\infty} (2N+2n-1)\cdot(2N+2n-3)\cdots(2n+3)\cdot\frac{(2n-1)!!}{(2n)!}x^{2n+2} \\
f_2(x) &= xF_1(x) = \\
&= \sum_{n=0}^{+\infty} (2N+2n-1)\cdot(2N+2n-3)\cdots(2n+5)\cdot\frac{(2n-1)!!}{(2n)!}x^{2n+4} \\
&\vdots \\
f_{N-1}(x) &= xF_{N-2}(x) = \sum_{n=0}^{+\infty} (2N+2n-1)\cdot\frac{(2n-1)!!}{(2n)!}x^{2N+2n-2} \\
F_{N-1}(x) &= \sum_{n=0}^{+\infty}\frac{(2n-1)!!}{(2n)!}x^{2N+2n-1} = x^{2N-1}\sum_{n=0}^{+\infty}\frac{\left(\frac{x^2}{2}\right)^n}{n!} = x^{2N-1}\mathrm{e}^{x^2/2}
\end{aligned}$$

and differentiation

$$\begin{aligned}
f_{N-1}(x) &= \frac{\mathrm{d}}{\mathrm{d}x}F_{N-1}(x) = (2N-1)\cdot x^{2N-2}\mathrm{e}^{x^2/2} + x^{2N}\mathrm{e}^{x^2/2} = xF_{N-2}(x) \\
f_{N-2}(x) &= \frac{\mathrm{d}}{\mathrm{d}x}F_{N-2}(x) = (2N-1)\cdot(2N-3)\cdot x^{2N-4}\mathrm{e}^{x^2/2} + \\
&\quad + 2\cdot(2N-1)\cdot x^{2N-2}\mathrm{e}^{x^2/2} + x^{2N}\mathrm{e}^{x^2/2} = xF_{N-3}(x) \\
&\vdots \\
f_0(x) &= \mathrm{e}^{x^2/2}\sum_{n=0}^{N}\binom{N}{n}\frac{(2N-1)!!}{(2n-1)!!}x^{2n} = s\left(x^2\right)\,.
\end{aligned}$$

The sum of the second power series is

$$\sum_{n=0}^{+\infty} b_n x^n = \mathrm{e}^{x/2}\sum_{n=0}^{N}\binom{N}{n}\frac{(2N-1)!!}{(2n-1)!!}x^n\,. \tag{8}$$

Now, we are able to construct the third power series

$$\sum_{n=0}^{+\infty} c_n x^n = \left(\sum_{n=0}^{+\infty} a_n x^n\right) \cdot \left(\sum_{n=0}^{+\infty} b_n x^n\right) = \sum_{n=0}^{N} \binom{N}{n} \frac{(2N-1)!!}{(2n-1)!!} x^n \,.$$

Finally, we have the coefficients

$$c_n = \begin{cases} \binom{N}{n} \frac{(2N-1)!!}{(2n-1)!!}\,, & \text{if } n \leq N\,, \\ 0\,, & \text{otherwise}\,. \end{cases} \tag{9}$$

$$\begin{aligned} &\sum_{j=0}^{n} (-1)^j \binom{2n}{2j} (2N+2n-2j-1)!!(2j-1)!! = \\ &= (2n)! \sum_{j=0}^{n} (-1)^j \frac{(2j-1)!!}{(2j)!} \frac{(2N+2n-2j-1)!!}{(2n-2j)!} = (2n)! \binom{N}{n} \frac{(2N-1)!!}{(2n-1)!!} = \\ &= (2n)! \frac{N!(2N)!2^n n!}{2^N N!(N-n)!(2n)!n!} = \frac{(2N)!}{2^{N-n}(N-n)!} = \frac{(2N)!}{(2N-2n)!!} = \frac{l!}{(l-m)!!} \end{aligned}$$

2. If $m = 2n+1$ is odd then $l = 2N+1$ is odd and we can simplify Eq. (5) to

$$\sum_{j=0}^{\lfloor \frac{m}{2} \rfloor} (-1)^j \frac{(2j-1)!!}{(2j)!} \frac{(l+m-2j-1)!!}{(m-2j)!} = \sum_{j=0}^{n} (-1)^j \frac{(2j-1)!!}{(2j)!} \frac{(2N+2n-2j+1)!!}{(2n-2j+1)!}$$

If we repeat the same procedure as in the previous case, we obtain the coefficients

$$c_n = \begin{cases} \binom{N}{n} \frac{(2N+1)!!}{(2n+1)!!}\,, & \text{if } n \leq N\,, \\ 0\,, & \text{otherwise}\,. \end{cases} \tag{10}$$

Hence, the result is

$$\begin{aligned} &\sum_{j=0}^{n} (-1)^j \binom{2n+1}{2j} (2N+2n-2j+1)!!(2j+1)!! = \\ &= (2n+1)! \sum_{j=0}^{n} (-1)^j \frac{(2j-1)!!}{(2j)!} \frac{(2N+2n-2j+1)!!}{(2n-2j+1)!} = \\ &= (2n+1)! \binom{N}{n} \frac{(2N+1)!!}{(2n+1)!!} = \frac{l!}{(l-m)!!} \end{aligned}$$

□